New polycyclic amines with biological activity

Matías Rey Carrizo

UNIVERSITAT DE BARCELONA

Facultat de Farmàcia

NEW POLYCYCLIC AMINES WITH BIOLOGICAL ACTIVITY

Matías REY CARRIZO

2014

UNIVERSITAT DE BARCELONA

Facultat de Farmàcia

Programa de doctorat: Química Orgànica Experimental i Industrial

NEW POLYCYCLIC AMINES WITH BIOLOGICAL ACTIVITY

Memòria presentada per Matías REY CARRIZO

Per obtenir el títol de Doctor per la Universitat de Barcelona.

Director i Tutor:

Dr. Santiago Vázquez Cruz

Barcelona, Novembre 2014

A mis abuelas Chichi y Marta.

A mis padres i a mi hermana.

I al meu trosset de cel.

"Trust the dreams, for in them is hidden the gate to eternity."

— Khalil Gibran, *The Prophet*

M'agradaria agrair a totes aquelles persones que m'han ajudat durant aquests quatre anys dur a terme aquest projecte:

Primer de tot, al Dr. Pelayo Camps, Catedràtic de Química Orgànica i Cap de la Unitat de Química Farmacèutica per acollir-me en el si del seu equip de treball i per acceptar ser membre del meu Tribunal de Tesi. En segona posició, però no per això menys important, al meu director de Tesi, el Dr. Santiago Vázquez, Professor Agregat del Departament de Farmacologia i Química Terapèutica. Todo empezó aquel jueves 6 de Mayo de 2010 en el que con tu tono característico, me convenciste para que me uniera a tu grupo de investigación. No me arrepiento de mi decisión y me esforzaré para que te sientas lo suficientemente orgulloso como para que nunca tengas que arrepentirte tú de la tuya. Gracias por todo lo que me has enseñado, has sido un gran maestro. Y especialmente gracias por la rápida corrección del manuscrito.

També voldria agrair als equips de farmacòlegs i de modelització amb qui hem col·laborat en aquest treball. Al grup de la Prof. Lieve Naesens, del *Rega Institute for Medicinal Research* (Bèlgica), per la determinació de l'activitat antiviral i del mecanisme d'acció d'alguns dels nostres compostos. Al Prof. Lawrence Pinto i al Dr. Chunlong Ma, de la Northwestern University (Evanston, Illinois, U.S.A.), per la determinació de la inhibició dels nostres compostos sobre canal M2. A la Prof. Anna Moroni i la Dra. Sabrina Gazzarrini, de la Università degli Studi di Milano, que van continuar assajant els nostres compostos sobre canal M2 després de la jubilació del Prof. Pinto. Al grup del Prof. Javier Luque, de la Universitat de Barcelona, per la realització dels càlculs de docking i dinàmiques moleculars, i particularment a la Salo i al Jordi que han estat els teòrics que s'han ocupat del tema. També vull agrair a la Dra. Gisela Colet per la breu col·laboració en els experiments de calorimetria diferencial d'escombrada.

Lògicament haig d'agrair al meu equip, els SVC, sense qui aquest treball no hagués estat possible. A la Eva, per ensenyar-me gran part del que sé, per estar sempre disposada a donar-me un cop de mà i per tots els moments compartits aquí i a l'estranger. A la Marta B., per l'ambient que aportes al lab i per tots els moments divertits que hem passat junts tant dintre com fora del lab. Als meus treballs dirigits; Rosana, la meva primera alumna aquell estiu 2011; espero haver-te ensenyat alguna cosa útil. Tu continues amb la tradició del canal M2, explota-ho tant com puguis, si algú pot, aquesta ets tu! A la Marta F., la meva estudiant més longeva, gràcies per fer divertits aquells mesos passats junts, en guardo un molt bon record. A l'Alèxia, la meva primera estudiant que no havia passat per cap tutor abans. Gràcies per les pràctiques de francès i per ensenyar-me a ensenyar. Bon courage avec ta thèse à l'étage en-dessous, tu peux y arriver!

A tots els treballs dirigits que han passat pel lab, que han rejovenit el laboratori amb la seva passada. Una menció especial a: en Salva, un gran investigador i més gran persona, gràcies per la bona rebuda a la meva arribada. A en Toni pels bons moments compartits fora del lab, al futbol, a les calçotades, als sopars, a les gresques, etc. I a l'Enric, pel bon rotllo i les rialles.

Als companys de química orgànica, que a més de compartir partits de futbol i alguna que altre sortida, m'han ajudat amb els reactius i el microones. Gràcies a en Guillaume, la Sònia, l'Elena, l'Alex, en Francesco, en Juan Andrés, en Claudio i a tota la colla.

Al grup d'escalada, que tot i que no ens hem vist molt últimament, vam passar bones estones i em va permetre alliberar tensions del lab. Sobretodo agradecer al profe, Luís, un grande.

A toda la gente de Andorra que me acompaña desde hace ya un buen puñado de años: el Guille, el Jose, el Didac, el Cris, el Carlos, el Guillem, el Oriol, el Javi, el Marc i el Iván C. Gracias por el apoyo, aunque no tengáis ni idea de lo que he estado haciendo. I al Iván P., mi vecino en el país de los Pirineos i en Toulouse, sin tu apoyo durante los primeros años no lo hubiera logrado. Y también te agradezco el esfuerzo de haber seguido manteniendo el contacto durante nuestros respectivos doctorados.

A mes potes français du master avec qui je suis resté en contact: Simon, Rémi et Fabrice. Merci pour le soutien et pour l'échange de galères de thèse, vous avec qui je partage un origine.

Me gustaría dar las gracias a la Dra. Luísa Pérez por brindarme la oportunidad de hacer mis primeras prácticas en un laboratorio, y sobre todo a Lucía, mi tutora, quién me enseño mucho (en particular a escribir la libreta!) i me instigó a que siguiera este camino. I want also to thank the people I did my stay with back in Japan, specially Kazuma and Chie, you really were the most helpful people I could met and I kindly appreciate what you taught me, I hope I will be able to return the favour sometime. どうもありがとうございました！I would also like to thank my lab mates in the Netherlands, and in particular Dr. Pieters and Francesca, my supervisor, who taught me a lot about lab organization and Núria who was always ready to give a hand, what she did quite often with me. I also want to express my gratitude to my colleagues during my 3 month internship in Manchester, specially Dr. Greaney who generously welcomed me in his group and Venu, my supervisor as well as José and Pete who made me feel as an integral member of the group.

RESULTS

The present Thesis has led to the following scientific publications and symposium communications:

Scientific publications

1. '3-Azatetracyclo[5.2.1.1^{5,8}.0^{1,5}]undecane derivatives: from wild-type inhibitors of the M2 ion channel of influenza A virus to derivatives with potent activity against the V27A mutant.' Rey-Carrizo, M.; Torres, E.; Ma, C.; Barniol-Xicota, M.; Wang, J.; Wu, Y.; Naesens, L.; Degrado, W. F.; Lamb, R. A.; Pinto, L. H.; Vazquez, S. *J. Med. Chem.* **2013**, *56*, 9265.
2. 'Azapropellanes with anti-influenza A virus activity'. Torres, E.; Leiva, R.; Gazzarrini, S.; Rey-Carrizo, M.; Frigolé-Vivas, M.; Moroni, A.; Naesens, L.; Vázquez, S. *ACS Med. Chem. Lett.* **2014**, *5*, 831.
3. 'Easily accessible polycyclic amines that inhibit the wild-type and amantadine-resistant mutants of the M2 channel of influenza A virus'. Rey-Carrizo, M.; Barniol-Xicota, M.; Ma, C.; Frigolé-Vivas, M.; Torres, E.; Naesens, L.; Llabrés, S.; Juárez-Jiménez, J.; Luque, F. J.; DeGrado, W. F.; Lamb, R. A.; Pinto, L. H.; Vázquez, S. *J. Med. Chem.* **2014**, *57*, 5738.
4. 'Dimerization of pyramidalized 3,4,8,9-tetramethyltetracyclo [4.4.0.0^{3,9}.0^{4,8}]dec-1(6)-ene to a hydrocarbon featuring four cyclohexane rings in boat conformations'. Rey-Carrizo, M.; Barniol-Xicota, M.; Font-Bardia, M.; Vázquez, S. *Angew. Chem. Int. Ed. Engl.* **2014**, *53*, 8195.
5. 'Exploring new polycyclic scaffolds targeting the V27A mutant M2 channel influenza A virus'. *Writing in progress.*

Book chapter

1. 'Inhibitors of the M2 channel of influenza A virus'. Duque, M. D.; Torres, E.; Valverde, E.; Barniol-Xicota, Guardiola, S.; Rey, M.; Vázquez, S. *Recent Advances in Pharmaceutical Sciences*, Transworld research Network, **2011**, 35.

Symposium communications

1. 'Synthesis of polycyclic amines with anti-influenza A virus activity'. Torres, E.; Rey-Carrizo, M.; Barniol-Xicota, M.; Vázquez, S. (Poster) Balticum Organicum Syntheticum, Tallinn, Estonia, **2012**.

2. 'New influenza A M2 channel inhibitors featuring tetracyclic scaffold'. Barniol-Xicota, M.; Rey-Carrizo, M.; Torres, E.; Ma, C.; Pinto, L. H.; Vázquez, S (Poster) Balticum Organicum Syntheticum, Tallinn, Estonia, **2012**.

3. 'Targeting the V27A mutant of the M2 channel of influenza A virus'. Rey-Carrizo, M.; Torres, E.; Ma, C.; Pinto, L. H.; Vázquez, S. (Poster) Balticum Organicum Syntheticum, Tallinn, Estonia, **2012**.

4. 'Synthesis and anti-influenza A activity of novel polycyclic amines'. Rey-Carrizo, M.; Torres, E.; Barniol-Xicota, M.; Vázquez, S. (Flash communication) XXIV Reunión Bienal de Química Orgánica, San Sebastián, Spain, **2012**.

5. 'Synthesis and anti-influenza A activity of novel polycyclic amines'. Rey-Carrizo, M.; Torres, E.; Barniol-Xicota, M.; Vázquez, S. (Flash communication) XXXVI Reunión Bienal de la Sociedad Española de Química, Santander, Spain, **2013**.

6. 'Hemagglutinin as a new target to fight the flu'. Leiva, R.; Gazzarrini, S.; Torres, E.; Rey-Carrizo, M.; Barniol-Xicota, M.; Moroni, A.; Naesens, L.; Vázquez, S. (Poster) I Simposio de Jóvenes Investigadores de la Sociedad Española de Química Terapéutica, Madrid, Spain, **2014**.

7. 'Influenza A virus: a wolf in sheep's clothing. Recent advances in new anti-influenza compounds'. Barniol-Xicota, M.; Rey-Carrizo, M.; Torres, E.; Leiva, R.; Ma, C.; Naesens, L.; Luque, F.J.; Pinto, L. H.; Vázquez, S. (Oral communication) I Simposio de Jóvenes Investigadores de la Sociedad Española de Química Terapéutica, Madrid, Spain, **2014**.

8. 'Exploring new polycyclic scaffolds targeting the V27A mutant M2 channel influenza A virus'. Rey-Carrizo, M.; Frigole-Vivas, M.; Gazzarrini, S.; Moroni, A.; Ma, C.; Pinto, L. H.; Vázquez, S. (Poster) I Simposio de Jóvenes Investigadores de la Sociedad Española de Química Terapéutica, Madrid, Spain, **2014**.

9. 'Grip A, alarmisme o perill real? Noves molècules actives contra soques resistents'. Rey-Carrizo, M.; Torres, E.; Barniol-Xicota, M.; Ma, C.; Pinto, L. H.; Naesens, L.; Gazzarrini, S.; Moroni, A.; Vázquez, S. (Oral communication) 8ns Debats de Recerca, Andorra la Vella, Principat d' Andorra, **2014**.

Research stay

1. 'Hemithioacetals as a new tool for Dynamic Combinatorial Chemistry'. Michael Greaney's group. School of Chemistry, Manchester, United Kingdom, October-December **2013**.

ABBREVIATIONS

Abs. EtOH = absolute ethanol

A/M2 = influenza A M2 channel

ACN = acetonitrile

AcOH = acetic acid

ATP = adenosine triphosphate

ATR = attenuated total reflectance

BM2 = influenza B M2 channel

b.r.s.m = based on recovered starting material

CDC = Centre for Disease Control and Prevention

Cp = cyclopentadiene

CPE = cytopathic effect

cRNA = complementary ribonucleic acid

DCM = dichloromethane

DIH = 1,3-diiodo-5,5-dimethylhydantoin

DMSO = dimethylsulfoxide

DNA = deoxyribonucleic acid

DSC = differential scanning calorimetry

EC_{50} = concentration producing 50% of antiviral effect

EC_{90} = concentration producing a reduction in viral RNA of 1 $\log_{10}$

EC_{99} = concentration producing a reduction in viral RNA of 2 $\log_{10}$

EI = electron impact

Et = ethyl

EtOAc = ethyl acetate

FDA = Food and Drug Administration

GC-MS = gas chromatography-mass spectrometry

GTP = guanosine-5'-triphosphate

HA = hemagglutinin

IC_{50} = half maximal inhibitory concentration

HMDS = hexamethyldisilazane

HOMO = highest occupied molecular orbital

IR = infrared

K_d = dissociation constant

LDA = lithium diisopropylamide

LiHMDS = lithium bis(trimethylsilyl)amide

LUMO = lowest unoccupied molecular orbital

M2TM = M2 channel transmembrane domain

MCC = minimum cytotoxic concentration

MD = molecular dynamics

MDCK = Madin-Darby Canine Kidney cells

MeOH = methanol

mRNA = messenger ribonucleic acid

mRNP = messenger ribonucleoprotein

MS = mass spectrometry

MTS = tetrazolium reduction assay

NA = neuraminidase

n-BuLi = *n*-butyllithium

NEP = nuclear export protein

NIH = National Institutes of Health

NMR = Nuclear Magnetic Resonance

NP = nucleoprotein

NS1 = non-structural protein 1

ORTEP = oak ridge thermal ellipsoid plot

PB1 = polymerase basic 1 protein

PB2 = polymerase basic 2 protein

PKR = protein kinase R

P-site = pore binding site

RBS = receptor binding site

RNA = ribonucleic acid

r.t. = room temperature

SET = single electron transfer

SOMO = singly occupied molecular orbital

S-site = surface binding site

ssNMR = solid state nuclear magnetic resonance

ssRNA = single stranded ribonucleic acid

t-BuLi = *tert*-butyllithium

TCAD = triple combination antiviral drug

TEVC = two-electrode voltage clamp

THF = Tetrahydrofuran

TMG = tetramethylguanidine

vRNA = viral ribonucleic acid

vRNP = viral ribonucleoprotein

WHO = World Health Organization

wt-M2 = wild-type M2 channel

μW = microwave apparatus

INDEX

Introduction

Medicinal chemistry is the discipline the present work belongs to. The field deals with the design, synthesis and pharmacological evaluation of new molecules that target a disease in the hope of getting a better insight into its mechanisms for eventually producing a new pharmaceutical agent.

We chose influenza, also known as the flu, as our target for carrying this three-year work chiefly for three reasons:

- Influenza causes a high mortality and morbidity through seasonal epidemics and sporadic pandemics.[1]
- Even excluding the fatalities, the flu causes a very big economic burden through hospitalization, absenteeism and loss of production.[2]
- There is currently no flawless treatment for the flu, meaning there is an urgent need for new ways to fight the illness.[3]

Having said that and taking into account that amantadine, a polycyclic amine (*vide infra*), has been used for decades as an anti-influenza drug and that our research group has an extended expertise in the synthesis of polycyclic molecules,[4] the aim of this thesis was to explore new polycyclic scaffolds with potential activity against influenza.

[1] Rossman, J. S.; Lamb, R. A. *Virology* **2011**, *411*, 229.

[2] Molinari, N.-A. M.; Ortega-Sanchez, I. R.; Messonnier, M. L.; Thompson, W. W.; Wortley, P. M.; Weintraub, E.; Bridges, C. B. *Vaccine* **2007**, *25*, 5086.

[3] a) De Clercq, E. *Nat. Rev. Drug Discov.* **2006**, *5*, 1015. b) Beigel, J.; Bray, M. *Antiviral Res.* **2008**, *78*, 91. c) Krug, R. M.; Aramini, J. M. *Trends Pharmacol. Sci.* **2009**, *30*, 269. d) Das, K.; Aramini, J. M.; Ma, L.-C.; Krug, R. M.; Arnold, E. *Nat. Struct. Mol. Biol.* **2010**, *17*, 530. e) Du, J.; Cross, T. A.; Zhou, H.-X. *Drug Discov. Today* **2012**, *17*, 1111. f) Das, K. *J. Med. Chem.* **2012**, *55*, 6263. g) Lee, S. M.-Y.; Yen, H.-L. *Antiviral Res.* **2012**, *96*, 391. h) Vanderlinden, E.; Naesens, L. *Med. Res. Rev.* **2014**, *34*, 301.

[4] a) Camps, P.; Pérez, F.; Vázquez, S.; Font-Bardia, M.; Solans, X. *Angew. Chem. Int. Ed. Engl.* **1995**, *34*, 912. b) Camps, P.; Estiarte, M. A.; Vázquez, S.; Pérez, F. *Synth. Commun.* **1995**, *25*, 1287. c) Camps, P.; Luque, F. J.; Orozco, M.; Pérez, F.; Vázquez, S. *Tetrahedron Lett.* **1996**, *37*, 8605. d) Camps, P.; Pérez, F.; Vázquez, S. *Tetrahedron* **1997**, *53*, 9727. e) Lange, H.; Schäfer, W.; Gleiter, R.; Camps, P.; Vázquez, S. *J. Org. Chem.* **1998**, *63*, 3478. f) Camps, P.; Fernández, J. A.; Vázquez, S.; Font-Bardia, M.; Solans, X. *Angew. Chem. Int. Ed. Engl.* **2003**, *42*, 4049. g) Vázquez, S.; Camps, P. *Tetrahedron* **2005**, *61*, 5147. h) Camps, P.; Muñoz, M. R.; Vázquez, S. *Tetrahedron* **2006**, *62*, 7645. i) Duque, M. D.; Camps, P.; Profire, L.; Montaner, S.; Vázquez, S.; Sureda, F. X.; Mallol, J.; López-Querol, M.; Naesens, L.; De Clercq, E.; Prathalingam, S. R.; Kelly, J. M. *Bioorg. Med. Chem.* **2009**, *17*, 3198. j) Duque, M. D.; Camps, P.; Torres, E.; Valverde, E.; Sureda, F. X.; López-Querol, M.; Camins, A.; Prathalingam, S. R.; Kelly, J. M.; Vázquez, S. *Bioorg. Med. Chem.* **2010**, *18*, 46.

1. The disease: influenza

To begin with, it should be clarified that there is a difference between seasonal influenza and pandemic influenza (i.e. when the disease has spread worldwide). Seasonal influenza can cause only mild symptoms (often mistakenly confused with a cold) or severe ones, even leading to death, depending on the virulence of the circulating strain and the immune system of the affected person. On the other hand, when seasonal influenza becomes pandemic, it generally displays a higher mortality rate due to the lack of preparation of the immune system to the completely new strain of the virus.

a. Seasonal influenza

The commonly known flu is caused by a virus, the influenza virus, which can be transmitted from an infected person to a new host by a range of different modes that are still debated today. They include: i) direct physical contact between the infected person and the host, ii) indirect contact by passive transfer through an intermediate object (e.g. contaminated hands), iii) droplet transmission generated from the respiratory tract of the infected individual when coughing, sneezing or talking, iv) airborne transmission via the dissemination of viruses in droplets that remain suspended for long periods of time.[5]

The risk of being infected with influenza is always present although it is especially common in winter, that is why it is sometimes referred as "seasonal flu". The reason for this prevalence is not clear but a likely scenario is that the cold temperatures and the low relative humidity of the season are favorable to the spread of influenza virus.[6]

Seasonal influenza is an acute viral infection of the respiratory tract that causes a sudden onset of cough, sore throat, runny or stuffy nose, body aches, headaches, fatigue and sometimes fever. Usually, people recover from these symptoms in a few days to less than two weeks with a symptomatic treatment or not treatment at all. However, more serious symptoms with fatal complications can happen to high-risk groups: elderly people (65 years and older), people of any age with certain chronic medical conditions (such as asthma, diabetes or heart disease), immunocompromised people, pregnant women and young children. But since anyone can catch the flu at any age, even healthy people, the menace of severe complications of the illness is always present.[7]

---

[5] a) Brankston, G.; Gitterman, L.; Hirji, Z.; Lemieux, C.; Gardam, M. *Lancet Infect. Dis.* **2007**, *7*, 257. b) Weber, T. P.; Stilianakis, N. I. *J. Infect.* **2008**, *57*, 361.

[6] Lowen, A. C.; Mubareka, S.; Steel, J.; Palese, P. *PLoS Pathog.* **2007**, *3*, 1470.

[7] CDC. Flu symptoms & severity http://www.cdc.gov/flu/about/disease/symptoms.htm (accessed Feb 25, 2014).

Taking for instance a developed country such as the U.S.A., it can be appreciated how overwhelming the death toll and the economic burden of influenza are: based on 2003 demographics, there were 24.7 million cases of the disease that brought about more than 40,000 deaths (mainly in elderly people). The total economic loss, accounting for medical costs and lost earnings, was estimated around $87.1 billion for that year only.[2]

The most dangerous feature of seasonal influenza is its inherent capacity of becoming a pandemic influenza, and this can happen for two reasons. The first is the high transmissibility; the ease with which the virus spreads principally via the airborne transmission route, make it very hard to contain the epidemic (i.e. when there is a substantial increase in the number of cases than previously reported or expected). The second one is its adaptive ability to elude treatments based on vaccination and this is mainly due to the virus property of mutating and evolving very rapidly; this is called the *antigenic drift*.

When someone gets the vaccine against seasonal influenza she or he is getting injected attenuated viruses of the most common circulating strains, these induce an immune response thereby producing antibodies against two major surface proteins of the viruses, namely hemagglutinin (HA) and neuraminidase (NA). They are the H and the N referred to for classifying virus strains, therefore the H5N1 strain means hemagglutinin type 5 and neuraminidase type 1. The body is then immunized to some strains but influenza viruses are very prone to mutations and together with the selective pressure exerted by the vaccine, these can induce changes in the shape of HA or NA antibodies' binding site, thus rendering the vaccine ineffective. Furthermore these cumulative alterations can gradually create a new strain with a different HA and NA combination. This phenomenon is known as *antigenic drift* [8] (Figure 1) and has caused heavier-than-normal flu seasons and even pandemics such as the H2N2 "Asian influenza" in 1957 or the H3N2 "Hong-Kong influenza" in 1968.[3a] The other very dangerous mutation process that more often leads to pandemic influenza is the *antigenic shift* (Figure 2) that will be explained hereafter.

---

[8] NIH. Antigenic drift
http://www.niaid.nih.gov/topics/flu/research/basic/pages/antigenicdriftillustration.aspx (accessed Feb 25, 2014).
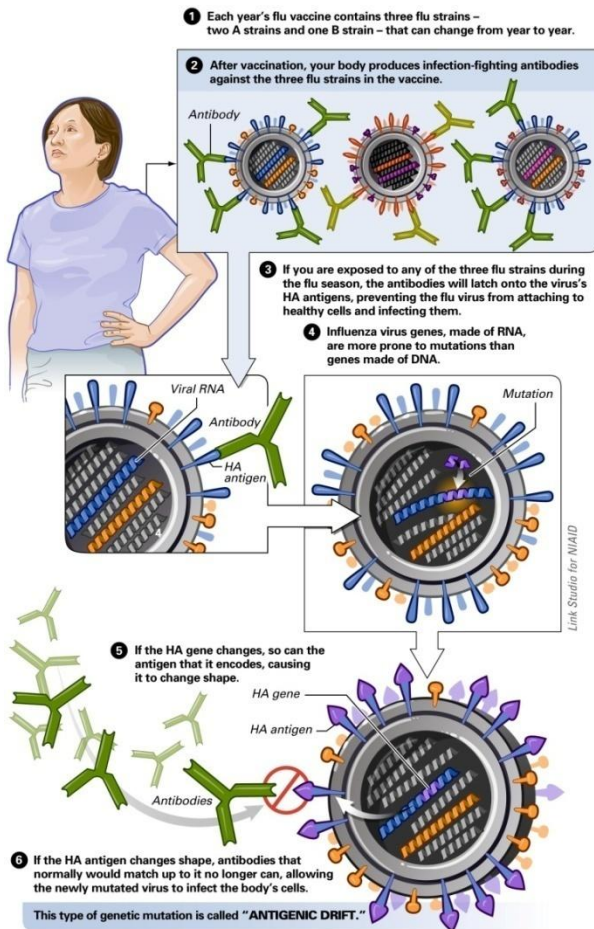
Figure 1. Antigenic drift[8]
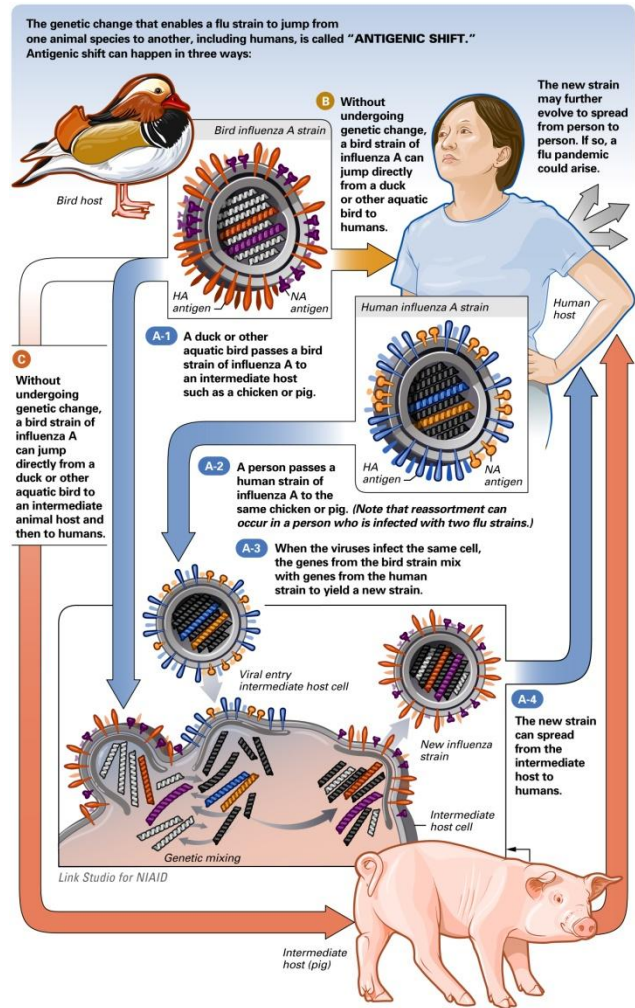
Figure 2. Antigenic shift[9]

b. *Pandemic influenza*

Pandemic influenza has the same characteristics as seasonal influenza; it is caused by influenza virus and the transmissibility is identical. By contrast the symptoms it can lead to are pneumonia or respiratory failures that might be lethal.[10] As stated before it may be caused by antigenic drift or by antigenic shift. The latter may happen in three ways: i) wild waterfowl (the natural reservoir of the virus) infects an intermediate host, a chicken or a pig, with a strain of influenza virus, then a person transmits another strain of influenza to the same

---

[9] NIH. Antigenic shift

http://www.niaid.nih.gov/topics/flu/research/basic/pages/antigenicshiftillustration.aspx (accessed Feb 25, 2014).

[10] a) Rello, J.; Rodríguez, A.; Ibañez, P.; Socias, L.; Cebrian, J.; Marques, A.; Guerrero, J.; Ruiz-Santana, S.; Marquez, E.; Del Nogal-Saez, F.; Alvarez-Lerma, F.; Martínez, S.; Ferrer, M.; Avellanas, M.; Granada, R.; Maraví-Poma, E.; Albert, P.; Sierra, R.; Vidaur, L.; Ortiz, P.; Prieto del Portillo, I.; Galván, B.; León-Gil, C. *Crit. Care* **2009**, *13*, R148. b) Perez-Padilla, R.; de la Rosa-Zamboni, D.; Ponce de Leon, S.; Hernandez, M.; Quiñones-Falconi, F.; Bautista, E.; Ramirez-Venegas, A.; Rojas-Serrano, J.; Ormsby, C. E.; Corrales, A.; Higuera, A.; Mondragon, E.; Cordova-Villalobos, J. A. *N. Engl. J. Med.* **2009**, *361*, 680.

host and the conditions are met for a recombinant mutant appearance, ii) a wild waterfowl strain can infect directly a human being, iii) wild waterfowl pass its influenza strain to an intermediate host that will transmit it to humans (Figure 2).[9] This phenomenon creates also a new strain of the virus usually combining high transmissibility with deadly virulence, for instance it is supposed that the H1N1 "Spanish flu" of 1918 started by an antigenic shift.[11]

There has been several documented influenza pandemics through the last and the current centuries starting with the deadliest natural disaster of human history: the 1918 "Spanish flu". Caused by the H1N1 subtype, its presumed origin is an avian-like influenza virus that spread simultaneously in three explosive waves during a 12 months period from three focuses: Europe, Asia and North-America, the latter being where the first wave was described in 1918. The actual inception is arguably Europe with France and Germany being the more plausible candidates. The virus had a unique feature displaying very high mortality rates in young population (15-34 years old), 20 times higher than in previous years. Altogether it caused around 50 million deaths and an estimate third of the population at the time (~500 million) was infected. The case-fatality rate was unusually high for an influenza pandemic (>2.5% compared with <0.1% for other pandemics) but this may be explained by many factors, wartime conditions and bacteria superinfections for example. Although another pandemic of such magnitude is not very likely, we must be cautious with its descendants.[12]

In 1957 the second pandemic of the 20th century occurred, generated this time by the H2N2 influenza virus subtype and appointed "Asian flu" due to its origin in Southeast Asia. The virus was possibly a reassortment, via antigenic shift, from an avian virus and the circulating H1N1 human strain, or it could have been through antigenic drift from H1N1.[3a] Its estimated mortality during 1957-1958 was between 1 to 4 million people touching principally Asia and North America. Even though this strain disappeared from the human population in only ten years, replaced by the H3N2 strain, it is still endemic in wild waterfowl. A major concern thus should be the absence of this subtype in humans for more than 50 years, meaning that a re-emergence of the H2N2 subtype or any related novel virus could catch people under 50 years old with no immunization at all against it.[13]

---

[11] Bouvier, N. M.; Palese, P. *Vaccine* **2008**, *26*, D49.

[12] a) Reid, A. H.; Taubenberger, J. K.; Fanning, T. G. *Microbes Infect.* **2001**, *3*, 81. b) Taubenberger, J. K.; Morens, D. M. *Emerg. Infect. Dis.* **2006**, *12*, 15. c) Oxford, J. S.; Lambkin, R.; Elliot, A.; Daniels, R.; Sefton, A.; Gill, D. *Vaccine* **2006**, *24*, 6742. d) Kilbourne, E. D. *Emerg. Infect. Dis.* **2006**, *12*, 9.

[13] Jones, J. C.; Baranovich, T.; Marathe, B. M.; Danner, A. F.; Seiler, J. P.; Franks, J.; Govorkova, E. A.; Krauss, S.; Webster, R. G. *J. Virol.* **2014**, *88*, 1175.

Then appeared the H3N2 "Hong Kong flu" in 1968; originated either by the reassortment of the circulating H2N2 human strain and an unknown avian influenza virus, or again by antigenic shift from H2N2.[3a] This new subtype was considered pandemic until 1970 but it was very mild, some years even showing a mortality rate inferior to seasonal flu. This was ascribed to the retention of the NA subtype from its parent H2N2, allowing some immunity to the infected population. Nevertheless it made around 700,000 victims worldwide and 34,000 only in the U.S.A. Afterwards, the virus became endemic and seasonal and has been present until today, though displaying a high mortality rate over the past decades.[14]

An unexpected event happened in 1977 with the re-emergence of the H1N1 strain this time under the sobriquet "Russian flu" even if the first case was reported in China. The extraordinariness of the case was the fact that this H1N1 subtype bore a close resemblance to the "Spanish flu" strain that disappeared in 1957, and it is considered remotely possible that a virus could survive unchanged after 20 years of immunity pressures. An accidental release of a frozen strain from the 1950s was the best explanation for the outbreak. Since the major part of the population was to some extent immune, the "pandemic" was really mild, affecting only people under 25 years old.[12d,14b,15] Contrary to the H2N2 strain, the H1N1 virus is still circulating today along with the H3N2.

FIGURE

Recorded human pandemic influenzas since 1885 (early sub-types inferred)

Source: European Centre for Disease Prevention and Control (ECDC) 2009
Reproduced and adapted (2009) with permission of Dr Masato Tashiro, Director, Center for Influenza Virus Research, National Institute of Infectious Diseases (NIID), Japan.
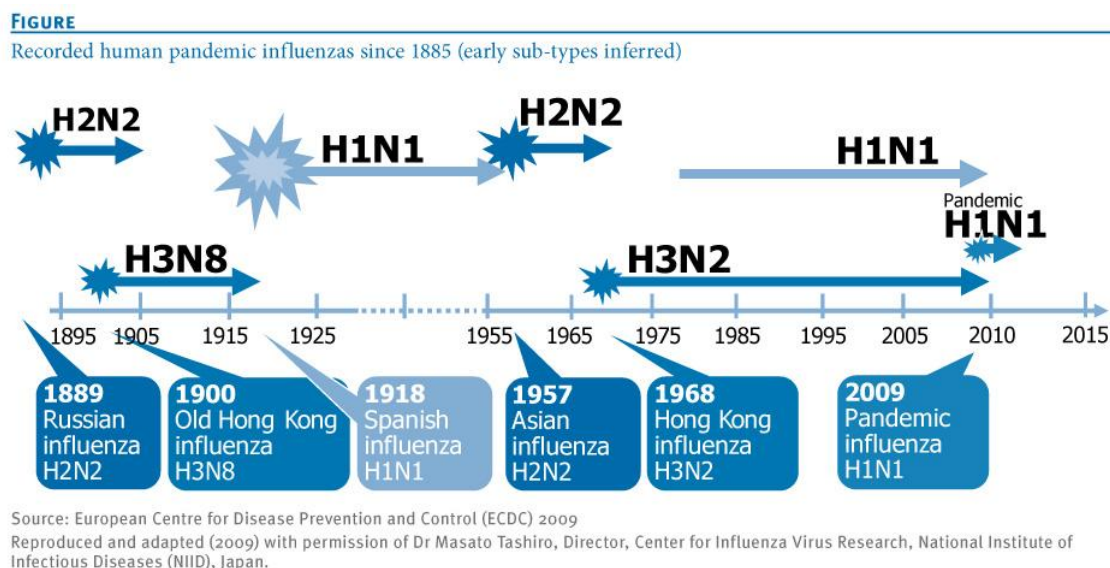
Figure 3. Influenza pandemics timeline[16]

[14] a) Rajagopal, S.; Treanor, J. *Semin. Respir. Crit. Care Med.* **2007**, *28*, 159. b) Taubenberger, J. K.; Kash, J. C. *Cell Host Microbe* **2010**, *7*, 440.

[15] a) Cox, N. J.; Fukuda, K. *Infect. Dis. Clin. North Am.* **1998**, *12,* 27. b) Neumann, G.; Noda, T.; Kawaoka, Y. *Nature* **2009**, *459*, 931.

[16] Nicoll, A. A new decade, a new seasonal influenza: the Council of the European Union Recommendation on seasonal influenza vaccination http://www.eurosurveillance.org/ViewArticle.aspx?ArticleId=19458 (accessed Feb 28, 2014).

In 1997 the first case of H5N1 "Avian flu" was declared in Hong Kong producing 6 casualties. Its origin had been entirely avian with birds and poultry as their main host, so their depopulation solved the problem. Nevertheless, associated with the movement of poultry, a new outbreak took place in 2003 in Asia and since then sporadic cases have occurred all over the world, the last being in North America on January 2014.[17] For still an unknown reason, the virus seems to affect mostly young populations (90% of the cases). But the major concern about this subtype is that, even if it does not have the ability to be transmitted between humans (hence the low number of cases), its mortality rate is as high as 60%.[15b,18] As of June the 27th 2014, 667 confirmed cases of H5N1 had been detected in 15 countries of which 393 were casualties.[19] The threat of the virus acquiring human-to-human transmission is a matter of great worry.

In early April 2009 the first case of H1N1 "Swine flu" was diagnosed in Mexico. The virus started spreading extremely fast, hitting very hard 8 countries (among which Spain) urging the WHO (World Health Organization) to declare it as the first pandemic of the 21st century as soon as early June. The high pathogenicity of the virus was ascribed to its inception, a triple reassortment from swine/avian/H3N2-human influenza viruses that renders most immune responses ineffective. The primary cause of death was atypical pneumonia which requires a heavy antibiotic treatment not available everywhere which could explain the high mortality. In August 2010 the WHO announced that H1N1 had moved to a post-pandemic period. A rough estimate of the death toll of the "Swine flu" first 12 months, stated there were nearly 290,000 deaths (80% were younger than 65 years) in 48 countries and 51% happened in Southeast Asia and Africa. We should not forget that the "Spanish flu" early phases were also considered mild and that the H1N1 strain continues to circulate in pigs and in humans as seasonal flu.[15b, 20]

---

[17] CDC. First Human Avian Influenza A (H5N1) Virus Infection Reported in Americas http://www.cdc.gov/flu/news/first-human-h5n1-americas.htm (accessed Feb 28, 2014).

[18] Abdel-Ghafar, A.; Chotpitayasunondh, T.; Zhancheng, G.; Hayden, F.; Hien, N.; de Jong, M.; Naghdaliyev, A.; Peiris, J.; Shindo, N.; Soeroso, S.; Uyeki, T. *N Engl J Med* **2008**, *358*, 261.

[19] WHO. Influenza at the human-animal interface. June 2014 http://www.who.int/influenza/human_animal_interface/Influenza_Summary_IRA_HA_interface_27June14.pdf?ua=1 (accessed Oct. 07th, 2014).

[20] a) Cohen, J.; Enserink, M. *Science* **2009**, *324*, 1496. b) Michaelis, M.; Doerr, H. W.; Cinatl, J. *Med. Microbiol. Immunol.* **2009**, *198*, 175. c) Dawood, F. S.; Iuliano, A. D.; Reed, C.; Meltzer, M. I.; Shay, D. K.; Cheng, P.-Y.; Bandaranayake, D.; Breiman, R. F.; Brooks, W. A.; Buchy, P.; Feikin, D. R.; Fowler, K. B.; Gordon, A.; Hien, N. T.; Horby, P.; Huang, Q. S.; Katz, M. A.; Krishnan, A.; Lal, R.; Montgomery, J. M.; Mølbak, K.; Pebody, R.; Presanis, A. M.; Razuri, H.; Steens, A.; Tinoco, Y. O.; Wallinga, J.; Yu, H.; Vong, S.; Bresee, J.; Widdowson, M.-A. *Lancet Infect. Dis.* **2012**, *12*, 687.

The last episode to date, is the newly found H7N9 subtype in China in end of March 2013. Its origin seems to be avian and it has caused 450 cases of which 165 deaths.[21] It has not acquired person-to-person transmission but the experts alert of its dangerousness if the virus was ever to cross this barrier.[22]

A better understanding of influenza virus and its infectivity mechanisms in order to prevent other disastrous pandemics seems a logical conclusion from these historical data.

2. The causal agent: influenza A virus

Influenza virus nomenclature was set by the WHO in 1980;[23] for example the strain A/Fujian/411/2002 (H3N2) means it is an influenza A virus which origin is Fujian with the strain number 411, it was isolated in 2002 and it possesses the H3N2 subtype. When not specified, the strain refers to human species, otherwise the animal is also included in the nomenclature, e.g. A/chicken/Spain/1664/2013 (H7N1). Wild waterfowl and waders are the natural reservoir hosts of influenza A virus where it remains hidden by asymptomatic infections until it crosses the species barrier.[14b]

The *Orthomyxoviridae* family includes influenzavirus A, influenzavirus B and influenzavirus C. All influenza viruses have a multipartite, negative-sense, single-stranded RNA and a lipid envelope. They can all infect humans, but their rate of antigenic variation differs from one genus to another. Influenza C has the smallest rate of mutation causing only mild infections and allowing lasting immunity. In contrast, influenza B possesses a rate of evolution high enough to force the sanitary authorities its consideration when producing seasonal vaccines.[24] But the real threat, the main source of the seasonal and pandemic flu, remains influenza A (Figure 4).[5b,25]

---

[21] WHO. Human infections with avian influenza A (H7N9) virus http://www.who.int/influenza/human_animal_interface/influenza_h7n9/riskassessment_h7n9_27june 14.pdf?ua=1 (accessed Oct. 7th, 2014).

[22] a) Lamb, R. A. *Am. J. Respir. Crit. Care Med.* **2013**, *188*, 1. b) Horby, P. *Nature* **2013**, *496*, 399.

[23] WHO. *Bull. World Health Organ.* **1980**, *58*, 585.

[24] Krystal, M.; Fitch, W. M.; Palese, P. *Virology* **1988**, *163*, 112.

[25] Cheung, T. K. W.; Poon, L. L. M. *Ann. N. Y. Acad. Sci.* **2007**, *1102*, 1.

Figure 4. Influenza A virus [26]

The lipid envelope, which is derived from the host's cell membrane, is where three surface proteins sit. The biggest is *hemagglutinin* (HA), a homotrimer glycoprotein made of approx. 540 amino acids, involved in receptor binding and membrane fusion. It has two distinct regions, a stem responsible for membrane fusion and a globular head containing the receptor binding site (Figure 5). HA binds to the host cell membrane through sialic (*N*-acetylneuraminic) acids, nine-carbon monosaccharides commonly found in many glycoconjugates. The carbon-2 of sialic acid can bind to carbon-3 or carbon-6 of galactose producing α-2,3- or α-2,6-linkages, yielding two different

---

[26] Kaiser, J. *Science* **2006**, *312*, 380.

steric configurations. HA in a virus from avian source binds preferentially to α-2,3-linkages which are only present in the lower respiratory tract of humans, thus helping explain the low infectivity but high pathogenicity (once the virus reaches the lungs of the infected person) of avian influenza. In host cells HA is first synthesized as its precursor protein HA0 which is subsequently cleaved into the two polypeptides HA1 and HA2 by host proteases.[11,25] There are seventeen subtypes of influenza A hemagglutinin known to date.[3h]
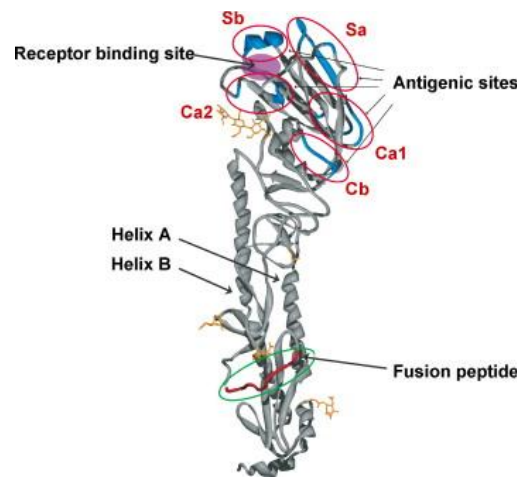
Figure 5. Hemagglutinin structure [11]

Another surface protein is *neuraminidase* (NA), also known as sialidase, a homotetramer of around 470 amino acids, with four domains: an *N*-terminal cytoplasmic domain followed by a transmembrane domain and a thin stem ending in a globular head (Figure 6). NA is a receptor-destroyer that cleaves the bond between sialic acid and HA from newly formed virions and prevents virus aggregation.[25, 28] Ten subtypes of influenza A neuraminidase have been found until now. HA and NA are the main proteins recognized by antibodies.[3h]
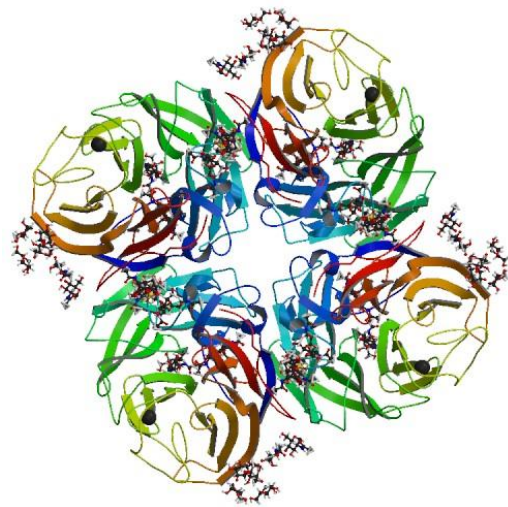
Figure 6. Neuraminidase structure [27]

[27] Varghese, J. N.; Colman, P. M. *J. Mol. Biol.* **1991**, *221*, 473.

[28] Air, G. M. *Influ. Other Respir. Viruses* **2012**, *6*, 245.

The last external protein of the virus is the smallest, the *M2 channel*. This homotetramer is formed by 97 amino acids with an external *N*-terminal domain, a transmembrane region and a cytoplasmic *C*-terminal tail. The transmembrane region forms a helical bundle that acts as a selective proton channel acidifying the interior of the virus when the conditions are suitable (Figure 7). The M2 protein is a proton channel integral to the release of the viral genetic material and is also essential in preventing HA premature inactivation during the process of new virus formation.[30]
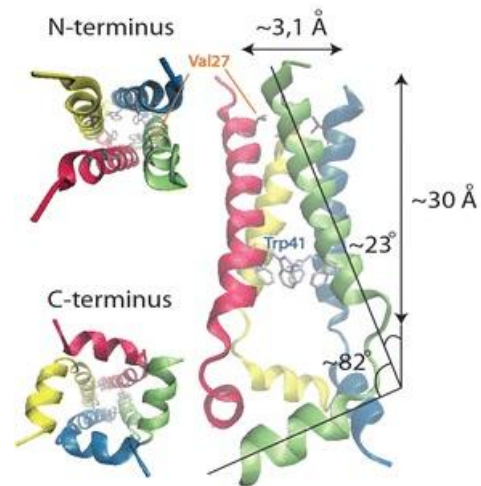
Figure 7. M2 channel structure [29]

Inside the virus lay the 8 segments of single stranded RNA (ssRNA) encoding for the 10 different proteins. But they are not free, the *nucleoprotein* (NP) encapsidates them forming what is known as the viral ribonucleoprotein (vRNP). The NP has a crescent shape with two distinct regions, a head and a body and in between sits the binding site of the ssRNA (Figure 8). Different NPs are attached to each other in a head-tail manner forming small oligomers, the actual structure of the vRNPs. The NP has been found to be involved in nuclear transport.[25,3d]
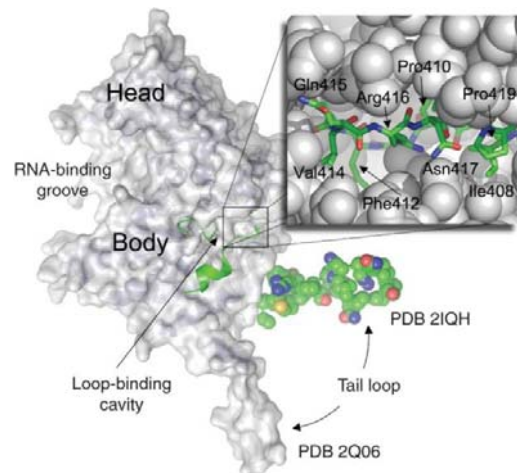
Figure 8. Nucleoprotein structure [3d]

[29] Sharma, M.; Yi, M.; Dong, H.; Qin, H.; Peterson, E.; Busath, D. D.; Zhou, H.-X.; Cross, T. A. *Science* **2010**, *330*, 509. (PDB: 2LOJ)

[30] Pinto, L. H.; Holsinger, L. J.; Lamb, R. A. *Cell* **1992**, *69*, 517.

Below the lipid envelope, the responsible of the membrane structure is the *matrix protein M1*. It binds both to the membrane and to the NP keeping the vRNP attached to the inner layer (Figure 9). Besides providing structural stability, the M1 protein seems to be involved in vRNP nuclear export and, in the later stages of infection, in vRNP transport.[1,3d]
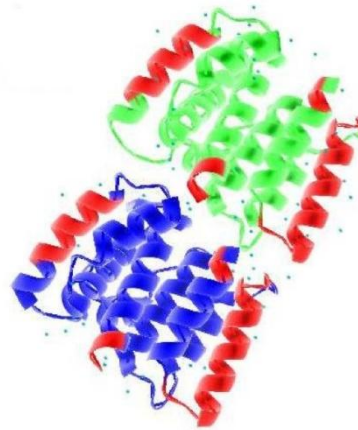
Figure 9. M1 matrix protein structure [31]

The *viral polymerase complex* (P complex) is an heterotrimer constituted by three subunits: PA, PB1 and PB2. The PB2 subunit is a cap-binding protein with endonuclease activity that is also able to generate cap primers for viral synthesis, using host mRNA. PB2 is associated with PB1 but little is known about the latter, only that it is key for RNA polymerization function. Finally, PA the smallest subunit, seems to be necessary for efficient nuclear accumulation of PB1. Besides, it has been found that it has helicase and ATP-binding activities (Figure 10).[25] The roles of P complex are: i) the transcription of negative-sense vRNA into ribosome-readable messenger RNA (mRNA, for translation into proteins) and ii) the replication via complementary RNA (cRNA) of vRNA. This viral polymerase is very prone to error which confers influenza A its high mutagenicity. A relatively recent discovered small protein, PB1-F2 encoded in the PB1 segment, has been found to induce apoptosis in the infected immune cells thus protecting the virus.[33]

Figure 10. PA, PB1 and PB2 structures [32]

[31] Goh, G. K.-M.; Dunker, A. K.; Uversky, V. N. *Virol. J.* **2008**, *5*, 126.

[32] Boivin, S.; Cusack, S.; Ruigrok, R. W. H.; Hart, D. J. *J. Biol. Chem.* **2010**, *285*, 28411.

[33] Chen, W.; Calvo, P. A.; Malide, D.; Gibbs, J.; Schubert, U.; Bacik, I.; Basta, S.; O'Neill, R.; Schickli, J.; Palese, P.; Henklein, P.; Bennink, J. R.; Yewdell, J. W. *Nat. Med.* **2001**, *7*, 1306.

The only nonstructural protein, i.e. encoded in the genome and produced in infected cells, but not part of the newly formed virion, is the *non-structural protein 1* (NS1). It is formed as an oligomer that interacts with the host cellular mechanisms to avoid interferences with viral replication (Figure 11).[25]
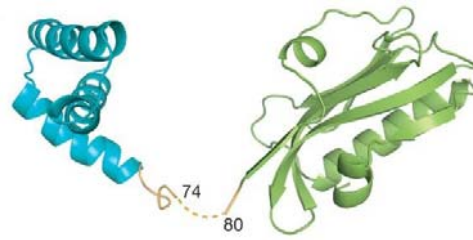
Figure 11. NS1 protein structure [34]

The NS2 protein was long thought to be a nonstructural protein but it was found that small quantities were present in the nascent virions, that is why it is also known as *nuclear export protein* (NEP). This 121 amino acids dimer is key, as its name suggest, in the export from the nucleus of the vRNPs (Figure 12). Through a complex system involving the M1 matrix protein, a small GTPase and a β-importin, the NEP mediates the nuclear export. [36] Nonetheless this is not its only function since recent studies have shown the NEP to have evolved and is now implicated also in the accumulation of

Figure 12. NEP protein structure [35]

different sorts of RNA within infected cells, a factor that could explain how avian influenza viruses overcome host-range restriction. Furthermore the NEP has been found to take part in the viral budding by recruiting an ATPase to the cell membrane.[37]

The cases of the new roles of the NEP as well as the recently discovered PB1-F2, illustrate how our understanding of the influenza A virus is still incomplete and needs constant research if we are to unveil its intricate mechanisms. Influenza A virus may seem simple, albeit it is not easy to find a suitable therapy that will not result in resistance, due to its error-prone RNA-polymerase as well as the immune pressure it is constantly subjected to. The striving in the subject can be inferred from the imposing number of molecules targeting different steps of the virus life cycle.[3]

---

[34] Bornholdt, Z. A.; Prasad, B. V. V. *Nature* **2008**, *456*, 985.

[35] Akarsu, H.; Burmeister, W. P.; Petosa, C.; Petit, I.; Müller, C. W.; Ruigrok, R. W. H.; Baudin, F. *EMBO J.* **2003**, *22*, 4646.

[36] O'Neill, R. E.; Talon, J.; Palese, P. *EMBO J.* **1998**, *17*, 288.

[37] Paterson, D.; Fodor, E. *PLoS Pathog.* **2012**, *8*, e1003019.

3. The virus: life cycle and current treatments

The primary defence against influenza virus is vaccination with inactivated or live attenuated viruses. Each year, a combination of the allegedly more common seasonal influenza strains based on a prediction of the genetic drift, is produced as a vaccine to protect the most vulnerable risk groups. As an example, the WHO vaccine recommendation for the 2014/2015 season is a trivalent formulation of: A/California/7/2009 (H1N1), A/Texas/50/2012 (H3N2) and B/Massachusetts/2/2012 (plus a B/Brisbane/60/2008 for quadrivalent formulations).[38]

Although very effective, vaccination has its own set of limitations; i) primarily the predicted strains must match the circulating ones in order to get an optimal benefit, ii) vaccines production takes more than 6 months rendering them unsuitable for a pandemic fast-spreading early phase, iii) since vaccination depends on the fitness of the subject, it may not be fully profitable for immunocompromised or certain age groups. Thus, there is a clear necessity of new antivirals and vaccines alike for the prophylaxis and treatment of influenza.[3c, 3d, 3g]

a. Viral attachment: hemagglutinin

Influenza A virus life cycle starts when a new host is infected, via one of the above mentioned modes, and the virus enters the respiratory tract. It binds to the sialic acid present in the host cell's membrane through the receptor binding site (RBS) of HA (Figure 13a).

This is the first antiviral target: to inhibit viral entry into the host cell. Three main strategies are employed: i) competitive binding to the RBS of HA, ii) block the sialic acid receptors, iii) destroy the sialic acid receptors. There is a wide variety of inhibitors of this first step and they comprehend: monoclonal antibodies (interacting with the RBS), lectins (causing virus particle aggregation), sialyl-containing macromolecules and sialomimetics (competitors of sialic acid for binding HA), sialic acid binding agents (competitors of HA) and fusion recombinant proteins that remove sialic acid.[3g,3h]

The main advantages of this strategy are the proven safety of some agents (e.g. lectins) and the good activities and selectivity of some therapies (e.g. monoclonal antibodies).[3g,3h]

---

[38] WHO. Recommended composition of influenza virus vaccines for use in the 2014-2015 northern hemisphere influenza season:
http://www.who.int/influenza/vaccines/virus/recommendations/2014_15_north/en/ (accessed Apr 15, 2014).

The main drawbacks are the high costs (for monoclonal antibodies) but mostly the large variation among HA subtypes that causes it to be a very challenging target.[3g, 3h]
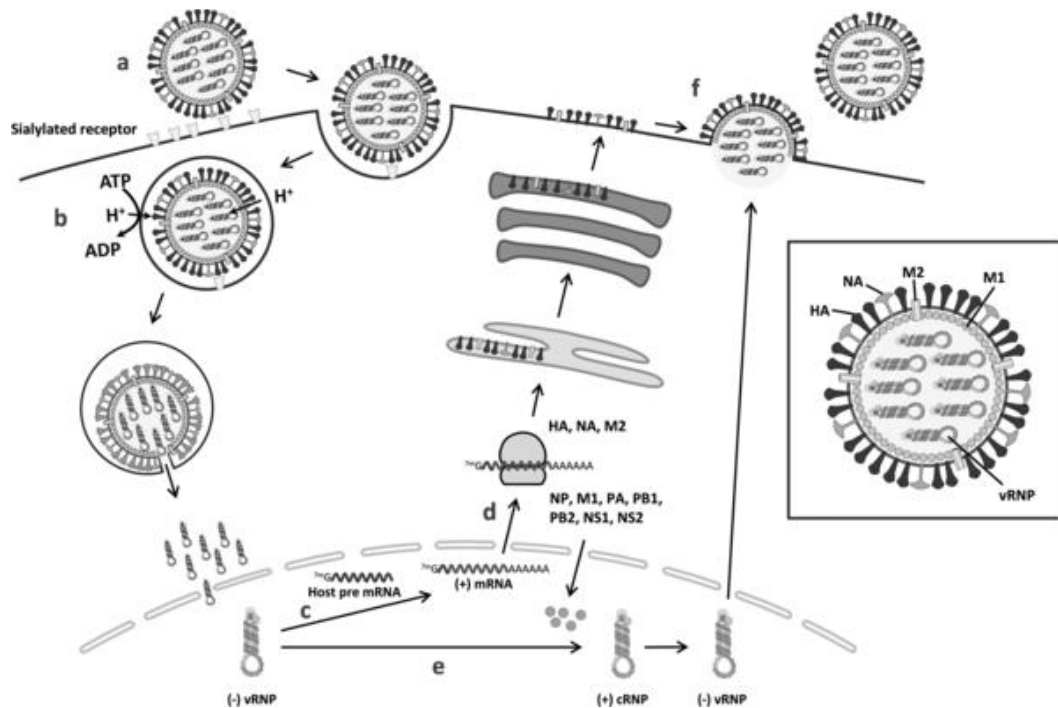
Figure 13. Influenza A virus life cycle [3h]

b. *Viral entry: endocytosis*

The virus is then internalized via a clathrin-mediated endocytosis and a macropinocytosis route in parallel.[39] The virus finds itself in an early endosome whose pH is lowered to pH ~6 by the cellular vacuolar proton ATPase (V-ATPase) (Figure 13b).

This is the next step liable to be targeted by antivirals: endocytosis. To impede the internalization, different approaches are considered: modulate membrane fluidity (glycyrrhizin), intercalate into viral membranes or disturb endocytic uptake (lipoglycopeptides).[3h]

The main advantage is again the safety of some molecules: glycyrrhizin has been used since many years in Japan with no apparent side-effects.[3h]

---

[39] de Vries, E.; Tscherne, D. M.; Wienholts, M. J.; Cobos-Jiménez, V.; Scholte, F.; García-Sastre, A.; Rottier, P. J. M.; de Haan, C. a M. *PLoS Pathog.* **2011**, *7*, e1001329.

The main drawbacks are the selectivity of some therapies but principally the ignorance of the interactions with the virus since the mechanism of viral endocytosis is not yet fully understood.[3h]

c. Membrane fusion: hemagglutinin

The early endosome continues to be transported and becomes a late endosome whose pH is again lowered by the V-ATPase. This event triggers a conformational change in the HA unmasking the fusion peptide that will merge the endosomal and viral membranes (Figure 13b).

Membrane fusion is also targeted by certain anti-influenza drugs with distinct strategies: stabilize the pre-fusion conformation of HA (TBHQ, arbidol), hinder membrane mixing (dextran sulfate), interact with surface glycoproteins to prevent membrane rearrangements (retrocyclin 2), alter membrane fluidity (arbidol), block the highly conserved fusion peptide (monoclonal antibodies, MBX2329 and MBX2546), inhibit the V-ATPase (e.g. bafilomycin A1) or elevate the endosomal pH (e.g. chloroquine and amantadine at high concentrations).[3h,41] Interestingly our group recently discovered some polycyclic amines (**1** and **2**) whose antiviral effect may be related to an elevation of the endosomal pH at much lower concentrations than amantadine (Figure 14).[40]

The main advantages are the safety of some molecules and the good results showed with some treatments, for instance, arbidol has extensively been used in Russia and China without any resistant-mutant yet isolated in the clinic. The main drawback is again the lack of a broad spectrum treatment due to the large variation among HA subtypes.[3c,3d,3e,3h,41]
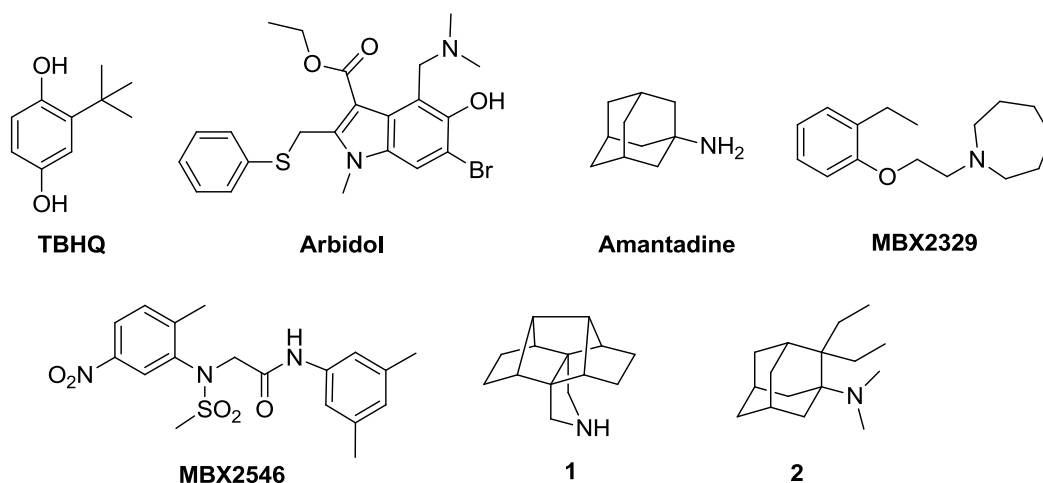
Figure 14. Some inhibitors of the membrane fusion process

[40] Torres, E.; Duque, M. D.; Vanderlinden, E.; Ma, C.; Pinto, L. H.; Camps, P.; Froeyen, M.; Vázquez, S.; Naesens, L. *Antiviral Res.* **2013**, *99*, 281.

[41] Basu, A.; Antanasijevic, A.; Wang, M.; Li, B.; Mills, D. M.; Ames, J. A.; Nash, P. J.; Williams, J. D.; Peet, N. P.; Moir, D. T.; Prichard, M. N.; Keith, K. A.; Barnard, D. L.; Caffrey, M.; Rong, L.; Bowlin, T. L. *J. Virol.* **2014**, *88*, 1447.

d. Virus uncoating: M2 channel

Simultaneously, the low endosomal pH also triggers the activation of the M2 channel, the proton channel that acidifies the interior of the virus leading to the release of the vRNPs from the M1 matrix; the uncoating event. The vRNPs are then released in the cytoplasm (Figure 13b).

Thus the M2 protein appears as an appealing target in the virus cycle and is the site of action of amantadine and rimantadine, both FDA (U.S. Food and Drug Administration) approved drugs for the treatment of influenza A (Figure 15). Rimantadine has an inherent superior activity compared with amantadine, but the latter displays improved pharmacokinetics.[42] Taking their structure as a base many research groups have worked on analogues trying to optimize and enhance their activity. Essentially their mechanism of action is the blocking of the channel to prevent proton trafficking.

The main advantages of amantadine and rimantadine were the bioavailability (>80%) due to their oral administration and the efficacy in both treatment and prophylaxis of influenza A. Furthermore, their stability at room temperature (at least for 25 years) renders them suitable for stockpiling.[43]

The main drawbacks of these treatments are, apart from being inactive against the influenza B M2 channel, that the protein mutates very easily producing resistant mutants and that amantadine displays a narrow toxic to therapeutic ratio (side effects in the central nervous system and in pregnant women). For these reasons amantadine and rimantadine use has been discouraged by the sanitary authorities.[44]

Since the M2 channel is the target of the compounds described in this thesis, a more detailed discussion will be carried further on.

Symmetrel® (amantadine)   **Flumadine® (rimantadine)**

Figure 15. M2 channel blockers Symmetrel® and Flumadine®

---

[42] a) Oxford, J.S.; Galbraith, A. *Pharmacol. Ther.* **1980**, *11*, 181. b) Belshe, R. B.; Burk, B.; Newman, F.; Cerruti, R. L.; Sim, I. S.; *J. Infect. Dis.* **1989**, *159*, 430

[43] WHO. Guidelines on the use of vaccines and antivirals during influenza pandemics. http://whqlibdoc.who.int/hq/2004/WHO_CDS_CSR_RMD_2004.8_eng.pdf?ua=1 (accessed on 15th October 2014).

[44] a) Hubsher, G.; Haider, M.; Okun, M. S. *Neurology* **2012**, *78*, 1096. b) WHO. Laboratory methodologies for testing the antiviral susceptibility of influenza viruses: M2 ion channel inhibitor. http://www.who.int/influenza/gisrs_laboratory/antiviral_susceptibility/m2inhibitor/en/ (accessed on 15th October 2014).

e. Nuclear import: nucleoprotein

The acidification of the interior of the virus induces a conformational change in the M1 matrix protein leading to the release of the vRNPs. After their exit through the fusion pores, the nuclear localization signal of the NP allows the vRNPs to be recognized by the host cell importin and to be internalized into the nucleus (Figure 13).

The NP is highly conserved through virus subtypes which renders tempting to work on it. Only two strategies are currently used: induce aggregation of the NP (ingavirin) and interfere with the replicative processes involving the NP (nucleozin).[3h]

The main advantage is that, as already stated, the target is highly conserved through the virus subtypes.

The main drawback is the poor activity of these compounds shown to date.[3h]

f. Transcription: viral polymerase complex

Once in the nucleus, the P complex starts from the negative-sense vRNA the synthesis of two positive-sense RNA: the mRNA for viral protein translation and the cRNA for replicating the vRNA. The mRNAs are bound to NPs to form mRNPs ready to be exported and the new vRNAs are then encapsidated by NPs to form novel vRNPs (Figure 13c, 13e). The viral polymerase complex, unlike human DNA polymerase, has no proof-reading function, readily inducing the production of mutant proteins of the virus.[3]

Targeting viral polymerase seems challenging but a few approaches have given good results: first, the inhibition of inosine 5'-monophosphate dehydrogenase a precursor of guanosine-5'-triphosphate (GTP), crucial for mRNA synthesis (ribavirin, viramidine). Secondly, nucleoside analogues that competitively inhibit the P complex (favipiravir) (Figure 16).

The main advantages of these treatments are the lack of drug-resistance and their availability by intravenous route making them the preferred therapy in acute infections (ribavirin, viramidine).

The main drawbacks are the toxicity and the poor to modest clinical efficacy of some of these compounds even at high doses.[3]
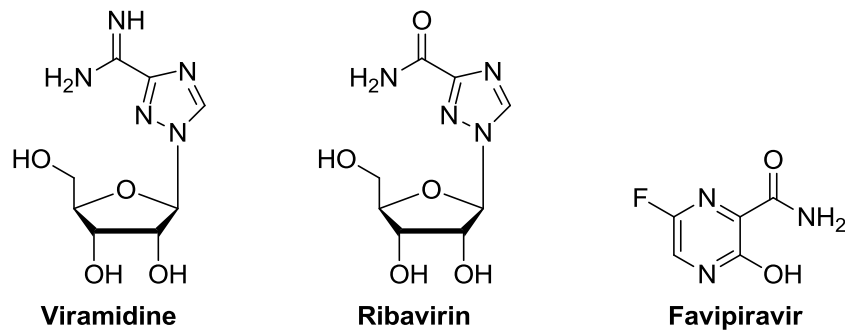
Figure 16. Viral polymerase inhibitors

g. Nuclear departure: nuclear export protein

In order to leave the nucleoplasm, the mRNPs co-opt the nuclear RNA export factor 1 (NXF1) pathway inherently used by the host cell to export its own mRNA (Figure 13d).[45]

The fact that the NFX1 export pathway is closely shared between host mRNA and viral mRNPs has prevented any attempt on considering it as an antiviral target.

In parallel, the newly formed vRNPs rely on the NS2/NEP protein. This one, through its nuclear export signal at its N-terminal, forms the termed nuclear export complex that will cross one of the many nuclear pore complexes formed by nucleoporins that guide the nucleocytoplasmic trafficking. The human nucleoporin 98 (hNup98) has been identified as an NS2-binding protein (Figure 13f).[46]

To consider this step of the viral replication as a target seems even more challenging than the transcription process, nevertheless a few strategies have been exploited: competitive inhibition of hNup98-NS2 interaction (GLFG-hNup98), inhibit the formation of the nuclear export complex (leptomycin B) and inhibition of the kinase signaling cascade that leads to nuclear export (U0126).[46]

The main advantages of this strategy are the good results obtained considering the recentness of nuclear export as an antiviral target.

The main drawbacks are the cytotoxicity of leptomycin B and the high concentrations needed of the other treatments.[46]

---

[45] York, A.; Fodor, E. *RNA Biol.* **2013**, *10*, 1274.

[46] a) Pleschka, S.; Wolff, T.; Ehrhardt, C.; Hobom, G.; Planz, O.; Rapp, U. R.; Ludwig, S. *Nat. Cell Biol.* **2001**, *3*, 301. b) Watanabe, K.; Takizawa, N.; Katoh, M.; Hoshida, K.; Kobayashi, N.; Nagata, K. *Virus Res.* **2001**, *77*, 31. c) Chen, J.; Huang, S.; Chen, Z. *J. Gen. Virol.* **2010**, *91*, 2474.

h. Translation: cellular ribosomes

The viral mRNPs hijack then the cellular mechanisms for translation; they free themselves from the NPs and are translated by the ribosomes into proteins. The HA, NA and M2 proteins are transported to the endoplasmic reticulum and the Golgi apparatus for maturation whereas the NP, M1, P complex, NS1 and NS2 enter the nucleus to form new vRNPs (Figure 13d).

As with the NFX1 pathway, it is not possible to aim at the viral protein translation without affecting the natural processes of the cell itself. Nonetheless small interfering RNAs have been developed with the aim of restricting mRNPs stability and hinder their translation.[3a]

i. Evasion of host response: NS1 protein

When the cell is under stress from, for instance, the lack of nutrients, a mechanical stress or the presence of a pathogen, it releases stress signals. They are interpreted by interferons that will activate the protein kinase R (PKR) responsible for inhibiting cellular translation. Inasmuch as the virus needs a high ribosomal activity for its protein production, the NS1 protein will interfere with PKR activation.[47] Besides binding to PKR, NS1 also interacts with CPSF30, responsible for processing of interferon-β pre-mRNAs. Furthermore NS1 has been shown to bind to phosphatidylinositol-3 kinase and double stranded RNA. Thus by interacting with all this molecules, NS1 prevents any immune response from the host cell.[3d]

It has not been until recently that NS1 has attracted any attention as a potential antiviral candidate and the few approaches undertaken until now have simply been the competitive inhibition of its multiple binding sites (e.g. NSC125044).

The main advantages of this strategy are that it is relying on the immune response of the body to take care of the virus and that the few molecules synthesized to date have yielded good results, rendering this novel target very promising.

The main drawback is also that it relies on the immune response of the body, since this treatment on immunocompromised, young children and elder people would have a poor effect.[3a, 3c, 3d, 3e, 3g]

j. Hemagglutinin maturation: M2 channel

As already mentioned, the HA, NA and M2 proteins are transported through the endoplasmic reticulum and the Golgi apparatus where they undergo

---

[47] Kash, J. C.; Goodman, A. G.; Korth, M. J.; Katze, M. G. *Virus Res.* **2006**, *119*, 111.

post-translational modification prior to reach the cell membrane. During its passage through the *trans*-Golgi network which has an intralumenal low pH, HA could suffer a premature irreversible conformational change to its fusion peptide extruded form. If this occurs the HA oligomers would aggregate hampering viral budding. To prevent this phenomenon, the M2 channel keeps the intralumenal pH of the transport vesicles above the threshold at which the HA conformational change happens (Figure 13d)[48].

Since this event is again controlled by the M2 channel, the same drugs (see 3d) targeting the protein for the uncoating process also affect the HA premature conformational change.

k. Packaging, budding and egress: neuraminidase

The external proteins (HA, NA and M2) aggregate in lipid raft domains of the plasma membrane. The vRNPs transported to the membrane are crosslinked by the M1 protein to HA. Then the concentration of HA and NA alter the membrane curvature (Figure 17A), enabling polymerization of M1 to further extend the budding virion (Figure 17B). Subsequently, the M2 protein is recruited at the neck of the budding virion, again altering the membrane curvature, which splits the virion from the plasma membrane (Figure 17C). Finally, since the virion can still be attached to the cell by the HA-sialic acid interaction, NA is entrusted with the cleavage of the sialic acid bond in order to release the newly formed virus (Figure 13f).[1,49]
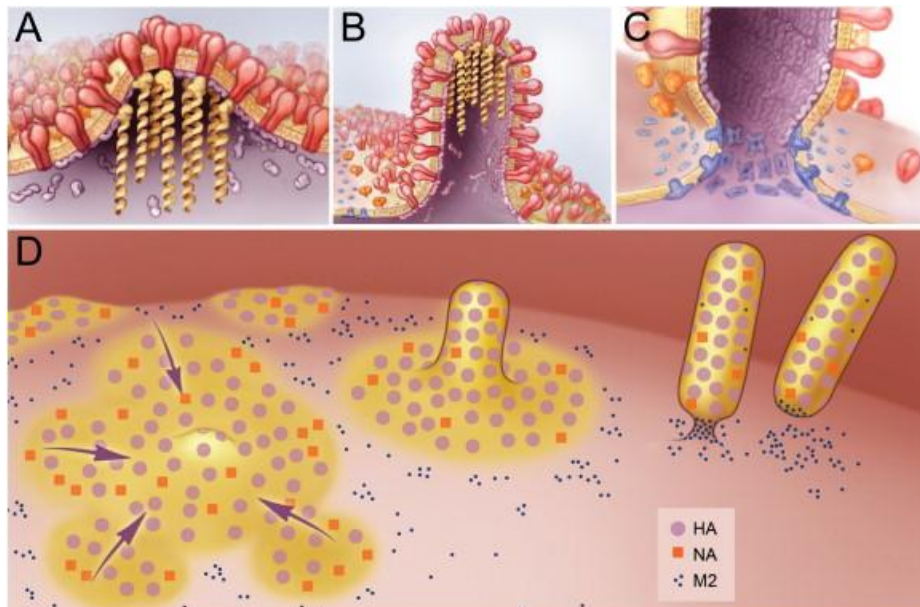
Figure 17. Viral budding[1]

---

[48] Takeuchi, K.; Lamb, R. A. *J. Virol.* **1994**, *68*, 911.

[49] Schmidt, N. W.; Mishra, A.; Wang, J.; DeGrado, W. F.; Wong, G. C. L. *J. Am. Chem. Soc.* **2013**, *135*, 13710.

The only new target in this process is the NA protein and it has proved to be the most successful one against influenza. The discovery of a conserved sialic acid binding site thanks to crystal structures of NA in 1983 was key to the development of the antiviral strategy: mimic the transition state of the interaction. The first neuraminidase inhibitor was zanamivir, approved by the FDA in 1999 and shortly after, also in 1999, oseltamivir was authorized improving zanamivir pharmacokinetics. It was not until recently, in 2010, that peramivir and laninamivir were given the green light to its human use in Japan and South Korea (Figure 18). Dimeric forms of zanamivir are also under study with very promising results. All these inhibitors are active against both influenza A and B and against a wide range of NA subtypes.[3,50]

Zanamivir main advantage is its prodigious activity ($IC_{50} < 1$ ng. mL^{-1}) although its administration route, inhaled, renders the treatment limiting for patients with severally affected lungs. To avoid this issue, an intravenous form of zanamivir is currently contemplated. Nonetheless zanamivir has an elevated cost of production.[3,50]

Oseltamivir retains the same formidable activity ($IC_{50} < 1$ ng. mL^{-1}) with the benefit of an oral route of administration, however resistant mutants (R292K, E119V and H274Y) have been detected of late. Furthermore, like zanamivir, oseltamivir has a high production cost.[3,50]

Peramivir has shown to be as active as zanamivir or oseltamivir with the convenience of a longer half-life of binding to the NA active site. Unfortunately it possesses a low oral bioavailability forcing its parenteral administration. Moreover there is evidence of cross-resistance with oseltamivir resistant mutant H274Y.[3,50]

Laninamivir combines the long-lasting effect of peramivir with the evasion of resistance from zanamivir. Its only handicap is, as zanamivir, its administration through inhalation that precludes its use in acute respiratory cases.[3,50]

---

[50] von Itzstein, M. *Nat. Rev. Drug Discov.* **2007**, *6*, 967.
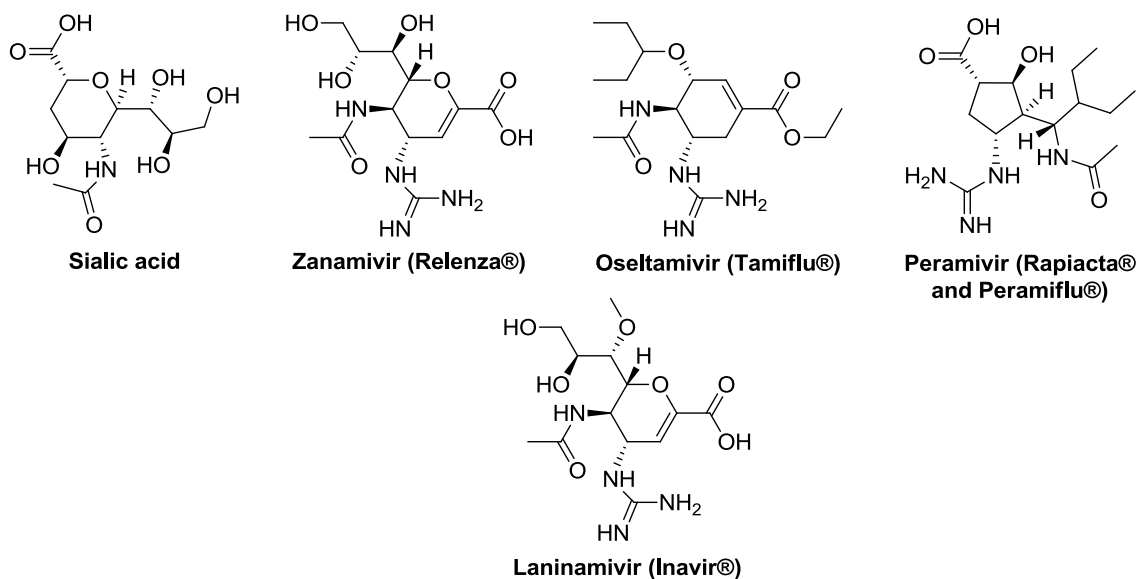
Figure 18. Sialic acid and neuraminidase inhibitors

It should be noted that some attention has recently been given to the entitled triple combination antiviral drug (TCAD). The strategy is also employed in HIV fighting; it consists of giving a cocktail of drugs acting at different stages of viral replication. For instance one of the TCAD described for influenza is composed of amantadine (M2 channel blocker), oseltamivir (neuraminidase inhibitor) and ribavirin (viral transcription inhibitor). The therapy has yielded very good results: i) better survival rates in mice than monotherapy, ii) recovered activity of amantadine and oseltamivir against resistant strains, iii) sustained protection against infection, and iv) no appearance of resistance due to its synergistic effect.[51, 3a]

For the sake of brevity, the antiviral targets, the therapies and their mode of action were not deeply reviewed. Nevertheless, three statements can be inferred from the data here presented:

- Only 4 neuraminidase inhibitors and 2 M2 channel blockers have ever been approved as therapeutics by any western country.
- As aforementioned, none of the available treatments is perfect, they all entail some disadvantages.
- Hence, there is a need for a constant quest of new approaches to fight influenza virus.

---

[51] a) Nguyen, J. T.; Smee, D. F.; Barnard, D. L.; Julander, J. G.; Gross, M.; de Jong, M. D.; Went, G. T. *PLoS One* **2012**, *7*, e31006. b) Seo, S.; Englund, J. A.; Nguyen, J. T.; Pukrittayakamee, S.; Lindegardh, N.; Tarning, J.; Tambyah, P. A.; Renaud, C.; Went, G. T.; de Jong, M. D.; Boeckh, M. J. *Antivir. Ther.* **2013**, *18*, 377.

4. The target: M2 channel

a. M2 channel structure and function

The influenza A M2 channel (A/M2) is a homotetramer; each monomer is composed of 97 amino acids forming 2 α-helices and they are further arranged as a left-handed parallel bundle with a tilt angle of 30⁰-35⁰ at the *N*-terminal part (Figure 19).[52] Each thread of the tetramer can be divided by its function as follows:

- Residues 1-24: *N*-terminal region pointing to the viral exterior and essential for incorporation into the virion.
- Residues 25-46: transmembrane domain (M2TM) entirely responsible for tetramerization, conduction of protons and binding site of drugs targeting the M2 channel.
- Residues 47-61: cytoplasmic amphipathic region implicated in membrane localization, budding and scission of newly formed virions. When studied together with the M2TM they are defined as M2TM + cyto.
- Residues 62-97: *C*-terminal tail accountable for the interaction with the M1 matrix protein inside the virus.[53]

The most often encountered domains in the literature are the M2TM and the M2TM + cyto, although the latter has been shown to have little to no effect on the proton flux, pH activation, drug-binding and backbone structure of the M2TM.[53] Thus the M2TM suffices to reproduce all the important features of the channel[54] and has been thoroughly studied by circular dichroism, raman spectroscopy,[55] electrophysiology, site directed mutagenesis and molecular dynamics simulations.[52b] Antiviral research took a giant leap with the publication in 2008 of solution NMR and crystallographic structures of the M2 channel.[56,57] This high resolution structures posed a cornerstone for future investigations and henceforward more accurate techniques such as X-ray crystallography, solution NMR and solid-state NMR (ssNMR) have been employed to determine precisely the structure of the M2 channel.[52b,58]

---

[52] a) Wang, J.; Kim, S.; Kovacs, F.; Cross, T. A. *Protein Sci.* **2001**, *10*, 2241.b) Hong, M.; DeGrado, W. F. *Protein Sci.* **2012**, *21*, 1620.

[53] Wang, J.; Qiu, J. X.; Soto, C.; DeGrado, W. F. *Curr. Opin. Struct. Biol.* **2011**, *21*, 68.

[54] Miao, Y.; Qin, H.; Fu, R.; Sharma, M.; Can, T. V; Hung, I.; Luca, S.; Gor'kov, P. L.; Brey, W. W.; Cross, T. A. *Angew. Chem. Int. Ed. Engl.* **2012**, *51*, 8383.

[55] Okada, A.; Miura, T.; Takeuchi, H. *Biochemistry* **2001**, *40*, 6053.

[56] Stouffer, A. L.; Acharya, R.; Salom, D.; Levine, A. S.; Di Costanzo, L.; Soto, C. S.; Tereshko, V.; Nanda, V.; Stayrook, S.; DeGrado, W. F. *Nature* **2008**, *451*, 596.

[57] Schnell, J. R.; Chou, J. J. *Nature* **2008**, *451*, 591.

[58] Williams, J. K.; Zhang, Y.; Schmidt-Rohr, K.; Hong, M. *Biophys. J.* **2013**, *104*, 1698.

Figure 19. a) crystal structure of the M2TM (PDB: 3LBW).[52b] The "front" helix has been removed for clarity. **b)** solution NMR structure of the M2TM + cyto (PDB: 2RLF) **c)** ssNMR structure of the M2TM + cyto (PDB: 2LOJ). Backbone is colored in grey and residues 49-60 in yellow. His37 are in cyan, Trp41 in green and water clusters in pink.[53]

The 22 residues forming the M2TM region are: Pro-Leu-Val_{27}-Val-Ala-Ala-Ser_{31}-Ile-Ile-Gly_{34}-Ile-Leu-His_{37}-Leu-Ile-Leu-Trp_{41}-Ile-Leu-Asp_{44}-Arg-Leu.[55]

As already stated, the A/M2 is a proton channel essential for viral replication. When the external pH attains a value close to 6, the A/M2 allows an inward flow of protons, whence the acidification that triggers the release of the vRNPs from the M1 matrix. Several models explain the proton conduction mechanism[29,30,55,57,58,59,60], albeit only one stands out with more supporting evidences; it is named the "shuttle" model and it suggests the following.

The channel has a truncated cone shape and is filled with water molecules forming clusters. Three water layers among five side chain layers fill the pore and ensure a continuous pathway for proton conduction. From the exterior to the interior of the virus, Val27 form a narrow valve to control proton entrance, then an entry cluster of 6 waters H-bonds His37 with the carbonyl backbone of Gly34. Below the His-box a bridging dimer connects the His-box with the Trp-basket, mediating a π-cation interaction between the charged His37 and the electron-rich indole of Trp41.[61] Finally, the exit cluster connects via H-bonds the Trp41 and the Asp44 (Figure20).[62]

---

[59] a) Hu, J.; Fu, R.; Nishimura, K.; Zhang, L.; Zhou, H.-X.; Busath, D. D.; Vijayvergiya, V.; Cross, T. A. *Proc. Natl. Acad. Sci. U. S. A.* **2006**, *103*, 6865. b) Phongphanphanee, S.; Rungrotmongkol, T.; Yoshida, N.; Hannongbua, S.; Hirata, F. *J. Am. Chem. Soc.* **2010**, *132*, 9782.

[60] Hu, F.; Schmidt-Rohr, K.; Hong, M. *J. Am. Chem. Soc.* **2012**, *134*, 3703.

[61] Bankura, A.; Klein, M. L.; Carnevale, V. *Chem. Phys.* **2013**, *422*, 156.

[62] Acharya, R.; Carnevale, V.; Fiorin, G.; Levine, B. G.; Polishchuk, A. L.; Balannik, V.; Samish, I.; Lamb, R. A.; Pinto, L. H.; DeGrado, W. F.; Klein, M. L. *Proc. Natl. Acad. Sci. U. S. A.* **2010**, *107*, 15075.

Figure 20. a) The backbone of three monomers is drawn in grey. From the *N*-terminal (exterior) to the *C*-terminal (interior): Val27 valve (orange), Ser31 (yellow), Ala30 (pink), His37 (green), Trp41 (cyan). Water molecules of the clusters are drawn in red.[63] **b)** Hydrogen bonding network in the M2 crystal structure (PDB: 3LBW). The carbonyl backbone of Gly/Ala34 is coloured in red, His37 in cyan, Trp41 in green and Asp44 in light blue. Grey lines indicate the water-protein H-bonds.[53]

The M2 channels of influenza A and influenza B (BM2) do not bear any similarity (explaining amantadine's inactivity against influenza B) except for the His-Xxx-Xxx-Xxx-Trp conserved motif in the M2TM, proving that it is integral for ion channel activity.[64]

The crystal structures show a pore lined by small lipophilic residues (Val27, Ala30/Ser31 and Gly34) that expose the only ionizable groups: His37's imidazoles. The fact that the pore is abundant in H-bond acceptors but lack H-bond donors coupled with the positioning of the histidines to accept but not to donate hydrogen bonds explains a key feature of the channel: the high pK_a of the first two histidines. Indeed, the pK_a's are 7.6 ± 0.1 for the first imidazole, 6.8 ± 0.1 for the second, 4.9 ± 0.3 for the third and 4.2 ± 0.6 for the last histidine (the pK_a of the imidazole side chain of L-histidine in water is around 6).[60,61] This deficit of H-bond donors when His37 is neutral, contributes to the driving force for binding H-bond donors like hydronium ions or drugs' ammonium group.[52b]

At near-physiological pH (7.5-8), the radius of the Val27 valve is approximately 3 Å,[65] the His-Box is found to be at the "neutral state" with just the first histidine of the tetrad protonated in Nδ1 or Nϵ2 (+1 state). His37's imidazoles form tightly packed electron-rich CH-π stacks avoiding water H-bonding. The Trp-basket blocks, by means of hydrophobic repulsion, the *C*-terminal end of the pore (Open$_{out}$-Closed$_{in}$) (Figure 21B).[62]

---

[63] Carnevale, V.; Fiorin, G.; Levine, B. G.; DeGrado, W. F.; Klein, M. L. *J. Phys. Chem. C* **2010**, *114*, 20856.

[64] Pinto, L. H.; Lamb, R. A. *J. Biol. Chem.* **2006**, *281*, 8997.

[65] Hu, F.; Luo, W.; Hong, M. *Science* **2010**, *330*, 505.

As the pH is lowered, the pore gets increasingly more hydrated and more dynamic. At pH 6.5 the charged imidazoles repel each other [65] inducing a slight bend and a rigid tilt of one of the helix that narrow the radius of the Val27 valve. The second histidine gets protonated (+2 state) but the charge is stabilized by the water clusters and the negative charge on Asp44. This is the "intermediate state". At the C-terminal end of the M2TM, the Trp41 flip to a conformation that projects its indolic NH towards the interior of the virus (Figure 21C).[62]

When the pH is close to 5 the third histidine becomes protonated (+3 state): the "conducting state" is reached. The further bend and tilt of the helix causes the Val27 valve to almost completely close. The charge cannot be further stabilized and the imidazolium groups move away from each other allowing microsecond ring reorientations for proton transfer to the waters in the C-terminal end of the pore (Figure 22A).[65] All this causes the Trp-basket to open by several Å (Closed$_{out}$-Open$_{in}$)(Figure 21D).[62]
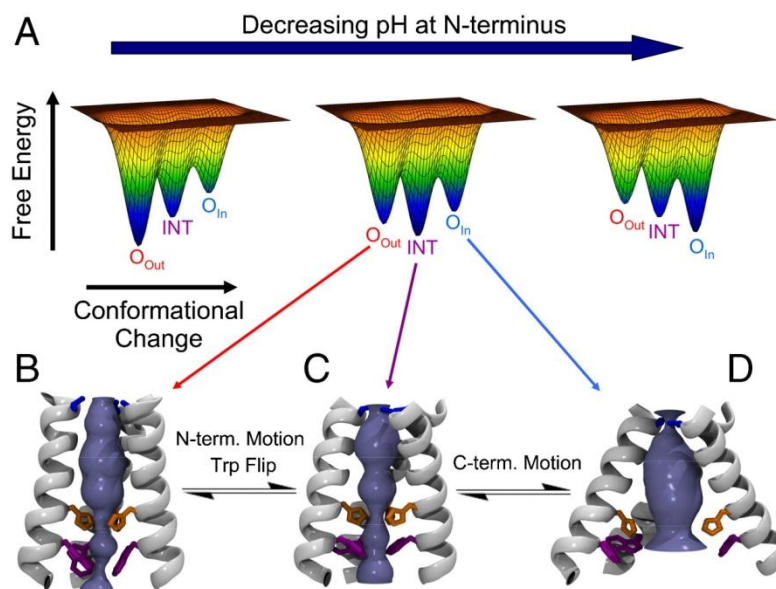
Figure 21. a) Cartoon illustrating the change in the energy landscape as function of the pH at the N-terminus of the channel. **b)** Neutral state. **c)** Intermediate state **d)** Conducting state.[62]

The protonation of the fourth histidine might also lead to proton conduction but when the positive charge inside the channel is lost due to proton transfer, the channel reverts to its intermediate state. [52b] The imidazoles then point their unprotonated nitrogen Nδ1 or Nϵ2 (Figure 22A) to the exterior of the virus to start a new cycle.[65] Disulphide bonds between cysteines at the *N*-terminal and at the *C*-terminal base of the protein ensure that conformational change of the channel does not provoke dissociation of the tetramer. [29,57]

The conformational change of the imidazoles represents the highest energy barrier of the conduction process. The His37's proton dissociation is considered the rate-limiting step and explains the M2 channel sigmoidal dependence on pH (saturation at low pH) (Figure 22B). [52b] Although only protons can be transported by this process, as the pH inside the virus decreases it becomes less selective allowing potassium cations to flow outward. This mechanism equilibrates the external and internal pH values and avoids a swift build up of a large electrical potential that would preclude additional proton flow before the final acidification is achieved. [53,66]
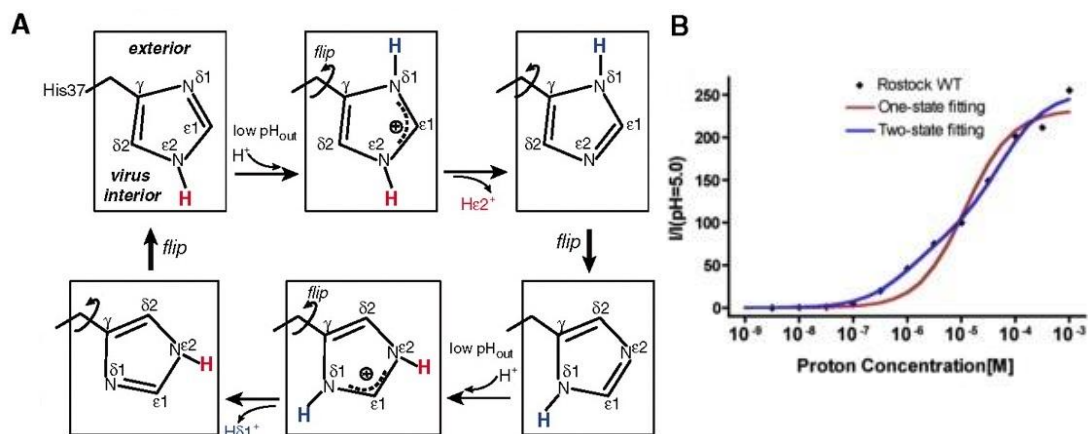
Figure 22. a) Imidazole ring reorientations in a cycle in which two protons are transported to the interior of the virus. [65] **b)** Sigmoidal pH dependence conduction of the M2 channel of an A/FPV/Rostock/34 strain. [67]

A variant proton relay model was proposed but was ruled out by ssNMR studies. [60] The M2 channel has many interesting features; one of them is that it is considered a "slow" channel since its absolute flux rate is small (100-1000 protons/s) but this is only due to the low concentration of protons at physiological pH (7.4) compared with other ions such as sodium or potassium. Another characteristic is its unexpected sigmoidal shape conduction profile: it evidences a levelling of the rate near the "conduction state" in agreement with the "shuttle" model; [62] the protonation/deprotonation of His37 occurs on the same time scale as proton turnover. [60] Lastly, the channel proton flux is greater when the external pH is lower than the internal pH ($pH_{out} < pH_{in}$) versus the reversed gradient ($pH_{out} > pH_{in}$). This property has been ascribed to the regulation exert by the electron-rich indole group of Trp41 in combination with Asp44 and Val27. [53]

[66] Leiding, T.; Wang, J.; Martinsson, J.; DeGrado, W. F.; Arsköld, S. P. *Proc. Natl. Acad. Sci. U. S. A.* **2010**, *107*, 15409.

[67] Ma, C.; Fiorin, G.; Carnevale, V.; Wang, J.; Lamb, R. A; Klein, M. L.; Wu, Y.; Pinto, L. H.; DeGrado, W. F. *Structure* **2013**, *21*, 2033.

b. Amantadine and rimantadine inhibition of the M2 channel

The anti-influenza activity of amantadine and rimantadine was found to be directed specifically against the M2 channel in 1985.[68] But we had to wait until 2008 for a more accurate description of their binding site. Oddly enough, at exactly the same time appeared two publications claiming two different binding modes for these drugs.[56,57]

The first model, proposed by Chou and co-workers, was deduced from the solution NMR of an M2TM + cyto construct in detergent micelles at pH 7.5. They found that rimantadine was bound at four sites on the outside of the four-helix bundle with the amine facing the inside of the pore at residues 40-45 of the M2TM (Figure 23B). They suggested therefore an allosteric inhibition with rimantadine stabilizing the closed conformation on the helix-lipid interface at the C-terminal end.[57,69] This was called the surface binding site (S-site).

The second hypothesis was put forward by DeGrado and co-workers based on a crystal structure of the M2TM region with amantadine at pH 5.3. From this study they concluded that a single molecule of amantadine was bound inside the pore between Val27 and Gly34 physically blocking the channel near its *N*-terminal (Figure 23A). This model was consistent with the resistant mutants (*vide infra*) and studies that demonstrated the slow kinetics of drug entrance due to the small space at the Val27 valve.[56] This was named the pore binding site (P-site).

A controversy was set between the two models to prove the right binding mechanism. Later this discrepancy was explained by the divergences in membrane solubilising conditions, the different employed pH, the type and concentration of the inhibitor and the length of the peptide used in the assays.[70] Fortunately, several studies using chimeric M2 channels (BM2-A/M2),[71] surface plasmon resonance,[70] ssNMR[72] and magic angle spinning NMR [73] supported the P-site over the S-site. In fact, they determined that the P-site was of high-affinity and the S-site of low-affinity for both adamantanes. Additional studies demonstrated that the P-site was thermodynamically favoured over the S-site which in turn was the kinetic binding site.[74]

---

[68] Hay, A. J.; Wolstenholme, A. J.; Shekel, J. J.; Smith, M. H. *EMBO J.* **1985**, *4*, 3021.

[69] Pielak, R. M.; Schnell, J. R.; Chou, J. J. *Proc. Natl. Acad. Sci. U. S. A.* **2009**, *106*, 7379.

[70] Rosenberg, M. R.; Casarotto, M. G. *Proc. Natl. Acad. Sci. U. S. A.* **2010**, *107*, 13866.

[71] a) Ohigashi, Y.; Ma, C.; Jing, X.; Balannik, V.; Pinto, L. H.; Lamb, R. A. *Proc. Natl. Acad. Sci. U. S. A.* **2009**, *106*, 18775. b) Pielak, R. M.; Oxenoid, K.; Chou, J. J. *Structure* **2011**, *19*, 1655.

[72] a) Cady, S. D.; Schmidt-Rohr, K.; Wang, J.; Soto, C. S.; Degrado, W. F.; Hong, M. *Nature* **2010**, *463*, 689. b) Cady, S. D.; Wang, J.; Wu, Y.; DeGrado, W. F.; Hong, M. *J. Am. Chem. Soc.* **2011**, *133*, 4274.

[73] Andreas, L. B.; Barnes, A. B.; Corzilius, B.; Chou, J. J.; Miller, E. A.; Caporini, M.; Rosay, M.; Griffin, R. G. *Biochemistry* **2013**, *52*, 2774.

[74] Gu, R.-X.; Liu, L. A.; Wei, D.-Q.; Du, J.-G.; Liu, L.; Liu, H. *J. Am. Chem. Soc.* **2011**, *133*, 10817.

The S-site was found to inhibit the activity of the channel by an allosteric mechanism, mainly by interaction of the drug's ammonium group with Asp44. However at a therapeutic dose, only the P-site was found to be relevant.[70]
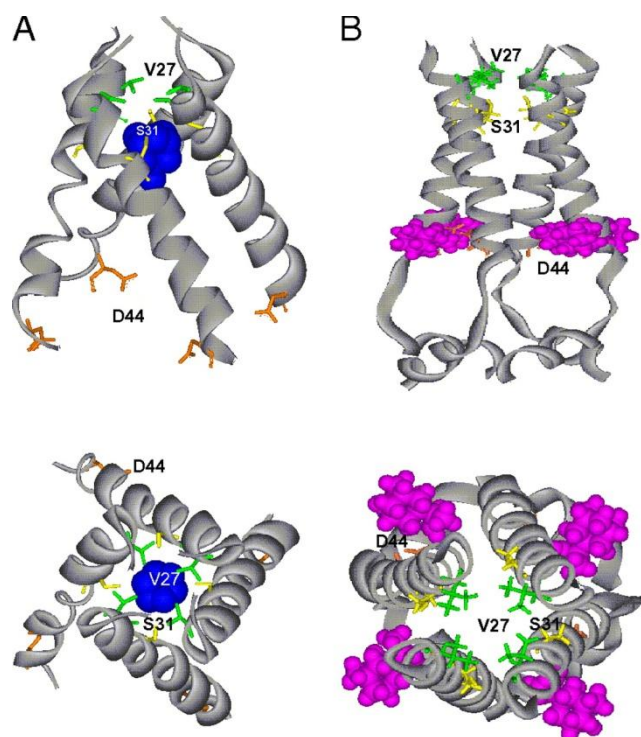
Figure 23. a) Side and top-down view of crystal structure of M2 (residues 22-46) bound to amantadine (blue). **b)** Side and top-down view of the solution NMR structure of M2 (residues 18-60) bound to rimantadine (magenta). Key active-site residues highlighted: Val27 (green), S31 (yellow) and Asp44 (orange).[70]

Adamantanes were found to inhibit the activity of the M2 channel by: i) physically occluding the pore inducing dehydration and thus preventing the protonation event, ii) locking the protein in a single state, hampering its plasticity, essential for conformational changes, and iii) perturbing the pK_a of the His37 tetrad by H-bonding through the entry water cluster (Figure 24).[72b] The orientation of the adamantanes' polar group inside the pore was also debated. Allegedly, it can fluctuate depending on the channel conformation.[75] The hydrophobic cage establishes Van der Wals interactions with the methyl groups of Val27 and Ala30 (Figure 25b).[71b] On the other side, the ammonium group can either point to the Val27 gate when it is more solvated (Open$_{out}$-Closed$_{in}$) or mimic the hydronium ions pointing towards the His37 when the Val27 gate is closed (Closed$_{out}$-Open$_{in}$).[75,76] The moiety is there hydrated near the entry cluster by four molecules of water and further stabilized by H-bonds to the carbonyl backbone of Ala30 (Figure25).[52b,76]

[75] Khurana, E.; Devane, R. H.; Dal Peraro, M.; Klein, M. L. *Biochim. Biophys. Acta* **2011**, *1808*, 530.

[76] Ghosh, A.; Wang, J.; Moroz, Y. S.; Korendovych, I. V; Zanni, M.; DeGrado, W. F.; Gai, F.; Hochstrasser, R. M. *J. Chem. Phys.* **2014**, *140*, 235105.
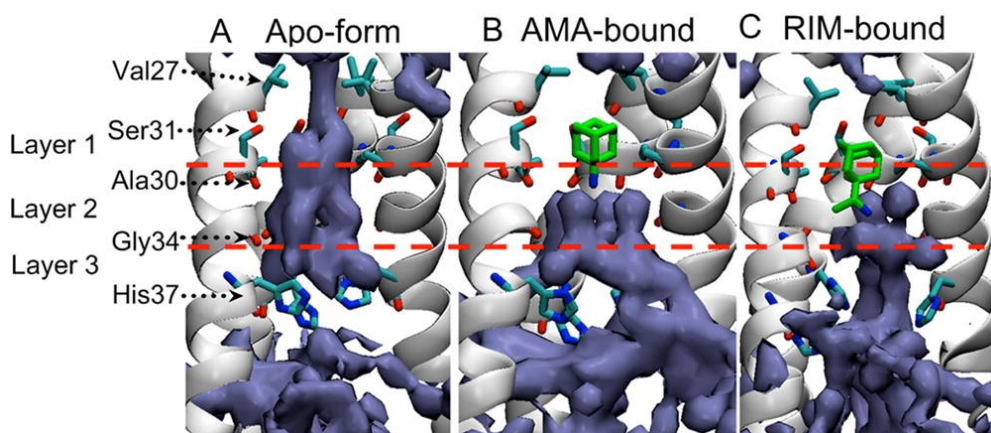
Figure 24. Water densities (blue) in the channel pore of the wild-type M2 channel of **a)** the apo-form (without ligand) **b)** the amantadine-bound form and **c)** the rimantadine bound form. Three water layers (red dashed lines), amantadine and rimantadine (green) and key active-site residues (cyan) are represented. Only three helices are shown for clarity.[77]

Rimantadine, with a bigger tilt angle than amantadine, has been demonstrated to directly interact through H-bonds with the backbone carbonyl of Ala30.[73] The intrinsic higher activity of rimantadine compared with amantadine has been explained by a better space filling and hence more dehydration of the pore, stemming from its bigger size and hydrophobicity.[72b]
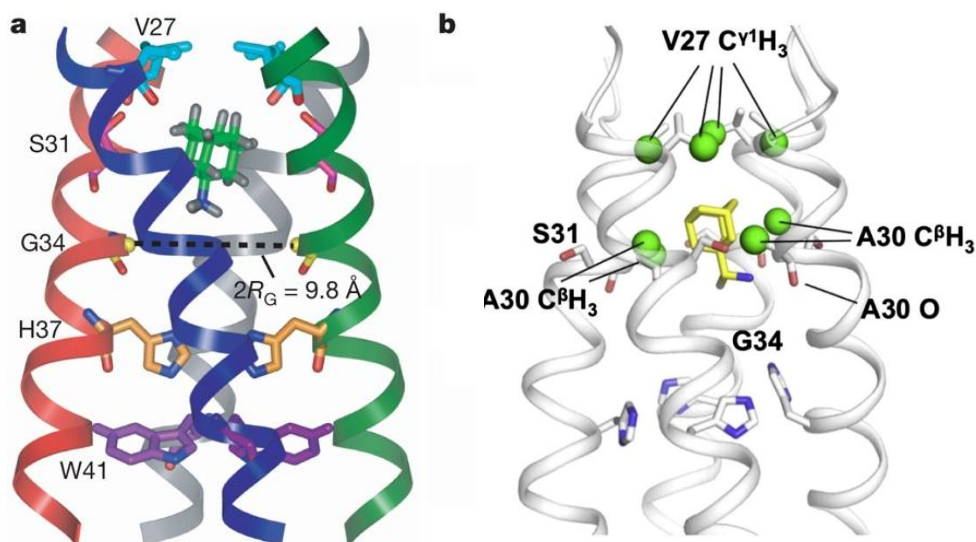
Figure 25. a) Side view showing amantadine (green) in the high affinity pore binding site. Key residues highlighted: Val27 (blue), S31 (pink), Gly34 (yellow), His37 (orange) and Trp41(magenta).[72a] **b)** Precise NMR structure of rimantadine bound to a chimeric A/M2-BM2 channel. Methyl groups interacting with the adamantane cage are highlighted in green.[78]

[77] Gu, R.-X.; Liu, L. A.; Wang, Y.-H.; Xu, Q.; Wei, D.-Q. *J. Phys. Chem. B* **2013**, *117*, 6042.

[78] Ouyang, B.; Chou, J. J. *Biochim. Biophys. Acta* **2014**, *1838*, 1058.

c. *Mutations in the M2 channel*

Even though amantadine and rimantadine were active drugs during a large period of time, the wild-type M2 channel (wt-M2) has developed escape mutants that efficiently avoid the blocking of its pore by these drugs. Many mutants can be obtained *in vitro*,[79] but 85% to 99% of reported resistance in transmissible virus is due to but three mutants. [52b,80]

The small number of viable mutations is attributable to the fact that mutants need to be finely tuned to ensure appropriate acidification while avoiding or minimising toxicity for the host cell. They should neither hinder sterically proton diffusion to the His-box at risk of slowing too much the conduction rate. Since mutations need to happen at four sites simultaneously, it becomes very hard to produce mutants well fitted to such conditions. The M2TM domain is then highly conserved [79] and the only mutants that retain the native proton flux and pH-activation curves that also match the HA maturation necessities, are the L26F, V27A and S31N mutations.[81]

The L26F mutant originates from the change of a leucine (isobutyl side chain) to a bigger and electron-richer phenylalanine (benzyl side chain). It is the less frequently encountered mutation although it has been isolated in H1N1-variant strains.[79] The residue is located at the *N*-terminal interhelical interface, hence the mutation produces a less efficient packing of the helix that destabilizes the tetramer and the water structure. According to molecular dynamics calculations, the result is a larger pore (approx. 0.5 Å) in the Val27 valve region compared with the wt-M2, consequently the drug has more freedom and cannot block properly the proton flux (Figure 26d).[77]

The V27A mutation consists of the change of a valine (isopropyl) to a smaller alanine (methyl). Its prevalence is superior to L26F and is also present in some H1N1-variant strains.[79] It used to predominate in the circulating strains but it lost its hegemony in favour of the S31N mutant.[81] The smaller side chain causes: i) the loss of activity of the Val27 valve as the first gate of the pore, now enlarged (from approx. 2 Å) compared with the wt-M2, ii) a weaker inter-helical packing and iii) faster proton conductance than wt-M2. Hence the inhibitor binds with no energetic barrier to the pore (compared with 5 kcal/mol in wt-M2) and is thus unable to stop proton conduction (Figure 26b).[77,82]

---

[79] Balannik, V.; Carnevale, V.; Fiorin, G.; Levine, B. G.; Lamb, R. A.; Klein, M. L.; Degrado, W. F.; Pinto, L. H. *Biochemistry* **2010**, *49*, 696.

[80] Suzuki, H.; Saito, R.; Masuda, H.; Oshitani, H.; Sato, M.; Sato, I. *J. Infect. Chemother.* **2003**, *9*, 195.

[81] Wang, J.; Ma, C.; Fiorin, G.; Carnevale, V.; Wang, T.; Hu, F.; Lamb, R. A.; Pinto, L. H.; Hong, M.; Klein, M. L.; DeGrado, W. F. *J. Am. Chem. Soc.* **2011**, *133*, 12834.

[82] a) Pielak, R. M.; Chou, J. J. *Biochem. Biophys. Res. Commun.* **2010**, *401*, 58. b) Gu, R.-X.; Liu, L. A.; Wei, D.-Q. *Trends Pharmacol. Sci.* **2013**, *34*, 571.

The S31N mutant arises from the change of a serine (hydroxymethyl) by an asparagine (methyl carboxamide). It is the more frequently encountered M2 channel mutation in the amantadine-resistant strains, principally in H3N2 and H1N1 strains.[79] The mutant displays an enlarged pore (by approx. 0.5 Å) near the Val27 valve and a narrower space in the Asn31 region (by approx. 1.5 Å) compared with the wt-M2. The resistance of this mutant is harder to explain but a hypothesis have been put forward that proposes a higher energy barrier (12 kcal/mol) [82b] for the entrance of the drug due to the larger asparagine and the shrunken pore, thus preventing any amantadine binding (Figure 26c).[77]
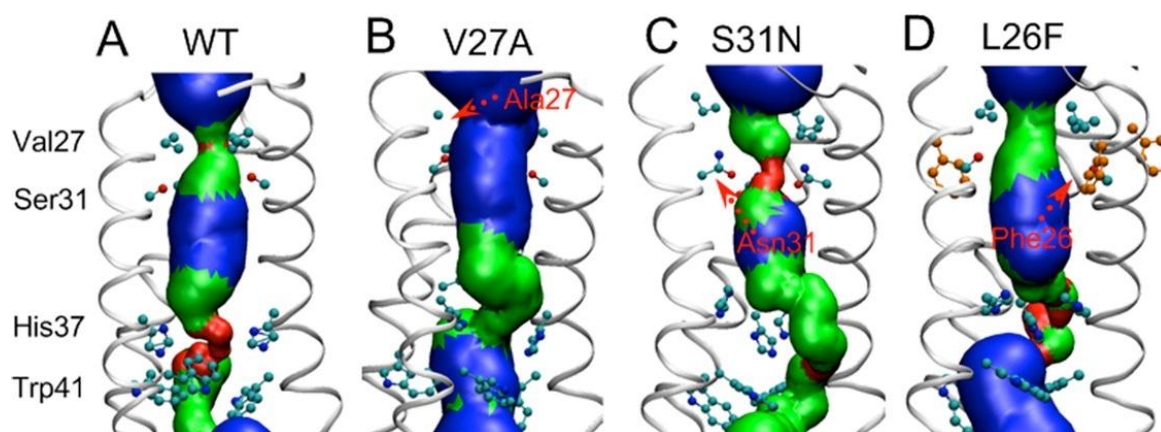
Figure 26. Pore radius profiles of **a)** wt-M2 **b)** V27A mutant **c)** S31N mutant and **d)** L26F mutant. The backbone protein is shown in white. The side chains key residues are represented in ball-and-stick models with carbons in cyan and orange, nitrogen in blue and oxygen in red. The channel pore is shown in different colours corresponding with the pore radii: red if the radius is < 1.4 Å, green if the radius is between 1.4 Å and 2.8 Å and blue if the radius is > 2.8 Å.[77]

Noteworthy, the drug pressure seems to be the source of only the V27A mutant,[81] the S31N emergence being attributed to the genetic drift and its predominance merely to evolutionary chance. [83] So, logically, this affects amantadine's activity: while in the S31N and the L26F mutant it exhibits a 10 to 20 order decrease in its IC_{50} compared with wt-M2, the V27A mutant is completely resistant to the drug (Figure 27).[81] Besides, some other less frequent resistant-mutants (A30T and G34E) have been identified reverting to wt-M2 in the absence of amantadine.[84]

Referred to the information about the A/M2 function, its inhibition by amantadine and the analysis of the mutant M2 channels described in this section, we should highlight that invaluable data were provided by classic

[83] Furuse, Y.; Suzuki, A.; Oshitani, H. *Antimicrob. Agents Chemother.* **2009**, *53*, 4457.

[84] Grambas, S.; Bennett, M. S.; Hay, A. J. *Virology* **1992**, *191*, 541.

molecular dynamics simulations and other computational calculations. [58,62,62,67,71b,72a,75,75,77,79,81,82,85] The furnished theoretical models proved to be of the uttermost importance for the study of this protein.

5. M2 channel inhibitors: state of the art

Amantadine's antiviral activity was first discovered in 1963 [86] and was subsequently confirmed by *in vivo* studies. [87] In 1965 α-methyl-1-adamatane methylamine hydrochloride (rimantadine) was reported to be more active than its parent compound (Figure 27). [88] These structures were considered as hits containing two distinct components: a primary pharmacophore, the amino group, assisted by the adamantane cage taken as the secondary pharmacophore.

amantadine
IC_{50} wt = 16 μM^a
IC_{50} S31N = 200 μM^a
IC_{50} V27A > 500 μM^a

rimantadine
IC_{50} wt = 10.8 μM^a
IC_{50} S31N > 500 μM^a
IC_{50} V27A > 500 μM^a
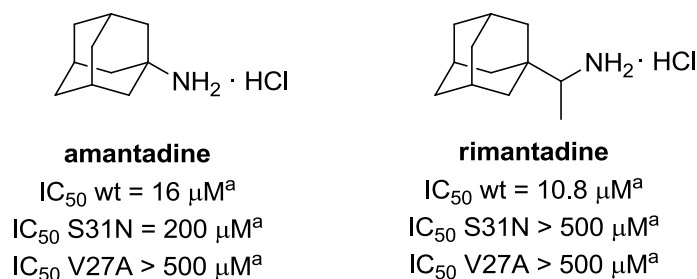
Figure 27. Amantadine and rimantadine M2 channel blocking activities. [a]Determined by two-electrode voltage clamp assay (TEVC) in *Xenopus laevis* frog oocytes.

a. Modifications of the amino pharmacophore

The first obvious strategy was to modify the amino part, hence the first variants synthesized were alkylaminoalkyl derivatives, albeit there were also derivatives featuring polar groups: alcohols, amines, guanidines and even some with no amino group (Figure 28). Unfortunately they were not more potent than amantadine and they even showed cross-resistance to both drugs. [89,90]

[85] a) Dong, H.; Yi, M.; Cross, T. A.; Zhou, H. *Chem. Sci.* **2013**, *4*, 2776. b) Wei, C.; Pohorille, A. *Biophys. J.* **2013**, *105*, 2036. c) Alhadeff, R.; Assa, D.; Astrahan, P.; Krugliak, M.; Arkin, I. T. *Biochim. Biophys. Acta* **2014**, *1838*, 1068.

[86] Jackson, G. G.; Muldoon, R. L.; Akers, L. W. *Antimicrob. Agents Chemother.* **1963**, *161*, 703.

[87] Davies, W. L.; Grunert, R. R.; Haff, R. F.; McGahen, J. W.; Neumayer, E. M.; Paulshock, M.; Watts, J. C.; Wood, T. R.; Hermann, E. C.; Hoffmann, C. E. *Science* **1964**, *144*, 862.

[88] Tsunoda, A.; Maassab, H. F.; Cochran, K. W.; Eveland, W. C. *Antimicrob. Agents Chemother.* **1965**, *5*, 553.

[89] Duque, M. D.; Torres, E.; Valverde, E.; Barniol, M.; Guardiola, S.; Rey, M.; Vázquez, S. In *Recent Advances in Pharmaceutical Science*; 2011; Vol. I pp. 1655–1663.

Figure 28. Amantadine analogs featuring polar groups. [a]Determined by TEVC in *Xenopus laevis* frog oocytes.

A range of heterocyclic derivatives of rimantadine were evaluated and proved that the introduction of an *N*-substituent was detrimental to antiviral activity (Figure 29).[91] Interestingly, an *L*-histidine derivative of amantadine (**17**) was shown to inhibit the wt-M2, the S31N mutant and a double mutant S31N/L26I even though the data were not confirmed by antiviral assays.[92]
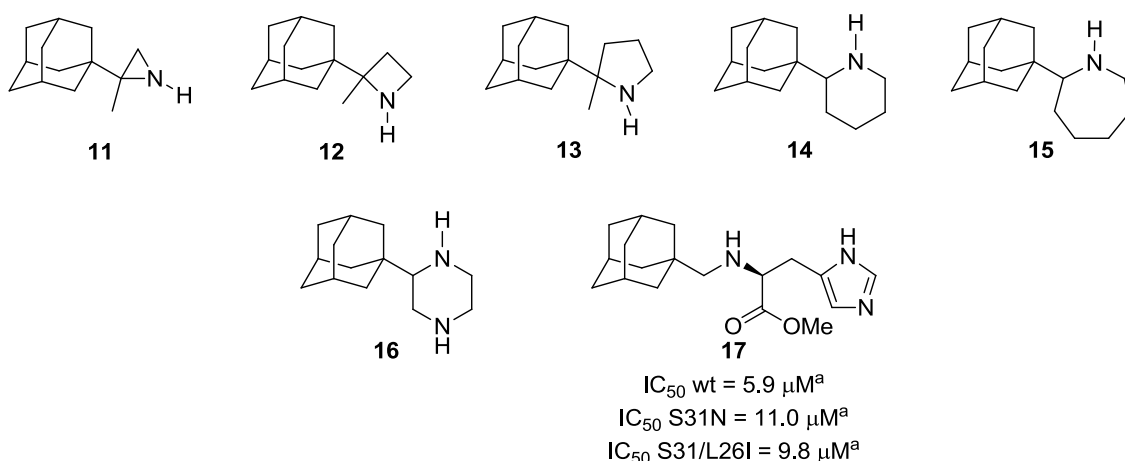
Figure 29. *N*-heterocyclic derivatives and *L*-histidine analogue of amantadine. [a]Determined by membrane currents of 293T-Rex cells that expressed the wt-M2, S31N and S31N/L26I.

[90] Wang, J.; Ma, C.; Balannik, V.; Pinto, L. H.; Lamb, R. A.; Degrado, W. F. *ACS Med. Chem. Lett.* **2011**, *2*, 307.

[91] a) Fytas, G.; Stamatiou, G.; Foscolos, G. B.; Kolocouris, A.; Kolocouris, N.; Witvrouw, M.; Pannecouque, C.; De Clercq, E. *Bioorg. Med. Chem.* **1997**, 7, 1887. b) Stamatiou, G.; Foscolos, G. B., Fytas, G.; Kolocouris, A.; Kolocouris, N.; Pannecouque, C.; Witvrouw, M.; Padalko, E.; Neyts, J.; De Clercq, E. *Bioorg. Med. Chem.* **2003**, 11, 5485. c) Zoidis, G.; Fytas, C.; Papanastasiou, I.; Foscolos, G. B.; Fytas, G.; Padalko, E.; De Clercq, E.; Naesens, L.; Neyts, J.; Kolocouris, N. *Bioorg. Med. Chem.* **2006**, *14*, 3341. d) Tataridis, D.; Fytas, G.; Kolocouris, A.; Fytas, C.; Kolocouris, N.; Foscolos, G. B.; Padalko, E., Neyts, J.; De Clercq, E. *Bioorg. Med. Chem.* **2007**, 17, 692.

[92] Zhang, W.; Xu, J.; Liu, F.; Li, C.; Jie, Y.; Chen, S.; Li, Z.; Liu, J.; Chen, L.; Zhou, G. *Chinese J. Chem.* **2010**, *28*, 1417.

The investigation of analogues of 2-amantadine led to the discovery of piperidines **18a-c** and pyrrolidine **19** (Figure 30) that although being slightly less active than amantadine or rimantadine, proved that amantadine is not fully optimized in the binding site, therefore the pore can accommodate larger compounds.[93]

The research at N. V. Philips-Duphar produced a series of azaspiroadamantanes of which **DU 34796**, (Figure 30) that had a wider antiviral spectrum *in vitro* than amantadine, entered clinical trials. Alas, it was not further developed after the discovery of cross-resistance with amantadine.[94] Following the same trend, Kolocouris' group synthesized azaspiroadamantane **23** that displayed an activity 230 times greater than amantadine but, regrettably, was toxic *in vivo*.[95]

18a R = Me
18b R = Et
18c R = -(CH$_2$)$_5$-

19   **20**   **21**   **22**   **23**   **DU34796**
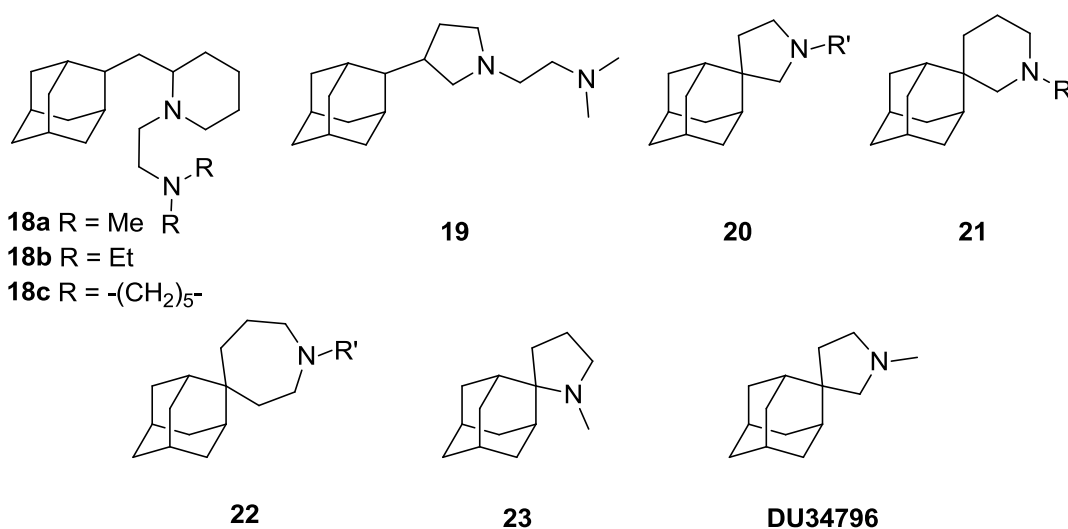
Figure 30. Piperidines, pyrrolidines and azaspiro-derivatives of amantadine.

---

[93] a) Kolocouris, A.; Tataridis, D.; Fytas, G.; Mavromoustakos, T.; Foscolos, G. B.; Kolocouris, N.; De Clercq, E. *Bioorg. Med. Chem. Lett.* **1999**, *9*, 3465. b) Stamatiou, G.; Kolocouris, A.; Kolocouris, N.; Fytas, G.; Foscolos, G. B.; Neyts, J.; De Clercq, E. *Bioorg. Med. Chem. Lett.* **2001**, *11*, 2137. c) Setaki, D.; Tataridis, D.; Stamatiou, G.; Kolocouris, A.; Foscolos, G. B.; Fytas, G.; Kolocouris, N.; Padalko, E.; Neyts, J.; De Clercq, E. *Bioorg. Chem.* **2006**, *34*, 248.
[94] a) Beare, A. S.; Hall, T. S.; Tyrrell, D. A. J. *Lancet* **1972**, *299*, 1039. b) Mathur, A.; Beare, A. S.; Reed, S. E. *Antimicrob. Agents Chemother.* **1973**, *4*, 421. c) Togo, Y. *Antimicrob. Agents Chemother.* **1973**, *4*, 641.
[95] a) Kolocouris, N.; Foscolos, G. B.; Kolocouris, A.; Marakos, P.; Pouli, N.; Fytas, G.; Ikeda, S.; De Clercq, E. *J. Med. Chem.* **1994**, *37*, 2896. b) Gkeka, P.; Eleftheratos, S.; Kolocouris, A.; Cournia, Z. *J. Chem. Theory Comput.* **2013**, *9*, 1272.

The M2 channel possesses two more putative binding sites capable of stabilizing an ammonium ion: i) one turn up from Ala30, where interactions with the carbonyl of Val27 and the hydroxyl of Ser31 would help stabilization and ii) one turn down from Ala30, where the interactions could be made with a cluster of four waters H-bonded to the carbonyl of Gly34 and the imidazole of His37.[52b] Investigation on aminospiroadamantanes was started by Kolocouris' group (**24-27**, Figure 31) with moderate results,[95] but it was DeGrado's work, targeting the lower binding pocket, that yielded compound **28**, equipotent to amantadine against wt, inactive against S31N but the most active compound until then against V27A (Figure 31).[81] Thus it seems that the distance and orientation between the amino group and the adamantane moiety is very relevant (Figure 35).[89]

24 a-c   **25 a-c**   **26 a-b**   **27 a-b**   **28**

a $R_1=R_2=H$ **b** $R_1=H$ $R_2=CH_3$ **a** R=H **b** R=CH$_3$
c $R_1=R_2=CH_3$

IC$_{50}$ wt = 18.7 μM[a]
IC$_{50}$ V27A = 0.3 μM[a]
IC$_{50}$ L26F = 5.6 μM[a]
S31N = not active[a]
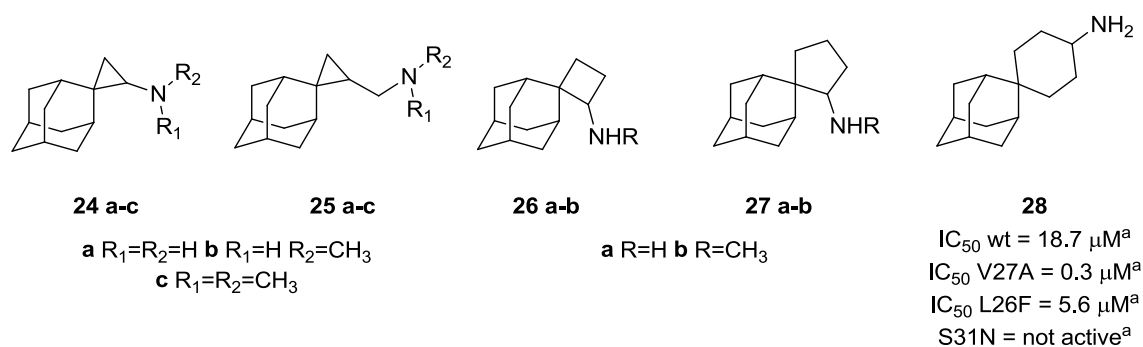
Figure 31. Aminospiroadamantanes. [a]Determined by TEVC in *Xenopus laevis* frog oocytes.

The biological evaluation of annulated derivatives (Figure 32) showed very potent activities of some derivatives against wt-M2 proving that a large lipophilic group close to the adamantane moiety does not hamper activity.[96]

29 a-c   **30 a-c**   **31 a-c**   **32**   **33 a-c**   **34 a-c**   **35 a-c**

a R=H **b** R=CH$_3$ **c** R=CH$_2$CH$_3$
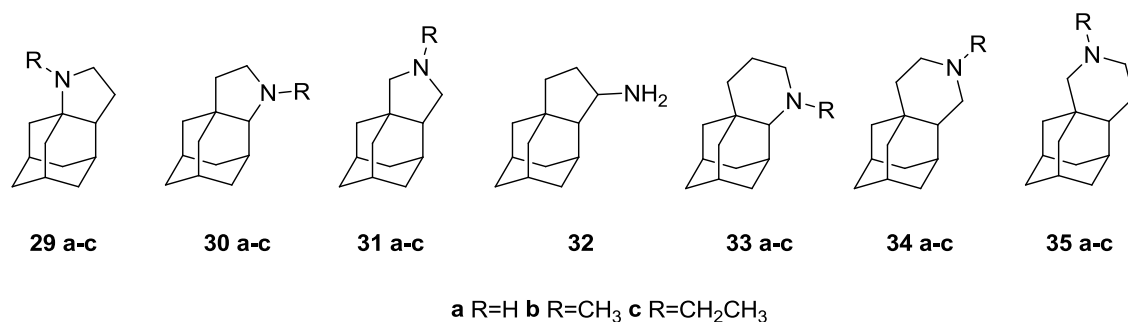
Figure 32. Annulated derivatives of amantadine.

---

[96] a) Zoidis, G.; Tsotinis, A.; Kolocouris, N.; Kelly, J. M.; Prathalingam, S. R.; Naesens, L.; De Clercq, E. *Org. Biomol. Chem.* **2008**, *6*, 3177. b) Zoidis, G.; Kolocouris, N.; Naesens, L.; De Clercq, E. *Bioorg. Med. Chem.* **2009**, *17*, 1534.

Very recently, DeGrado's group published the first dual agents against wt-M2 and S31N (Figure 33) along with the solution NMR structure of their most potent compound trapped inside the mutant channel (Figure 33b). Interestingly the structure shows an unexpected binding mode, with the adamantane group in a lower binding pocket (Ala30-Gly34) and with the amine pointing up for interactions with the Asn31. These results proved that the S31N mutant is a druggable target and that there are multiple ammonium interaction sites, opening the door to new antiviral designs.[97]
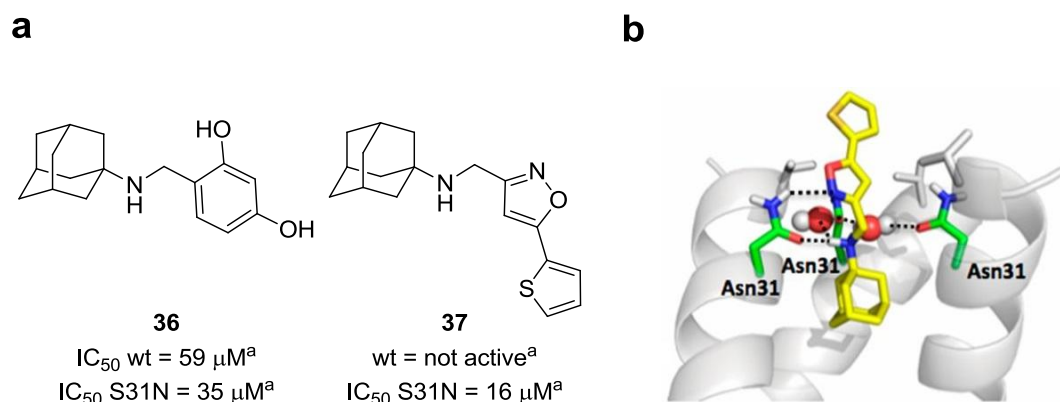
Figure 33. a) Inhibitors of the S31N mutant. [a]Determined by TEVC in *Xenopus laevis* frog oocytes. **b)** Model of **37** binding mode in the S31N channel.

b. *Modifications of the adamantane pharmacophore*

In 1995 Bristol-Myers Squibb undertook a high-throughput screening which yielded BL-1743 (Figure 34), a compound equipotent to amantadine against wt-M2, cross-resistant but showing faster kinetics than its parent compound.[98] With the recent published crystal structure of the M2 channel, Pinto's and DeGrado's groups extensively explored the BL-1743 scaffold which led to several structures (Figure 34) with increased potencies against wt-M2, L26F and V27A but inactive against S31N. Moreover, ssNMR experiments demonstrated that **41**'s ammonium was interacting with the putative lower binding site (Figure 35).[99]

---

[97] a) Wang, J.; Wu, Y.; Ma, C.; Fiorin, G.; Wang, J.; Pinto, L. H.; Lamb, R. A.; Klein, M. L.; Degrado, W. F. *Proc. Natl. Acad. Sci. U. S. A.* **2013**, *110*, 1315. b) Wang, J.; Ma, C.; Wang, J.; Jo, H.; Canturk, B.; Fiorin, G.; Pinto, L. H.; Lamb, R. A.; Klein, M. L.; DeGrado, W. F. *J. Med. Chem.* **2013**, *56*, 2804. c) Williams, J. K.; Tietze, D.; Wang, J.; Wu, Y.; DeGrado, W. F.; Hong, M. *J. Am. Chem. Soc.* **2013**, *135*, 9885.

[98] Kurtz, S.; Luo, G.; Hahnenberger, K. M.; Brooks, C.; Gecha, O.; Ingalls, K.; Numata, K.; Krystal, M. *Antimicrob. Agents Chemother.* **1995**, *39*, 2204.

[99] a) Wang, J.; Cady, S. D.; Balannik, V.; Pinto, L. H.; DeGrado, W. F.; Hong, M. *J. Am. Chem. Soc.* **2009**, *131*, 8066. b) Balannik, V.; Wang, J.; Ohigashi, Y.; Jing, X.; Magavern, E.; Lamb, R. A.; DeGrado, W. F.; Pinto, L. H. *Biochemistry* **2009**, *48*, 11872.

Figure 34. Spiro compounds related to BL-1743. [a]Determined by TEVC in *Xenopus laevis* frog oocytes.
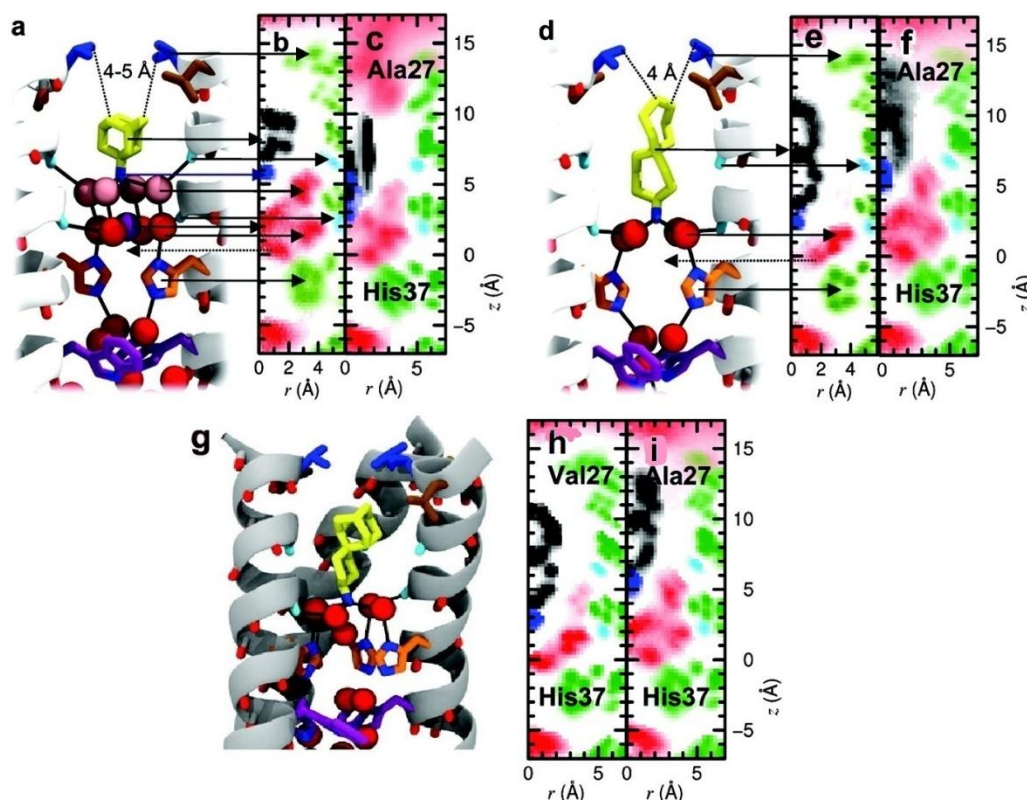
Figure 35. a) Amantadine, **d)** spiropiperidine **41** and **g)** aminospiroadamantane **28** within the wt-M2 pore with water molecules in red, pink and purple. Side chains of Leu26 (brown), Val27 (blue), His37 (orange) and Trp41 (purple) are represented. Backbone carbonyls of Ala30 and Gly34 involved in H-bonds with water are in light blue. **(b,e,h)** Density maps in cylindrical coordinates of the heavy atoms of wt-M2 (green), water (red) and polycycles (black). Oxygen atoms of Ala30 and Gly34 are in light blue. **(c,f,i)** Density maps of the V27A mutant in complex with the different polycyles.[81]

In the exploration of new carbon skeletons, DeGrado's group envisioned the use of silicon since the C-Si bond is longer than a C-C bond. This approach produced two compounds **44** and **45**, (Figure 36) active against wt-M2 and **45** endowed with fair activity against the V27A mutant.[100]

Again, completely reinventing the adamantane pharmacophore, Hu *et. al.* published a series of isopinocamphenylamines (Figure 36) that displayed good activities against wt-M2 albeit being inactive against resistant-mutants.[101]

As a proof that the M2 channel can accommodate bigger structures, homoadamantanes (Figure 36) have shown similar activities to amantadine against wt-M2 with some marginal activities against L26F, V27A and S31N.[90]

44
IC_{50} wt = 2.6 μM^a

45
IC_{50} wt = 13.7 μM^a
IC_{50} V27A = 31.3 μM^a

46
EC_{50} wt = 1.4 μM^b

47
EC_{50} wt = 0.1 μM^b

48

49
IC_{50} wt = 29.0 μM^a

50
IC_{50} wt = 24.0 μM^a

51
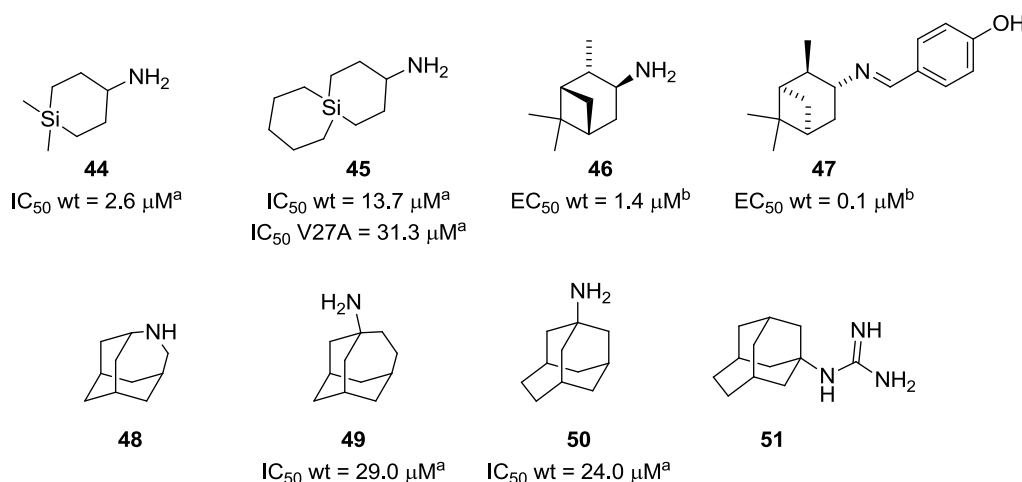
Figure 36. Silicon derivatives, isopinocamphenylamines and homoadamantanes. $^a IC_{50}$ determined by TEVC in *Xenopus laevis* frog oocytes. $^b EC_{50}$ determined by viral inhibition assay using A/Hong Kong/8/68 (H3N2).

From the myriad of structures that have been explored, not all of them here revised, the following conclusions may be drawn:

- Amantadine is not fully optimized in the channel leaving space for bulkier derivatives.
- The distance and orientation between the two pharmacophores seems to be relevant.
- The introduction of polar groups is not deleterious to activity but it does not improve it either.
- *N*-Alkylating the amino group does not improve potency and the bulkier the substituent the less active the compound.
- The work herein described has exposed that modifications of the polycyclic cage have a potential not yet fully explored .[89]

[100] Wang, J.; Ma, C.; Wu, Y.; Lamb, R. A.; Pinto, L. H.; DeGrado, W. F. *J. Am. Chem. Soc.* **2011**, *133*, 13844.
[101] Zhao, X.; Li, C.; Zeng, S.; Hu, W. *Eur. J. Med. Chem.* **2011**, *46*, 52.

6. Previous work of our group

As already mentioned, our group has an extended expertise in the synthesis of polycyclic scaffolds,[4] so taking advantage of this knowledge our research group started its own approach based on modifying the adamantane scaffold to yield polycyclic amines with possible antiviral activity. Below are shown some examples.

Among the polycyclic structures explored by the group, there have been ring-rearranged analogues of amantadine, oxo-adamantanes and benzo-homoadamantanes. Benzo-homoadamantanes [102] were inactive as M2 channel blockers, but the pentacyclic structures and the oxo-adamantanes had some interesting activities against wt-M2 (Figure 37).[103]

52·HCl
wt = not active[a]

53·HCl
wt = not active[a]

54·HCl
wt = not active[a]

55·HCl
IC_{50} wt = 33.5 μM[a]

56·HCl
wt = not active[a]

57·HCl
IC_{50} wt = 24.0 μM[a]

58·HCl
IC_{50} wt = 29.2 μM[a]

59·HCl
IC_{50} wt = 22.9 μM[a]

60·HCl
R = H, Alkyl
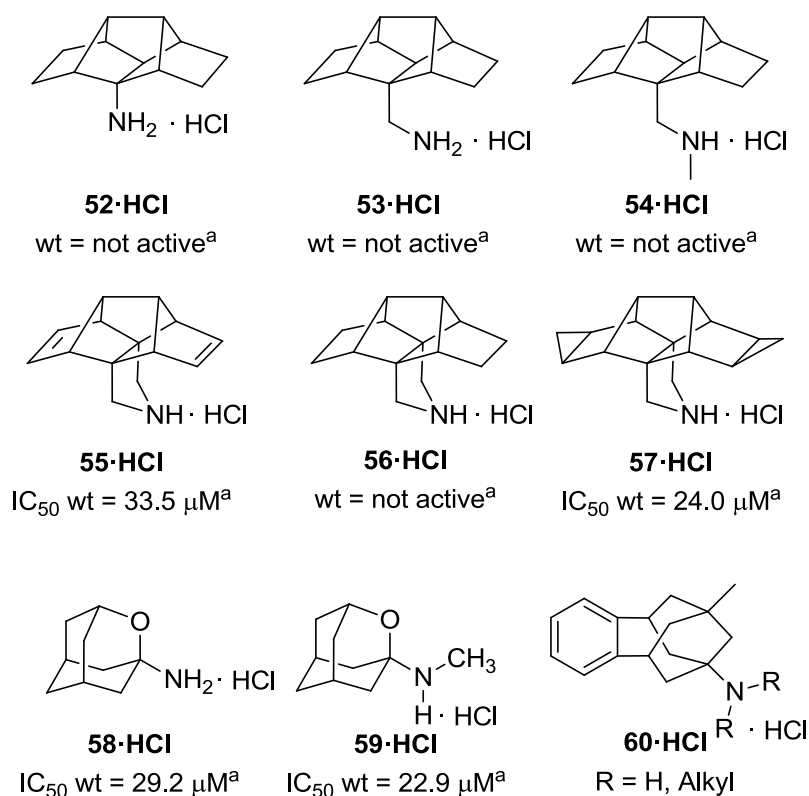
Figure 37. Ring-rearrangement analogues of adamantane, oxo-adamantanes and benzo-homoadamantanes synthesized by our research group. [a]Determined by TEVC in *Xenopus laevis* frog oocytes.

---

[102] Torres, E., Synthesis of polycyclic compounds with antiviral activity. Ph.D. Thesis, University of Barcelona, Barcelona, Spain, 2013.

[103] Duque, M. D.; Ma, C.; Torres, E.; Wang, J.; Naesens, L.; Juárez-Jiménez, J.; Camps, P.; Luque, F. J.; DeGrado, W. F.; Lamb, R. A.; Pinto, L. H.; Vázquez, S. *J. Med. Chem.* **2011**, *54*, 2646.

Rationally targeting the S31N mutant, the group synthesized a series of smaller analogues of amantadine by ring-contraction (noradamantane) and double ring-contraction (bisnoradamantane). Their pharmacological evaluation revealed that although active against the wt-M2 channel, they were devoid of activity against the S31N mutant. Surprisingly, the longest compound within this series, guanidine **70·HCl** unfolded as a dual agent with low micromolar activity against wt-M2 and the V27A mutant (Figure 38).[102,104,105]

61·HCl
EC_{50} wt = 26.5 μM^a

62·HCl
EC_{50} wt = 52.0 μM^a

63·HCl
wt = not active
% inh. V27A = 0%[b]

64·HCl
IC_{50} wt = 3.0 μM
% inh. V27A = 0%[b]

65·HCl
IC_{50} wt = 11.7 μM
% inh. V27A = 6%[b]

66·HCl
IC_{50} wt = 1.1 μM
% inh. V27A = 0%[b]

67·HCl
IC_{50} wt = 17.0 μM
% inh. V27A = 11%[b]

68·HCl
IC_{50} wt = 7.2 μM
% inh. V27A = 18%[b]

69·HCl
IC_{50} wt = 9.7 μM
% inh. V27A = 26%[b]

70·HCl
IC_{50} wt = 6.1 μM
% inh. V27A = 84%[b]
IC_{50} V27A = 11.4 μM
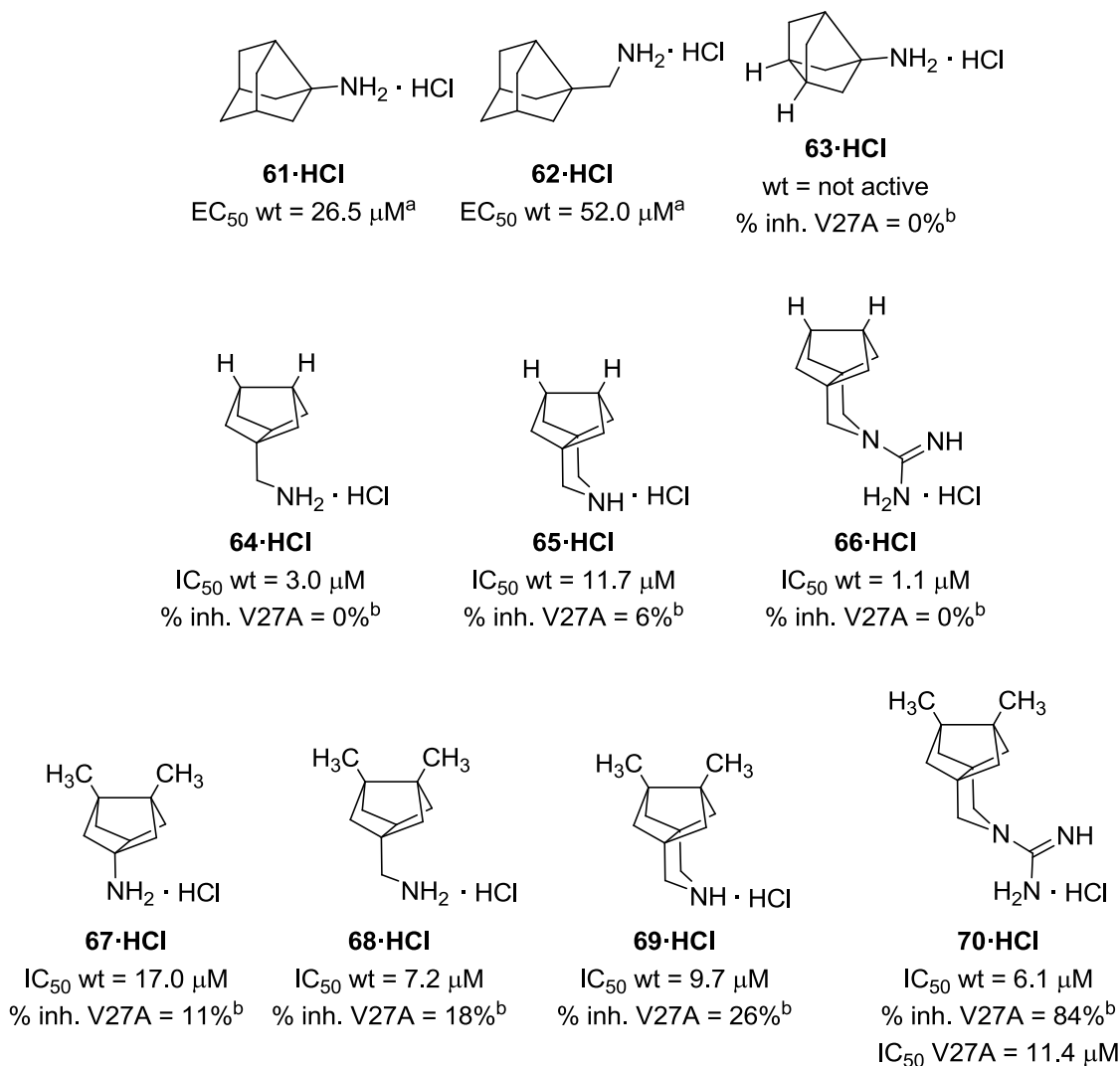
Figure 38. Noradamantanes and bisnoradamantanes synthesized by our research group. [a]EC_{50} determined by viral inhibition assay using A/Hong Kong/7/87 (H3N2). [b]Determined by TEVC in *Xenopus laevis* frog oocytes at 100 µM for 2 min.

[104] Rey-Carrizo, M.; Torres, E.; Ma, C.; Barniol-Xicota, M.; Wang, J.; Wu, Y.; Naesens, L.; DeGrado, W. F.; Lamb, R. A.; Pinto, L. H.; Vázquez, S. *J. Med. Chem.* **2013**, *56*, 9265.

[105] Camps, P.; Duque, M. D.; Vázquez, S.; Naesens, L.; De Clercq, E.; Sureda, F. X.; López-Querol, M.; Camins, A.; Pallàs, M.; Prathalingam, S. R.; Kelly, J. M.; Romero, V.; Ivorra, D.; Cortés, D. *Bioorg. Med. Chem.* **2008**, *16*, 9925.

From the scaffolds presented in both Figure 37 and 38 a structure activity relationship can be inferred:

- From the comparison of primary amines **52·HCl** and **53·HCl** with pyrrolidines **55·HCl** and **57·HCl** we moved from inactivity to compounds nearly as active as amantadine against wt-M2.
- More important, if we rely solely on the percentage of inhibition values, it seems that the activity against V27A is also favoured by a conformationally more rigid structure, e.g. pyrrolidine **65·HCl** vs. primary amines **63·HCl** and **64·HCl** or pyrrolidine **69·HCl** vs. primary amines **67·HCl** and **68·HCl**.
- The activity against V27A increases with the methyl derivatives compared with its parent non-methylated compounds (see **63·HCl** vs. **67·HCl** , **64·HCl** vs. **68·HCl**, **65·HCl** vs. **69·HCl** and **66·HCl** vs. **70·HCl**)
- The guanidines **66·HCl** and **70·HCl** are more active against wt-M2 than their parent amines **65·HCl** and **69·HCl**, respectively.
- The guanidine **70·HCl** is also more active against V27A than **66·HCl**.

So, it seemed that reducing the conformational freedom of the amine pharmacophore improved both the activity against wt-M2 and V27A and that the bulkier the molecule the better it filled the extra space in the enlarged binding pocket of V27A. The guanidine derivatives, longer than their amine counterparts, seemed to interact deeper in the channel therefore yielding more activity against wt-M2 and V27A.

Objectives

At the beginning of this thesis:

- the only druggable protein was the V27A since the S31N mutant was thought to be unattainable,
- the V27A mutant was an appealing target by reason of its absolute resistance to amantadine,
- this mutant M2 channel was studied in depth and globally well understood.

Taking into consideration these facts, we decided to focus the present work towards the rational synthesis of amantadine analogues active against the V27A mutant channel and ideally being dual agents active also against the wt-M2 channel. Having said that, we should bear in mind that the M2 channel as a target was shared between three Ph.D. students and that the objectives were reshaped through an iterative process according to the pharmacological results obtained by the whole team. Thus, these were the main goals of this dissertation:

1. The synthesis and pharmacological evaluation of a family of amines with general structures **I** and **II** that were designed as longer though tighter derivatives of amantadine to explore new polycyclic scaffolds.
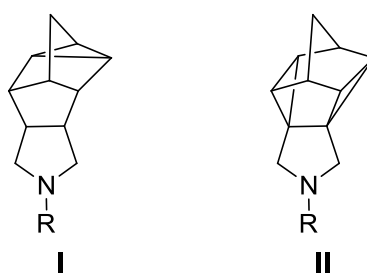
Figure 39

2. Following the exploration of new polycyclic structures, we considered the synthesis of 4-azatetracyclo[5.3.2.0^{2,6}.0^{8,10}]dodecane derivatives **III** to assess their activity as M2 channel blockers.
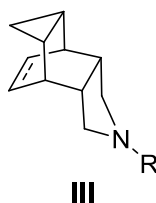
Figure 40

3. Based on the good activities obtained with the 4-azatetracyclo[$5.4.2.0^{2,6}.0^{8,11}$]tridecane scaffold (synthesized by the Ph.D. student M. Barniol), we envisioned longer derivatives that would penetrate deeper inside the cavity of the V27A mutant, that is the pyrrolidines with general structures **IV** and **V**.
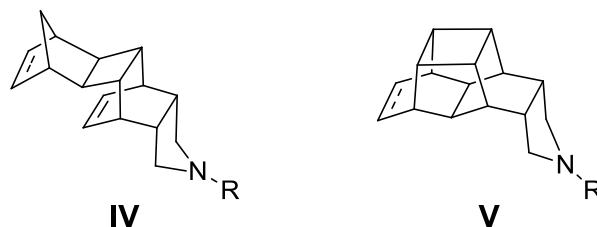
Figure 41

4. Centred on the structure activity relationship of the compounds previously synthesized by Dr. E. Torres during her Ph.D. (Figure 38), we designed a synthetic route to obtain bulkier structures founded on **VI** that would fill better the extra available space in the V27A mutant.
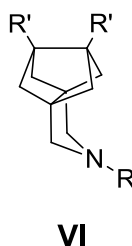
Figure 42

5. Bearing in mind that the synthesis of the molecules described in the previous point would be long and tedious, we also planned the synthesis and pharmacological evaluation of 7,8,9,10-tetramethyl-3-azapentacyclo[$7.2.1.1^{5,8}.0^{1,5}.0^{7,10}$]tridecane derivatives **VII** as synthetically more affordable compounds that would maintain the desired bulkiness to target the V27A mutant.

VII
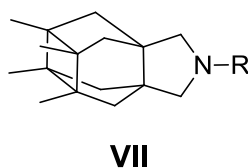
Figure 43

Results and discussion

1. Longer and more compact amantadine analogues

1.1 Synthesis: 11-azahexacyclo[7.3.0.0^{1,3}.0^{2,6}.0^{4,8}.0^{7,9}]dodecane and related compounds

The design of new polycyclic scaffolds and their evaluation as potential A/M2 channel blockers was the goal sought with this first family of amines. Our plan was to appraise a structure longer than amantadine to see if it could improve the activity by interacting deeper in the wild-type A/M2 channel. At the same time, we desired to assess a more compact structure to gain a better insight into the hydrophobic interactions in the upper part of the channel. Based on the structure described by Forman *et al.*[106] we pursued the synthesis of pyrrolidine analogues of their polycycle (Figure 44).
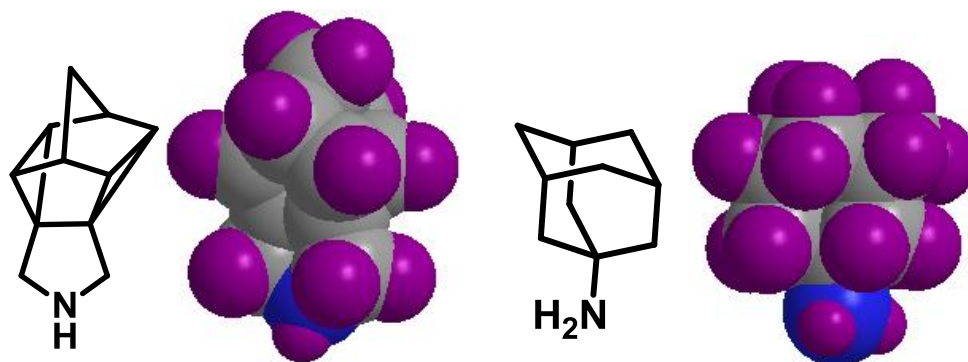
Figure 44. Qualitative space filling models of 11-azahexacyclo[7.3.0.0^{1,3}.0^{2,6}.0^{4,8}.0^{7,9}]dodecane and amantadine. Hydrogen atoms are shown in purple. Source: ChemBio3D Ultra. Energy minimized through MM2.

Therefore the 11-azahexacyclo[7.3.0.0^{1,3}.0^{2,6}.0^{4,8}.0^{7,9}]dodecane exhibited a longer distance between the amine and the furthest carbon of the polycycle (5.28 Å) than amantadine (4.30 Å) while being tighter, that is, the width of the molecule (2.24/2.47 Å, depending on the alignment along the y-axis) was smaller than amantadine's (2.95 Å) (Figure 45).

The distances shown in this figure and the subsequent are illustrative and, depending on the binding orientation of the molecule, might not reflect the distances considered to be significant, so they must be regarded carefully.

---

[106] Forman, M. A.; Moran, C.; Herres, J. P.; Stairs, J.; Chopko, E.; Pozzessere, A.; Kerrigan, M.; Kelly, C.; Lowchyj, L.; Salandria, K.; Gallo, A.; Loutzenhiser, E. *J. Org. Chem.* **2007**, *72*, 2996.
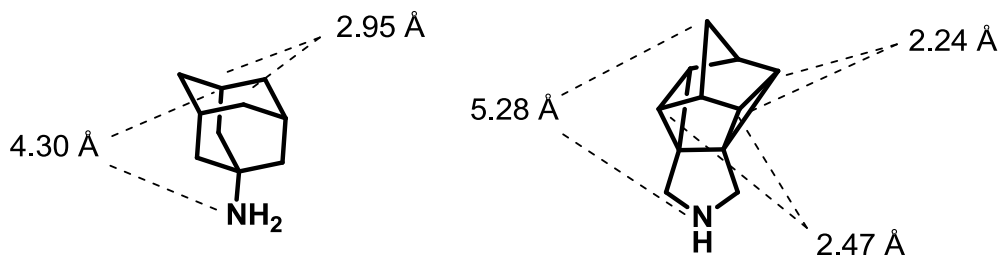
Figure 45. Most representative distances of amantadine and 11-azahexacyclo[7.3.0.0^{1,3}.0^{2,6}.0^{4,8}.0^{7,9}]dodecane. Source: ChemBio3D Ultra. Energy minimized through MM2.

The first part of the synthetic route was logically identical to the one described in the literature.[106] The basic scaffold was obtained through a homo-Diels-Alder reaction between the commercially available 2,5-norbornadiene and dimethylacetylene dicarboxylate in the presence of a catalytic amount of hydroquinone as an antioxidant (Scheme 1). The reaction produced the diester **71** in an 82% yield.
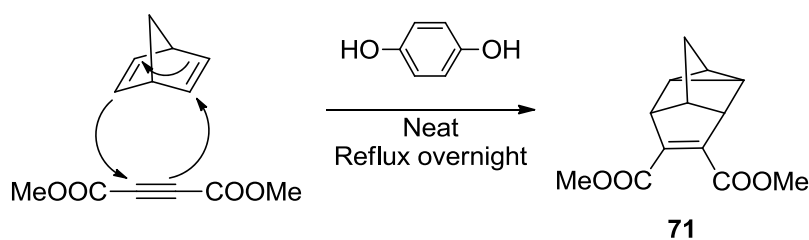
Scheme 1. Mechanism of the homo-Diels-Alder of 2,5-norbornadiene and dimethylacetylene dicarboxylate

The cycloaddition was followed by a basic hydrolysis of the diester **71** to the diacid **72** with an 86% yield. Then took place the central reaction to obtain the desired skeleton: a [2+2] photocycloaddition (Scheme 2).
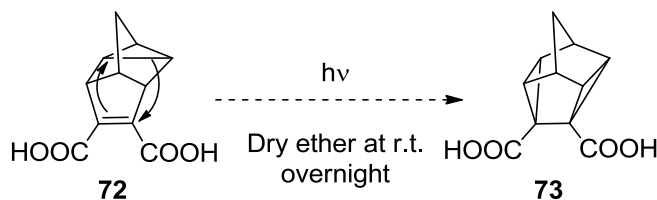
Scheme 2. Mechanism of the [2+2] photocycloaddition of **72**

Regrettably we could not reproduce the yields published by Forman *et al.* even though they were already low (typically between 20-25%). After several attempts we were unable to attain full conversion of the starting material and the mixture of **72** and **73** was inseparable through column chromatography. We ascribed the failure to the fact that the reported reaction was carried out in a Rayonet photochemical reactor (an apparatus containing 8 to 12 lamps of a non specified power)[106] whereas our reactor consisted of a single mercury lamp of 125 W.

The mixture of **72** and **73** was reacted with urea in order to get the corresponding imides. The reaction consists in inducing urea pyrolysis (150 °C) to produce a wide range of decomposition products, among which ammonia, allegedly the reactive species responsible for the formation of the imide.[107]

We assumed the two imides **74** and **75** would be more easily separated by column chromatography (Scheme 3). Unfortunately, the reaction did not yield the expected products, most certainly due to the harsh conditions of the reaction (200 °C). This synthetic route was thus abandoned.
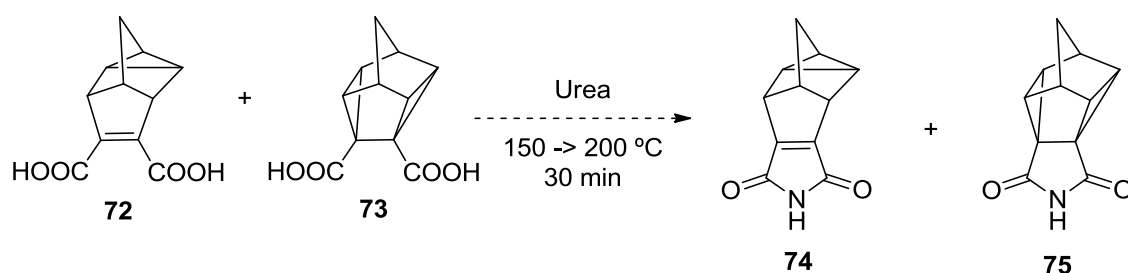
Scheme 3. Reaction of the mixture of **72** and **73** with urea

---

[107] a) Wynne, A. M. *J. Chem. Educ.* **1987**, *64*, 180. b) Schaber, P. M.; Colson, J.; Higgins, S.; Thielen, D.; Anspach, B.; Brauer, J. *Thermochim. Acta* **2004**, *424*, 131. c) Bernhard, A. M.; Peitz, D.; Elsener, M.; Wokaun, A.; Kröcher, O. *Appl. Catal. B Environ.* **2012**, *115-116*, 129.

1.2 Synthesis: 5-azapentacyclo[6.4.0.0^{2,10}.0^{3,7}.0^{9,11}]dodecane and related compounds

Simultaneously, we were also keen on the obtention of the 5-azapentacyclo[6.4.0.0^{2,10}.0^{3,7}.0^{9,11}]dodecane structure that, although not being as symmetrical as the hexacyclo derivative, possessed also some interesting features (Figure 46).
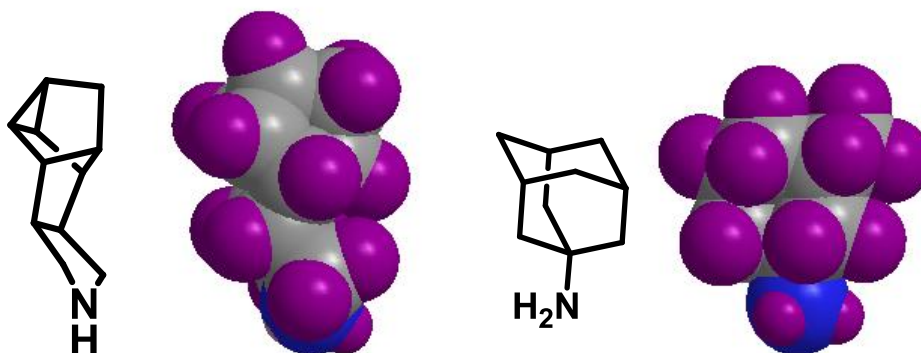
Figure 46. Qualitative space filling models of 5-azapentacyclo[6.4.0.0^{2,10}.0^{3,7}.0^{9,11}]dodecane and amantadine. Hydrogen atoms are shown in purple. Source: ChemBio3D Ultra. Energy minimized through MM2.

This scaffold presented a much longer distance between the amine and the furthest carbon of the polycyclic skeleton (5.68 Å) than amantadine (4.30 Å) while possessing a smaller polycycle width (2.25/2.29 Å) compared with amantadine (2.95 Å) (Figure 47). It was thus thought that this scaffold would penetrate deeper in the A/M2 channel while establishing different hydrophobic interactions with the residues of the entry gate (Val27, Ala30/Ser31).
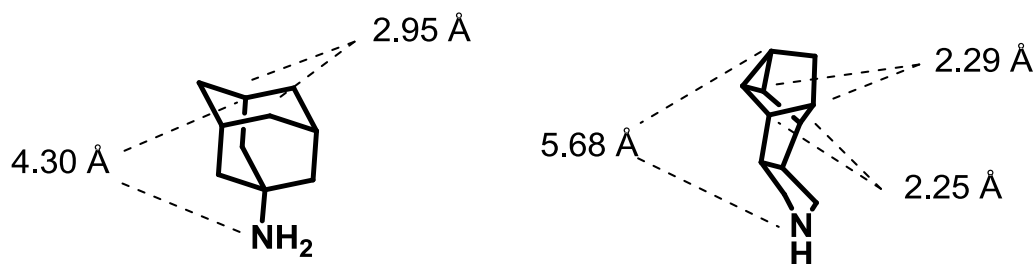
Figure 47. Most representative distances of amantadine and 5-azapentacyclo[6.4.0.0^{2,10}.0^{3,7}.0^{9,11}]dodecane. Source: ChemBio3D Ultra. Energy minimized through MM2.

Starting from the already synthesized diacid **72** we first tried to obtain the unsaturated cyclic imide by reacting it with urea. However, as aforementioned, the conditions seemed too harsh for the C-C double bond to be stable and only decomposition products were obtained from this reaction. So the diacid **72** was hydrogenated with hydrogen in the presence of palladium on activated carbon to yield the saturated diacid **76** in 90% yield. As expected, the single stereoisomer the hydrogenation produced was the *endo*-isomer which was confirmed by X-ray diffraction of a subsequent product and will be discussed in due time. Reaction of **76** with urea furnished imide **77** with a 79% yield (Scheme 4).
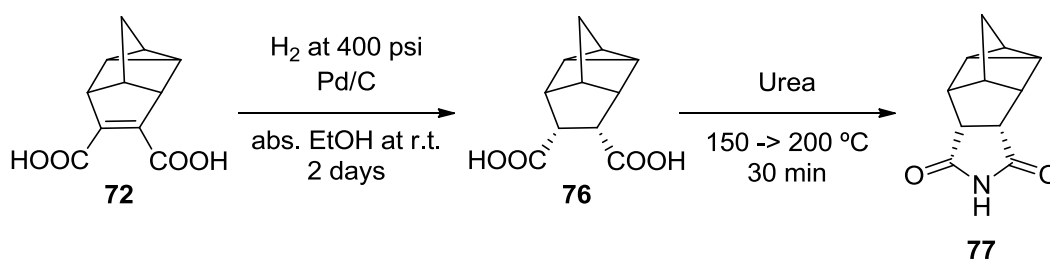
Scheme 4. Synthetic route for the obtention of imide **77**

Imide **77** was reduced with sodium bis(2-methoxyethoxy)aluminium hydride (Red-Al®), since our first attempts with lithium aluminium hydride did not yield good results. The main advantage of Red-Al® is its solubility in organic solvents, rendering the reaction mixture homogenous and the work-up cleaner than with other aluminium hydrides.[108] The oil obtained after the reduction was precipitated with HCl/Et$_2$O to form the hydrochloride salt **78** in 47% yield (Scheme 5).
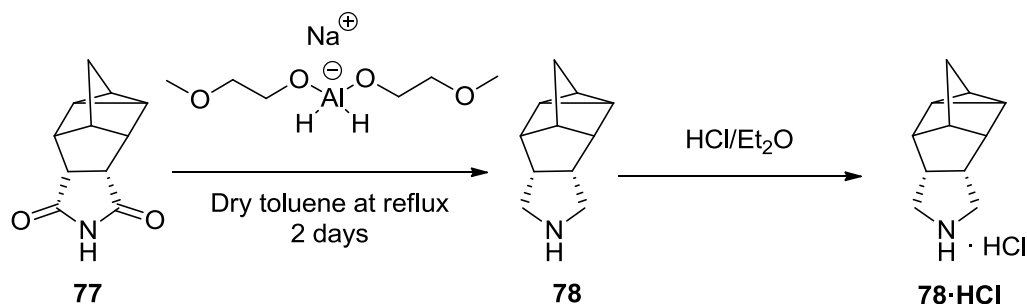
Scheme 5. Reduction of imide **77** with Red-Al® and subsequent precipitation as the hydrochloride salt **78·HCl**

---

[108] Kalo, J.; Ginsburg, D.; Vogel, E. *Tetrahedron* **1977**, *33*, 1177.

The next step was the formation of the guanidine derivative. The reaction involves the attack by a primary or a secondary amine to 1*H*-pyrazole-1-carboxamidine hydrochloride salt in the presence of a weak base such as triethylamine (Scheme 6).[109]
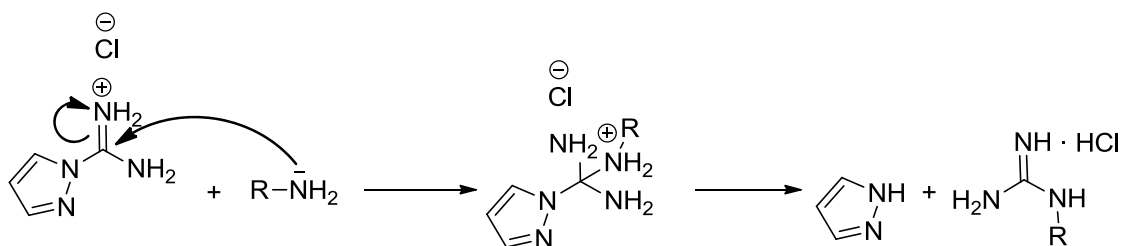
Scheme 6. Mechanism of the formation of guanidines with 1*H*-pyrazole-1-carboxamidine hydrochloride

Hence, pyrrolidine **78·HCl** was transformed to guanidine **79·HCl** with a 70% yield (Scheme 7).
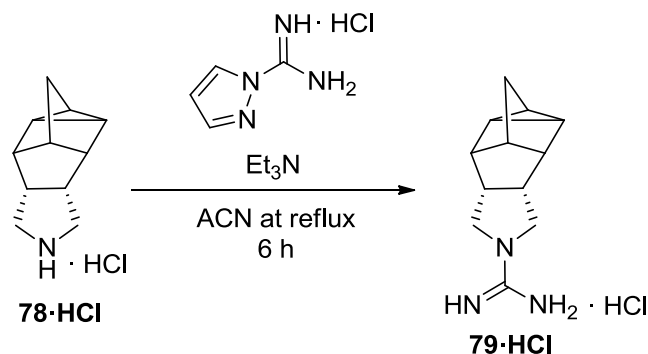
Scheme 7. Guanylation of amine **78.HCl**

As we have already mentioned, the catalytic hydrogenation of **72** was stereoselective, furnishing only one stereoisomer of **76**. In order to unequivocally determine the stereoselectivity of this family of compounds, we performed an X-ray diffraction analysis from a sample of **78·HCl** crystallized from 2-propanol. As shown in Figure 48, the hydrogenation of the double bond had taken place by the *exo-* face, rendering the ring in the *endo-* position (Figure 48).

---

[109] Bernatowicz, M. S.; Wu, Y.; Matsueda, G. R. *J. Org. Chem.* **1992**, *57*, 2497.
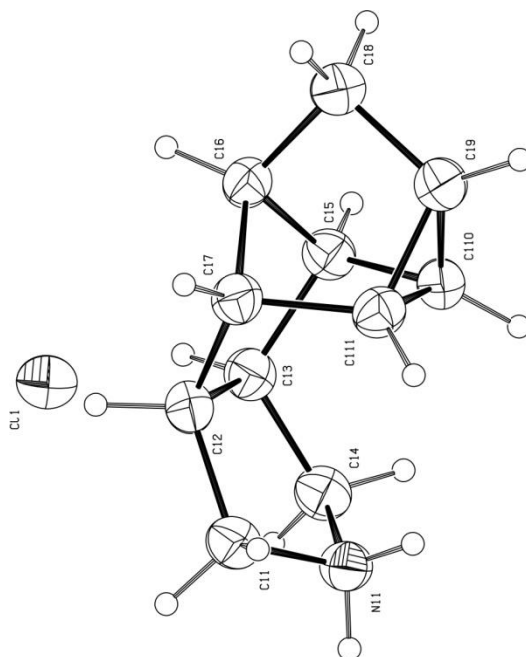
Figure 48. X-ray crystal structure (ORTEP) of amine **78** as hydrochloride salt

The *exo-* isomer would have been longer from the amine to the furthest carbon of the polycycle (5.68 Å), nevertheless the *endo-* isomer (5.14 Å) was still longer than amantadine (4.30 Å) and theoretically fulfilled the sought property of a deeper penetration into the A/M2 channel (Figure 49).
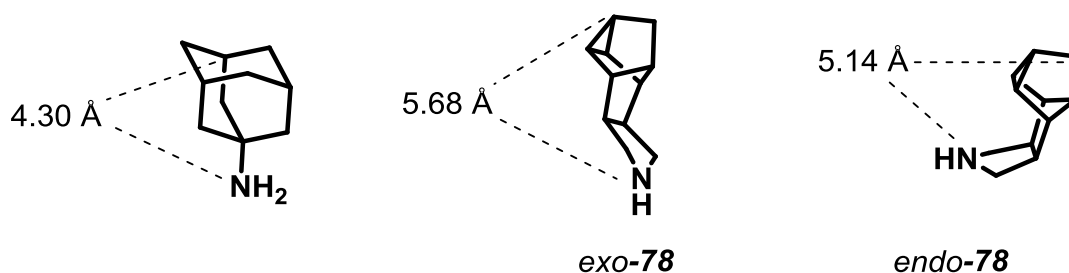
Figure 49. Distances from the amino moiety to the furthest carbon of the skeleton of amantadine and both *endo-* and *exo-* isomers of 5-azapentacyclo[6.4.0.0^{2,10}.0^{3,7}.0^{9,11}]dodecane. Source: ChemBio3D Ultra. Energy minimized through MM2.

1.3 Pharmacology: 5-azapentacyclo[6.4.0.0^{2,10}.0^{3,7}.0^{9,11}]dodecane and related compounds

The synthesized compounds were first evaluated as M2 channel blockers in non-human cells expressing the M2 channel. We should clarify that this procedure measures the M2 blocking activity exclusively. This work was carried out by the group of Professor Anna Moroni (University of Milano).

The group of Professor Lawrence H. Pinto, in the Northwestern University, and the group of Professor Moroni, are highly specialized in the use of a molecular biology technique named two-electrode voltage clamp or TEVC. The assay involves the injection of mRNA of the protein to be studied in oocytes from *Xenopus laevis* (an African frog). These cells are very convenient due to their size, big enough to be manipulated, and to the little number of channels or receptors endogenously expressed. After an incubation period, the oocytes can then be impaled with two microelectrodes, one for voltage sensing (electrode 1) connected to a voltage follower (A1), and the other for current injection (electrode 2) relied to a clamping amplifier (A2) for applying the desired voltage to the cell (Figure 50)[110].
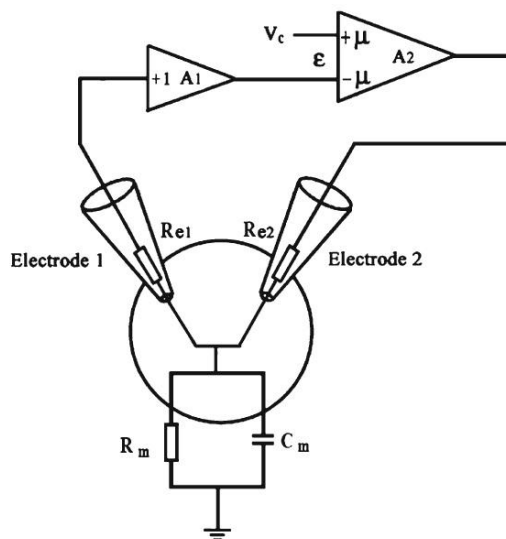
Figure 50. Electric diagram of two-electrode voltage clamp on an oocyte [110]

---

[110] Bingcai, G.; Chen, X.; Zhang, H. In *Ion channels. Methods in Molecular Biology*; 2nd Ed. Gamper, N., Ed.; Springer: New York, 2013; pp. 79–89.

The oocyte's membrane voltage is then clamped to -40 mV (a typical membrane potential value),[111] defined as the resting level, in a non-activating buffer solution at pH 8.5, hence the A/M2 channel is in a closed state (first blue bar in Figure 51). Then, the oocytes are bathed in an activating buffer at pH 5.5 that opens the A/M2 channel (red bar) and the measured current is taken as being the 100% activity of the channel. Next, the tested molecule is added at 100 µM (yellow bar) in the same activating solution. After 2 minutes, the oocytes are poured in the non-activating solution at pH 8.5 (second blue bar) for 5 minutes to allow current recovery. Following that, the activating solution at pH 5.5 is again applied (second red bar in Figure 51) and the current measured can be extrapolated to the percentage of the A/M2 channel activity remaining after the passage of the tested compound.[99b]
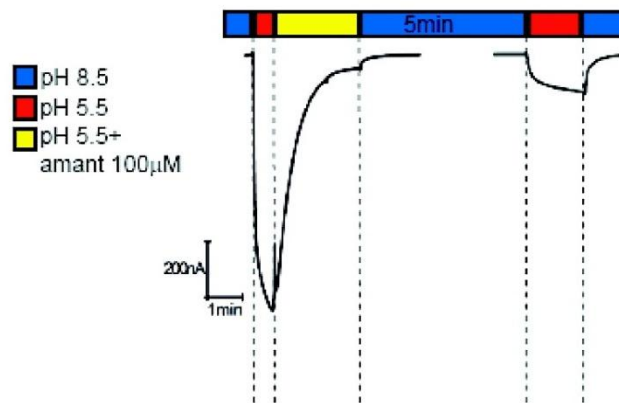
Figure 51. Representative trace of wt-M2 channel activity inhibited by amantadine at saturated concentration (100 µM) determined by TEVC [99b]

The molecules exhibiting an inhibition of A/M2 of 80% or superior, have their IC_{50} determined using the same technique. The channel activity is measured with varying concentrations of the compound (I) and it is normalized to the current provoked by the activating solution at pH 5.5 (I_o). The IC_{50} is the concentration needed to inhibit 50% of the activity of A/M2 (Figure 52).
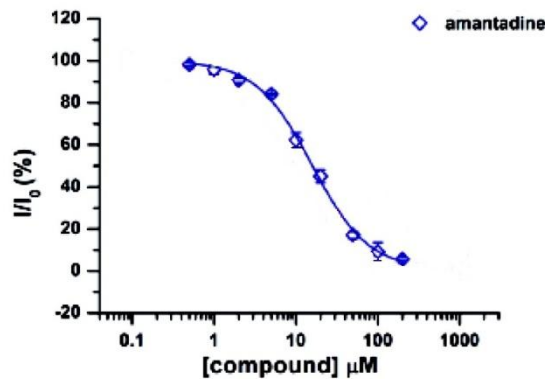
Figure 52. A/M2 activity assayed by TEVC at varying concentrations of amantadine [99b]

---

[111] Shimbo, K.; Brassard, D. L.; Lamb, R. A.; Pinto, L. H. *Biophys. J.* **1996**, *70*, 1335.

Professor Moroni's group did the evaluation as A/M2 channel blockers of this first set of compounds namely, **78.HCl** and **79·HCl**, using the TEVC technique (Table 1).

Table 1. Inhibition of the wt, V27A and S31N M2 channels by amine and guanidine derivatives of 5-azapentacyclo[6.4.0.0^{2,10}.0^{3,7}.0^{9,11}]dodecane scaffold

Compound	wt-M2		V27A-M2		S31N-M2	
	%inh.[a]	IC$_{50}$ (μM)	%inh.[a]	IC$_{50}$ (μM)	%inh.[a]	IC$_{50}$ (μM)
Amantadine	91.0 ± 2.1	16.0 ± 1.2	10.8 ± 2.0	ND[b]	35.6 ± 1.5	200 ± 3.5
78.HCl	93.7 ± 0.8	3.3	0	ND	0	ND
79·HCl	99.0 ± 0.5	0.84	2.0 ± 1.1	ND	0	ND

[a]Percentage inhibition at 100 μM for 2 min. Average of at least three experiments.
[b]ND: not determined

Gratifyingly, both amine **78·HCl** and guanidine **79·HCl** were active against the wild-type A/M2 channel. Indeed, they were both at least one order of magnitude more active than the reference amantadine, guanidine **79·HCl** being more active than its parent pyrrolidine **78·HCl**, as expected. Regrettably, neither of them inhibited any of the two tested mutant channels, V27A and S31N.
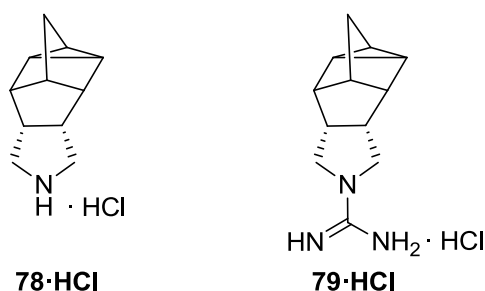
Figure 53. Active compounds against wt-M2 in the 5-azapentacyclo[6.4.0.0^{2,10}.0^{3,7}.0^{9,11}]dodecane series

The antiviral *in vitro* activity and cytotoxicity of these molecules were assessed by Professor Lieve Naesens of the Rega Institute for Medical Research in Leuven, Belgium, by two methods: the cytopathic effect (CPE) reduction assay and the tetrazolium reduction assay (MTS).

The CPE assay consists, first, in the incubation of healthy cells, in this case Madin-Darby canine kidney cells (MDCK), with influenza virus. When the virus attacks the cells a cell damage occurs, namely a cytopathic effect, that can be seen through a microscope and therefore deteriorated cells can be counted. In the presence of the tested compound, if it shows some activity, there will be a protection of the cells, a reduction in the CPE. However the compound can, in addition, be detrimental to cell growth and display a cytotoxic effect that can also be scored.

On the other hand, the MTS is a colorimetric assay based on the reduction of a tetrazolium reagent (MTS) by NADH in the cytoplasm, producing formazan in quantities, presumably, directly proportional to the number of viable cells (Scheme 8). Formazan absorbs light and can thus be quantified by UV-vis spectroscopy. Hence, the same procedure than with CPE is applied, the MTS simply allows a different method for scoring the viable cells.[112]
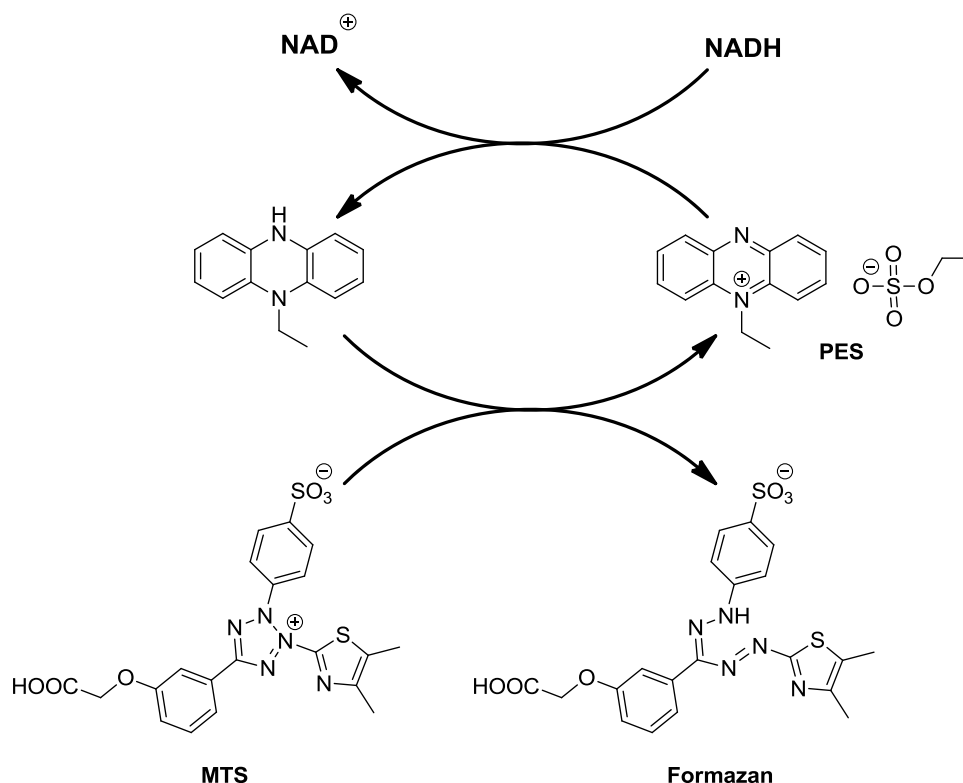
Scheme 8. Reduction of MTS to formazan by cytoplasmic NADH through an intermediate: phenazine ethosulfate (PES) [112]

---

[112] Riss, T. L.; Moravec, R. A.; Niles, A. L.; Benink, H. A.; Worzella, T. J.; Minor, L. In *Assay Guidance Manual*; Sittampalam, G. S., Ed.; Eli Lilly & Company and the National Center for Advancing Translational Sciences, 2013.

Thus, Professor Naesens tested the antiviral activity and cytotoxicity in MDCK cells of this first family of compounds against a variety of influenza viruses (Table 2):

- A/PR/8/34 (H1N1): an amantadine-resistant influenza A strain carrying a double mutation on the M2 channel (V27T and S31N).
- A/HK/7/87 (H3N2): an amantadine-sensitive influenza A strain bearing a wild-type M2 channel.
- B/HK/5/72: an amantadine-resistant influenza B strain.

Table 2. Antiviral activity against influenza A and B determined in MDCK cells of amine and guanidine derivatives of 5-azapentacyclo[$6.4.0.0^{2,10}.0^{3,7}.0^{9,11}$]dodecane

| Compound | Antiviral EC$_{50}$^{a} (μM) | | | | | | Toxicity |
| | Influ. A (H1N1) | | Influ. A (H3N2) | | Influenza B | | MCC^b |
	CPE	MTS	CPE	MTS	CPE	MTS	
Amantadine	212	192	0.45	0.50	>500	>500	>500
78.HCl	>100	>100	>100	>100	>100	>100	>100
79·HCl	>100	>100	>100	>100	>100	>100	>100

^{a}Effective concentration producing 50% of inhibition of viral replication. Values shown are the mean of 2-3 determinations.

^{b}Minimum compound concentration causing minimal changes in cell morphology.

These antiviral results mean that neither **78·HCl** nor **79·HCl** were active against influenza A (H1N1), influenza A (H3N2) or influenza B. They did not show any cytotoxicity either.

Founded on the activities as M2 channel blockers of **78·HCl** and **79·HCl** we expected them to be, at least, active against the H3N2 strain, carrying a wt-M2, in the antiviral assay. The fact that they were not, may be due to multiple factors: permeability issues with the cell, too rapid degradation by the host cell, side interactions and trapping of the molecule with other components of the virus or the host cell, etc.

Noteworthy, Professor Naesens possesses a wide collection of DNA and RNA viruses (e.g. parainfluenza-3 virus, coxsackie virus, vesicular stomatitis virus, herpes virus, etc.), all of which were subjected to our compounds. None of the molecules presented in this dissertation displayed any activity against them (data not shown).

This first approach with new polycyclic structures led to some interesting results:

- Both amine **78·HCl** and guanidine **79·HCl** were very active wt-M2 channel blockers, guanidine **79·HCl** being a submicromolar inhibitor.
- Guanidine **79·HCl** was more active than amine **78·HCl**, as expected.

- None of them displayed any activity whatsoever in the *in vitro* assays.
- None of them were cytotoxic at the measured concentrations.

Although the results of the TEVC experiment could not be extrapolated to the antiviral *in vitro* assay, the obtained activities encouraged us to proceed with the exploration of new polycyclic scaffolds.
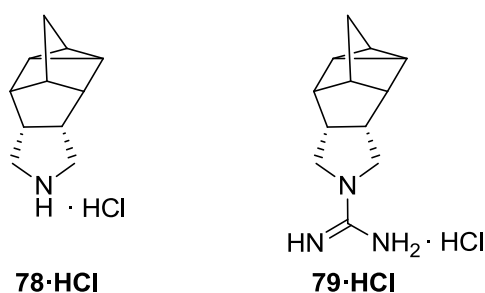
Figure 54. Active compounds against wt-M2 but inactive through *in vitro* assays in the 5-azapentacyclo[6.4.0.0^{2,10}.0^{3,7}.0^{9,11}]dodecane series

2. More elongated structures: attempts to reach the lower binding site at Gly34

2.1 Synthesis: 4-azatetracyclo[5.3.2.0²,⁶.0⁸,¹⁰]dodecane and related compounds

Following our quest for new polycyclic structures, we were attracted by some of the molecules reported by Abou-Gharbia and co-workers [113] : particularly, we desired to synthesize and evaluate the 4-azatetracyclo[5.3.2.0²,⁶.0⁸,¹⁰]dodecane scaffold that was readily available in a reduced number of steps and presented some attractive features (Figure 55).
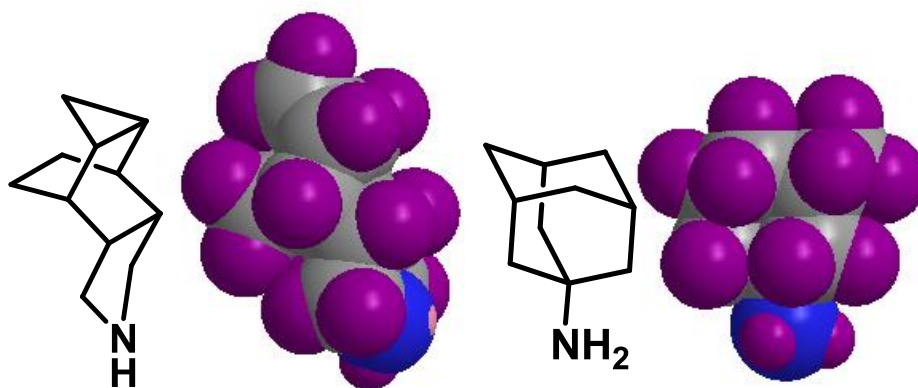
Figure 55. Qualitative space filling models of 4-azatetracyclo[5.3.2.0²,⁶.0⁸,¹⁰]dodecane and amantadine. Hydrogen atoms are shown in purple. Source: ChemBio3D Ultra. Energy minimized through MM2.

This structure was, from the amine to the furthest carbon, longer (5.83 Å) than amantadine (4.30 Å) and longer than the previous scaffold (5.14 Å, see Figure 49). The width of the polycyclic cage (2.55 Å) was smaller than amantadine's (2.95 Å), although being wider compared with the previous scaffold (2.25/2.29 Å, see Figure 47). Thus, this structure was longer than amantadine in an attempt to establish interactions with the lower binding site at Gly34 and disrupt the deeper water clusters.[52b] Even so, it was still more compact than amantadine to appraise the influence of the lipophilic polycyclic cage (Figure 56).

---

[113] Abou-Gharbia, M.; Patel, U. R.; Webb, M. B.; Moyer, J. A.; Andree, T. H.; Muth, E. A. *J. Med. Chem.* **1988**, *31*, 1382.
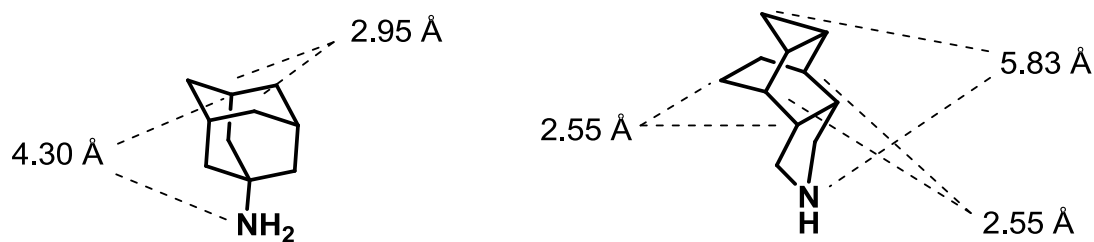
Figure 56. Most representative distances of amantadine and 4-azatetracyclo[5.3.2.0^{2,6}.0^{8,10}]dodecane. Source: ChemBio3D Ultra. Energy minimized through MM2

The first part of the synthesis was taken from the literature and consisted in a Diels-Alder reaction between cycloheptatriene and maleimide.[113] In fact, cycloheptatriene, stable at room temperature, has a valence isomer, norcaradiene, whose isomerization is triggered thermically.[114] It was this isomer that reacted with maleimide (Scheme 9) to get imide **80** with a 64% yield. The *endo-* product was obtained, as expected for a Diels-Alder with maleimide,[115] since there is a bonding interaction, stabilizing this isomer, between the carbonyl groups and the developing double bond at the back of norcaradiene.
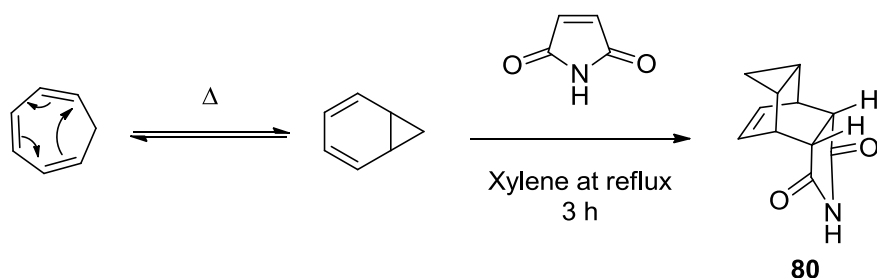
Scheme 9. Diels-Alder reaction of norcaradiene with maleimide to yield imide **80**

The synthetic route continued with the reduction of **80** with Red-Al® to produce amine **81** that was subsequently converted to the hydrochloride salt **81·HCl** via the use of HCl/Et$_2$O with a 79% overall yield (Scheme 10).
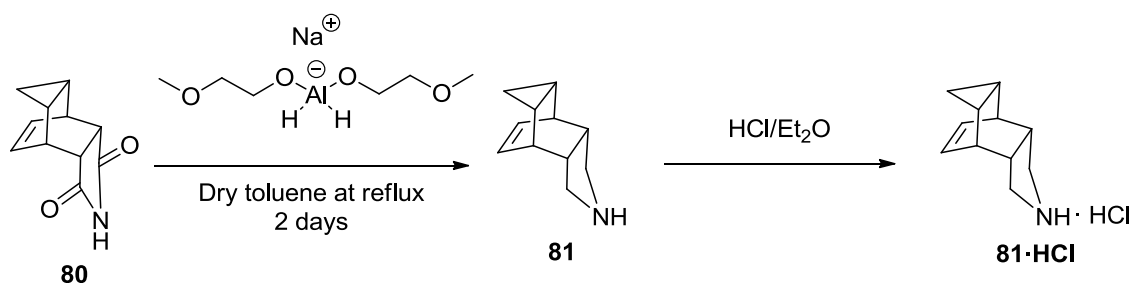
Scheme 10. Reduction of imide **80** and succeeding formation of the hydrochloride salt

---

[114] McNamara, O. A.; Maguire, A. R. *Tetrahedron* **2011**, *67*, 9.

[115] Martin, J. G.; Hill, R. K. *Chem. Rev.* **1961**, *61*, 537.

These two simple steps supplied the first compound to be tested pharmacologically, pyrrolidine **81·HCl**, that was also central to access every other final compound. First, it was submitted to a guanylation reaction with 1*H*-pyrazole-1-carboxamidine hydrochloride in the presence of triethylamine to get guanidine **82·HCl** in an 85 % yield. In order to afford the saturated guanidine, **82·HCl** was hydrogenated with palladium on activated carbon at high pressure of hydrogen to furnish guanidine **83·HCl** in a 77% yield (Scheme 11) We synthesized the guanidine derivatives since our previous data predicted they would be more potent M2 channel blockers than their amine counterparts (see page 64).
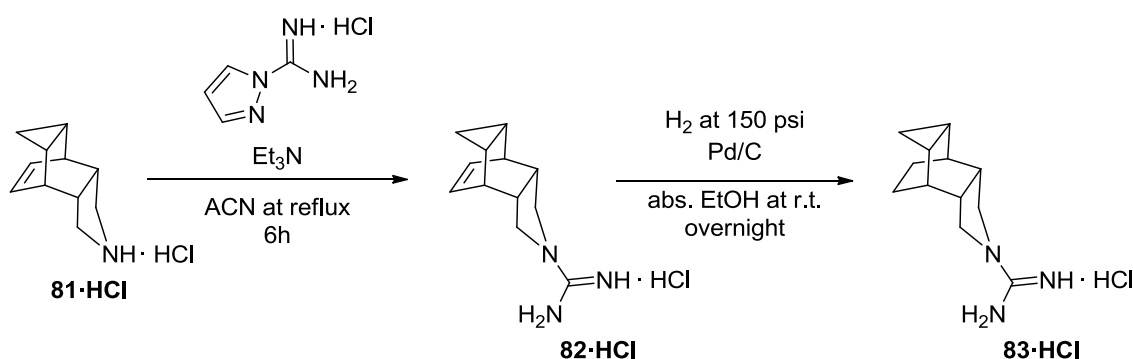
Scheme 11. Guanylation of amine **81·HCl** and subsequent hydrogenation of guanidine **82·HCl** to afford guanidine **83·HCl**

Amine **81·HCl** was also hydrogenated with palladium on activated carbon at high pressure of hydrogen to get the saturated pyrrolidine **84.HCl** in quantitative yield (Scheme 12). We wanted to assess the pharmacological effect of the presence versus the absence of the terminal C-C double bond.
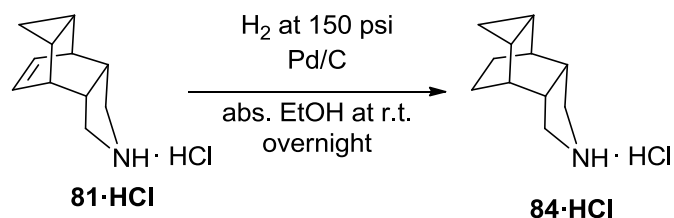
Scheme 12. Hydrogenation of amine **81·HCl**

Amine **81** was then subjected to reductive alkylation procedures to get tertiary amines. This reaction between an amine and a ketone or an aldehyde, produce imines that can be reduced to the alkylated amines (Scheme 13).
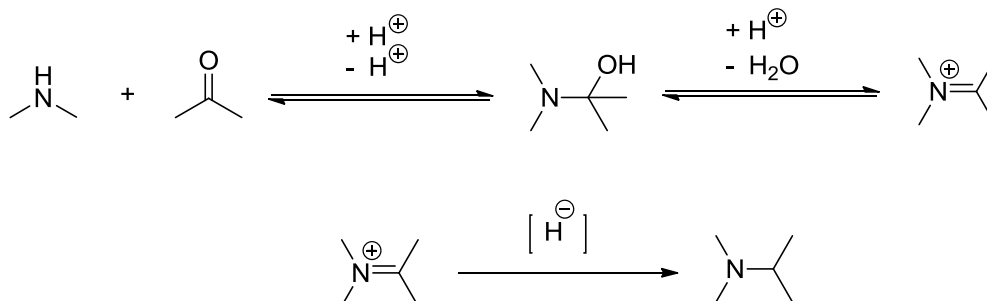
Scheme 13. Reductive amination process

The reduction of the imine can be carried out by catalytic hydrogenation or by a number of hydride donors. One of the most commonly used is sodium cyanoborohydride which selectively reduces the imine without reducing the ketone or aldehyde to the unreactive alcohol.[116] This phenomenon is due to the electron withdrawing cyano moiety that stabilizes the negative charge on the boron thus rendering it less reactive. Hence, in slightly acidic conditions, there is a kinetic difference between the reduction of the imine by sodium cyanoborohydride, that happens fast, and the reduction of the carbonyl group of either the ketone or the aldehyde, that is negligible.[116] Consequently, the whole reductive amination reaction can be carried out in a one-pot fashion (Scheme 14).
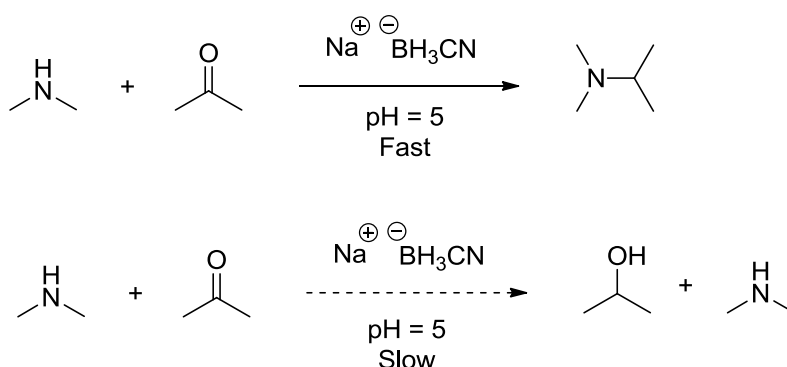
Scheme 14. One-pot synthesis of an alkylated amine from an amine and a ketone or aldehyde

---

[116] a) Borch, R. F.; Bernstein, M. D.; Durst, H. D. *J. Am. Chem. Soc.* **1971**, *93*, 2897. b) Lane, C. F. *Synthesis* **1975**, 135.

Accordingly, we synthesized alkylated amine **86·2HCl** through reductive alkylation. First, commercially available 1-Boc-4-piperidone and free amine **81** in the presence of acetic acid, formed the imine that was rapidly reduced by sodium cyanoborohydride to the protected alkylated amine **85**. The use of Boc-protected piperidone was justified by the possibility of unwanted reductive aminations between unprotected piperidones themselves. The protecting group was removed with hydrochloric acid to obtain alkylated amine **86·2HCl** as the dihydrocloride salt in 76 % yield over the 2 steps (Scheme 15).
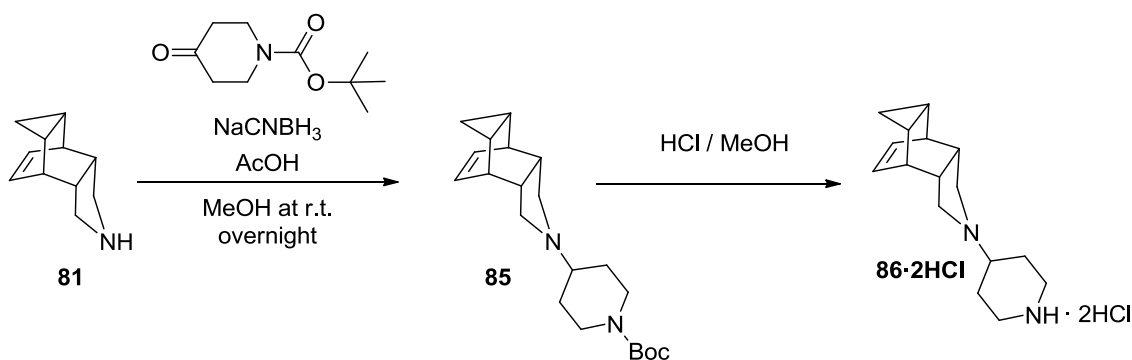
Scheme 15. Synthesis of the alkylated diamine **86·2HCl**

The alkylated diamine **86·2HCl** was also hydrogenated with palladium on activated carbon at high pressure of hydrogen to get the saturated piperidine **87·2HCl** in 85 % yield (Scheme 16). Both **86·2HCl** and **87·2HCl** answered our desire of compounds long enough to penetrate deeper in the channel, closer to the lower binding site at Gly34 and disturb the rigidity of the four water molecules present in there.[52b,76]
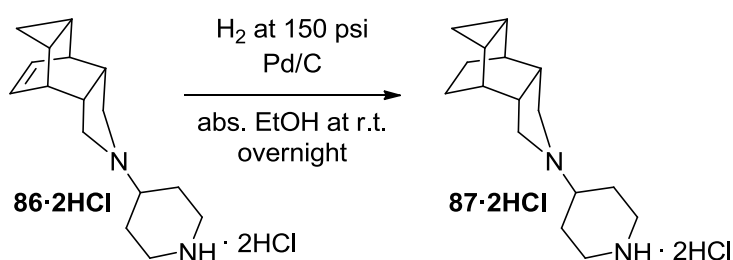
Scheme 16. Hydrogenation of **86·2HCl**

Another reductive alkylation of **81** was achieved, this time with formaldehyde as the carbonyl partner. The reaction was again performed with sodium cyanoborohydride as the reducing agent in the presence of acetic acid. Unfortunately, although the reaction did yield the product, both the hydrochloride salt and the tartrate salt were hygroscopic compounds, meaning they caught ambient water rapidly giving sticky oils not easily handled and thus not suitable for pharmacological evaluation (Scheme 17).
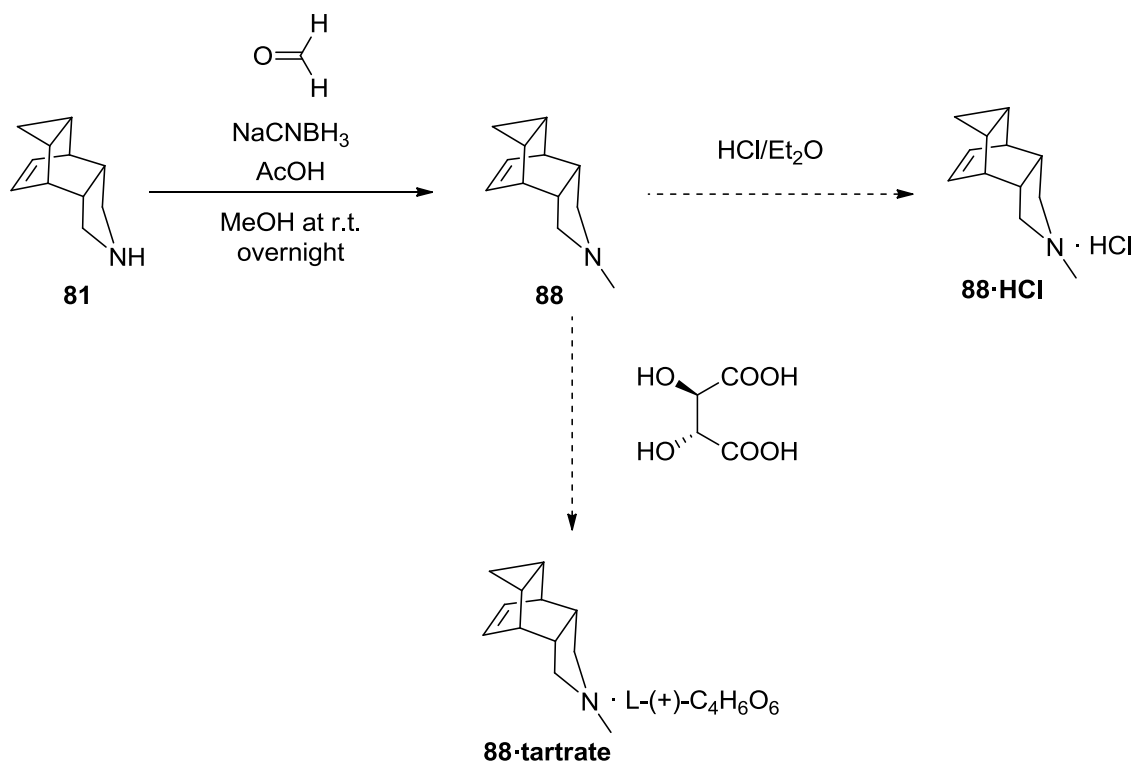
Scheme 17. Attempted syntheses of **88·HCl** and **88·tartrate**

Even if we were aware that *N*-alkylating the amine of the polycyclic compounds usually diminished the antiviral activity, we wished, as a mean of reinforcing our previous knowledge, to appraise the effect of *N*-alkylating this particular scaffold.

2.2 Pharmacology: 4-azatetracyclo[5.3.2.0^{2,6}.0^{8,10}]dodecane and related compounds

This series of compounds was tested, using the above mentioned TEVC technique, by the group of Professor Pinto in the Northwestern University. All but **87·2HCl**, that was not soluble neither in DMSO nor in methanol, so no TEVC assay could be performed with this molecule (Table 3).

Table 3. Inhibition of the wt, V27A and S31N M2 channels by 4-azatetracyclo[5.3.2.0^{2,6}.0^{8,10}]dodecane derivatives

Compound	wt-M2		V27A-M2		S31N-M2	
	%inh.[a]	IC$_{50}$ (µM)	%inh.[a]	IC$_{50}$ (µM)	%inh.[a]	IC$_{50}$ (µM)
Amantadine	91.0 ± 2.1	16.0 ± 1.2	10.8 ± 2.0	ND[b]	35.6 ± 1.5	200 ± 3.5
81·HCl	88.8 ± 1.3	2.92	0	ND	2.4 ± 1.3	ND
82·HCl	90.7 ±0.9	1.50	0	ND	9.5 ± 0.6	ND
83·HCl	93.4 ± 1.2	1.64	2.5 ± 0.4	ND	14.5 ± 1.7	ND
84·HCl	90.9 ± 1.0	3.38	5.7 ± 0.9	ND	3.4 ± 2.2	ND
86·2HCl	1.3 ± 1.3	ND	3.1 ± 0.5	ND	0	ND
87·2HCl	NS[c]	NS	NS	NS	NS	NS

[a]Percentage inhibition at 100 µM for 2 min. Average of at least three experiments.

[b]ND: not determined.

[c]NS: not soluble.

Pleasantly, amines **81·HCl**, **82·HCl**, **83·HCl** and **84·HCl** displayed low micromolar activities against the wt-M2 channel, one order of magnitude lower than amantadine. Regrettably, none of the compounds of this family inhibited neither the S31N nor the V27A mutant channels. Disappointingly, **86·2HCl** did not show any activity whatsoever against any of the M2 channels, perhaps due to unfavorable clashes between the pore lining residues and the piperidine ring or the tertiary amine. Alternatively, the lack of activity of this compound may have been related to the fact that it was a diamine and, as such, doubly protonated at physiological pH, rendering it too polar to enter into the channel. As already expected no compound was active against the S31N mutant.

Nevertheless, two interesting trends could be inferred:

- As expected, guanidines were more potent than their parent amines (**81.HCl** vs. **82·HCl** and **84·HCl** vs. **83·HCl**).
- The double bond had little effect on the activity of the compounds against the wt-M2 channel (**81·HCl** vs. **84·HCl** and **82·HCl** vs. **83·HCl**).
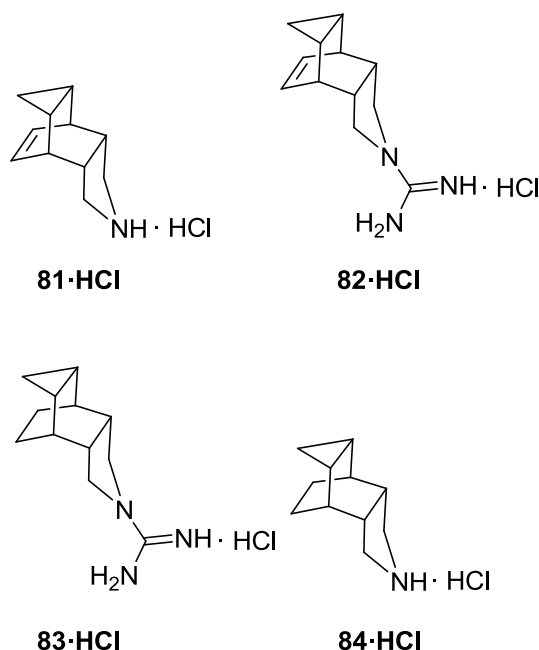
Figure 57. Active compounds against wt-M2 in the 4-azatetracyclo[5.3.2.0^{2,6}.0^{8,10}]dodecane series

Professor Naesens in the Rega Institute for Medical Research in Belgium performed the antiviral and cytotoxicity assays in MDCK cells of this second family of compounds, using the same methods described previously (see page 65), against three influenza virus strains (Table 4):

- A/PR/8/34 (H1N1): an amantadine-resistant influenza A strain carrying a double mutation on the M2 channel (V27T and S31N).
- A/HK/7/87 (H3N2): an amantadine-sensitive influenza A strain bearing a wild-type M2 channel.
- B/HK/5/72: an amantadine-resistant influenza B.

Table 4. Antiviral activity against influenza A and B determined in MDCK cells of 4-azatetracyclo[5.3.2.0^{2,6}.0^{8,10}]dodecane derivatives

| Compound | Antiviral EC$_{50}$^{a} (µM) | | | | | | Toxicity |
| | Influ. A (H1N1) | | Influ. A (H3N2) | | Influenza B | | MCC^b |
	CPE	MTS	CPE	MTS	CPE	MTS	
Amantadine	30	34	1.4	1.4	>500	>500	>500
81.HCl	>100	>100	6.2	8.0	>100	>100	>100
82·HCl	>100	>100	>100	>100	>100	>100	>100
83·HCl	>100	>100	>100	>100	>100	>100	>100
84·HCl	>100	>100	6.0	2.7	>100	>100	>100
86·2HCl	<0.8	<0.8	>100	>100	>100	>100	>100
87·2HCl	>100	>100	>100	>100	>100	>100	20

^{a}Effective concentration producing 50% of virus induced cytopathic effect. Values shown are the mean of 2-3 determinations.

^{b}Minimum compound concentration causing minimal changes in cell morphology.

Amines **81·HCl** and **84·HCl** presented a favourable antiviral activity against the H3N2 strain bearing a wt-M2 channel, their activities confirming the higher potency of the fully saturated compounds. Yet, guanidines **82·HCl** and **83·HCl** did not display any antiviral activity, the probable causes being the same already stated (see page 66). None of the compounds evidenced any activity against influenza B and none of them were cytotoxic except for guanidine **87·2HCl** that displayed some toxicity.

Surprisingly, piperidine **86·2HCl** was very active against the H1N1 strain carrying a double mutation on the M2 channel (V27T and S31N) albeit not exhibiting any activity against the S31N mutant channel in the TEVC assay. This effect could be explained by the ability of some polycyclic compounds to slightly increase the endosomal pH: it has been found lately that the A/PR/8/34 (H1N1) strain is very sensitive to these changes.[40,117]

In order to confirm the activities of **81·HCl** and **84·HCl**, Professor Naesens carried out two more experiments with the A/HK/7/87 (H3N2) strain: a virus yield assay and a plaque reduction assay. The virus yield assay consists in seeding MDCK cells then infect them with the influenza virus and next expose them to serial dilutions of the compounds to be tested. After an incubation period, the supernatants containing the newly formed virions released from the infected cells, are lysed to disrupt the viral particles and release the vRNA. This one is quantified by quantitative real time reverse transcription polymerase chain reaction (qRT-PCR) and it is compared with the untreated virus control in a plotted graph. The EC_{90} is calculated by extrapolation and is defined as the concentration of compound causing a 1-$\log_{10}$ reduction in the amount of viral genetic material released compared with the control. Similarly, the EC_{99} is considered as being the concentration of compound causing a 2-$\log_{10}$ reduction.[118] This assay usually circumvents the cytotoxicity of the molecules since the exposure time to the cells is reduced compared with the CPE or MTS assays. The results for **81·HCl** and **84·HCl** are hereafter presented (Table 5).

Table 5. Antiviral activities against influenza virus A/HK/7/87 (H3N2) determined with MDCK cells by virus yield assay of **81·HCl** and **84·HCl**

Compound	Antiviral activity (µM) Influenza A/HK/7/87 (H3N2)		
	CPE (EC_{50})[a]	MTS (EC_{50})[a]	Virus yield (EC_{99})[b]
Amantadine	1.4	1.4	1.1
81.HCl	6.2	8.0	20
84·HCl	6.0	2.7	<0.4

[a]Effective concentration producing 50% of inhibition of viral replication.

[b]Compound concentration producing a 2-$\log_{10}$ reduction in virus yield determined by qRT-PCR.

[117] Kolocouris, A.; Tzitzoglaki, C.; Johnson, F. B.; Zell, R.; Wright, A. K.; Cross, T. A.; Tietjen, I.; Fedida, D.; Busath, D. D. *J. Med. Chem.* **2014**, *57*, 4629.

[118] Meneghesso, S.; Vanderlinden, E.; Stevaert, A.; McGuigan, C.; Balzarini, J.; Naesens, L. *Antiviral Res.* **2012**, *94*, 35.

The virus yield assay confirmed the activities of both **81·HCl** and **84·HCl** against the A/HK/7/87 (H3N2) strain of influenza and reaffirmed again that the saturated amine **84·HCl** was more potent than the unsaturated **81·HCl**.

The other experiment was a plaque reduction assay and it is achieved as follows. First, the influenza virus is incubated for 1 hour with different concentrations of the compounds, after what they are added to MDCK cells and incubated again 1 hour. The excess virus is removed, replaced by fresh medium containing more of the compounds and after another incubation period of 72 hours, the viral plaques are visualized by staining with crystal violet. The plaques are cell destruction regions generated by the virus spreading, so they are considered to account for viral replication. The putative antiviral molecule could have two effects on the cell: it could either reduce the number of plaques (red circled Petri dishes in Figure 58c) compared with the mock-treated virus control (Figure 58b) or it could have a cytotoxic effect killing the MDCK cells (non-circled Petri dish in Figure 58c).

A) <u>Cell control</u>   B) <u>Influenza virus control</u>

C) <u>Putative antiviral molecule</u>

3 μM   10 μM   50 μM
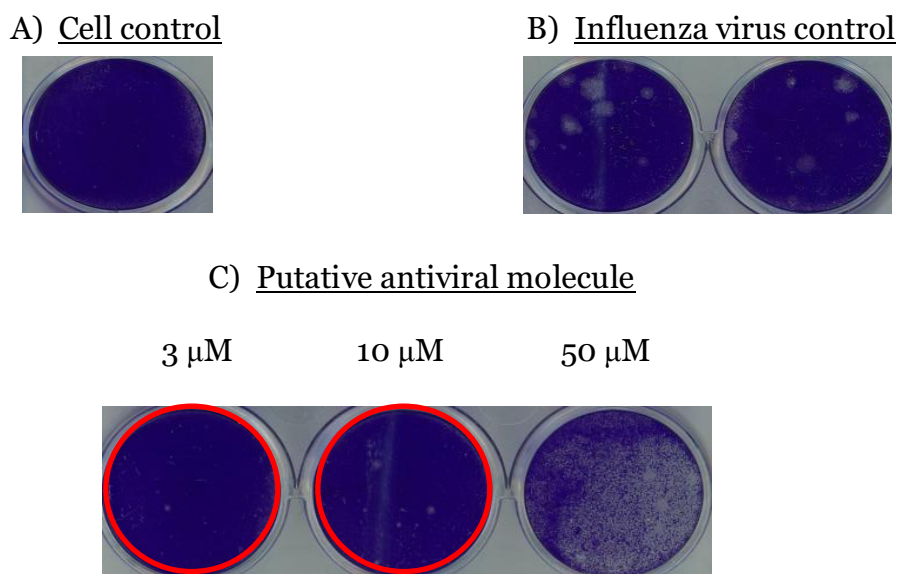
Figure 58. a) MDCK cells in culture media **b)** MDCK cells infected with influenza virus produces viral plaques (white spots) **c)** MDCK cells, influenza virus and a putative inhibitor at different concentrations. The red circled Petri dishes (3 μM and 10 μM) show a reduction in plaques compared with the control whereas the non-circled one (50 μM) indicates a cytotoxic effect. Source: Professor Lieve Naesens

The second family of compounds was thus tested by Professor Naesens in a plaque reduction assay with influenza virus A/HK/7/87 (H3N2) strain at three different concentrations (Figure 59).
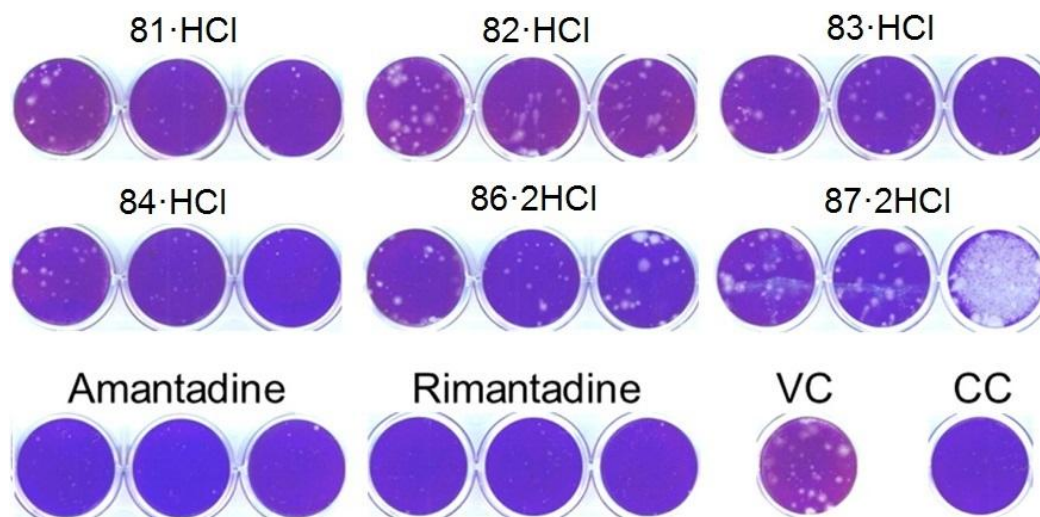
Figure 59. Virus plaque reduction assay of 4-azatetracyclo[5.3.2.0^{2,6}.0^{8,10}]dodecane derivatives. MDCK cells infected with influenza virus A/HK/7/87 (H3N2) in the presence of tested compounds. Concentrations, from left to right: 0.5, 2 and 8 µM. Plaques visualized by crystal violet staining. VC: mock-treated virus control. CC: uninfected cell control

From this experiment we confirmed that **81·HCl** and **84·HCl** were very active antiviral compounds (clear plaque reduction at 8 and 2 µM and modest reduction at 0.5 µM) against the influenza strain carrying a wt-M2. The other molecules (**82·HCl**, **83·HCl**, **86·2HCl**, **87·2HCl**) exhibited no plaque reduction at all at any concentration and **87·2HCl** was cytotoxic at 8 µM. These results validated the CPE and MTS assays (see page 77).

Thus, in terms of cell culture activity, the more promising compounds were **81·HCl** and **84·HCl** (Figure 66).
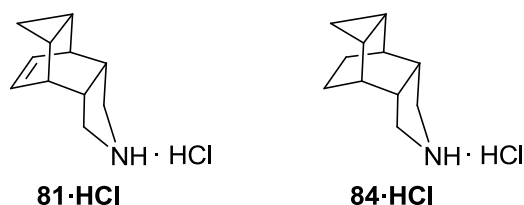
Figure 60. Most promising compounds according to *in vitro* assays

Despite not having a direct correlation for all the tested compounds between the TEVC and the antiviral assays, some promising molecules were unveiled:

- Amines **81·HCl** and **84·HCl** were low micromolar wt-M2 channel blockers.
- Both **81·HCl** and **84·HCl** displayed low micromolar antiviral activities against an H3N2 influenza strain bearing a wt-M2.
- The fully saturated amine **84·HCl** was more active than its unsaturated counterpart amine **81·HCl**.
- Neither **81·HCl** nor **84·HCl** were cytotoxic at the measured concentrations.

- Guanidines **82·HCl** and **83·HCl** were low micromolar wt-M2 channel blockers, more active than their parent amines.
- Unfortunately no antiviral activity was detected for **82·HCl** nor for **83·HCl**. This could be due to issues once in presence of the cell and the whole virus.
- No toxicity was detected for **82·HCl** nor for **83·HCl** at the measured concentrations.

- Disappointingly the *N*-alkylated compounds, **86·2HCl** and **87·2HCl**, exhibited no activity as M2 channel inhibitors or as *in vitro* antivirals against the A/HK/7/87 (H3N2) strain although being long enough to establish deeper and more robust interactions within the channel pore.
- Oddly enough, diamine **86·2HCl** displayed a high antiviral activity against the A/PR/8/34 (H1N1) strain, yet it seemed not to involve M2 channel blocking.
- Diamine **86·2HCl** was not cytotoxic at the measured concentrations, contrary to **87·2HCl**.

81·HCl   **82·HCl**   **83·HCl**   **84·HCl**
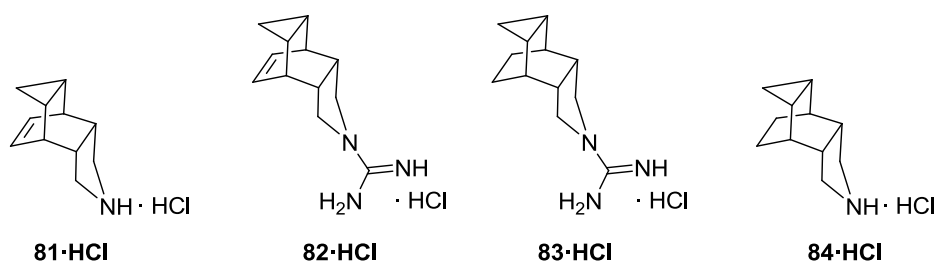
Figure 61. Active compounds of the 4-azatetracyclo[5.3.2.0^{2,6}.0^{8,10}]dodecane series either as *in vitro* antivirals and/or M2 channel blockers

3. Elongated compounds: targeting the V27A mutant

3.1 Synthesis: 13-azahexacyclo[8.5.2.1^{4,7}.0^{2,9}.0^{3,8}.0^{11,15}]octadecane and related compounds

There were other scaffolds among the structures described by Abou-Gharbia and co-workers that also caught our attention.[113] So, whilst we were dealing with the previously mentioned scaffold, the Ph.D. student M. Barniol synthesized the 4-azatetracylo[5.4.2.0^{2,6}.0^{8,11}]tridecane derivatives **89·HCl**, **90·HCl**, **91·HCl** and **92·HCl** that were also evaluated by the pharmacologists (Figure 62).

89·HCl
IC$_{50}$ wt = 5.5 μM
% inh. V27A = 6%[a]

90·HCl
IC$_{50}$ wt = 1.2 μM
% inh. V27A = 17%[a]

91·HCl
IC$_{50}$ wt = 4.9 μM
% inh. V27A = 34%[a]

92·HCl
IC$_{50}$ wt = 2.1 μM
% inh. V27A = 76%[a]
IC$_{50}$ V27A = 22.6 μM
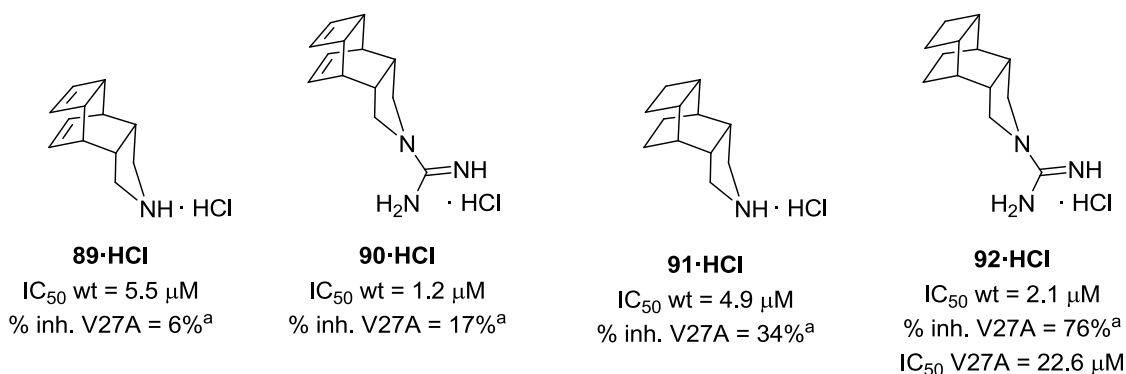
Figure 62. M2 channel blocking activities of 4-azatetracylo[5.4.2.0^{2,6}.0^{8,11}]tridecane derivatives synthesized by M. Barniol. [a]Determined by TEVC in *Xenopus laevis* frog oocytes at 100 μM for 2 min.

The activities displayed in this series were very enlightening: taking into account that the only difference between guanidines **83·HCl** and **92·HCl** was the replacement of a cyclopropane by a cyclobutane, this small change entailed a dramatic increase in the inhibition of the V27A mutant (14% vs. 76%) whilst retaining wt-M2 activity (1.6 μM vs. 2.1 μM).

Hence, taking as a basis the 4-azatetracylo[5.4.2.0^{2,6}.0^{8,11}]tridecane scaffold we designed another structure that would extend the cyclobutane part, to explore the lipophilic interactions of the upper part of the channel, whilst maintaining all the other features from this scaffold; namely the 13-azahexacyclo[8.5.2.1^{4,7}.0^{2,9}.0^{3,8}.0^{11,15}]octadecane structure (Figure 63).
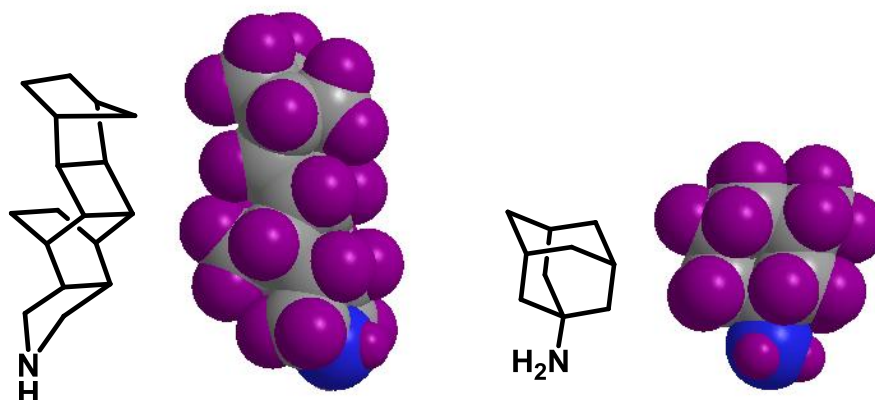
Figure 63. Qualitative space filling models of 13-azahexacyclo[8.5.2.1^{4,7}.0^{2,9}.0^{3,8}.0^{11,15}]octadecane and amantadine. Hydrogen atoms are shown in purple. Source: ChemBio3D Ultra. Energy minimized through MM2.

The skeleton of the 13-azahexacyclo[8.5.2.1^{4,7}.0^{2,9}.0^{3,8}.0^{11,15}]octadecane displayed a much longer distance between the amine and the furthest carbon (8.60 Å), in fact twice the distance, compared with amantadine (4.30 Å). We were again targeting the lower binding site at Gly34,[52b] but especially we desired to explore the effect of this elongated series on the V27A mutant to see if the lengthening of the molecule would permit a higher degree of disruption of the increased number of waters present in the mutant channel.[81] The width of the scaffold (2.53/2.59 Å) was still lower than amantadine (2.95 Å) but since it had given good results with the 4-azatetracylo[5.4.2.0^{2,6}.0^{8,11}]tridecane, we decided to modify only one parameter at a time (Figure 64).
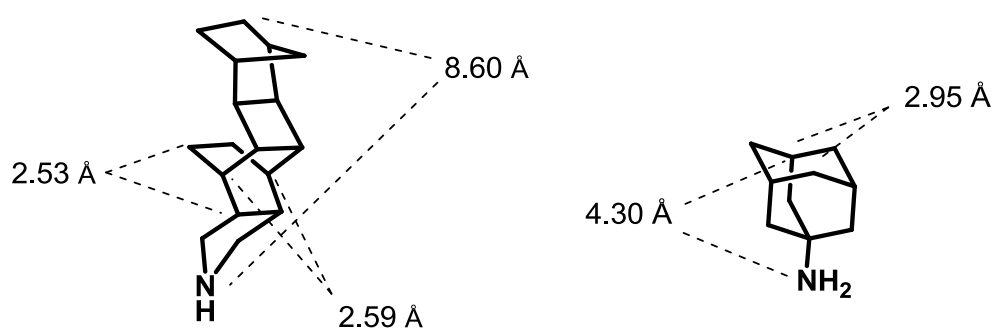
Figure 64. Most representative distances of 13-azahexacyclo[8.5.2.1^{4,7}.0^{2,9}.0^{3,8}.0^{11,15}]octadecane and amantadine. Source: ChemBio3D Ultra. Energy minimized through MM2

The beginning of the synthetic route was taken from the literature [119] and it started with the Diels-Alder reaction of cyclooctatetraene with maleimide. Cyclooctatetraene, stable at room temperature, possesses a valence isomer, bicyclo[4.2.0]octa-2,4,7-triene, and just like cyclohepatriene (see page 70) the tautomerization is triggered thermally (Scheme 18).
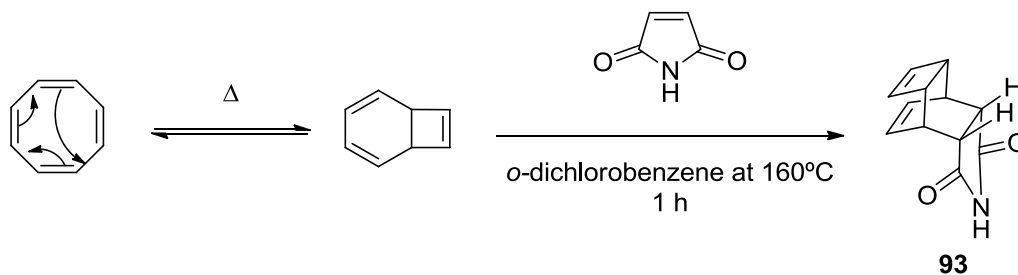
Scheme 18. Diels-Alder reaction between bicyclo[4.2.0]octa-2,4,7-triene and maleimide

Again the *endo-* product was formed due to the bonding interaction between the carbonyl and the developing π-bond of bicyclo[4.2.0]octa-2,4,7-triene, inexistent in the *exo-* isomer (Scheme 19)[115].
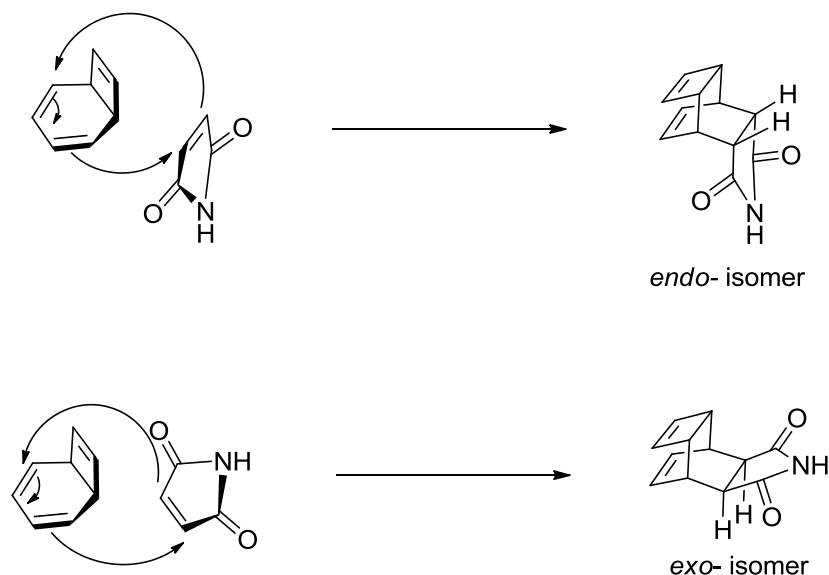
Scheme 19. Difference between the *exo-* and the *endo-* isomer in the Diels-Alder reaction of bicyclo[4.2.0]octa-2,4,7-triene and maleimide

---

[119] Arya, V. P.; Shenoy, S. J. *Indian J. Chem., Sect. B.* **1976**, *14*, 780.

Because our goal was to elongate the scaffold synthesized by M. Barniol, the 4-azatetracylo[5.4.2.0^{2,6}.0^{8,11}]tridecane, we tried different dienes for a Diels-Alder reaction with imide **93**. We expected that the energy gain from the "strain release" of the cyclobutene ring (dienophile) under conditions of high pressure and temperature, would be sufficient for driving the reaction equilibrium to the products side, even if the diene was not activated. Thus we reacted imide **93** with butadiene and 1,3-dimethylbutadiene in a pressure reactor at 120°C for 20 hours. Unfortunately no reaction occurred (Scheme 20).
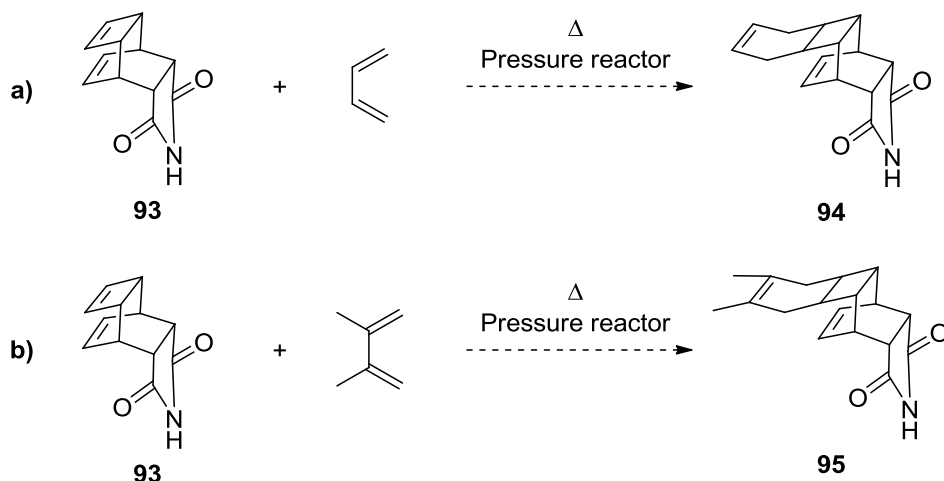
Scheme 20. Diels-Alder reactions of imide **93** with **a)** butadiene and **b)** 1,3-dimethylbutadiene

Our first thought was that since butadiene is a gas at room temperature, maybe the build up of pressure was preventing the reaction. Moreover, butadiene being sold dissolved in toluene, the control over its actual concentration was complicated. In order to avoid the pressure coming from this source and trying to get a better handle of its concentration, we decided to react imide **93** with 3-sulfolene, a reagent known to release butadiene upon heating, through a cheleotropic reaction (when two σ bonds terminating at a single atom are made or broken in concert) (Scheme 21).[120] Regrettably, this reaction did not yield the cycloaddition product **94** either.
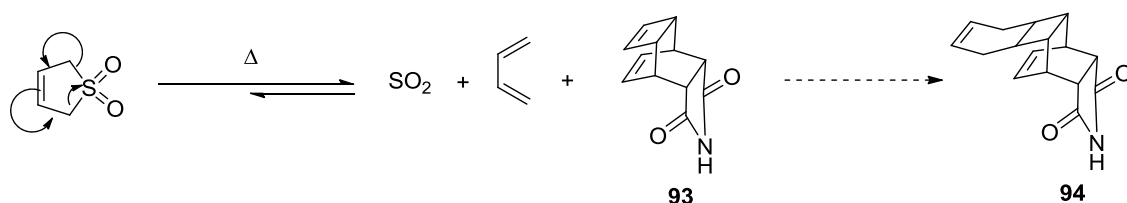
Scheme 21. Diels-Alder reaction of 3-sulfolene with imide **93**

---

[120] a) Drake, L. R.; Stowe, S. C.; Partansky, A. M. *J. Am. Chem. Soc.* **1946**, *68*, 2521. b) Woodward, R. B.; Hoffmann, R. *Angew. Chem. Int. Ed. Engl.* **1969**, *8*, 781.

We thought the problem came from the very poor reactivity of the used dienes, hard to overcome even with our harsh conditions. So we looked for a more reactive diene: cyclopentadiene (Cp). This one owes its instability to the 4π electrons in a five-membered ring and prefers to dimerize at room temperature to yield the more stable dicyclopentadiene (Scheme 22a). In order to obtain the monomer, the latter has to be cracked at 160 ºC and cyclopentadiene is collected by distillation (Scheme 22b). It is a highly reactive diene in the Diels-Alder reaction.[121]
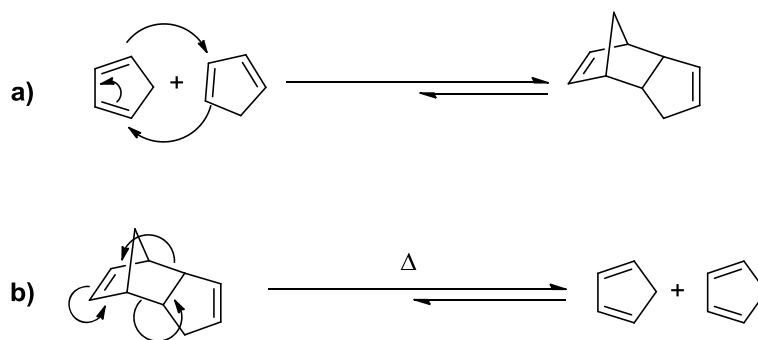
Scheme 22. a) Diels-Alder reaction at room temperature of cyclopentadiene to produce dicyclopentadiene. **b)** Retro Diels-Alder at 160 ºC of dicyclopentadiene to obtain cyclopentadiene

Thus imide **93** was reacted with Cp in a Diels-Alder reaction. The high reactivity of Cp and the gain in energy through "strain release" in the strained cyclobutene ring in imide **93**, led us think that this time the Diels-Alder reaction could be possible.

Disappointingly, our first attempt only yielded the unreacted starting materials (entry 1 in Table 6). Then we switched to the microwave apparatus (μW) because we thought that the conditions that can be applied in the machine might suit our reaction. We could not use toluene, our first choice until then for the Diels-Alder reactions, since it does not absorb very well microwave radiation, so we choose *o*-dichlorobenzene due to its unique features as a solvent, combining good microwave absorbing capacity and good solubilisation of the highly lipophilic imide **93** and Cp as well. Our first experiment yielded only the starting materials (entry 2) but we imagined that the sensibility of the solvent to microwaves could be impaired by water, so we removed it from the solvent through distillation. To our satisfaction, when using dry *o*-dichlorobenzene we obtained **96** in low yield (entry 3). By extending the reaction time we improved the yield (entry 4) but sadly the reaction was not scalable with the available microwave equipment (entry 5).

---

[121] Magnusson, G. *J. Org. Chem.* **1985**, *50*, 1998.

Table 6. Different conditions for the Diels-Alder reaction of imide **93** and cyclopentadiene

Entry	Imide 93	Cp	Solvent	Setup	Yield
1	200 mg (1 eq)	0.33 mL (4 eq)	Toluene	Pressure reactor (120°C)	-
2	200 mg (1 eq)	1.30 mL (15 eq)	*o*-dichlorobenzene	μW (210°C) 30 min	-
3	200 mg (1 eq)	1.30 mL (15 eq)	Dry *o*-dichlorobenzene	μW (210°C) 30 min	17%
4	200 mg (1 eq)	1.30 mL (15 eq)	Dry *o*-dichlorobenzene	μW (210°C) 120 min	81%
5	3.60g (1 eq)	22.4 mL (15 eq)	Dry *o*-dichlorobenzene	μW (210°C) 120 min	-

Most discouraging was the fact that the reaction yielded two stereoisomers (Scheme 23) in a 95:5 ratio (determined by GC-MS), inseparable through column chromatography. If we had continued the synthesis with such a mixture, we would have never known which isomer was responsible for how much antiviral activity, so we decided to abandon this synthetic route.
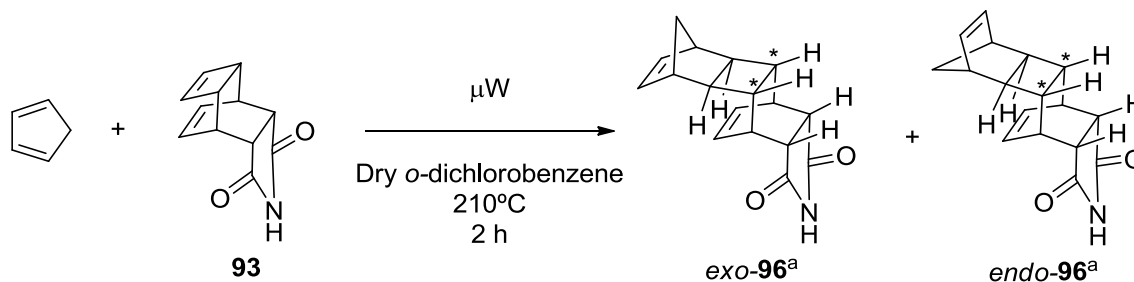
Scheme 23. Diels-Alder reaction between Cp and imide **93** producing *exo*- and *endo*-**96**. [a]*Exo*- and *endo*- adducts refers to the carbon substituents (*) of the dienophile.

3.2 Synthesis: 14-azaheptacyclo[8.6.1.0^{2,5}.0^{3,11}.0^{4,9}.0^{6,17}.0^{12,16}]heptadecane and related compounds

This last failure did not discourage us to persist in the quest of longer derivatives of the 4-azatetraclo[5.4.2.0^{2,6}.0^{8,11}]tridecane scaffold. By the means of another Diels-Alder reaction we found that we could access the 14-azaheptacyclo[8.6.1.0^{2,5}.0^{3,11}.0^{4,9}.0^{6,17}.0^{12,16}]heptadecane structure that, even if not being as long as the previously described scaffold, had still some appealing features (Figure 65).
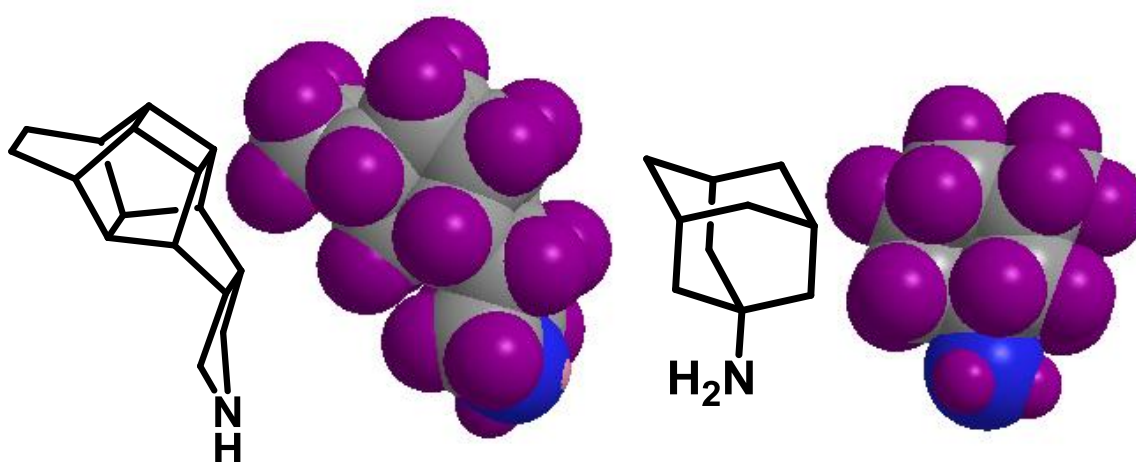
Figure 65. Qualitative space filling models of 14-azaheptacyclo[8.6.1.0^{2,5}.0^{3,11}.0^{4,9}.0^{6,17}.0^{12,16}]heptadecane and amantadine. Hydrogen atoms are shown in purple. Source: ChemBio3D Ultra. Energy minimized through MM2.

This new skeleton was longer from the amine to the furthest carbon of the polycycle, on a straight line, (5.91 Å) than amantadine (4.30 Å) but the approximate width of the polycyclic cage when the amine was along the y-axis (2.60/2.85 Å) was inferior to amantadine (2.95 Å). This structure was thought to penetrate deeper in the channel targeting the lower binding site at Gly34[52b] but the tilt of the molecule may render it wider, and although knowing that the wt-M2 can accommodate larger molecules than amantadine it might be possible that not enough space is available for such a big compound. In any case, we desired to test the effect of wide compounds like this one in the V27A mutant, displaying an enlarged cavity (Figure 66).
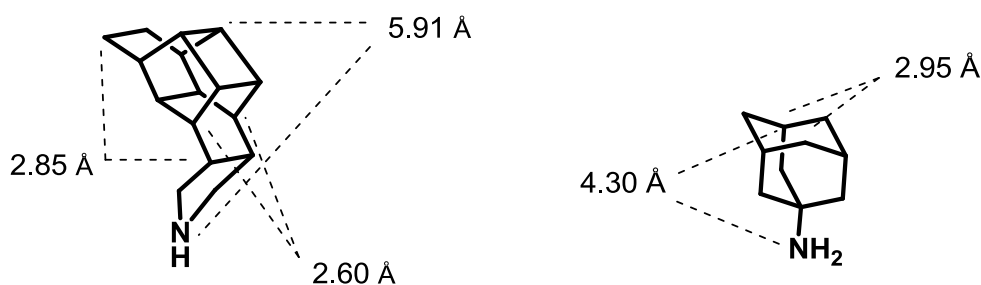
Figure 66. Most representative distances of 14-azaheptacyclo[8.6.1.0^{2,5}.0^{3,11}.0^{4,9}.0^{6,17}.0^{12,16}]heptadecane and amantadine. Source: ChemBio3D Ultra. Energy minimized through MM2

The synthesis was based on the work of Srikrishna[122] and started by using the same imide **93** previously described. This one was subjected to a Diels-Alder reaction with neat 5,5-dimethoxy-1,2,3,4-tetrachlorocyclopentadiene, and the reaction mixture was heated in a pressure reactor. The Diels-Alder adduct was obtained in 89% yield (Scheme 24).
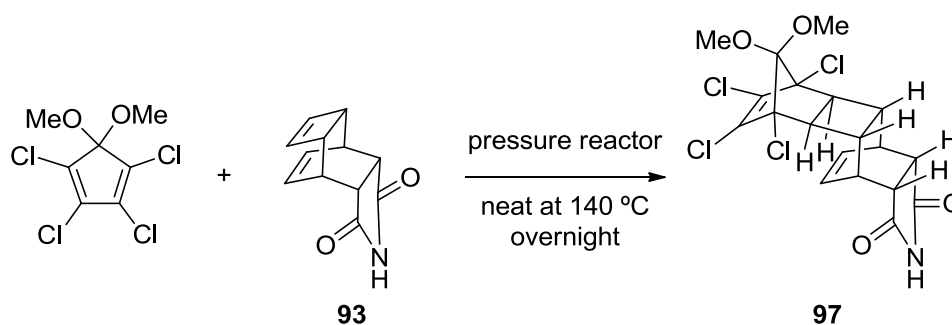
Scheme 24. Diels-Alder reaction between 5,5-dimethoxy-1,2,3,4-tetrachlorocyclopentadiene and imide **93**

Then, again following the procedure described by Srikrishna,[122] the chlorine atoms and the ketal were removed in a one-pot dechlorination/ deprotection reaction. The first part, the dechlorination, took place in liquid ammonia at -60 °C with sodium. When these reagents are mixed, they form a salt in which the electrons are the anion (electride salt) giving the solution an intense blue colour;[123] these free electrons are the active species of the reaction. They added to **97** thus forming a radical anion that subsequently expelled a chloride anion to give a radical. Another free electron is then added to form the anion which in turn picked a proton from methanol, ammonia not being acidic enough.[124] The reaction continued until all the chlorine atoms were removed from **97** (Scheme 25).

---

[122] Srikrishna, A. *Synth. Commun.* **1990**, *20*, 279.

[123] Dye, J. L. *Science* **2003**, *301*, 607.

[124] Smith, M. B.; March, J. *March's Advanced Organic Chemistry*, 6th ed.; Wiley: New Jersey, 2007.
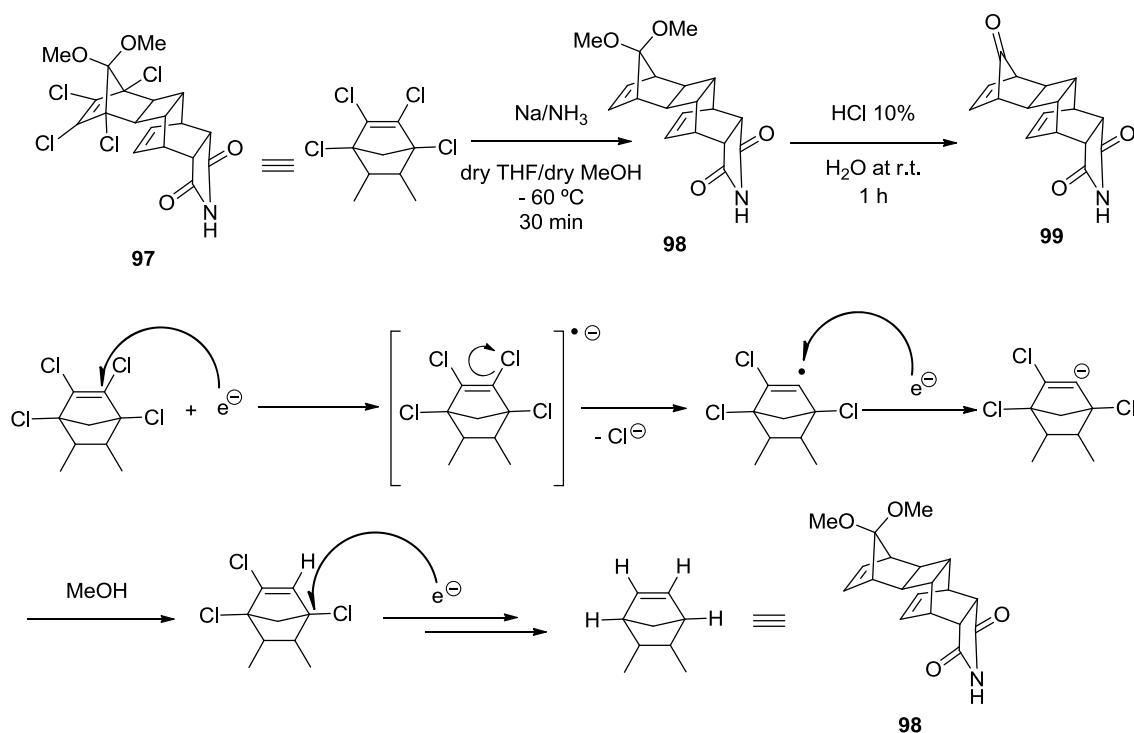
Scheme 25. Dechlorination reaction of **97**

As already stated, compound **98** was not isolated and with an acidic work-up the ketal was deprotected to produce **99** in 41% yield over the two steps (Scheme 26).
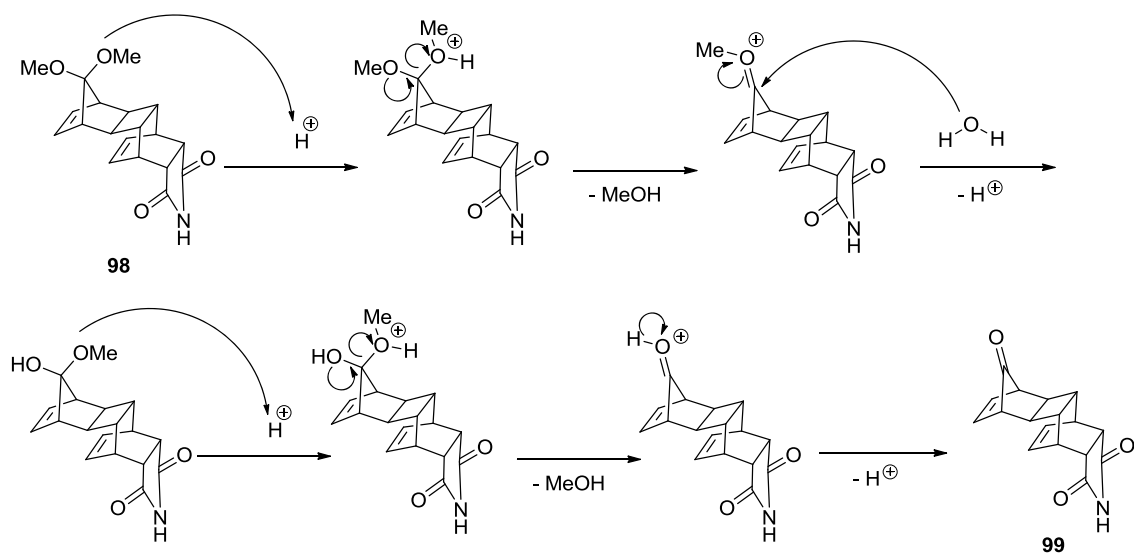
Scheme 26. Ketal deprotection of **98**

The next step of the route was also described in the literature [122] and consisted of a one-pot thermal decarbonylation followed by an intramolecular Diels-Alder reaction. The reaction was set in a pressure reactor in the presence of hydroquinone as an antioxidant, and was heated to 180 ℃. The first step was the thermal decarbonylation that produced the non-isolated intermediate **100** which underwent two disrotatory retroelectocyclic rearrangements that provided a molecule with the suitable configuration for the intramolecular Diels-Alder reaction. These harsh conditions led to **101** in 44% yield (Scheme 27).
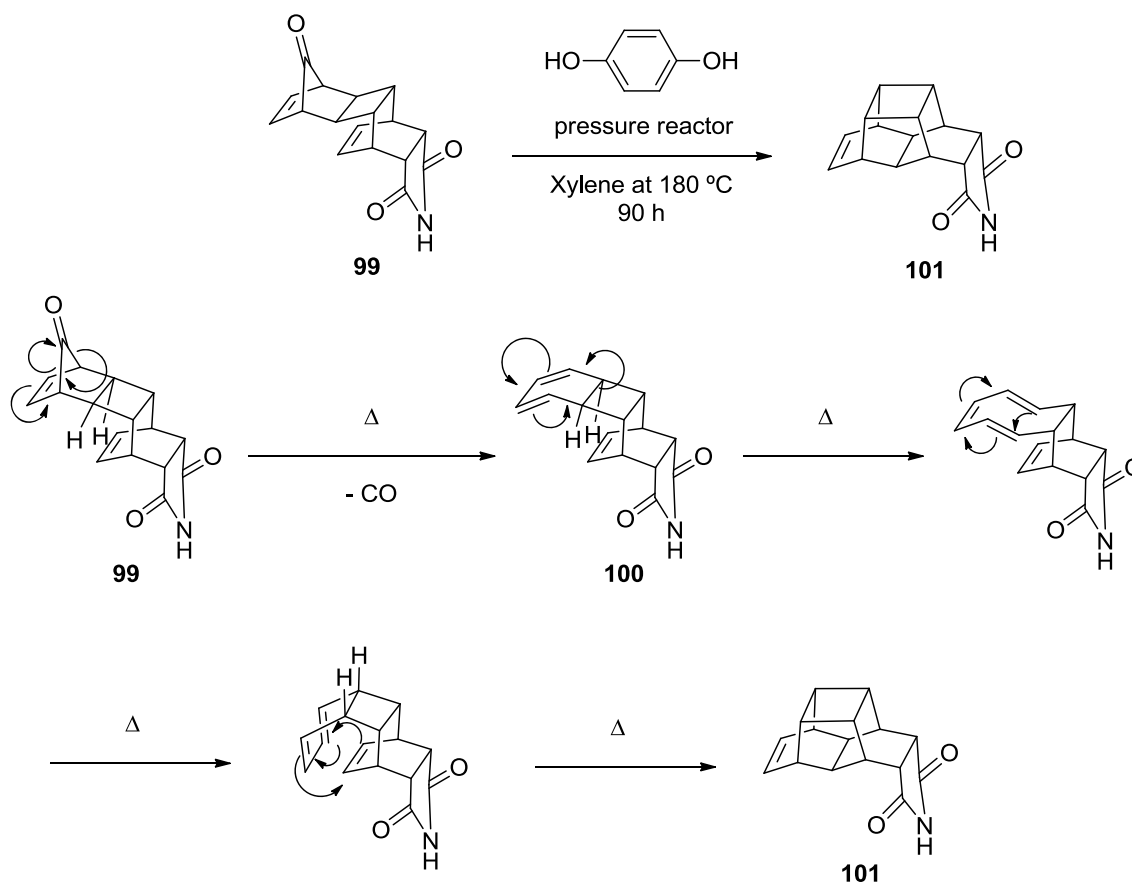
Scheme 27. Decarbonylation and intramolecular Diels-Alder reactions of **99**

Imide **101** was then subjected to a reduction process with Red-Al® in order to get amine **102** that was readily converted to its hydrochloride salt **102·HCl** in 74% yield (Scheme 28).
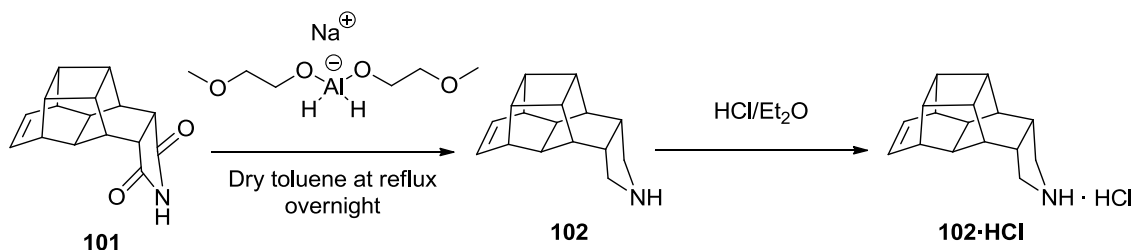
Scheme 28. Reduction of **101** and subsequent conversion to hydrochloride salt

This one was in turn submitted to a hydrogenation with palladium on activated carbon to produce **103·HCl** with a yield of 79%, and to a guanylation with 1*H*-pyrazole-1-carboxamidine to get guanidine **104·HCl** in a 31% yield. The low yield of the reaction might be due to the partial solubility of the hydrochloride salt in the organic solvent, whence the small precipitation of the salt, an effect magnified by the reduced scale of the reaction (0.3 mmol). Last, amine **103·HCl** was also submitted to a guanylation process to get guanidine **105·HCl** in 42% yield, proving again the solubility problem of this scaffold (Scheme 29).
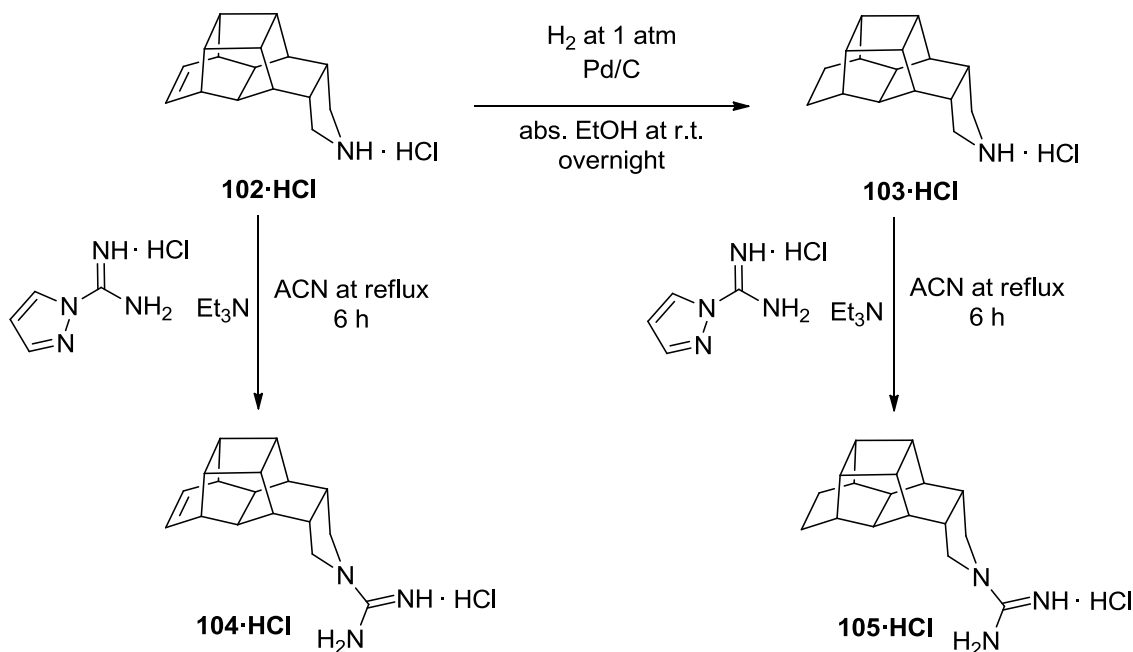
Scheme 29. Hydrogenation of **102·HCl** and guanylation reactions to obtain **104·HCl** and **105·HCl**

3.3 Pharmacology: 14-azaheptacyclo[8.6.1.0^{2,5}.0^{3,11}.0^{4,9}.0^{6,17}.0^{12,16}]heptadecane and related compounds

These compounds were tested as M2 channel blockers of both wild-type and mutants V27A and S31N, by Professor Moroni in the University of Milano. Their activities were determined by the already explained TEVC assay (Table 7).

Table 7. Inhibition of the wt, V27A and S31N M2 channels by 14-azaheptacyclo[8.6.1.0^{2,5}.0^{3,11}.0^{4,9}.0^{6,17}.0^{12,16}]heptadecane derivatives

Compound	wt-M2		V27A-M2		S31N-M2	
	%inh.[a]	IC$_{50}$ (μM)	%inh.[a]	IC$_{50}$ (μM)	%inh.[a]	IC$_{50}$ (μM)
Amantadine	91.0 ± 2.1	16.0 ± 1.2	10.8 ± 2.0	ND[b]	35.6 ± 1.5	200 ± 3.5
102.HCl	96.4 ± 1.3	2.6	49.0± 2.8	ND	0	ND
103·HCl	98.1 ± 0.5	2.1	83.9 ± 0.7	17.2	0	ND
104·HCl	89.6 ±0.9	6.5	54.0 ±0.6	ND	0	ND
105·HCl	90.6 ± 3.1	3.7	71.2 ± 3.9	32.2	4.7 ± 0.7	ND

[a]Percentage inhibition at 100 μM for 2 min. Average of at least three experiments.
[b]ND: not determined.

Satisfyingly, amines **102·HCl** and **103·HCl** and guanidines **104·HCl** and **105·HCl** inhibited the wt-M2 better than amantadine. The most active compound, amine **103·HCl**, displayed an activity against wt-M2 one order of magnitude lower than amantadine. Although only by a small difference, the saturated compounds were slightly more active than the unsaturated ones. Interestingly, as we will see along the study of the different related polycycles, this family is the only one with guanidines performing worst than amines in the TEVC assay. This effect might be due to the scaffold being longer and the amine moiety already occupying the volume limit of the wt-M2 channel lumen, thus the lengthening with a guanidine group would be deleterious to the activity by provoking steric clashes with the pore lining residues.

Regarding the V27A mutant, only the saturated molecules **103·HCl** and **105·HCl** exhibited a detectable activity as M2 channel blockers, so the saturated compounds were more active than their unsaturated counterparts. Inexplicably though, amine **103·HCl** was more active than its guanidine derivative **105·HCl** against this mutant, when the contrary was logically expected. Gratifyingly, at least one compound, amine **103·HCl** was more active against the V27A mutant than its predecessor **92·HCl** (17.2 μM vs. 22.6 μM), implying our hypothesis was right, the 4-azatetraclo[5.4.2.0^{2,6}.0^{8,11}]tridecane scaffold was not fully optimized regarding the V27A mutant.

Therefore some intriguing trends could be deduced from these data:

- The fully saturated compounds (**103·HCl** and **105·HCl**) were slightly more active against both wt-M2 and V27A than their unsaturated analogues (**102·HCl** and **104·HCl**).

- Surprisingly, amines seemed to be more potent against wt-M2 and the V27A mutant than their guanidine counterparts (**102·HCl** vs. **104·HCl** and **103·HCl** vs. **105·HCl**).

- This fact could be explained for the wt-M2 channel by invoking the big size of the scaffold, but no interpretation of this phenomenon was found so far for the V27A mutant.
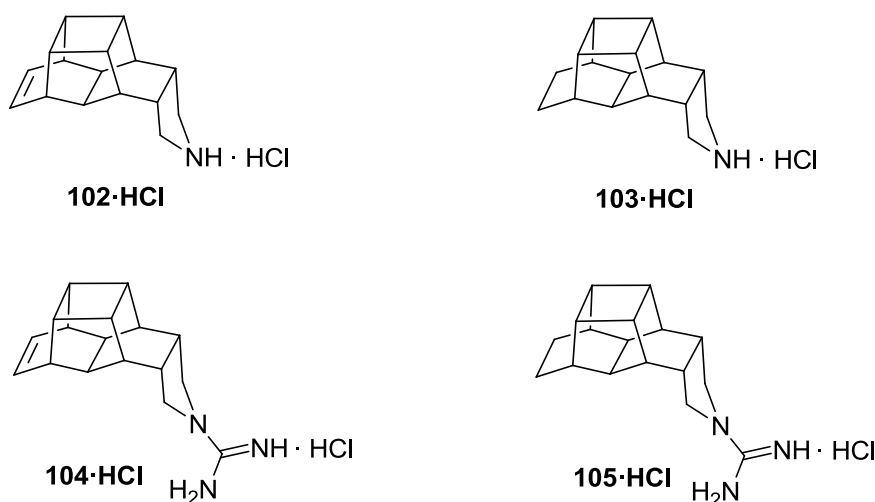
Figure 67. Active compounds against wt-M2 (**103·HCl** and **105·HCl** also active against V27A) in the 14-azaheptacyclo[8.6.1.0^{2,5}.0^{3,11}.0^{4,9}.0^{6,17}.0^{12,16}]heptadecane series

Professor Naesens in the Rega Insitute for Medical Research in Belgium, performed the antiviral and cytotoxicity assays in MDCK cells of this family of compounds, using the same methods described previously (see page 65), against an array of influenza virus strains (Table 8):

- A/PR/8/34 (H1N1): an amantadine-resistant influenza A strain carrying a double mutation on the M2 channel (V27T and S31N).
- A/HK/7/87 (H3N2): an amantadine-sensitive influenza A strain bearing a wild-type M2 channel.
- B/HK/5/72: an amantadine-resistant influenza B strain.

Table 8. Antiviral activity against influenza A and B determined in MDCK cells of 14-azaheptacyclo[$8.6.1.0^{2,5}.0^{3,11}.0^{4,9}.0^{6,17}.0^{12,16}$]heptadecane series

| Compound | Antiviral EC$_{50}$^{a} (µM) | | | | | | Toxicity |
| | Influ. A (H1N1) | | Influ. A (H3N2) | | Influenza B | | MCC^b |
	CPE	MTS	CPE	MTS	CPE	MTS	
Amantadine	138	203	0.45	0.50	>500	>500	>500
102.HCl	>100	>100	>100	>100	>100	>100	20
103·HCl	>100	>100	>100	>100	>100	>100	4.0
104·HCl	>100	>100	>100	>100	>100	>100	7.0
105·HCl	>100	>100	>100	>100	>100	>100	2.0

^{a}Effective concentration producing 50% of virus induced cytopathic effect. Values shown are the mean of 2-3 determinations.

^{b}Minimum compound concentration causing minimal changes in cell morphology.

Frustratingly, the antiviral assays did not reveal any activity at all among the tested compounds and to make matters worse, all the molecules of this series displayed some cytotoxicity. Guanidines seemed to be more cytotoxic than their parent amines (**102·HCl** vs. **104·HCl** and **103·HCl** vs. **105·HCl**). The fully saturated compounds were also more cytotoxic than their unsaturated counterparts (**102·HCl** vs. **103·HCl** and **104·HCl** vs. **105·HCl**). As expected, none of the assayed compounds were active against influenza B.

To sum up the results of the TEVC and the antiviral assays of this family of compounds, we could retain that:

- Although an unexpected behaviour was detected between amines and guanidines, all the tested compounds, i.e. **102·HCl**, **103·HCl** **104·HCl** and **105·HCl** exhibited M2 channel blocking activities against wt-M2.

- Saturated amine **103·HCl** and saturated guanidine **105·HCl** were active against V27A, amine **103·HCl** being more active than its simpler analogue guanidine **92·HCl**.

- None of the compounds were active in the cell culture assays and all of them were cytotoxic.

- Regarding cytotoxicity, guanidines were more cytotoxic than amines and the saturated compounds were more cytotoxic than the unsaturated ones.
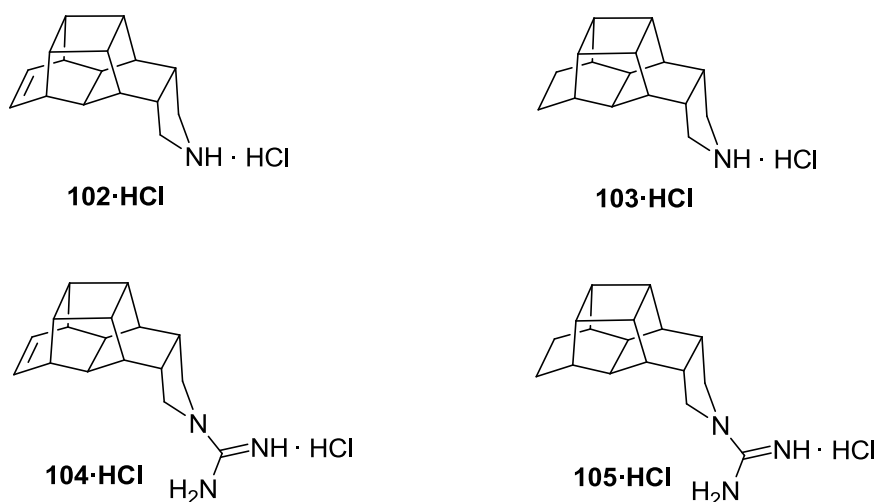
Figure 68. Active compounds as M2 channel blockers but not active through antiviral assays in the 14-azaheptacyclo[8.6.1.0^{2,5}.0^{3,11}.0^{4,9}.0^{6,17}.0^{12,16}]heptadecane series

4. The longest and more active compounds against V27A

4.1 Synthesis: 7,8-disubstituted 3-azatetracyclo[5.2.1.1^{5,8}.0^{1,5}]undecane

As already mentioned before, Dr. E. Torres had synthesized during her Ph.D. thesis some bisnoradamantane derivatives (see Figure 38) that had yielded promising activities against the V27A mutant channel (Figure 69).[102]

65·HCl
IC$_{50}$ wt = 11.7 μM
% inh. V27A = 6%[a]

66·HCl
IC$_{50}$ wt = 1.1 μM
% inh. V27A = 0%[a]

69·HCl
IC$_{50}$ wt = 9.7 μM
% inh. V27A = 26%[a]

70·HCl
IC$_{50}$ wt = 6.1 μM
% inh. V27A = 84%[a]
IC$_{50}$ V27A = 11.4 μM
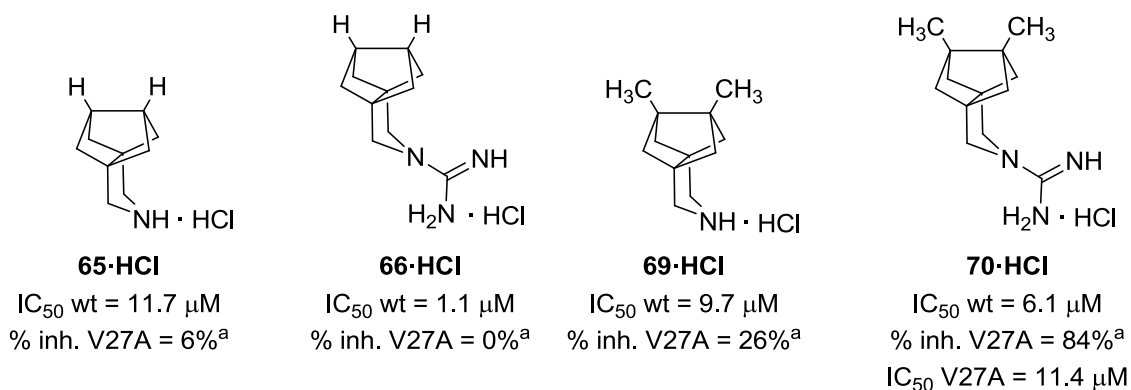
Figure 69. Bisnoradamantanes synthesized by Dr. E. Torres. [a]Determined by TEVC in *Xenopus laevis* frog oocytes at 100 μM for 2 min.

Taking into account that the longer compounds **69·HCl** and **70·HCl** were more potent against the V27A mutant channel than the unsubstituted **65·HCl** and **66·HCl**, logically, the next step was to develop even longer derivatives, always maintaining the pyrrolidine moiety. Hence, we first thought of switching the methyl groups of the bridgehead positions to ethyl groups. This furnished the 7,8-diethyl-3-azatetracyclo[5.2.1.1^{5,8}.0^{1,5}]undecane scaffold (Figure 70).
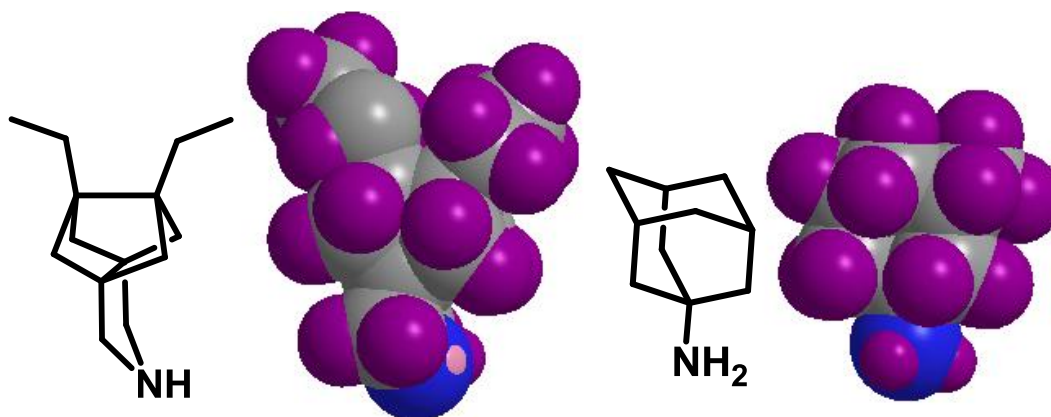
Figure 70. Qualitative space filling models of 7,8-diethyl-3-azatetracyclo[5.2.1.1^{5,8}.0^{1,5}]undecane and amantadine. Hydrogen atoms are shown in purple. Source: ChemBio3D Ultra. Energy minimized through MM2.

This new structure was difficult to appraise due to the free rotation inherent to the ethyl group. We supposed it to be at its lowest energetic level inside the M2 channel, that is with a conformation that sets the methyl groups of the ethyl moiety away from each other. In any case, the 7,8-diethyl-3-azatetracyclo[5.2.1.1^{5,8}.0^{1,5}]undecane scaffold could be wider or not, depending on the orientation of the molecule, (3.07/2.31 Å) than amantadine (2.95 Å) but it was always longer, from the amine to the furthest carbon (7.01 Å, in this conformation) than amantadine (4.30 Å). With this scaffold we desired to assess the effect of the free rotation of the ethyl groups on the entry gate (Ala27, Ala30/Ser31) of the larger V27A mutant, whilst maintaining the longitude of the molecule, always targeting the Gly34 binding site (Figure 71).[52b]
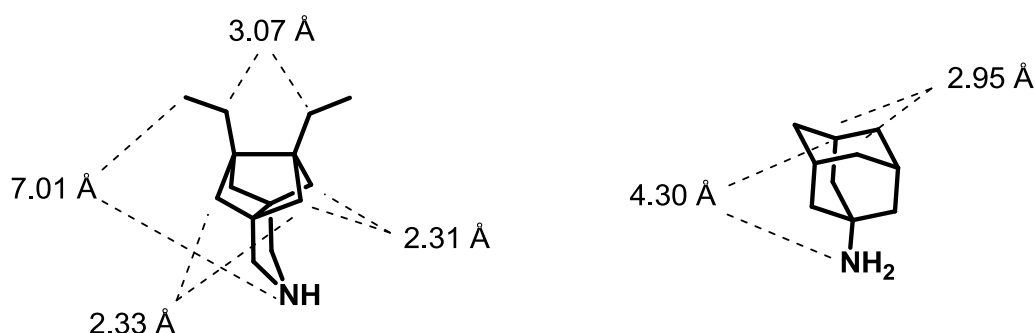
Figure 71. Most representative distances of 7,8-diethyl-3-azatetracyclo[5.2.1.1^{5,8}.0^{1,5}]undecane and amantadine. Source: ChemBio3D Ultra. Energy minimized through MM2

In a second approach, we decided to synthesize a more rigid structure: the 12-azapentacyclo[6.5.1.1^{3,10}.0^{1,10}.0^{3,8}]pentadecane scaffold (Figure 72).
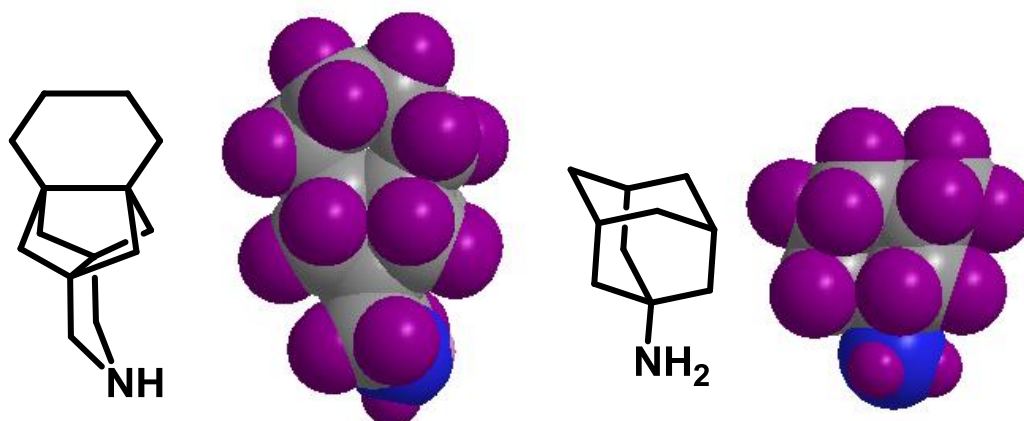
Figure 72. Qualitative space filling models of 12-azapentacyclo[6.5.1.1^{3,10}.0^{1,10}.0^{3,8}]pentadecane and amantadine. Hydrogen atoms are shown in purple. Source: ChemBio3D Ultra. Energy minimized through MM2.

This scaffold was also much longer from the amine to the furthest carbon of the polycycle (6.64 Å) than amantadine (4.30 Å) but this time the rigidity of the upper part of the molecule provided a frozen conformation of a small chair-like twist of the cyclohexane ring. The width of the molecule (2.36/3.07 Å) could be similar or less than amantadine (2.95 Å) depending on the orientation of the compound. The goal of this scaffold was again to target the lower binding site at Gly34,[52b] and to appraise the effect the wider upper part of the molecule could have on the entry gate of the V27A mutant. This structure was more rigid than the previous one to evaluate the influence of rigidity against the free rotation of the ethyl moieties (Figure 73).
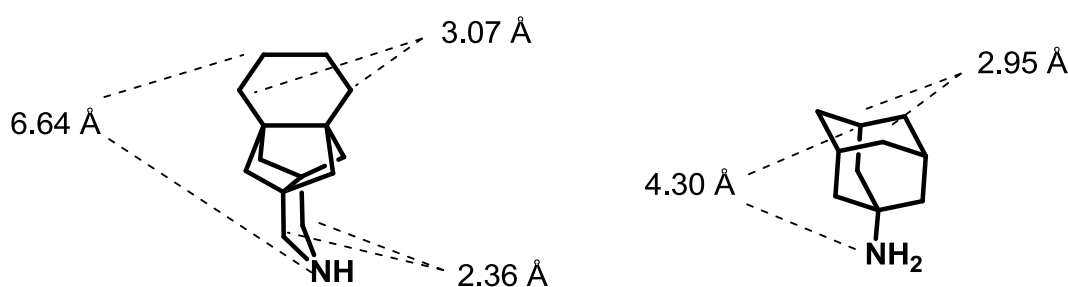
Figure 73. Most representative distances of 12-azapentacyclo[6.5.1.1^{3,10}.0^{1,10}.0^{3,8}]pentadecane and amantadine. Source: ChemBio3D Ultra. Energy minimized through MM2

The synthetic route was inspired from a previous work of the group and was applied to both the 7,8-diethyl-3-azatetracyclo[5.2.1.1^{5,8}.0^{1,5}]undecane and the 12-azapentacyclo[6.5.1.1^{3,10}.0^{1,10}.0^{3,8}]pentadecane scaffolds.[125]

The first step was the preparation of diketones **108** and **109** through a Weiss-Cook condensation in a multigram scale. The reaction consisted in the condensation of two equivalents of dimethyl-1,3-acetonedicarboxylate and an α-dicarbonylic compound, either 3,4-hexanedione or 1,2-cyclohexanedione. The reaction was set in basic media and took advantage of the keto-enol tautomerism of dimethyl-1,3-acetonedicarboxylate to furnish, after two consecutive aldol condensations, the 1:1 adduct, never isolated. The reaction progressed with two Michael additions of the second equivalent of the β-ketoester to produce the dienol-tetraester **106** and **107** (Scheme 30).[126]

---

[125] Ayats, C.; Camps, P.; Duque, M. D.; Font-Bardia, M.; Muñoz, M. R.; Solans, X.; Vázquez, S. *J. Org. Chem.* **2003**, *68*, 8715.

[126] a) Weiss, U.; Edwards, J. M. *Tetrahedron Lett.* **1968**, *47*, 4885. b) Yang, S.; Cook, J. M. *J. Org. Chem.* **1976**, *41*, 1903. c) Bertz, S. H.; Cook, J. M.; Gawish, A.; Weiss, U. *Org. Synth.* **1986**, *64*, 27.
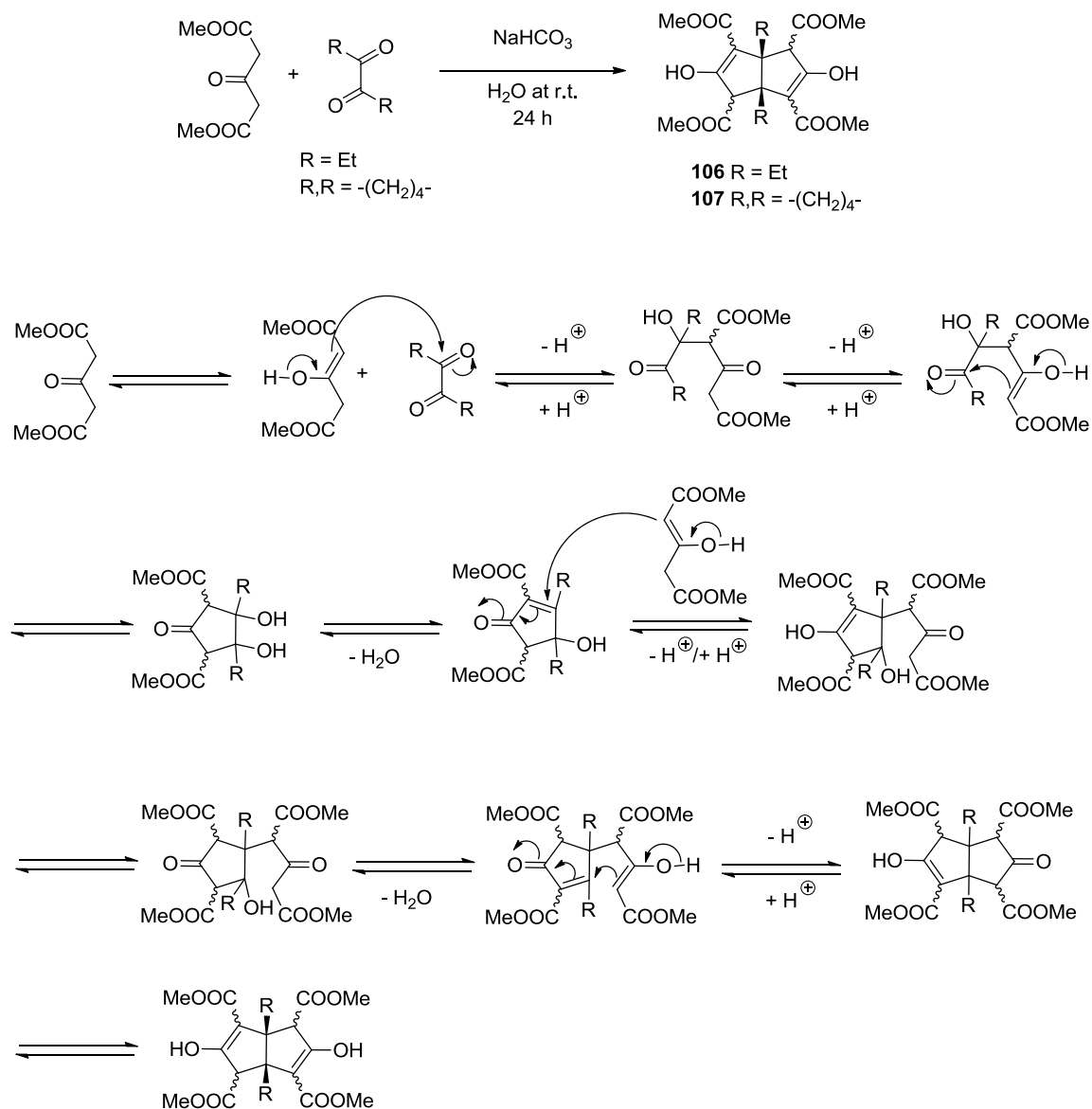
Scheme 30. Weiss-Cook condensation of dimethyl-1,3-acetonedicarboxylate and 3,4-hexanedione or 1,2-cyclohexanedione

Dienol-tetraesters **106** and **107** were used without purification in the next reaction; an acid hydrolysis followed by a decarboxylation. This process furnished diketones **108** and **109** in an overall 42% and 50% yield, respectively calculated from diketones 3,4-hexanedione or 1,2-cyclohexanedione (Scheme 31).[127]

---

[127] a) Weber, R. W.; Cook, J. M. *Can. J. Chem.* **1978**, *56*, 189. b) Makhseed, S.; McKeown, N. B. *Chem. Commun.* **1999**, 255.
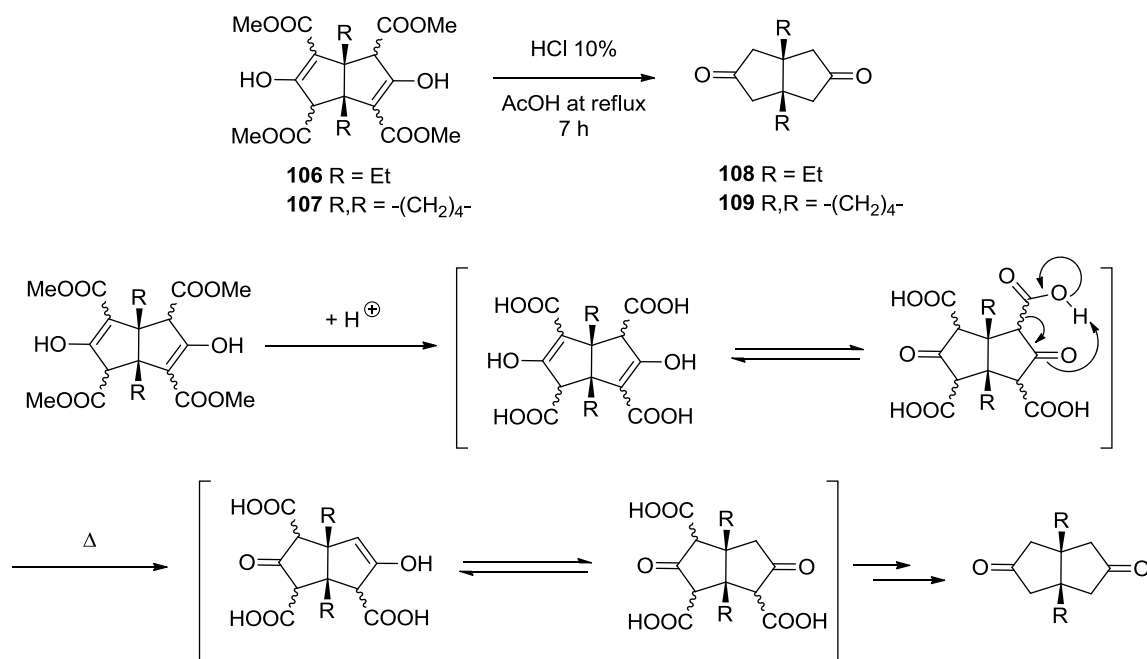
Scheme 31. Acid hydrolysis and decarboxylation reactions of dienol-tetraesters **106** and **107**

The synthesis continued with the preparation of hydrazone derivatives using hydrazine monohydrate. This simple nucleophilic attack produced hydrazones **110** and **111** in 87% and 99% yield, respectively (Scheme 32). These ones were transformed into vinyl iodides in the presence of iodine and tetramethylguanidine (TMG) as a base, through the Barton vinyl iodine reaction. The reaction begins with the iodine oxidation of the hydrazone to a diazo compound. Further N_2 elimination and deprotonation gives the vinyl iodide.[128] Mixtures of *syn-* and *anti*-vinyl iodides **112** and **113** were obtained in 47% and 57% yield respectively (Scheme 32).

The medium yields of both reactions can be explained by the possible formation of undesired products from the reactive carbocation: it could give the azine product from the reaction with the starting hydrazone, the geminal diiodide product from the reaction with iodine and the ketone from the reaction with water (Scheme 32). To minimise these side reactions, Barton and co-workers investigated the factors that should favour the formation of the vinyl iodide over the undesired products and found that, among other reasons, the use of a strong, highly hindered, non-nucleophilic base such as TMG was very important.[128]

[128] a) Barton, D. H. R.; Bashiardes, G.; Fourrey, J.-L. *Tetrahedron Lett.* **1983**, *24*, 1605. b) Barton, D. H. R.; Bashiardes, G.; Fourrey, J. *Tetrahedron* **1988**, *44*, 147. c) Barton, D. H. R.; Chen, M.; Jászberényi, J. C.; Taylor, D. K.; Hartz, R. A.; Smith, A. B. *Org. Synth.* **1997**, *74*, 101.
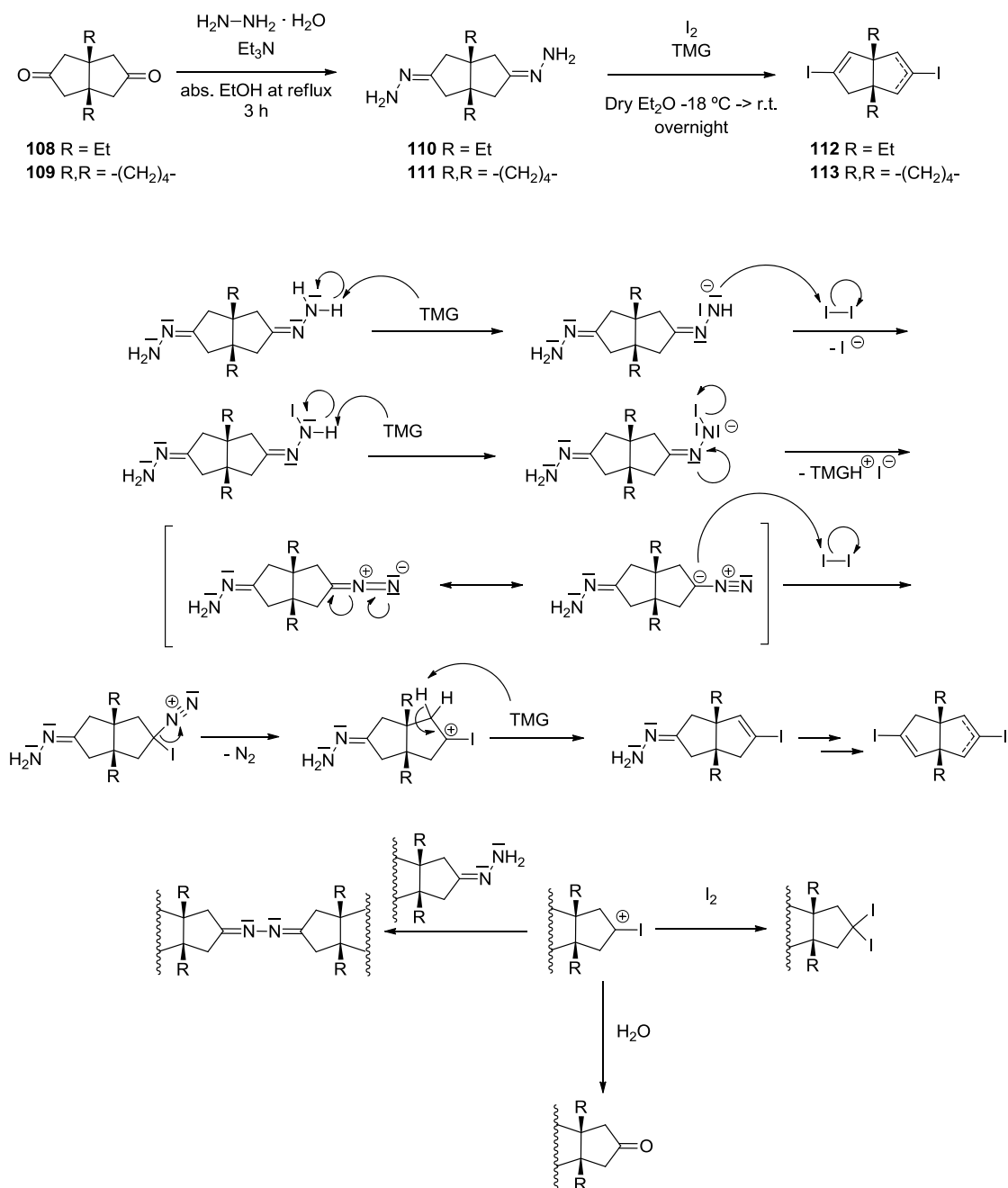
Scheme 32. Barton vinyl iodine reaction of hydrazones **109** and **110** and side-reactions

Following the group procedure,[125] the *syn-* and *anti-*mixtures of both vinyl iodides **112** and **113** were transformed into the *syn-* and *anti-*mixtures of the methyl esters **114** and **115** through a methoxycarbonylation using a palladium(II) catalyst. The reaction starts with the reduction, by triethylamine, of Pd(II) to the reactive species Pd(0). Then begins a catalytic cycle whose actual mechanism is still debated; an illustrative one develops as follows.[129]

---

[129] a) Schoenberg, A.; Bartoletti, I.; Heck, R. F. *J. Org. Chem.* **1974**, *39*, 3318. b) Barnard, C. F. J. *Organometallics* **2008**, *27*, 5402.

First, an oxidative addition of the vinyl iodide takes place reforming a Pd(II) species. The latter then undergoes a carbonyl insertion into its coordination sphere, modifying this one from a square planar to a trigonal bipyramidal geometry. The carbonyl moiety is then inserted into the coordinated alkene forming an acyl group that next suffers a nucleophilic attack from the solvent, methanol. This attack expels the desired ester and produces a hydrido-palladium complex that endures a reductive elimination to reform the catalyst, ejecting HI neutralized by the base.[129] This reaction furnished the *syn*- and *anti*-mixtures of the diesters **114** and **115** in 62% and 64% yield, respectively (Scheme 33).
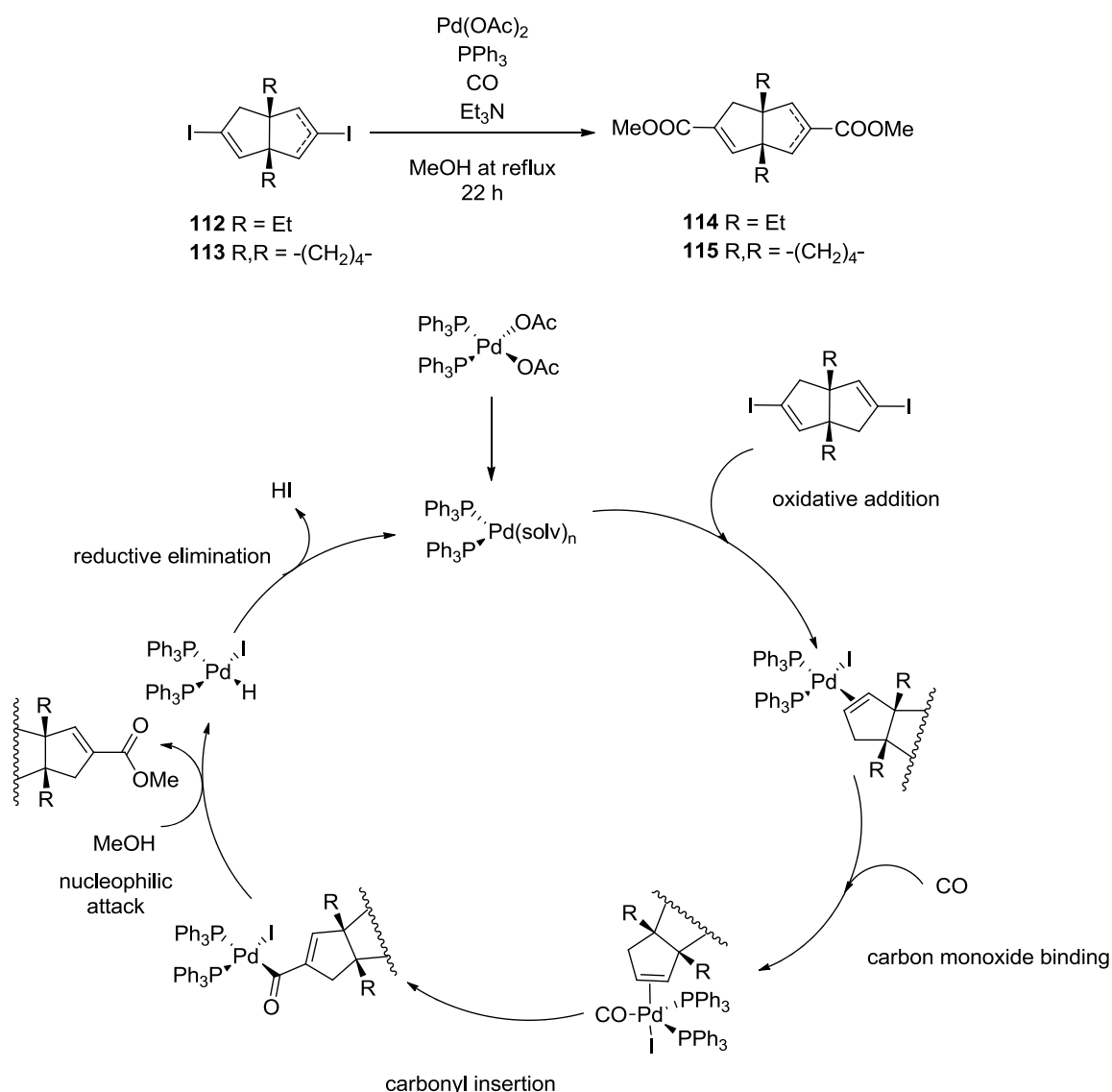
Scheme 33. Methoxycarbonylation reaction of vinyl iodides **112** and **113**

The next step was a very slow catalytic hydrogenation, due to the steric congestion around the double bonds, of the vinylic diesters **114** and **115** that produced a more complex mixture of *exo,endo-* , *endo,endo-*, and *exo,exo-* saturated diesters **116** and **117** in 77% and 74% yield, respectively (Scheme 34).
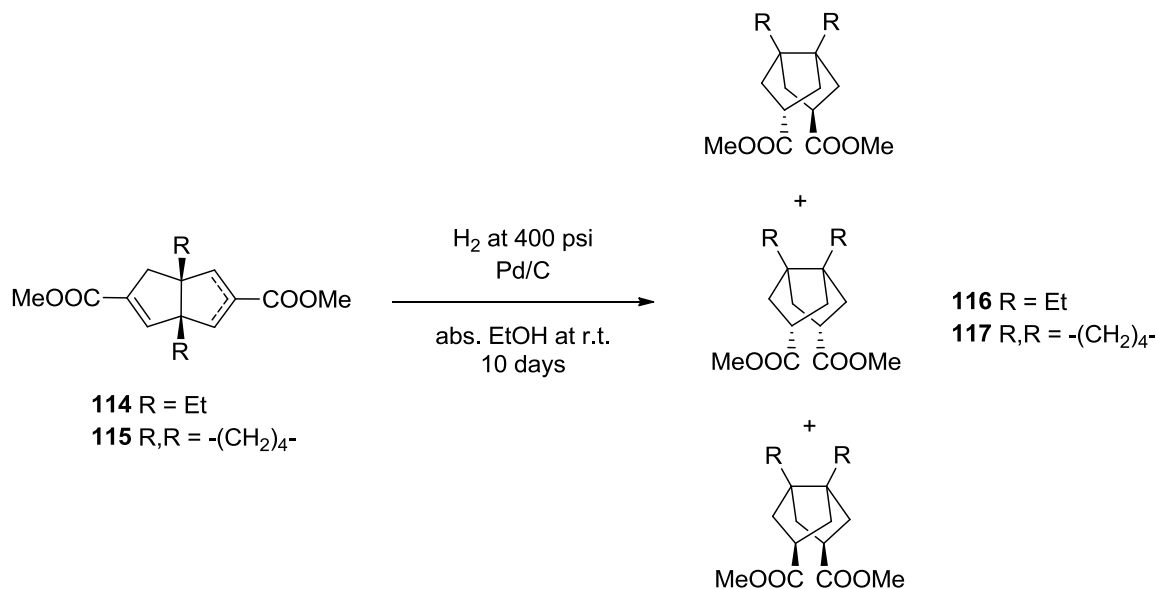
Scheme 34. Hydrogenation of the vinylic diesters **114** and **115** that yielded a mixture of *exo,endo-* , *endo,endo-*, and *exo,exo-* saturated diesters **116** and **117**

The following reaction was the key step of the whole synthesis; an intramolecular enolate homocoupling of the saturated diesters **116** and **117**. The dimerization of enolates was first described in a seminal work by Ivanoff and Spassoff where they generated the enolate of the sodium salt of a carboxylic acid with a Grignard reagent which was then treated with bromine to give the desired dimer.[130] Hitherto many other methods have been developed, such as: generation of the enolate with lithium *N*-(*tert*-butyl)cyclohexanamide and coupling with copper(II) bromide,[131] heterocoupling of two different enolates generated by lithium diisopropylamide (LDA) and coupled with copper(II) chloride,[132] generation of the enolate, again with LDA, and coupling with iron(III) chloride,[133] or enolate generation with an amine and titanium(IV) chloride or iodine as oxidants.[134] More recently, Baran and co-workers established an heterocoupling method using LDA and either iron(III) or copper(II) as oxidants.[135]

---

[130] Ivanoff, D.; Spassoff, A.; *Bull. Soc. Chim. Fr.* **1935**, *2*, 76-78.

[131] Rathke, M. W.; Lindert, A. *J. Am. Chem. Soc.* **1971**, *93*, 4605.

[132] Ito, Y.; Konoike, T.; Saegusa, T. *J. Am. Chem. Soc.* **1975**, *97*, 2912.

[133] Frazier, R. H.; Harlow, R. L. *J. Org. Chem.* **1980**, *45*, 5408.

[134] Kise, N.; Tokioka, K.; Aoyama, Y.; Matsumura, Y. *J. Org. Chem.* **1995**, *60*, 1100.

[135] a) Baran, P. S.; DeMartino, M. P. *Angew. Chem. Int. Ed. Engl.* **2006**, *45*, 7083. b) DeMartino, M. P.; Chen, K.; Baran, P. S. *J. Am. Chem. Soc.* **2008**, *130*, 11546.

In our particular case, we chose to persist with the method already employed by the group.[125] Our first attempt was with LDA, generated from diisopropylamine and *n*-butyllithium (*n*-BuLi), but the reaction yielded a messy mixture of by-products from side reactions. It could be that the LDA bulkiness was not enough to avoid undesired reactions with iodine.[136] Therefore we switched to hexamethyldisilazane, a much hindered base, whose amide (LiHMDS) was originated also with *n*-BuLi. The actual mechanism of this reaction is still unclear, but it seems that only two different reaction pathways exist. The treatment of the diesters with LiHMDS generated the enolates that could undergo a single electron transfer (SET) process with iodine and form the diradical species that would collapse into the desired polycylic diesters.[135] Alternatively, the enolates could react with iodine via an ionic mechanism and form the iodide that would readily give an intramolecular nucleophilic substitution to afford the polycyclic diesters.[134] All in all, diesters **118** and **119** were obtained with a 47% and 57% yield, respectively.
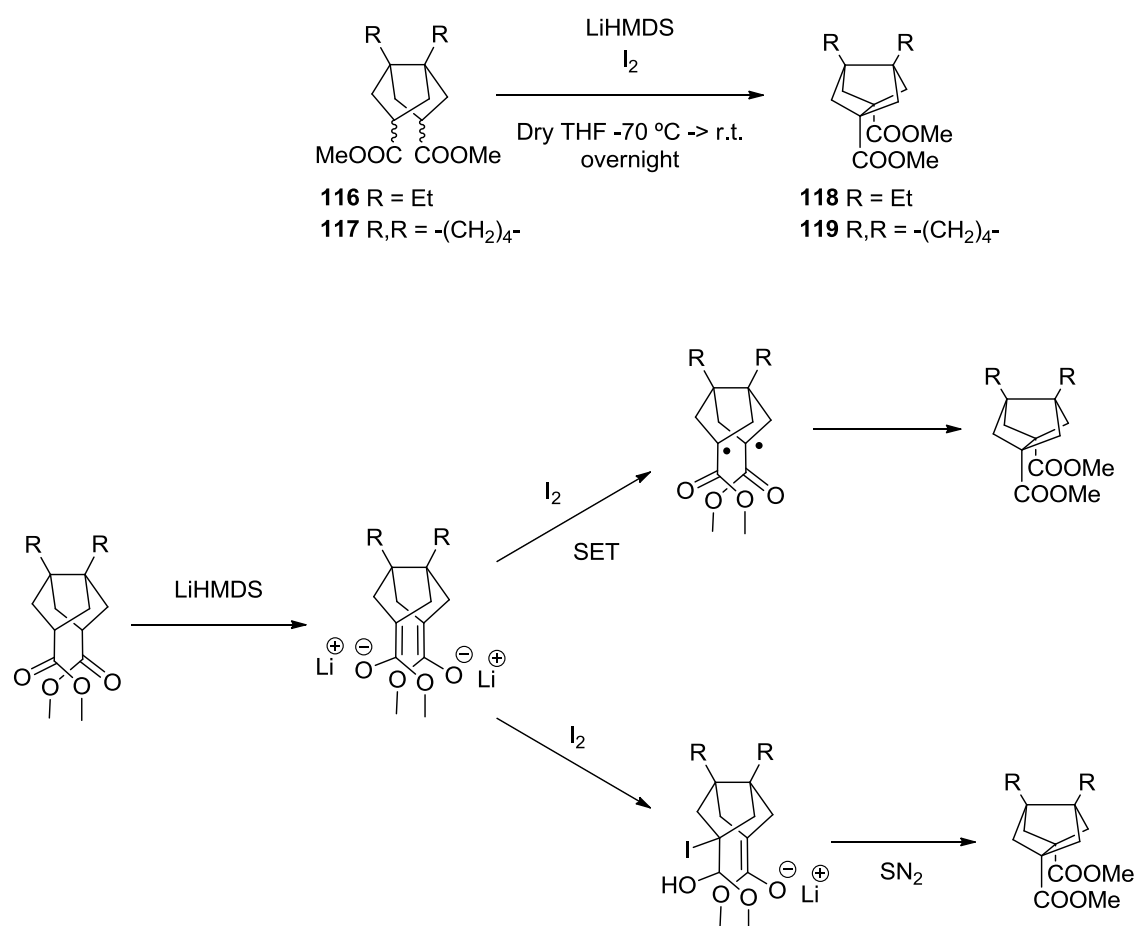
Scheme 35. Intramolecular enolate homocoupling of diesters **116** and **117**

---

[136] Renaud, P.; Fox, M. A. *J. Org. Chem.* **1988**, *53*, 3745.

With the polycyclic structure already formed, we subjected diesters **118** and **119** to a basic hydrolysis that furnished diacids **120** and **121** in 63% and 80% yield, respectively. After that, the aforementioned treatment with urea produced imides **122** and **123** in 87% and 83% yield, respectively (Scheme 36).
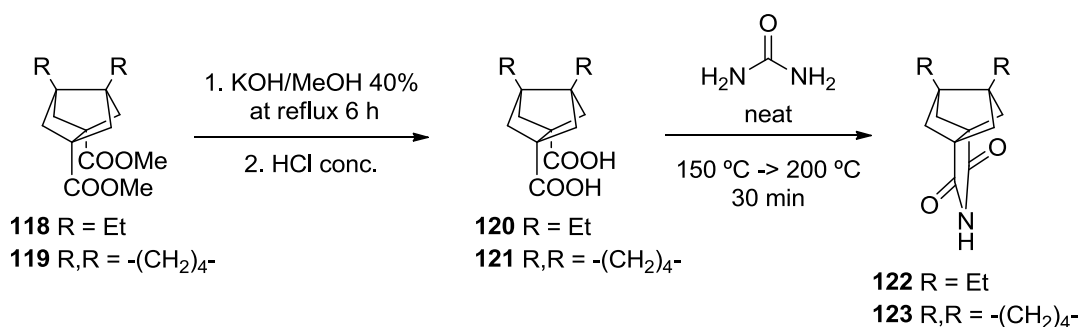
Scheme 36. Basic hydrolysis of diesters **118** and **119** and subsequent transformation of the formed diacids **120** and **121** to the corresponding imides **122** and **123**

Next, imides **122** and **123** were reduced, again using Red-Al®, to afford their corresponding amines. The issue appeared with the formation of the salts; the hydrochloric salts were hygroscopic so we were forced to precipitate amines **124** and **125** as the tartrate salts. Amines **124·tartrate** and **125·tartrate** were obtained in 33% yield and 83% yield, respectively (Scheme 37).
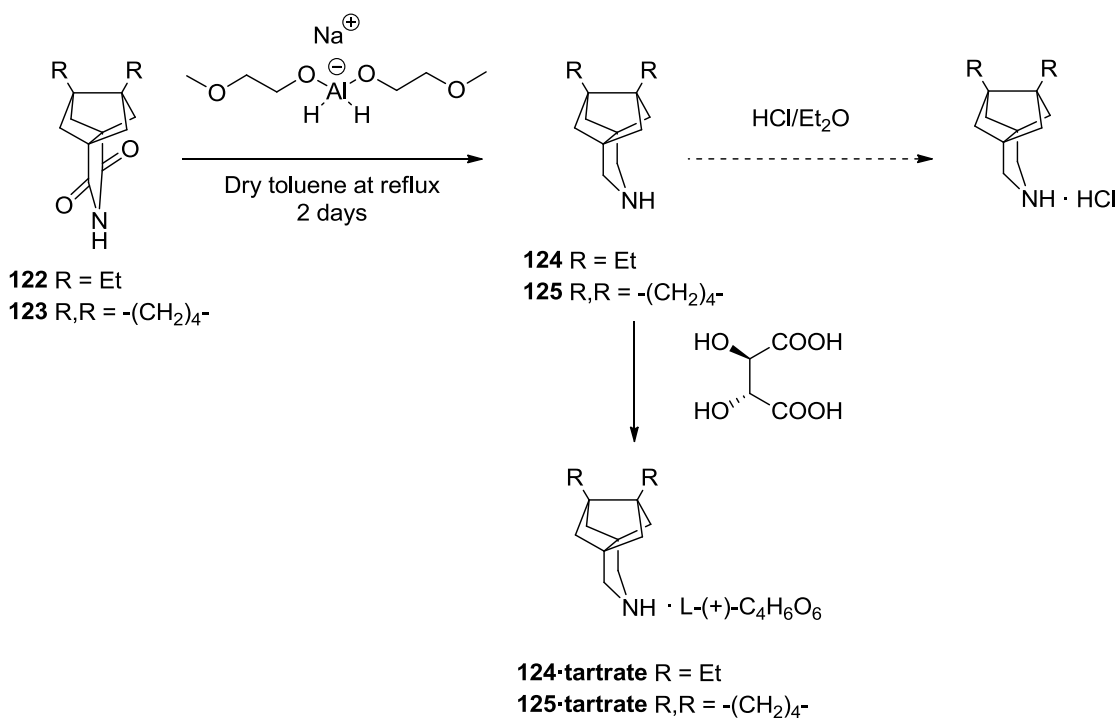
Scheme 37. Reduction of imides **122** and **123** to form amines **124** and **125** as tartrate salts

These amines, once freed from the L-(+)-tartaric acid salt, were submitted to the guanylation process with 1*H*-pyrazole-1-carboxamidine hydrochloride to furnish guanidines **126·HCl** and **127·HCl** in 76% and 63% yield, respectively. Paradoxically, guanidines were not hygroscopic as hydrochloride salts, maybe thanks to the higher number of hydrogen bonds, forming a tight network, compared with amines.

124·tartrate R = Et
125·tartrate R,R = -(CH$_2$)$_4$-

124 R = Et
125 R,R = -(CH$_2$)$_4$-

126·HCl R = Et
127·HCl R,R = -(CH$_2$)$_4$-
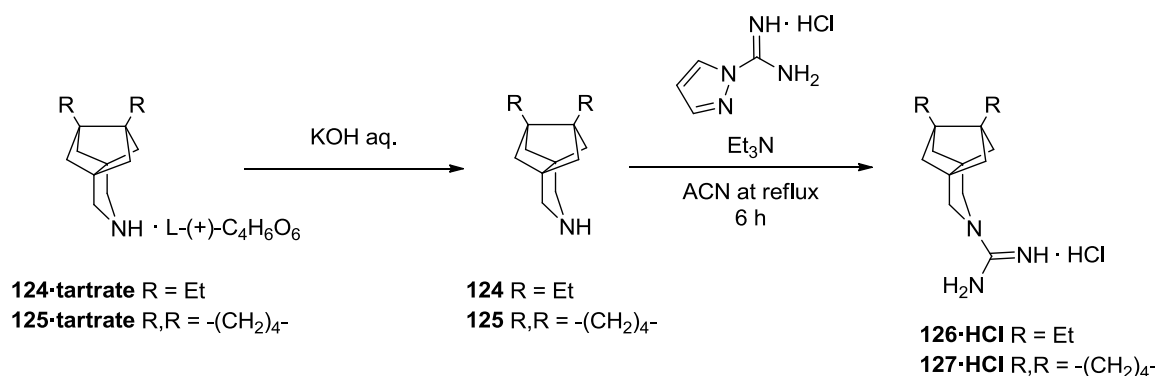
Scheme 38. Guanylation of free amines **124** and **125**

This synthetic route comprehended 10 steps for the obtention of the amines with an overall yield of 0.7% for **124.tartrate** and 3.2% for **125.tartrate**. Guanidine derivatives were logically obtained in 11 steps with an overall yield of 0.5% for **126.HCl** and 2.0% for **127·HCl**.

4.2 Pharmacology:
7,8-disubstituted 3-azatetracyclo[5.2.1.1^{5,8}.0^{1,5}]undecane

This family of compounds was tested, using the TEVC technique, by the group of Professor Pinto in the Northwestern University (Table 9).

Table 9. Inhibition of the wt, V27A and S31N M2 channels by 7,8-diethyl-3-azatetracyclo[5.2.1.1^{5,8}.0^{1,5}]undecane derivatives and 12-azapentacyclo[6.5.1.1^{3,10}.0^{1,10}.0^{3,8}]pentadecane derivatives

Compound	wt-M2		V27A-M2		S31N-M2	
	%inh.[a]	IC$_{50}$ (µM)	%inh.[a]	IC$_{50}$ (µM)	%inh.[a]	IC$_{50}$ (µM)
Amantadine	91.0 ± 2.1	16.0 ± 1.2	10.8 ± 2.0	ND[b]	35.6 ± 1.5	200 ± 3.5
124·tartrate	65.0 ± 1.7	ND	15.8 ± 2.7	ND	13.1 ± 1.7	ND
125·tartrate	85.3 ±0.8	4.5	76.2 ± 0.3	20.5	11.9 ± 1.0	ND
126·HCl	42.8 ± 1.8	ND	79.2 ± 0.4	13.8	10.8 ± 1.2	ND
127·HCl	93.1 ± 2.5	3.4	93.8 ±0.9	0.29	5.7 ± 2.0	ND

[a]Percentage inhibition at 100 µM for 2 min. Average of at least three experiments.
[b]ND: not determined.

The 7,8-diethyl-3-azatetracyclo[5.2.1.1^{5,8}.0^{1,5}]undecane derivatives, both amine **124·tartrate** and guanidine **126·HCl**, showed a low activity against wt-M2. This may be caused by steric clashes between the free rotating ethyl groups and either the narrow entry gate of the channel or the protein backbone. On the other hand, the more rigid derivatives, both amine **125·tartrate** and guanidine **127·HCl,** from the 12-azapentacyclo[6.5.1.1^{3,10}.0^{1,10}.0^{3,8}]pentadecane scaffold, displayed activities one order of magnitude less than amantadine against wt-M2, seconding our theory for the inactivity of **124·tartrate** and **126·HCl**.

Strikingly, amine **124·tartrate** was not very active against the V27A mutant although this one possesses a larger entry gate. It seemed that even the V27A entry gate was not large enough to avoid the steric clashes of the free rotating ethyl moieties, since guanidine **126·HCl**, although exhibiting a mid-micromolar IC_{50} against V27A, was less active than the methyl derivative **70·HCl** (see Figure 69). In contrast, the higher conformational rigidity of the 12-azapentacyclo[6.5.1.1^{3,10}.0^{1,10}.0^{3,8}]pentadecane scaffold, satisfyingly had a positive effect, supporting the very high activities of amine **125·tartrate** and guanidine **127·HCl** against the V27A mutant. *To our delight, guanidine* **127·HCl** *displayed a sub-micromolar IC_{50} against the V27A mutant channel, being, to date and to the best of our knowledge, the most active M2 channel blocker ever synthesized against this particular mutant.* As expected none of the tested compounds were active against the S31N mutant.

These data allowed us to deduce the following:

- The more rigid scaffold of **125·tartrate** and **127·HCl** proved to be more active against wt-M2 than the freely rotating structure of **124·tartrate** and **126·HCl**.
- Guanidine **127·HCl** was slightly more active against wt-M2 than its amine counterpart **125·tartrate**.
- Of note, **125·tartrate** and **127·HCl** were also more active against wt-M2 than the methyl analogues **69·HCl** and **70·HCl** (see Figure 69).

- Amine **124·tartrate** was not active against the V27A mutant with an enlarged binding cavity.
- Likewise, guanidine **126·HCl** showed a fair activity against V27A although it was less active than its methylated counterpart **70·HCl** (see Figure 69).
- The more rigid analogues **125·tartrate** and **127·HCl** were very active against the V27A mutant with **127·HCl** displaying an outstanding sub-micromolar IC_{50}.
- Guanidine **127·HCl** was more active against V27A than **126·HCl**, reinforcing the belief that the more rigid the structure the higher the activity.
- The cyclohexyl derivatives **125·tartrate** and **127·HCl** were also more active against V27A mutant than the methyl analogues **69·HCl** and **70·HCl** (see Figure 69).

Furthermore, the group of Professor William F. DeGrado, at the University of Pennsylvania, tested the binding affinity of our most potent compound against wt-M2, i.e. **127·HCl**. They reconstituted a tetramer of the M2TM domain in dodecylphosphocholine micelles and exposed it to different concentrations of **127·HCl**; in other words, drug titration. The concentration of **127·HCl** inside the M2 channel was followed by solution NMR, more specifically by ^{1}H NMR focusing on the peak of Hε1 of Trp41.[72b] A new signal at 10.9 ppm appeared as the concentration of **127·HCl** was increasing (corresponding to the drug-bound form) and simultaneously the peak at 10.4 ppm (associated with the apo-form) became weaker (Figure 74).
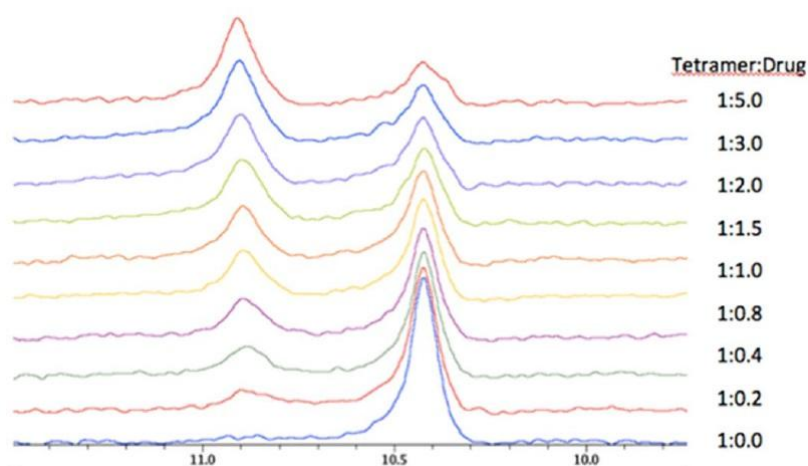
Figure 74. ^{1}H spectra showing the chemical shift in ppm of Hε1 of Trp41.

A plot of the integral of the peak at 10.9 ppm against the concentration of **127·HCl** revealed that this compound bound the wt-M2 channel with a stoichiometry ratio of 1.37 ± 0.28 per tetramer and possessed a dissociation constant K_d of 40 ± 24 μM (Figure 75).
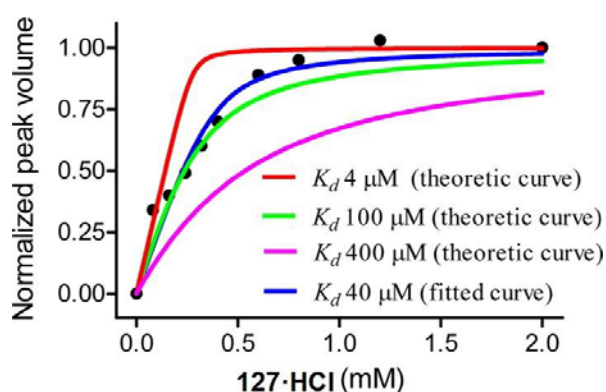
Figure 75. Binding affinity of **127·HCl** to wt-M2TM as determined by solution NMR drug titration. The normalized integral of Hε1 of Trp41 was plotted agains **127·HCl** concentration. Theoretical curve fittings with fixed stoichiometry (N = 1) and K_d of 4 (red), 40 (blue), 100 (green) and 400 μM (pink) are shown.

If we define the equilibrium between a drug and a receptor as:
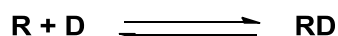
$$R + D \rightleftharpoons RD$$

Then the dissociation constant K_d obeys to the equation:

$$K_d = \frac{[R] \times [D]}{[RD]}$$

Where [R] is the concentration of free receptor, [D] is the concentration of free drug and [RD] is the concentration of the complex receptor-drug. Hence when 50% of the receptors are bound to the drug [R] = [RD] therefore K_d = [D]. This means that K_d can be assimilated with the concentration of free drug producing a 50% binding, in other words the IC_{50}.

The difference between the IC_{50} and the K_d of **127·HCl** can be attributed to the slow binding of M2 channel blockers obeying a second order rate constant,[137] thus meaning that the IC_{50} depends on the drug exposure time to the channel. The K_d for **127·HCl** of 40 ± 24 µM has to be compared with the K_d of amantadine of 15.2 ± 3.8 µM determined also through drug titration but followed by circular dichroism.[99b] The K_d of **127·HCl** is approximate since in the conditions employed for the titration, the concentration of protein was significantly above K_d, implying that the determination of the actual K_d is very difficult.

This experiment confirmed that guanidine **127·HCl** and possibly its whole series, owed their activity to binding inside the channel in a ratio 1 to 1 per tetramer.
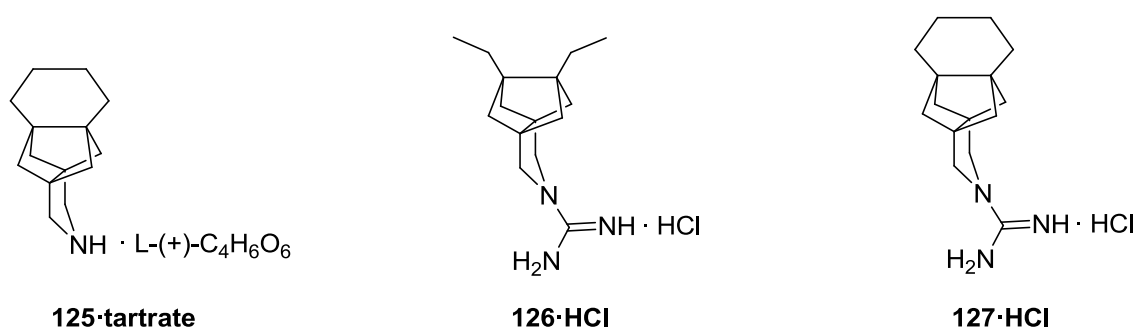
Figure 76. Active compounds as M2 channel blockers against wt-M2 and/or V27A mutant in the 7,8-disubstituted 3-azatetracyclo[5.2.1.1^{5,8}.0^{1,5}]undecane series

---

[137] Ma, C.; Polishchuk, A. L.; Ohigashi, Y.; Stouffer, A. L.; Schön, A.; Magavern, E.; Jing, X.; Lear, J. D.; Freire, E.; Lamb, R. A.; DeGrado, W. F.; Pinto, L. H. *Proc. Natl. Acad. Sci. U. S. A.* **2009**, *106*, 12283.

On the other hand, Professor L. Naesens performed the antiviral and cytotoxicity assays in MDCK cells of this new series of compounds, using the same methods described previously (see page 65), against three influenza virus strains (Table 10):

- A/PR/8/34 (H1N1): an amantadine-resistant influenza A strain carrying a double mutation on the M2 channel (V27T and S31N).
- A/HK/7/87 (H3N2): an amantadine-sensitive influenza A strain bearing a wild-type M2 channel.
- B/HK/5/72: an amantadine-resistant influenza B strain.

Table 10. Antiviral activity against influenza A and B determined in MDCK cells of 3-azatetracyclo[5.2.1.1^{5,8}.0^{1,5}]undecane derivatives series

| Compound | Antiviral EC$_{50}$^{a} (μM) | | | | | | Toxicity |
| | Influ. A (H1N1) | | Influ. A (H3N2) | | Influenza B | | MCC^b |
	CPE	MTS	CPE	MTS	CPE	MTS	
Amantadine	30	38	0.84	0.82	>500	>500	>500
124·tartrate	>100	>100	>100	>100	>100	>100	20
125·tartrate	>100	>100	>100	>100	>100	>100	4.0
126·HCl	>100	>100	>100	>100	>100	>100	4.0
127·HCl	>100	>100	>100	>100	>100	>100	4.0

^{a}Effective concentration producing 50% of inhibition of viral replication. Values shown are the mean of 2-3 determinations.

^{b}Minimum compound concentration causing minimal changes in cell morphology.

Sadly, all the tested compounds, that is, amines **124·tartrate** and **125·tartrate** and guanidines **126·HCl** and **127·HCl** were inactive as *in vitro* antivirals against all the tested influenza strains. Moreover they all displayed high cytotoxicity against MDCK cells. One of the probable causes might be the amphiphilic nature of the compounds, that may cause a membrane disrupting effect if the exposure time is high enough. The CPE assay is a 3-day assay that favours this kind of behaviour, so even though the compounds did not exhibited a high selectivity, it might be that their cytotoxicity masked their antiviral activity.

In order to unmask the possible activities of **125·tartrate** and **127·HCl**, Professor Naesens performed a virus yield assay (see page 78) in which the supernatant containing the virus released is collected and quantified 24 hours after exposure. The compounds were tested against the A/HK/7/87 (H3N2) strain bearing a wt-M2 (Table 11).

Table 11. Antiviral activities against influenza virus A/HK/7/87 (H3N2) determined with MDCK cells by virus yield assay of **125·tartaric** and **127·HCl**

Compound	Antiviral activity (μM) Influenza A/HK/7/87 (H3N2)		
	CPE (EC$_{50}$)[a]	Virus yield (EC$_{90}$)[b]	Virus yield (EC$_{99}$)[c]
Amantadine	0.84	0.22	1.1
125.tartrate	>100	0.85	>10
127·HCl	>100	0.37	>2

[a]Effective concentration producing 50% of inhibition of viral replication.

[b]Compound concentration producing a 1-log$_{10}$ reduction in virus yield determined by qRT-PCR.

[c]Compound concentration producing a 2-log$_{10}$ reduction in virus yield determined by qRT-PCR.

As we suspected, both compounds, **125·tartrate** and **127·HCl** belonging to the 12-azapentacyclo[6.5.1.1^{3,10}.0^{1,10}.0^{3,8}]pentadecane sub-family, possessed an antiviral activity *in vitro* reflected by their EC$_{90}$ determined through the virus yield assay. As in the TEVC assay, guanidine **127·HCl** was more active than amine **125·tartrate**, both displaying EC$_{90}$ values close to amantadine but still far from it, as the EC$_{99}$ determination confirmed. In spite of that, this experiment demonstrated that our compounds, although not exhibiting a high selectivity, were active in cell culture assays.
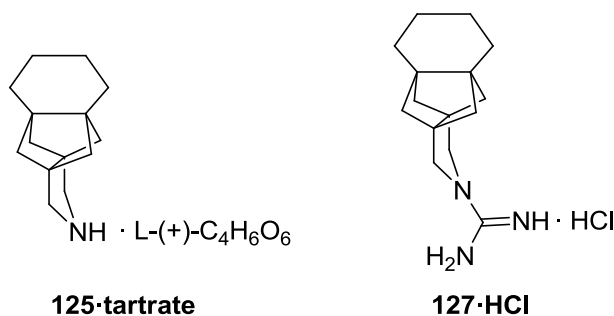
Figure 77. Active compounds according to *in vitro* assays

Although the TEVC results were not straightforwardly confirmed by antiviral assays, this family of compounds had some features worth mentioning:

- The ethyl derivatives **124·tartrate** and **126·HCl** were not active as M2 channel blockers against wt-M2, most certainly by the steric handicap of the free rotation of the ethyl groups.
- Surprisingly, amine **124·tartrate** was not active against V27A although this mutant bears an enlarged cavity.
- Similarly, guanidine **126·HCl** was active against V27A but less than its methyl analogue **70·HCl**.
- Neither amine **124·tartrate** nor guanidine **126·HCl** presented any antiviral activity, even exhibiting a high cytotoxicity.
- The conformational freedom of the ethyl moieties seemed thus to be detrimental to wt-M2 activity and also slightly deleterious to V27A activity.

- The cyclohexyl derivatives **125·tartrate** and **127·HCl** were very active as M2 channel blockers against wt-M2, pleasantly more than their methyl counterparts **69·HCl** and **70·HCl**.
- Amine **125·tartrate** and guanidine **127·HCl** were also very active against the V27A mutant, again being more active than their methyl analogues **69·HCl** and **70·HCl**.
- As expected, guanidine **127·HCl** was more active against wt-M2 and V27A than amine **125·tartrate**.
- Guanidine **127·HCl** was proven to bind inside the M2 channel with a ratio close to 1 to 1 tetramer and a K_d of 40 ± 24 μM.
- Unfortunately, both **125·tartrate** and **127·HCl** were inactive as antivirals in the CPE assay, even displaying a high cytotoxicity.
- The virus yield assay circumvented this toxicity and demonstrated that both amine **125·tartrate** and guanidine **127·HCl** were to some extent active *in vitro*.
- The conformational rigidity of these longer derivatives seemed thus to be a very positive effect for M2 channel blocking activity.

125·tartrate   **126·HCl**   **127·HCl**
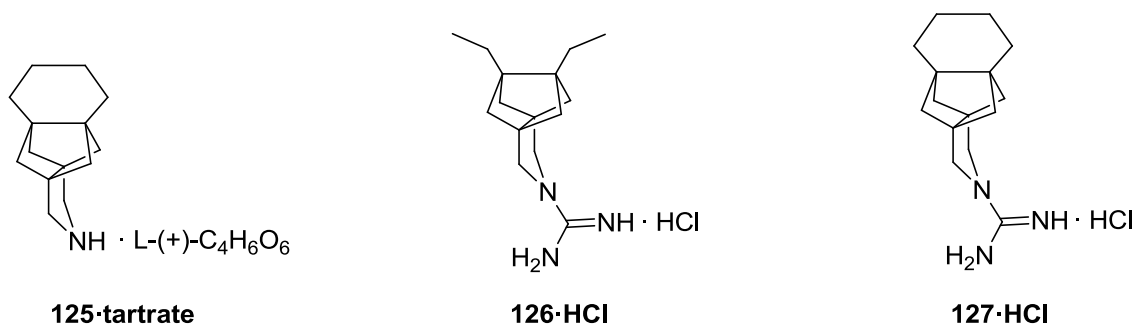
Figure 78. Active compounds of the 7,8-disubstituted 3-azatetracyclo[$5.2.1.1^{5,8}.0^{1,5}$]undecane series either as M2 channel blockers and/or as *in vitro* antivirals

5. Bulkier compounds with a shorter synthetic route

5.1 Synthesis:
7,8,9,10-Tetramethyl-3-azapentacyclo[7.2.1.1^{5,8}.0^{1,5}.0^{7,10}]tridecane and derivative

As above mentioned, the previous synthetic route to compounds **124**, **125**, **126** and **127** was very long, 10 to 11 steps for the obtention of the final amines or guanidines. Nevertheless, their pharmacological results were very encouraging. Thus, motivated by those good activities, we designed a synthetic route for, in fewer steps, obtaining a similar scaffold in length. However, this time we desired to expand the volume of its upper part to better fill the extra space available in the enlarged entry gate of the V27A mutant. We found inspiration in the work of Silva and Ginsburg for the design of a shorter and more synthetically available route leading to the 7,8,9,10-tetramethyl-3-azapentacyclo[7.2.1.1^{5,8}.0^{1,5}.0^{7,10}]tridecane scaffold (Figure 79).[138]
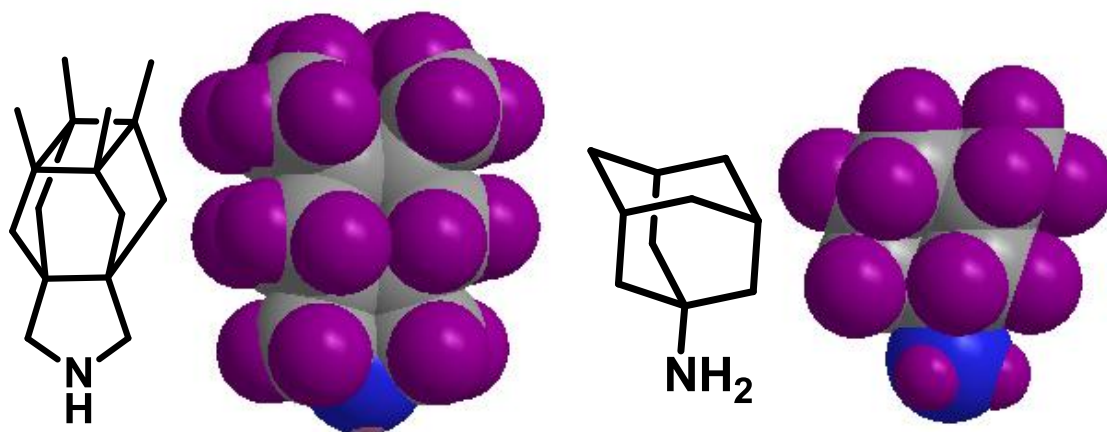
Figure 79. Qualitative space filling models of 7,8,9,10-tetramethyl-3-azapentacyclo[7.2.1.1^{5,8}.0^{1,5}.0^{7,10}]tridecane and amantadine. Hydrogen atoms are shown in purple. Source: ChemBio3D Ultra. Energy minimized through MM2.

---

[138] a) Avila, W. B.; Silva, R. A. *J. Chem. Soc. D Chem. Commun.* **1970**, 94. b) Ashkenazi, P.; Ginsburg, D. *Tetrahedron* **1979**, *35*, 1317.

This scaffold is still longer from the amine to the furthest carbon of the structure (6.08 Å) than amantadine (4.30 Å) even though it is shorter than the 12-azapentacyclo[6.5.1.1^{3,10}.0^{1,10}.0^{3,8}]pentadecane scaffold (6.64 Å, see Figure 73). But comparing the width of these structures, the 7,8,9,10-tetramethyl-3-azapentacyclo[7.2.1.1^{5,8}.0^{1,5}.0^{7,10}]tridecane scaffold (2.98 Å/3.00 Å) resembles more amantadine (2.95 Å) than the former scaffold does (3.07/2.36 Å, see Figure 73) in that they both have a "ball-like" shape with a similar width and depth. Besides, the main polycycle (excluding the pyrrolidine ring) possesses two cyclohexanes, two cyclopentanes and a cyclobutane ring, filling a comparable space to the four cyclohexane rings of amantadine (Figure 80).
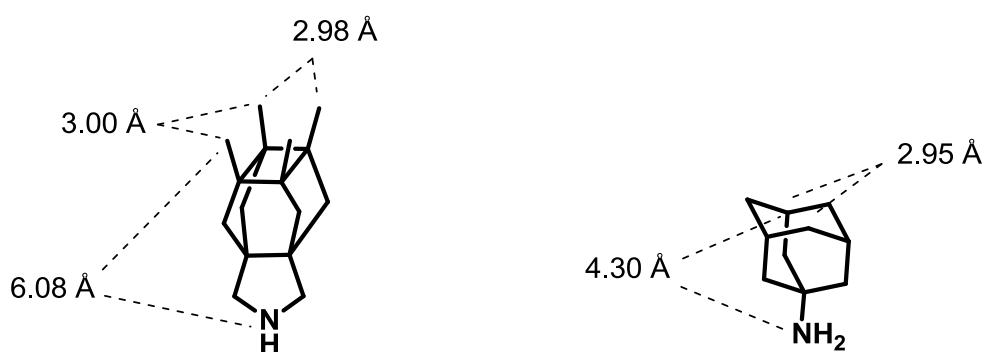
Figure 80. Most representative distances of 7,8,9,10-tetramethyl-3-azapentacyclo[7.2.1.1^{5,8}.0^{1,5}.0^{7,10}]tridecane and amantadine. Source: ChemBio3D Ultra. Energy minimized through MM2

We started the synthesis, following the procedures described by Avila and Silva,[138] by reacting one equivalent of acetylene dicarboxylic acid with two equivalents of 2,3-dimethyl-1,3-butadiene in a pressure reactor. Mechanistically the reaction has three steps: first, a Diels-Alder reaction producing the non-isolated intermediate diacid **128** followed by a dehydration yielding the neither isolated intermediate anhydride **129**. Most likely, the second equivalent of 2,3-dimethyl-1,3-butadiene preferred to react with the anhydride **129** rather than with diacid **128**, the former being a better dienophile. Thus **129** underwent another Diels-Alder reaction forming the final anhydride **130** with 86% yield (Scheme 39).
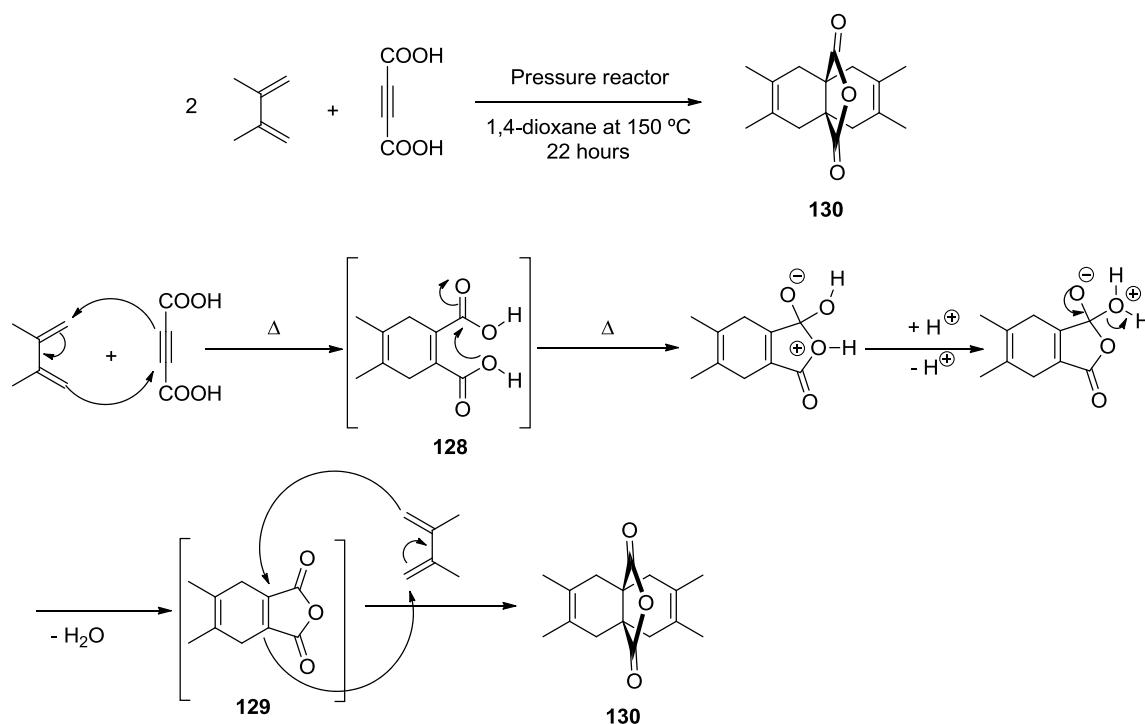
Scheme 39. Diels-Alder and dehydration reactions of 2,3-dimethyl-1,3-butadiene and acetylene dicarboxylic acid producing anhydride **130**

Anhydride **130** was then subjected to a basic hydrolysis with sodium hydroxide to afford diacid **131** in a 64% yield. The latter was treated with urea, in the previously mentioned reaction, to provide imide **132** in a 75% yield (Scheme 40).
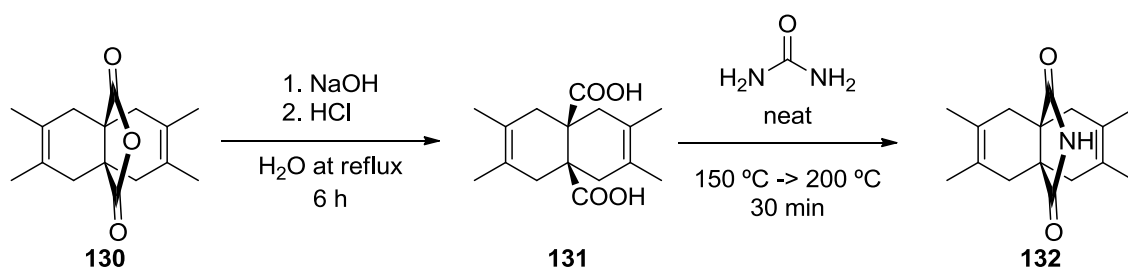
Scheme 40. Basic hydrolysis of **130** and subsequent reaction of diacid **131** with urea to furnish imide **132**

Next, the key step of this synthetic route took place: a [2+2] photocycloaddition. Imide **132** was submitted to the UV radiation of a 125 W mercury lamp in order to form the cyclobutane derivative **133**. A plausible mechanism would involve the sensitization of the reaction by acetone, which would be excited to its triplet state by the UV radiation. Acetone then transfers the energy to one of the C-C double bonds of **132** exciting it to a triplet state also, which SOMO swiftly reacts with the LUMO of the spare C-C double bond producing a diradical intermediate that collapses into the polycyclic imide **133**.[139] This one was obtained in 36% yield, based on recovered starting material, with increased reaction times having no effect on the yield and increased concentrations of starting material being deleterious (Scheme 41).
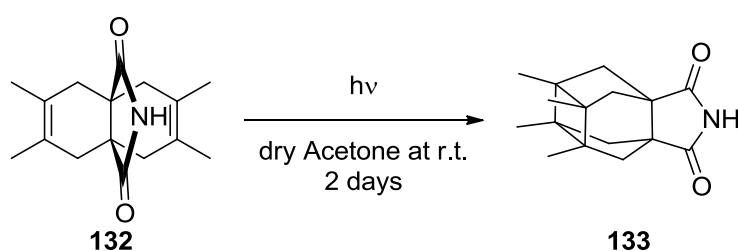
Scheme 41. [2+2] Photocycloaddition of imide **132** to form imide **133**

Imide **133** was then reduced with Red-Al® and subsequently treated with hydrochloric acid in diethyl ether to furnish novel amine **134·HCl** in 71% yield (Scheme 42).
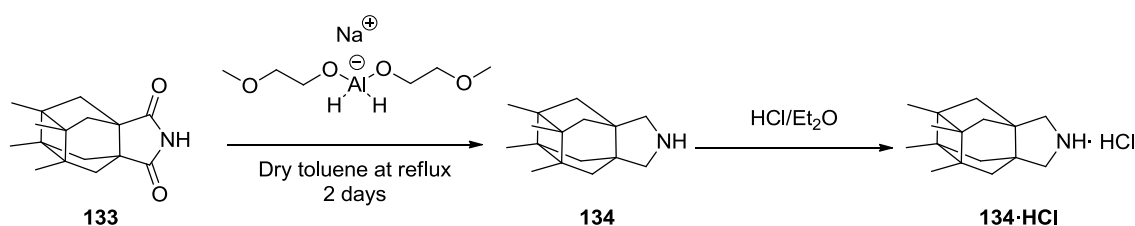
Scheme 42. Reduction with Red-Al® of imide **133** and subsequent precipitation as hydrochloride salt to obtain **134·HCl**.

---

[139] a) Tada, M.; Kokubo, T.; Sato, T. *Tetrahedron* **1972**, *28*, 2121. b) Kosugi, H.; Sekiguchi, S.; Ryu-ichi, S.; Uda, H. *Bull. Chem. Soc. Jpn.* **1976**, *49*, 520. c) Loufty, R. O.; De Mayo, P. *Can. J. Chem.* **1972**, *50*, 3465.

Amine **134·HCl** was guanylated with 1*H*-pyrazole-1-carboxamidine to afford guanidine **135·HCl** in 66% yield (Scheme 43).
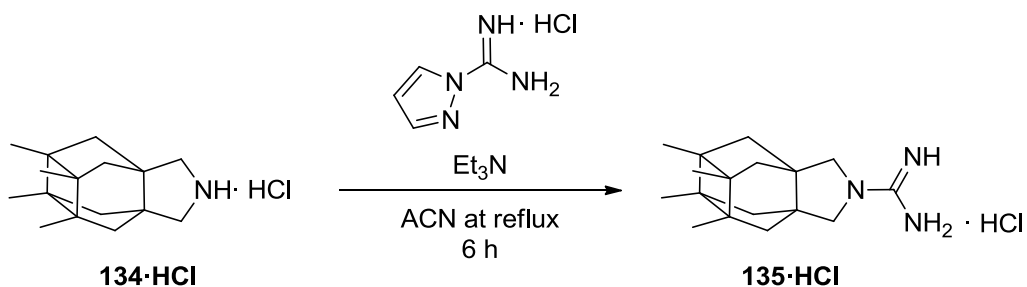
Scheme 43. Guanylation reaction of amine **134·HCl** to afford guanidine **135·HCl**

This synthetic route was much shorter than the one leading to the 12-azapentacyclo[6.5.1.1^{3,10}.0^{1,10}.0^{3,8}]pentadecane scaffold. It consisted of 5 steps to obtain amine **134·HCl** in 10.6% overall yield and 6 steps to secure guanidine **135·HCl** in 6.4% overall yield (cf. 10 to 11 steps with an average overall yield of 2% for the 12-azapentacyclo[6.5.1.1^{3,10}.0^{1,10}.0^{3,8}]pentadecane scaffold).

5.2 Pharmacology: 7,8,9,10-Tetramethyl-3-azapentacyclo[7.2.1.1^{5,8}.0^{1,5}.0^{7,10}]tridecane and derivative

This last small family of compounds was tested, using the TEVC technique, by the group of Professor Pinto in the Northwestern University. Furthermore, at that time the laboratories of Professor Pinto succeeded in obtaining an oocyte expressing the L26F mutant M2 channel upon which they also tested our compounds (Table 11).

Table 11. Inhibition of the wt, V27A, S31N and L26F M2 channels by 7,8,9,10-tetramethyl-3-azapentacyclo[7.2.1.1^{5,8}.0^{1,5}.0^{7,10}]tridecane derivatives

Compound	wt-M2		V27A		S31N		L26F	
	%inh.[a]	IC$_{50}$ (μM)	%inh.[a]	IC$_{50}$ (μM)	%inh.[a]	IC$_{50}$ (μM)	%inh.[a]	IC$_{50}$ (μM)
Amt.	91.0 ± 2.1	16.0 ± 1.2	10.8 ± 2.0	ND[b]	35.6 ± 1.5	200 ± 3.5	48.2 ± 3.5	164.5
134·HCl	90.2 ± 0.9	18.0	96.4 ± 0.5	0.70	1.1 ± 1.1	ND	90.6 ± 1.1	8.6
135·HCl	91.7 ± 1.2	10.7	96.7 ± 0.5	0.50	2.7 ± 1.5	ND	88.4 ± 0.6	7.5

Amt. = amantadine

[a]Percentage inhibition at 100 μM for 2 min. Average of at least three experiments.

[b]ND: not determined.

Satisfyingly, both amine **134·HCl** and guanidine **135·HCl** displayed an activity against wt-M2 close to amantadine, although they were less active than the previous 12-azapentacyclo[6.5.1.1^{3,10}.0^{1,10}.0^{3,8}]pentadecane scaffold (4.5 μM for amine **125·tartaric** and 3.4 μM for guanidine **127·HCl**, see Table 9). Nevertheless, both were sub-micromolar inhibitors of the V27A mutant and low-micromolar inhibitors of the L26F mutant possessing an entry gate bigger than wt-M2 but smaller than V27A. These data suggest that this new structure was less suited for the wt-M2 binding cavity than the previous scaffold but fitted much better in the V27A enlarged cavity than the latter, since, not only guanidine **135·HCl** but also amine **134·HCl**, exhibited a high potency against this mutant. None of the tested compounds were active against the S31N mutant.

Accordingly, the following conclusions, concerning M2 channel blocking, may be drawn for this scaffold:

- Both amine **134·HCl** and guanidine **135·HCl** were good inhibitors of the wt-M2 with activities close to amantadine's.
- Not surprisingly, guanidine **135·HCl** was more active than its parent amine **134·HCl**.
- Sadly, they were less active than amine **125·tartaric** and guanidine **127·HCl** from the previous scaffold.
- This might be interpreted as the 7,8,9,10-tetramethyl-3-azapentacyclo[7.2.1.1^{5,8}.0^{1,5}.0^{7,10}]tridecane structure fitting in the wt-M2 binding cavity in a manner resembling amantadine owed to the similar shape of their polycycle. The four methyl groups could establish van Der Waals interactions with the Val27 residues and the pyrrolidine could reach deeper, getting a little closer to the water clusters at Gly34 and explaining the small difference in the IC$_{50}$ of **134·HCl** and **135·HCl** with amantadine.

- Both amine **134·HCl** and guanidine **135·HCl** were sub-micromolar inhibitors of the V27A mutant.
- Again, guanidine **135·HCl** was more active than its parent amine **134·HCl**.
- Although guanidine **135·HCl** was not more active than guanidine **127·HCl** against V27A, their IC$_{50}$ values were very close (see Table 9).
- On the contrary, amine **134·HCl** was more active than amine **125·tartaric** (see Table 9).
- These results suggest that the activity against the V27A mutant of these compounds comes more from the interactions of the methyl moieties with the Ala27 than from the length of the molecule.

- Both amine **134·HCl** and guanidine **135·HCl** inhibited the amantadine-resistant L26F mutant displaying also a wider pore lumen.

134·HCl   **135·HCl**
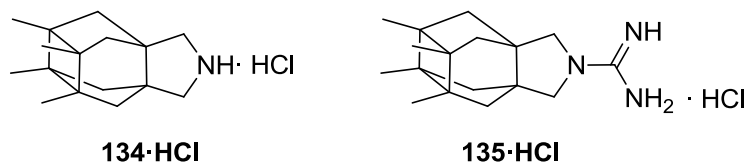
Figure 81. Active compounds as M2 channel blockers against wt-M2, V27A and L26F from the 7,8,9,10-tetramethyl-3-azapentacyclo[7.2.1.1^{5,8}.0^{1,5}.0^{7,10}]tridecane series

To gain insight on the mode of inhibition of amine **134·HCl**, the group of Professor F. Javier Luque of the University of Barcelona examined the binding of **134·HCl** on wt-M2 and V27A through molecular dynamics simulations.

In the wt-M2 complex these were the features found for **134·HCl**:

- the centre of the inhibitor was close to the plane defined by the Ser31 tetrad,
- the amine's nitrogen was pointing to the His37, termed the *down* orientation, with an average distance of 6.1 Å,
- the molecule exhibited a tilt angle, deviation of the amine nitrogen from the pore axis, of 16.1 º (see Figure 82a).

Thus, they confirmed that **134·HCl** binds in wt-M2 in a comparable manner to amantadine, the lipophilic cage occupying the same pocket in the lumen of the channel. The only difference being the further reach of the amino group and the extra lipophilic interactions of the four methyl groups in **134·HCl** (see Figure 82b).

The binding of amantadine to the V27A mutant yielded the following characteristics in the simulations:

- the centre of the molecule was in the plane defined by the four Ala27 (distance 2.2 Å) and the four Ser31 (distance 2.1 Å),
- the amine's nitrogen was pointing up, named the *up* orientation, with a tilt angle of 159 º,
- the distance of the centre of amantadine to the plane formed by the His37 tetrad was 14.5 Å (see Figure 82c).

In the V27A simulations, the distance between the His37 was reduced by approx. 0.8 Å which contributed to amantadine's nitrogen orientation being swung towards Ala27 in the *up* orientation, and even in one of the replicas ran, amantadine was expelled from the mutant channel.

Amine **134·HCl**, was in two out of the three replicas ran, in the *down* orientation, with its nitrogen further away from the His37 plane compared with the wt-M2 complex, precisely:

- the centre of the molecule was shifted 1.1 Å from the Ser31 plane towards the N-terminal,
- the distance between the amine's nitrogen and the His37 tetrad was 7.7 Å,
- and the tilt angle of the molecule was close to 12 º (see Figure 82d).

In the third replica, amine **134·HCl** was turned over to the *up* orientation: its centre was moved further away from the Ser31 plane, specifically to a distance of 2.3 Å, the distance between the amine's nitrogen and the His37 tetrad was close to 15 Å, and the tilt angle was 145 º (see Figure 82e).

Probably, amine **134·HCl** was in equilibrium between the *up* and *down* orientations but its bigger size compared with amantadine, conferred by the methyl groups, prevented the exchange rate to be too fast to induce the release of the molecule, as was the case with amantadine.
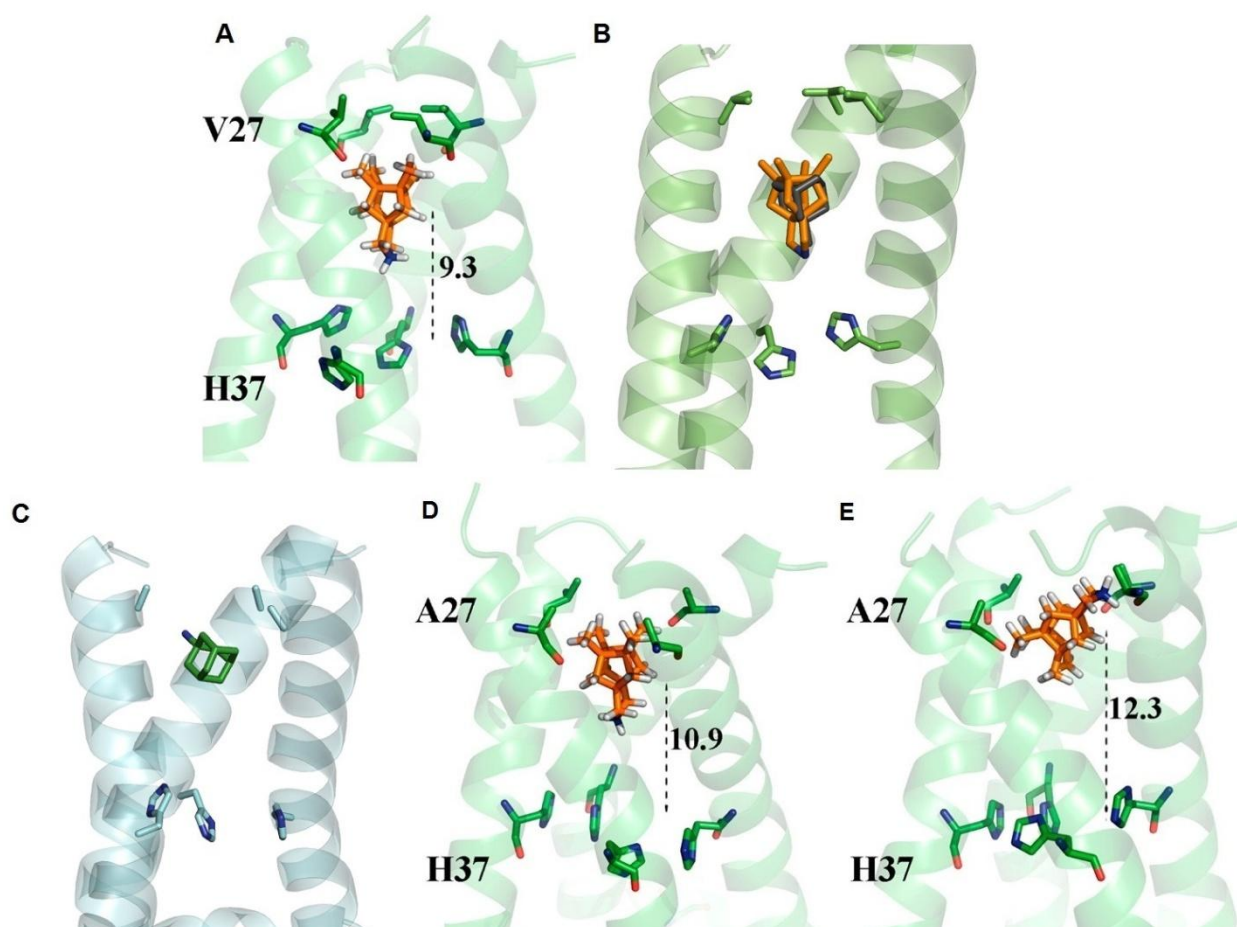
Figure 82. a) Amine **134·HCl** bound to wt-M2. **b)** Amine **134·HCl** (orange) and amantadine (black) superposed in the wt-M2. **c)** Amantadine in the V27A mutant channel. **d)** Amine **134·HCl** bound to V27A, *down* variant. **e)** Amine **134·HCl** bound to V27A, *up* variant. Dashed lines represent the distance in Å between the centre of the molecule and the plane formed by the His37 tetrad. The "front" helix has been removed for clarity.

Professor Naesens performed the antiviral and cytotoxicity assays in MDCK cells of this last series of compounds, using the same methods described previously (see page 65), against three influenza virus strains (Table 12):

- A/PR/8/34 (H1N1): an amantadine-resistant influenza A strain carrying a double mutation on the M2 channel (V27T and S31N).
- A/HK/7/87 (H3N2): an amantadine-sensitive influenza A strain bearing a wild-type M2 channel.
- B/HK/5/72: an amantadine-resistant influenza B strain.

Table 12. Antiviral activity against influenza A and B determined in MDCK cells of the 7,8,9,10-tetramethyl-3-azapentacyclo[7.2.1.1^{5,8}.0^{1,5}.0^{7,10}]tridecane series

| Compound | Antiviral EC$_{50}$[a] (μM) | | | | | | Toxicity |
| | Influ. A (H1N1) | | Influ. A (H3N2) | | Influenza B | | MCC[b] |
	CPE	MTS	CPE	MTS	CPE	MTS	
Amantadine	30	34	1.4	1.4	>500	>500	>500
134·HCl	1.8	3.0	>100	>100	>100	>100	100
135·HCl	>100	>100	>100	>100	>100	>100	≥4

[a]Effective concentration producing 50% of inhibition of viral replication. Values shown are the mean of 2-3 determinations.

[b]Minimum compound concentration causing minimal changes in cell morphology.

Disappointingly, neither amine **134·HCl** nor guanidine **135·HCl** were active against the H3N2 strain bearing a wt-M2 channel. Since both **134·HCl** and **135·HCl** displayed some cytotoxicity, their antiviral activity could be masked by their toxicity. Besides, they could have some permeability problems in the cell culture, a plausible cause already taken into account for other molecules (see page 66).

Shockingly, amine **134·HCl** was active against the A/PR/8/34 (H1N1) strain carrying a double mutation, one of them the S31N, although the TEVC assay showed no activity of the molecule against this mutant. This behaviour was already seen with one of our molecules (see Table 4) and elsewhere,[40,117] and could be the consequence of the capacity of some molecules to slightly increase the endosomal pH, effect to which the A/PR/8/34 (H1N1) strain is very sensitive (see page 78).

In order to confirm or to refute the previous statements, Professor Naesens performed a virus yield and a plaque reduction assays with the A/HK/7/87 (H3N2) strain.

The virus yield assay, exposing the cells to the compounds only 24 hours as opposed to the 3 days of the CPE assay, can, in principle, circumvent the cytotoxicity issue (see page 78). The assay yielded the following results (Table 13):

Table 13. Antiviral activities against influenza virus A/HK/7/87 (H3N2) determined with MDCK cells by virus yield assay of **134·HCl** and **135·HCl**

Compound	Antiviral activity (μM) Influenza A/HK/7/87 (H3N2)		
	CPE (EC_{50})[a]	MTS (EC_{50})[a]	Virus yield (EC_{99})[b]
Amantadine	1.4	1.4	1.1
134.HCl	>100	>100	>50
135·HCl	>100	>100	>10

[a]Effective concentration producing 50% of inhibition of viral replication.
[b]Compound concentration producing a 2-$\log_{10}$ reduction in virus yield determined by qRT-PCR.

Unfortunately, neither amine **134·HCl** nor guanidine **135·HCl** displayed any activity through this experiment. Thus, two possible sources for the inactivity of these molecules could be some permeability issues or some poor selectivity, that is a high cytotoxicity, since through this assay that avoids in principle the cytotoxicity, both compounds were inactive.

Then, Professor Naesens carried out the virus plaque reduction assay again using the A/HK/7/87 (H3N2) bearing a wt-M2 (see page 79). The compounds were tested at three different concentrations (Figure 83).
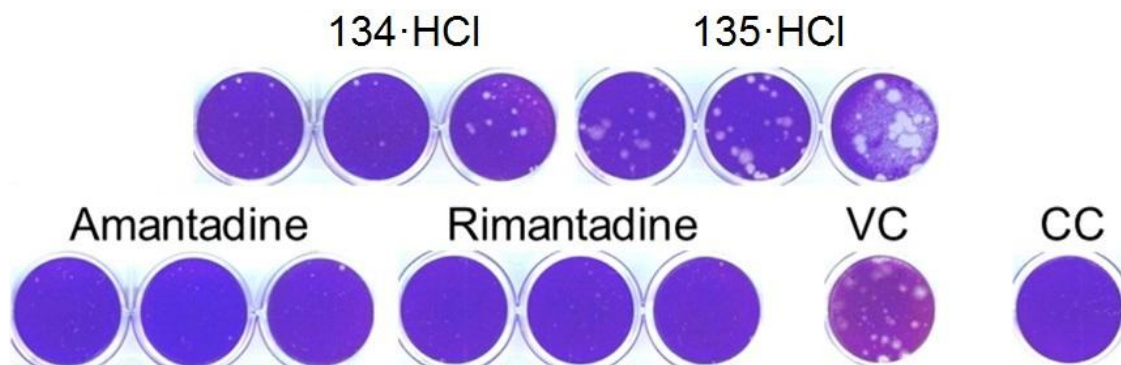
Figure 83. Plaque reduction assay using influenza virus A/HK/7/87 (H3N2) of amine **134·HCl** and guanidine **135·HCl**. Concentrations, from left to right: 0.5, 2 and 8 μM. Plaques visualized by crystal violet staining. VC: mock-treated virus control. CC: uninfected cell control

Amine **134·HCl** caused a visible plaque reduction at 0.5 μM and 2 μM and a slight cytotoxicity at 8 μM. In contrast, guanidine **135·HCl** was inactive at 0.5 μM and 2 μM and displayed cytotoxicity at 8 μM. This experiment showed that amine **134·HCl** was active as an antiviral and that guanidine **135·HCl** was cytotoxic at a concentration in agreement with the one determined by the CPE assay.

Taking all the antiviral data into account, we can conclude that:

- Amine **134·HCl** was not active as an antiviral in the CPE assay nor in the virus yield reduction assay but it did show a strong activity through the plaque reduction assay.
- Through the CPE assay, amine **134·HCl** displayed a low-moderate cytotoxicity.
- The inactivity of **134·HCl** seemed thus not to stem from a cytotoxicity problem although this was not confirmed by the virus yield assay.
- Amine **134·HCl** was active against the A/PR/8/34 (H1N1) strain although it appeared not to be related with M2 channel blocking.

- Guanidine **135·HCl** was not active as antiviral through the CPE assay, the plaque reduction assay nor the virus yield assay.
- According to the CPE and the plaque reduction assays, guanidine **135·HCl** was highly cytotoxic.
- The issue with guanidine **135·HCl** could be a high cytotoxicity or a permeability problem, among others.

The conclusions that may be drawn for the 7,8,9,10-tetramethyl-3-azapentacyclo[7.2.1.1^{5,8}.0^{1,5}.0^{7,10}]tridecane series are:

- Amine **134·HCl** presented an activity against wt-M2 close to amantadine's.
- Their similar activity may be due to their close resembling binding mode inside the channel as seen by molecular dynamics simulations.
- The lower activity of amine **134·HCl** compared with amine **125·tartaric** against wt-M2 may be explained by the latter being longer than the former.
- Amine **134·HCl** proved to be inactive as an antiviral against the H3N2 strain carrying a wt-M2 channel although some activity was detected by virus plaque reduction.
- Amine **134·HCl** was a sub-micromolar inhibitor of the V27A channel.
- Against this mutant, **134·HCl** was more active than **125·tartaric** possibly because, albeit not being so long, the methyl groups of this molecule filled better the extra space available in the V27A mutant.
- Satisfyingly, amine **134·HCl** was active against the L26F mutant possessing an enlarged entry gate as well.
- Amine **134·HCl** was also active against the A/PR/8/34 (H1N1) although it appeared not to be related with M2 channel blocking.
- Through the antiviral assays, amine **134·HCl** displayed no activity *in vitro* and a low-moderate cytotoxicity which could be the source of its inactivity.

- Guanidine **135·HCl** was active against wt-M2 and as expected was more active than its parent amine **134·HCl**.
- For the same reason previously stated, guanidine **127·HCl** was more active than guanidine **135·HCl** against wt-M2.
- Guanidine **135·HCl** was not active by *in vitro* assays.
- This inactivity could be due to permeability issues or to cytotoxicity problems.
- As presumed, guanidine **135·HCl** was more cytotoxic than amine **134·HCl**.
- Although their activities against V27A were close, guanidine **127·HCl** was more active than guanidine **135·HCl**.
- As expected, guanidine **135·HCl** was more active against V27A than its parent amine **134·HCl**.
- Guanidine **135·HCl** was also active against the L26F mutant and was again more active than amine **134·HCl**.

Conclusions

1. During this Thesis, 48 compounds were synthesized, of which 40 were not previously described in the literature and have been thoroughly characterized by spectroscopic and analytical means. Among them, 18 were pharmacologically evaluated. Concretely, the families prepared in this work were:

    a. The amine and guanidine of the 5-azapentacyclo[6.4.0.0^{2,10}.0^{3,7}.0^{9,11}]dodecane series, a tighter though longer than amantadine analogue scaffold.

    b. A diversity of amines, guanidines, fully saturated and unsaturated derivatives of the 4-azatetracyclo[5.3.2.0^{2,6}.0^{8,10}]dodecane series as a mean of exploring the antiviral activity of this different polycyclic scaffold.

    c. The amine and guanidine of the saturated and unsaturated 14-azaheptacyclo[8.6.1.0^{2,5}.0^{3,11}.0^{4,9}.0^{6,17}.0^{12,16}]heptadecane scaffold to elongate a former structure endowed with good activity against the V27A mutant.

    d. The amine and guanidine of the 7,8-diethyl-3-azatetracyclo[5.2.1.1^{5,8}.0^{1,5}]undecane and of the 12-azapentacyclo[6.5.1.1^{3,10}.0^{1,10}.0^{3,8}]pentadecane scaffolds in order to continue the exploration of the 3-azatetracyclo[5.2.1.1^{5,8}.0^{1,5}]undecane polycyclic core.

    e. The amine and guanidine of the 7,8,9,10-tetramethyl-3-azapentacyclo[7.2.1.1^{5,8}.0^{1,5}.0^{7,10}]tridecane to afford in a relatively short synthetic route a bulky compound targeting the V27A mutant.

2. From the pharmacological activity point of view:

    a. Out of the 18 tested compounds, 14 displayed an activity, at least in the same range as amantadine, against the wt-M2 channel in the TEVC assay. The most active compound, **79·HCl**, belonged to the 5-azapentacyclo[6.4.0.0^{2,10}.0^{3,7}.0^{9,11}]dodecane series and exhibited an IC$_{50}$ of 0.83 μM.

    b. According to the *in vitro* assays, only 4 molecules out of the 18 tested yielded any activity against the H3N2 strain carrying a wt-M2 channel. The most active compound against it, **84·HCl**, from the 4-azatetracyclo[5.3.2.0^{2,6}.0^{8,10}]dodecane series, possessed an EC$_{50}$ of 6.0 μM in the CPE assay and an EC$_{99}$ inferior to 0.4 μM in the virus yield assay.
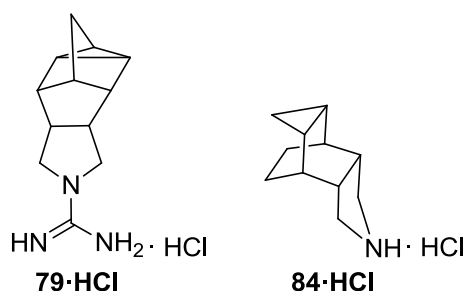
Figure 84. Most active compounds according to the TEVC assay (**79·HCl**) and the *in vitro* assays (**84·HCl**) against wt-M2

c. Regarding the activity against the V27A mutant, 7 molecules out of the 18 tested in the TEVC assay yielded any activity against this mutant. The most active compound, **127·HCl**, was part of the 12-azapentacyclo[6.5.1.1^{3,10}.0^{1,10}.0^{3,8}]pentadecane series and displayed an IC$_{50}$ of 0.29 μM. Besides, to date, this is the most active compound ever synthesized against this particular strain.
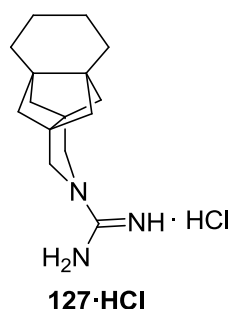
Figure 85. Most active compound against the V27A mutant M2 channel according to the TEVC assay

d. Two molecules, **86·2HCl** and **134·HCl**, showed an activity in the CPE assay against the H1N1 strain bearing a V27T and an S31N mutant M2 channel. Regrettably, their activity was not attributed to an M2 channel blocking mechanism.

e. A dual activity in wt-M2 and in V27A was achieved for 6 molecules: **103·HCl** and **105·HCl**, belonging to the 14-azaheptacyclo[8.6.1.0^{2,5}.0^{3,11}.0^{4,9}.0^{6,17}.0^{12,16}]heptadecane series and **125·HCl**, **127·HCl**, **134·HCl** and **135·HCl**. Even a triple activity in wt-M2, V27A and L26F channels was observed for **134·HCl** and **135·HCl**, belonging to the 7,8,9,10-tetramethyl-3-azapentacyclo[7.2.1.1^{5,8}.0^{1,5}.0^{7,10}]tridecane.
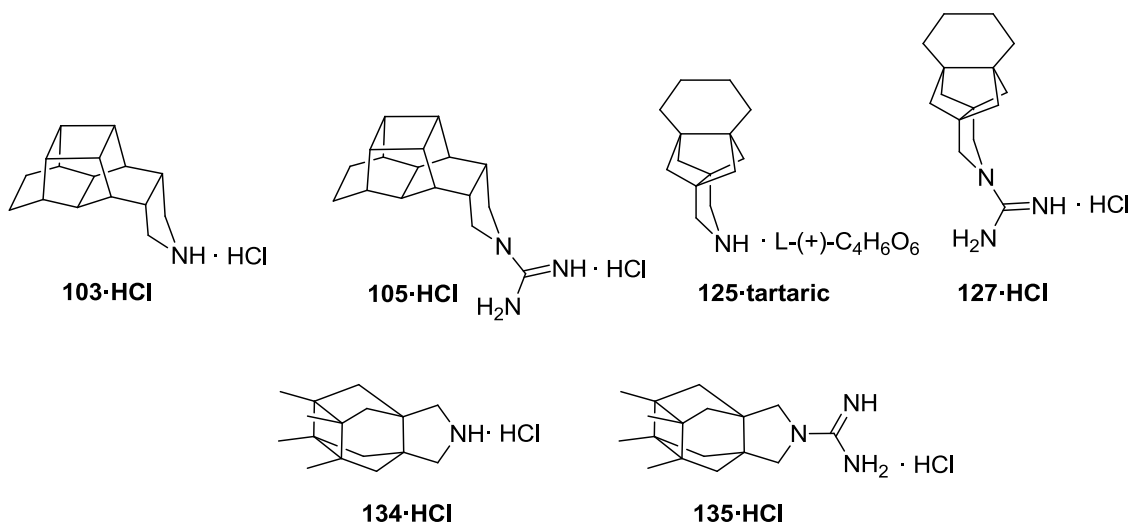
Figure 86. Dual compounds active against wt-M2 and the V27A mutant according to the TEVC assay. **134·HCl** and **135·HCl** are also active against L26F.

f. Unfortunately none of the tested compounds displayed any activity against the S31N mutant M2 channel.

3. As a general conclusion for this dissertation, we have fulfilled the objectives presented in the introductory part:

a. We have assessed new scaffolds as M2 channel blockers, proving again that the polycyclic cage of amantadine is not fully optimized in the channel lumen.

b. We have obtained very good M2 channel blocking activities against both wt-M2 and V27A and even dual agents that would ideally circumvent part of the resistance problem.

c. Based on these pharmacological data, we have designed shorter synthetic routes to secure compounds with similar activities.

d. Our exploration of new polycyclic structures as M2 channel blockers has helped us and others to gain more insight into the design of novel compounds to fight influenza A.

Additional results

Synthesis and trapping of the pyramidalized 3,4,8,9-tetramethyltetracyclo[4.4.0.0^{3,9}.0^{4,8}]dec-1(6)-ene

As we have already mentioned in the introductory part, our group has an extended expertise in the synthesis of polycyclic molecules,[4] mainly with the aim of studying highly pyramidalized alkenes. The chemistry of highly pyramidalized alkenes has received significant attention from synthetic and computational chemists due to their unusual reactivity.[4h,106,140]

If we talk about pyramidalized olefins, they are defined as molecules whose C-C double bond possess one or both atoms not in the plane defined by the three atoms attached to it. As a consequence, the geometry of the double bond becomes distorted, which induces a mixing of the 2s orbital into the π bond. This rehybridazation stabilizes the π* molecular orbital (LUMO) through the reduction of the antibonding overlap but the energy of the π orbital (HOMO) remains constant since the effects of the increased 2s character and the reduced overlap cancel each other (Figure 87).

The reduction of the gap between the HOMO and the LUMO is responsible for the high reactivity of pyramidalized alkenes and explains the ease of reduction of such compounds, their ability to form stable complexes with transition metals like platinum and their higher reactivity towards nucleophiles compared with electrophiles.[141] This high reactivity renders pyramidalized alkenes very prone to Diels-Alder reactions, oxidation to epoxides by atmospheric oxygen, to nucleophilic addition reactions and to dimerization reactions (Scheme 44).[141] Besides, again thanks to the lower energy of the π* compared with regular C-C double bonds, pyramidalized alkenes display special spectroscopic features: a deshielding in ^{13}C NMR of the C-C double bond (typical values 150-170 ppm)[142] and a shift of their UV absorption maximum towards longer wavelengths.[141]

---

[140] a) Theophanous, F. A.; Tasiopoulos, A. J.; Nicolaides, A.; Zhou, X.; Johnson, W. T. G.; Borden, W. T. *Org. Lett.* **2006**, *8*, 3001. b) Camps, P.; Colet, G.; Delgado, S.; Muñoz, M. R.; Pericàs, M. A.; Solà, L.; Vázquez, S. *Tetrahedron* **2007**, *63*, 4669. c) Pillekamp, M.; Alachraf, W.; Oppel, I. M.; Dyker, G. *J. Org. Chem.* **2009**, *74*, 8355. d) Gavrish, S. P. *J. Comput. Chem.* **2012**, *33*, 2173. e) Ioannou, S.; Krassos, H.; Nicolaides, A. V. *Tetrahedron* **2013**, *69*, 8064.

[141] Vázquez, S.; Camps, P. *Tetrahedron* **2005**, *61*, 5147.

[142] Vazquez, S. *J. Chem. Soc. Perkin Trans. 2* **2002**, 2100.
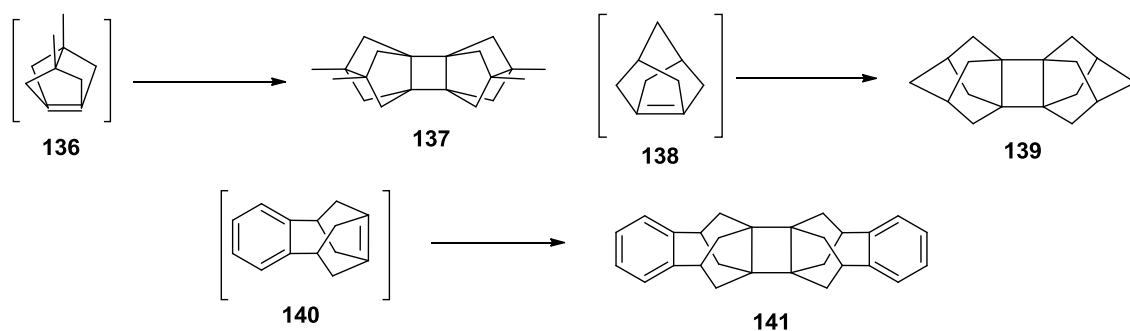
Scheme 44. Dimerization of some pyramidalized alkenes[141]

A convenient way of defining pyramidalization is via a geometrical parameter, the pyramidalization angle Φ. This one was introduced by Borden and co-workers,[143] and describes the angle between the plane containing one of the doubly bonded carbon atoms and the two substituents attached to it as well as the extension of the double bond (Figure 87).
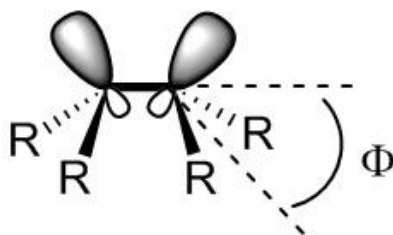
Figure 87. Schematic representation of a pyramidalized alkene and the pyramidalization angle Φ[141]

Taking advantage of the knowledge on this sort of chemistry present in the group and our recent experience with this structure (cf. part on the 7,8,9,10-tetramethyl-3-azapentacyclo[7.2.1.1^{5,8}.0^{1,5}.0^{7,10}]tridecane scaffold), we decided to undertake the synthesis and trapping of the pyramidalized alkene **142**. Theoretical calculations using B3LYP/6-31G(d) on the pyramidalized alkene **142** predicted a pyramidalization angle Φ = 47.5⁰, a C-C double bond length of 1.360 Å (cf. 1.333 Å for ethylene)[144] and a HOMO-LUMO gap of 5.64 eV (cf. 8.0 eV for ethylene),[144] meaning the molecule should be accessible. We were also attracted by the symmetry and the uniqueness of dimer **143** featuring three planar cyclobutane rings, four cyclopentane rings and four cyclohexane rings in boat conformations (Figure 88).

---

[143] Volland, W. V; Davidson, E. R.; Borden, W. T. *J. Am. Chem. Soc.* **1979**, *101*, 533.

[144] Daday, C.; Smart, S.; Booth, G. H.; Alavi, A.; Filippi, C. *J. Chem. Theory Comput.* **2012**, *8*, 4441.
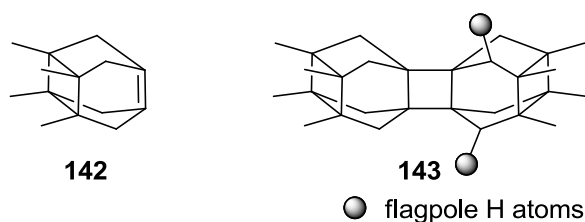
Figure 88. Pyramidalized alkene **142** and dimer **143**

The characteristic of **143** of possessing cyclohexanes in a "frozen" boat conformation with methylenic units whose hydrogen atoms are termed flagpoles (Figure 88), attracted particularly our attention all the more that, apart from a few exceptions,[145] the examples of cyclohexane rings in boat conformation that can be found in the literature, lack this H-H flagpole interaction.[146]

Hence we started the synthesis from the known anhydride **130** and we applied to it the UV radiation of a 125 W mercury lamp to produce the [2+2] photocycloaddition of its double bonds (see Scheme 41).[138] We obtained the polycyclic anhydride **144** with a 30% yield b.r.s.m.[147] This one was then submitted to a basic hydrolysis that produced diacid **145** in 82% yield (Scheme 45).
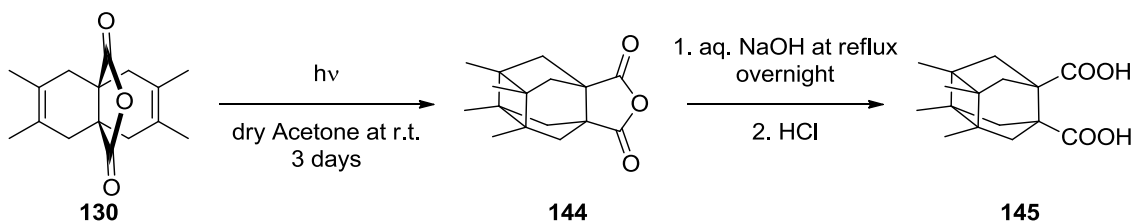
Scheme 45. [2+2] Photocycloaddition of **130** and subsequent hydrolysis of the polycyclic anhydride **144** to furnish diacid **145**

---

[145] a) Biethan, U.; Gizycki, U. V.; Musso, H. *Tetrahedron Lett.* **1965**, *6*, 1477. b) Musso, H.; Biethan, U. *Chem. Ber.* **1967**, *100*, 119. c) Musso, H.; Klusacek, H. *Chem. Ber.* **1970**, *103*, 3076. d) Ahlquist, B.; Almenningen, A.; Benterud, B.; Traetteberg, M.; Bakken, P.; Lüttke, W. *Chem. Ber.* **1992**, *125*, 1217. e) Cupas, C. A.; Hodakowski, L. *J. Am. Chem. Soc.* **1974**, *96*, 4668. f) Hamon, D. P. G.; Taylor, G. F. *Tetrahedron Lett.* **1974**, *15*, 155 g) Hamon, D. P. G.; Taylor, G. F. *Aust. J. Chem.* **1976**, *29*, 1721.

[146] a) Balasubramanian, M. *Chem. Rev.* **1962**, *62*, 591. b) Sauers, R. R. *J. Chem. Educ.* **2000**, *77*, 332. c) Kakhiani, K.; Lourderaj, U.; Hu, W.; Birney, D.; Hase, W. L. *J. Phys. Chem. A* **2009**, *113*, 4570.

[147] During the writing of this thesis, M. Barniol repeated this reaction with a 400 W mercury lamp and irradiating during 5 days, she obtained **144** in 70% yield.

Furthermore, the obtention of the polycyclic anhydride **144** was confirmed by X-ray diffraction (Figure 89).
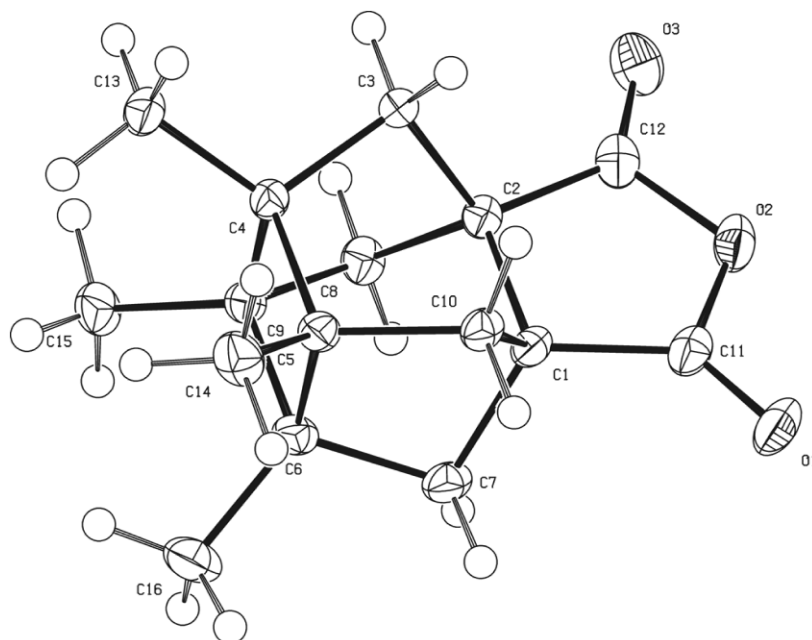
Figure 89. X-ray crystal strucuture (ORTEP) of anhydride **144**

Next, we desired to obtain the diiodo derivative through a iododecarboxylation reaction. Unfortunately, our first attempts with lead(IV) tetraacetate furnished mixtures enriched in unreacted starting material. So we subjected diacid **145** to the procedure described by Gandelman and co-workers, [148] where they use 1,3-diiodo-5,5-dimethylhydantoin (DIH) as the reaction initiator and source of iodines. The radical-chain reaction begins with the homolytic cleavage of the N-I bond of DIH. The radical produced abstracts one proton from the diacid which is left as the acyloxyl radical. This one spontaneously undergoes a decarboxylation process that furnishes a radical on the carbon atom which will be iodinated with another molecule of DIH closing the cycle (Scheme 46).[148] In our case, the reaction of **145** with DIH in dry 1,2-dichloroethane under irradiation at reflux produced **146** in 51% yield.

---

[148] Kulbitski, K.; Nisnevich, G.; Gandelman, M. *Adv. Synth. Catal.* **2011**, *353*, 1438.
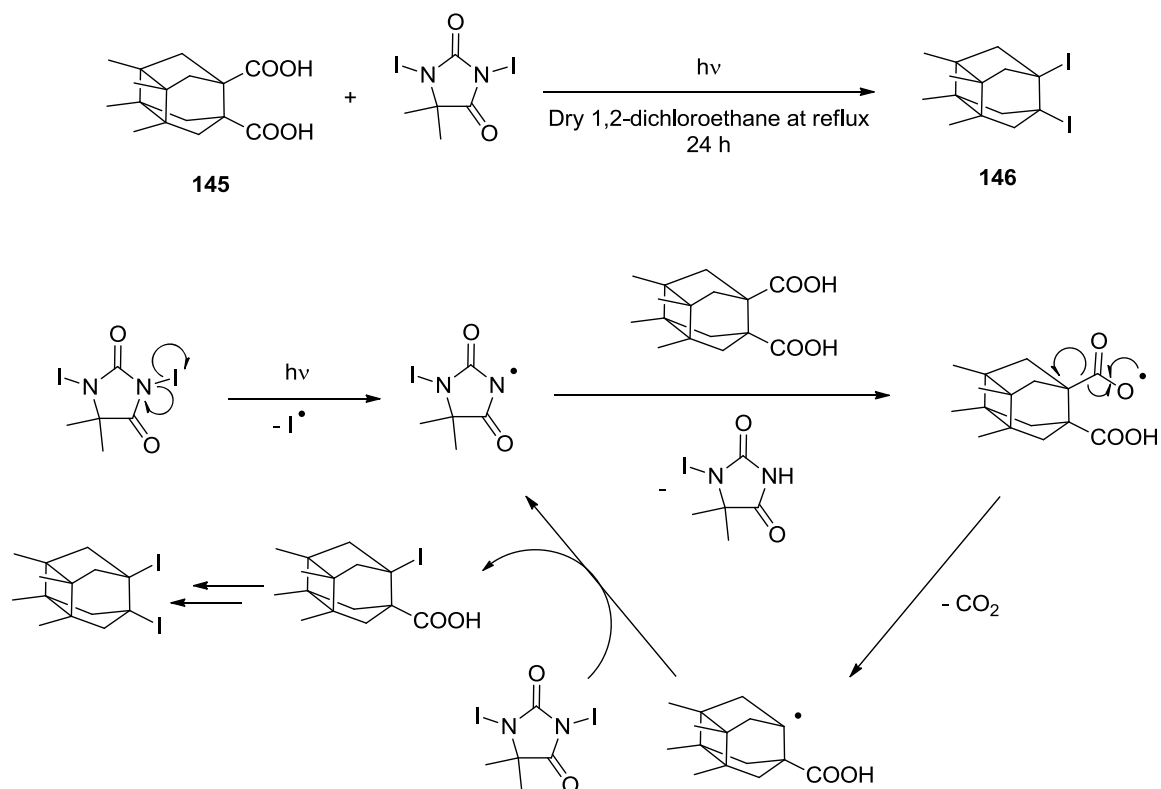
Scheme 46. Iododecarboxylation of diacid **145** using 1,3-diiodo-5,5-dimethylhydantoin

The structure of diiodo compound **146** was also confirmed by X-ray diffraction (Figure 90).
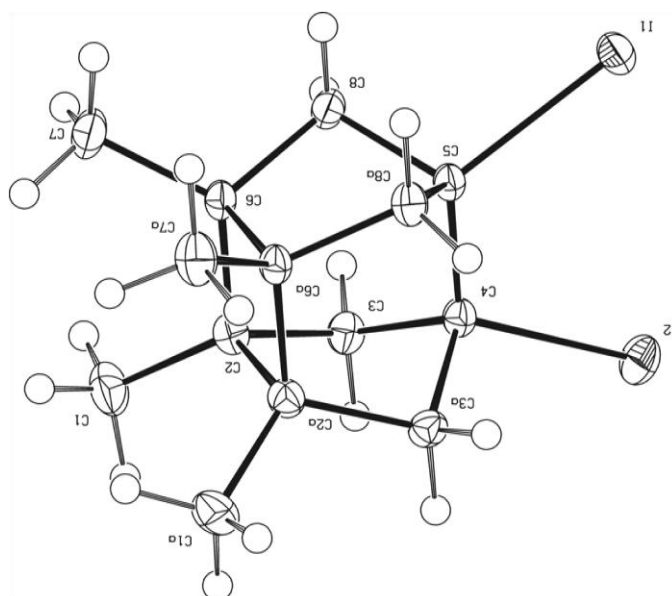
Figure 90. X-ray crystal structure (ORTEP) of diiodo compound **146**

Pyramidalized alkenes are highly reactive compounds impossible to isolate, thus a commonly used method to prove their existence is to trap them as Diels-Alder adducts. In our case we submitted diiodo compound **146** to a lithium-halogen exchange with *tert*-butyllithium, which furnished an alkyllithium species that, upon releasing lithium iodide, formed the pyramidalized alkene **142**. This one was trapped as its Diels-Alder adduct with 1,3-diphenylisobenzofuran **147**. The reaction proceeded with a 37% yield (Scheme 47).
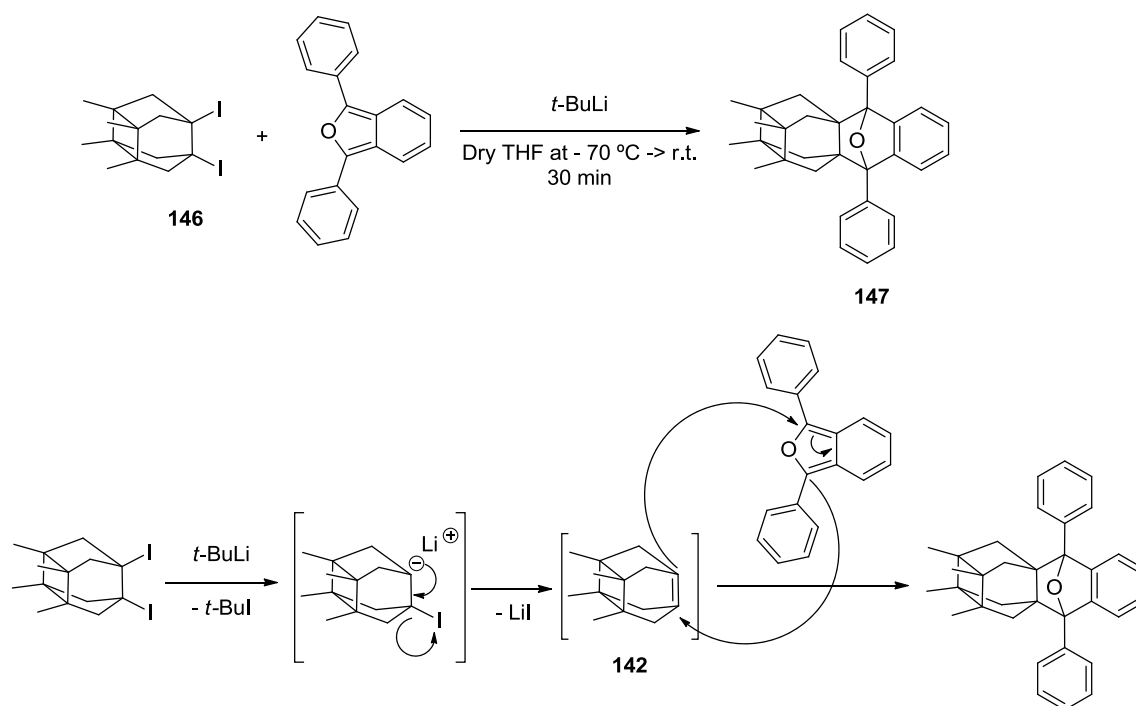
Scheme 47. Trapping of the pyramidalized alkene **142** as its Diels-Alder adduct with 1,3-diphenylisobenzofuran **147**

144

This adduct was crystallized from dichloromethane and its X-ray structure was determined, unveiling a dichloromethane molecule inside the crystal (Figure 91).
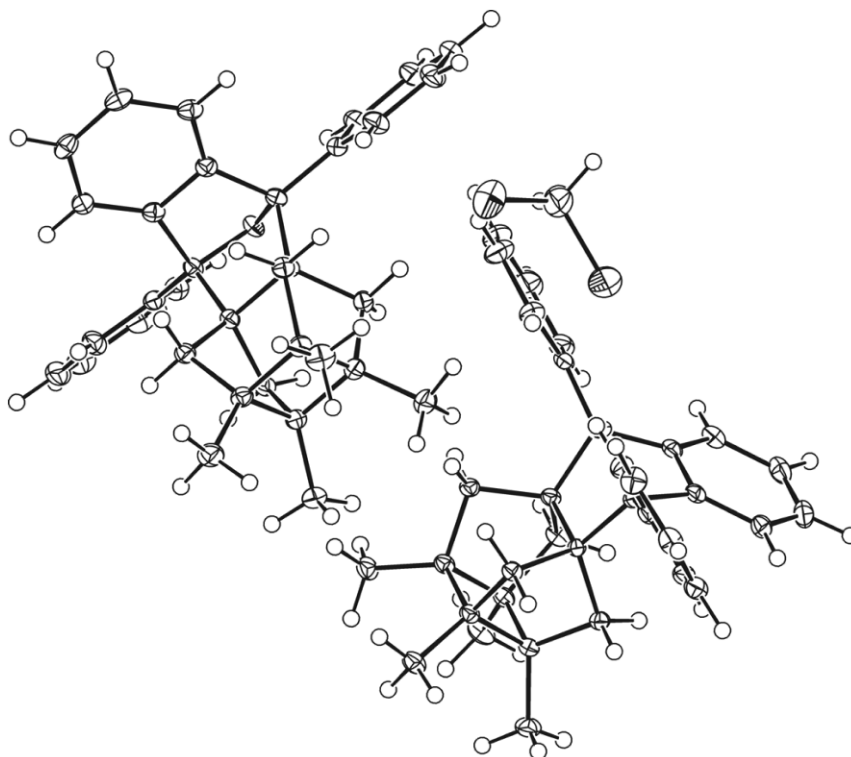
Figure 91. X-ray crystal structure (ORTEP) of the Diels-Alder adduct **147**

As we have already seen, the reaction of 1,2-diiodocompounds with *tert*-butyllithium is a convenient method for the generation of highly pyramidalized alkenes. However, in order to dimerize them, the use of *tert*-butyllithium is not always the best option as the nascent alkene may undergo nucleophylic attack by *tert*-butyllithium. For these reasons, in order to obtain the desired dimer we switched to a different way of generating the pyramidalized alkene. Our group has pioneered the use of molten sodium as an alternative, non-nucleophilic reagent for the generation of highly pyramidalized alkenes.[4a]

In this way, metallic sodium was melted in refluxing 1,4-dioxane, readily reacting with the diiodo compound to produce a radical anion intermediate which, after the loss of an iodide, was left as the alkyl radical. This one had then two paths to follow: i) being further reduced to the diradical, which would collapse as the pyramidalized alkene **142** and subsequently dimerize through a [2+2] cycloaddition to form the dimer **143** or ii) abstract a hydrogen from the medium before being reduced again to a tertiary alkyl radical. Similarly, this

intermediate could also follow two possible reaction pathways: i) abstract another hydrogen to afford the reduced compound **148** or ii) dimerize to furnish the dihydrodimer **149**. After a careful separation of the reaction mixture, the reduced compound **148** was isolated in 5% yield, the dihydrodimer **149** in 9% yield and the dimer **143** in 9% yield as well (Scheme 48).
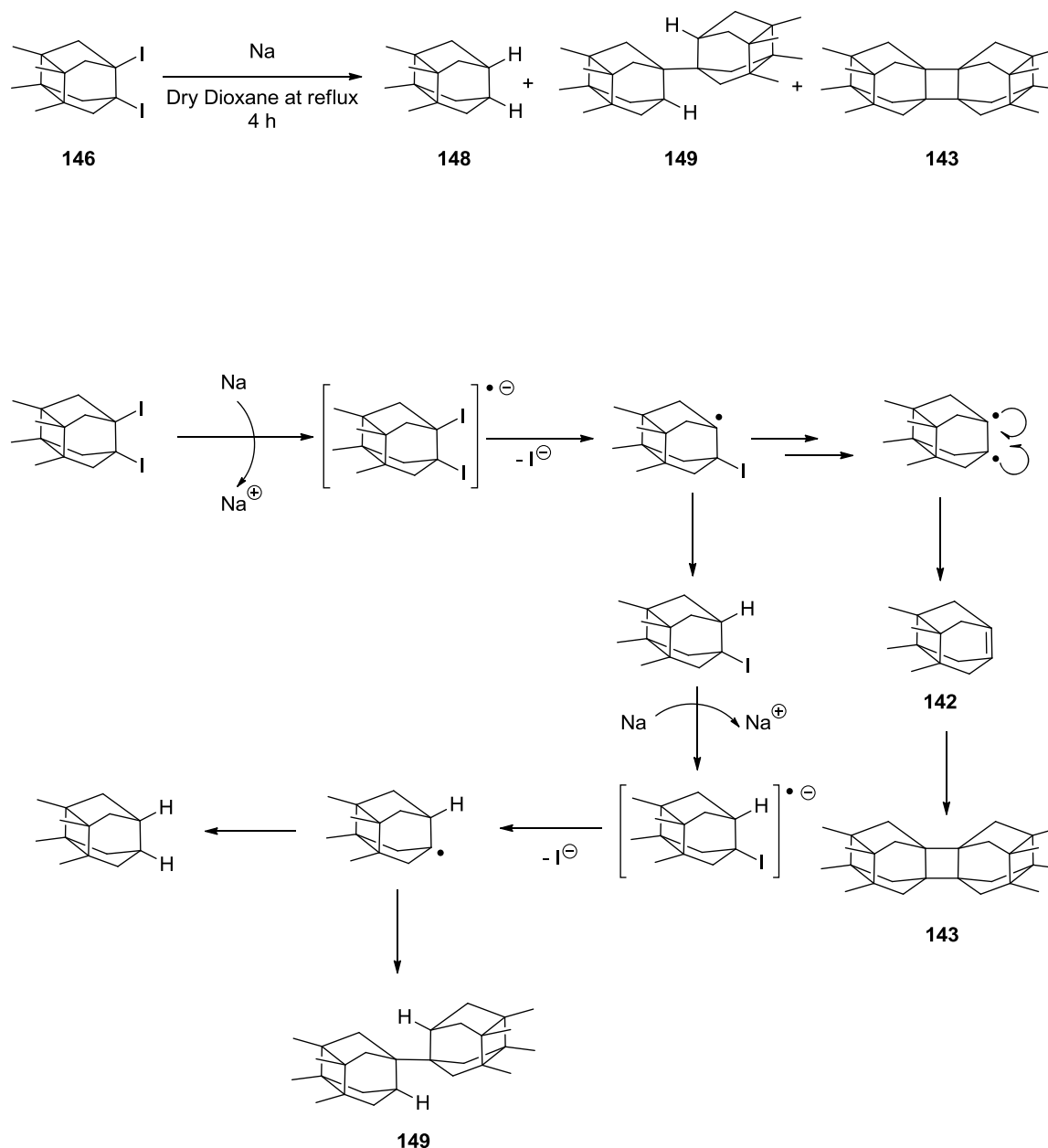
Scheme 48. Formation of the reduced product **148**, the dihydrodimer **149** and the dimer **143**

Unfortunately, we were unable to obtain a crystal good enough to diffract by X-ray the reduced compound **148**. However, we managed to secure crystals for X-ray diffraction of the dihydrodimer **149** (Figure 92) and the dimer **143** (Figure 93).
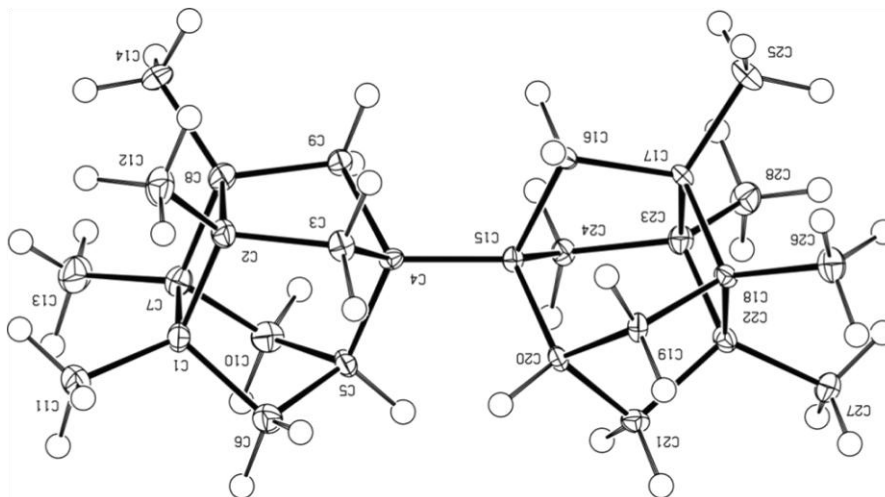
Figure 92. X-ray crystal structure (ORTEP) of the dihydrodimer **149**
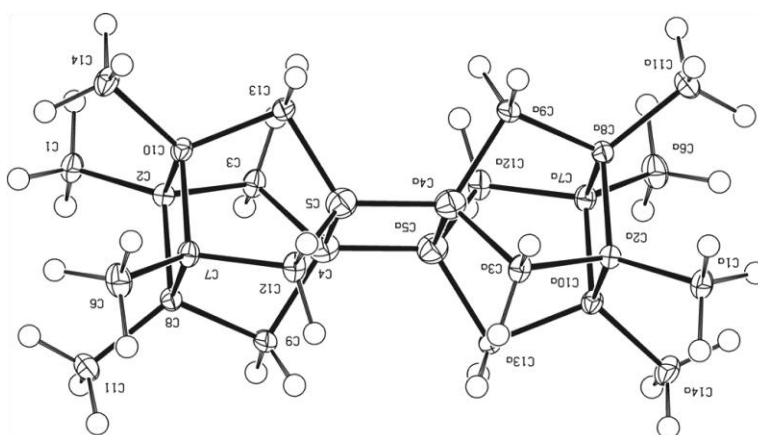
Figure 93. X-ray crystal structure (ORTEP) of dimer **143**

Besides, in collaboration with Professor J. Luque from the University of Barcelona, we performed theoretical calculations using two methods (B3LYP and MP2) on the abovementioned flagpole distances of the boat conformer of cyclohexane and on compounds **148** and **143** (Table 14).

Table 14. H-H and C-C distances between the flagpole H atoms and the C atoms attached to them in the boat conformer of cyclohexane, the reduced compound **148** and the dimer **143**

Compound	H-H distance (Å)			C-C distance (Å)		
	B3LYP/ 6-31G(d)	MP2/ 6-31G(d)	Crystal struct.	B3LYP/ 6-31G(d)	MP2/ 6-31G(d)	Crystal struct.
Cyclohex.	2.349	2.289	-	2.739	2.710	-
148	2.035	2.027	-	2.655	2.639	-
143	2.054	2.042	1.999	2.684	2.668	2.619

From these data we can extract some valuable information:

- Although the distances given by the two methods are very close, in our particular case, the prediction done with the MP2 ab initio method is more in accord with our experimental data than the one given by the B3LYP method.
- The calculated distances for the reduced compound **148** and for the dimer **143** are very similar, meaning that the C-C exocyclic bond does not have any particular effect on these flagpole distances.
- The distances found for our compounds are shorter than the ones displayed by the boat conformer of cyclohexane. This implies that the cyclobutane and cyclopentane rings on **143** and **148** hamper the ability of the boat cyclohexane to relieve the flagpole interaction.

Analyzing the crystal structures of dimer **143** and dihydrodimer **149** we discovered some features worth mentioning:

- About the dimer **143**, one interesting aspect are its cyclobutanes; the ones attached to the methyl groups are nearly perfect squares (1.584(4) Å/ 1.584(1) Å) whereas the central cyclobutane is not so symmetric (1.589 Å/ 1.542 Å), its newly formed C-C bond being shorter than the other two bonds. Nevertheless all the cyclobutanes are planar, their angles being between 89.90-90.05 º.

- Regarding the dihydrodimer **149** its H-H flagpole distances (between 1.93 Å and 2.03 Å) and the C-C distances of the carbons bearing the flagpoles H (average of 2.64 Å) were very similar to the ones found for **143**.

- Another interesting characteristic of **149** is its C-C exocyclic intercage distance with a value of 1.539(3) Å (cf. C-C bond of ethane is 1.531 Å). This length is the expected for a single bond and is halfway between the short intercage C-C bond of bicubyl derivatives and tetrahedranyltetrahedrane (1.44-1.46 Å) and the very long displayed in 1,1'-biadamantyl (1.578 Å) (Figure 94). The shortening of the former has been attributed to an increased s character and a hyperconjugative effect, [149] whereas the latter lengthening has been explained by the six H-H repulsions of the vicinal atoms. [150] Hence, this could mean that in our dihydrodimer **149** with C-C-C angles at the linking carbon atoms between 98.35-114.48 º, the effects of the increased s character due to the small distortion and the five H-H repulsions of the vicinal atoms, would cancel each other.

bicubyl   **tetrahedranyltetrahedrane**   **1,1'-biadamantyl**
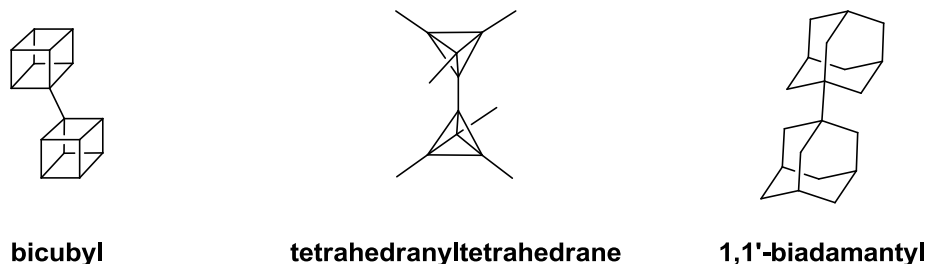
Figure 94. Bicubyl, tetrahedranyltetrahedrane and 1,1'-biadamantyl strucutres

---

[149] Mo, Y. *Org. Lett.* **2006**, *8*, 535.

[150] Alden, R. A.; Kraut, J.; Traylor, T. G. *J. Am. Chem. Soc.* **1968**, *90*, 74.

Finally, in collaboration with Dra. Gisela Colet, from the Institut Català d'Investigació Química, we performed a differential scanning calorimetry (DSC) measurement of dimer **143**. From previous experiences of the group with similar structures,[4a,4c,151] we envisioned that, upon exposing the sample to very high temperatures, a likely scenario was the opening of one or more cyclobutane rings through a [2+2] retrocycloaddition. MP2/6-311++G(d,p)//MP2/6-31G(d) calculations predicted endothermic processes for all the three possible ring openings; specifically the transformation from **143** to **150** required 17.8 kcal.mol^{-1} and the ring opening from **143** to **151** needed 11.5 kcal.mol^{-1}, very close to the energetic demand to afford **152**, 11.4 kcal.mol^{-1} (Scheme 49).
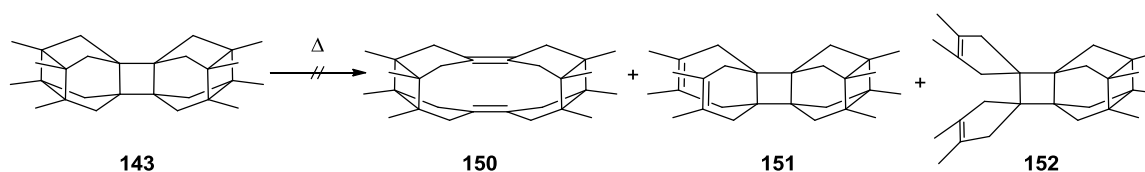
Scheme 49. Three different possibilities for the [2+2] retrocycloaddition of dimer **143**

Regrettably, the DSC experiment did not detect any of these ring openings when the dimer **143** was subjected to temperatures up to 500 °C. The only endothermic process was detected at 380 °C with a value of 0.005 kcal.mol^{-1} but was attributed to the melting of the sample (see blue area in Figure 95).
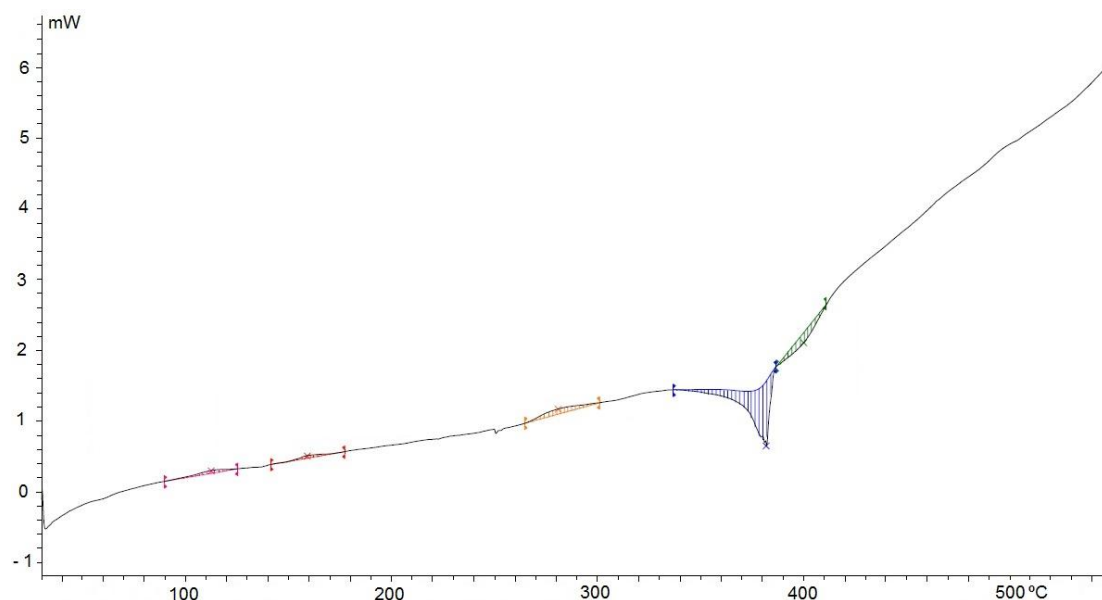
Figure 95. Plot of DSC of dimer **143**

---

[151] Camps, P.; Colet, G.; Delgado, S.; Muñoz, M. R.; Pericàs, M. A.; Solà, L.; Vázquez, S. *Tetrahedron* **2007**, *63*, 4669.

In conclusion, we have synthesized, trapped and dimerized a new pyramidalized alkene that bears four characteristic cyclohexane rings in frozen boat conformation, being a novel entry to the few molecules possessing this cyclohexane conformer with flagpole hydrogens. Many of the intermediates permitting the obtention of the pyramidalized alkene, as well as its Diels-Alder adduct, were crystallized and studied in detail through X-ray diffraction. Contrary to the previous molecules synthesized by the group, the polycyclic rings of the dimer **143** were thermally stable.

Materials and methods

General methods

Melting points were determined in open capillary tubes with a MFB 595010M Gallenkamp or a Büchi B‑540 melting point apparatuses.

300 MHz ^{1}H spectra, 400 MHz ^{1}H/100.6 MHz ^{13}C NMR spectra, and 500 MHz ^{1}H/125.7 MHz ^{13}C NMR spectra were recorded on Varian Gemini 300, Varian Mercury 400, and Varian Inova 500 spectrometers, respectively. The chemical shifts are reported in ppm (δ scale) relative to internal tetramethylsilane, and coupling constants are reported in Hertz (Hz). The used abbreviations were: s, singlet; d, doublet; t, triplet; q, quadruplet; quint, quintuplet; hept, septet; m, multiplet; or combinations thereof.

IR spectra were run on FTIR Perkin‑Elmer Spectrum RX I spectrophotometer using potassium bromide (KBr) pellets or attenuated total reflectance (ATR) Technique. Absorption values are expressed as wavenumbers (cm^{-1}); only significant absorption bands are given.

The GC/MS analyses were carried out in an inert Agilent Technologies 5975 gas chromatograph equipped with a DB‑5MS (30 m × 25 mm) capillary column with a stationary phase of phenylmethylsilicon (5% diphenyl − 95% dimethylpolysiloxane), using the following conditions: initial temperature of 50 ºC (1 min), with a gradient of 15 ºC / min up to 300 ºC, and a temperature in the source of 230 ºC. Solvent Delay (SD) of 3 minutes and pressure of 7,5 psi.

The accurate mass analyses were carried out at Unitat d'Espectrometria de Masses dels Centres Científics i Tecnològics de la Universitat de Barcelona (CCiTUB), Chemistry Faculty, using a LC/MSD‑TOF spectrophotometer.

The elemental analyses were carried out in a Flash 1112 series Thermofinnigan elemental microanalyzator (A5) to determine C, H and N, and in a titroprocessor Methrom 808 to determine Cl, at the Servei de Microanàlisi of IIQAB (CSIC) of Barcelona.

The X ray analyses were carried out in the Serveis Científico‑Tècnics of Universitat de Barcelona, using MNAR345 difractometer.

To concentrate solvents in vacuo a Büchi GKR‑50 rotavapor was used.

Column chromatography was performed on silica gel 60 Å (35-70 mesh, SDS, ref 2000027).

Thin‑layer chromatography was performed with aluminium‑backed sheets with silica gel 60 F254 (Merck, ref 1.05554), and spots were visualized with UV light and 1% aqueous solution of KMnO4.

All the new compounds that were subjected to a pharmacological evaluation, possessed a purity ≥ 95% as evidenced by their analytical data.

Solvent purification was carried out following the procedures described in: Perrin, D. D.; Armarego, W. L. F. *Purification of Laboratory Chemicals*, 4th Edition, Butterworth‑Heinemann: Oxford, 1996.

The NMR data and the synthetic procedure of all the compounds synthesized for the first time in our laboratory is included in the current manuscript. Regarding the compounds described previously in the literature, the synthetic procedure is described along with the literature reference corresponding with their first preparation.

A complete characterization of all the new compounds synthesized in this thesis was carried out including ^{1}H and ^{13}C, IR, elemental analysis and GC/MS. All ^{1}H and ^{13}C NMR signals were assigned by reason of homocorrelation (COSY ^{1}H/^{1}H and NOESY) and heterocorrelation ^{1}H/^{13}C (HSQC) experiments.

1. **5-azapentacyclo[6.4.0.0^{2,10}.0^{3,7}.0^{9,11}]dodecane and related compounds**

(1R, 2R, 3S, 7S)-Dimethyl tetracyclo[4.3.0.0²,⁴.0³,⁷]non-8-ene-8,9-dicarboxylate, 71.[106]
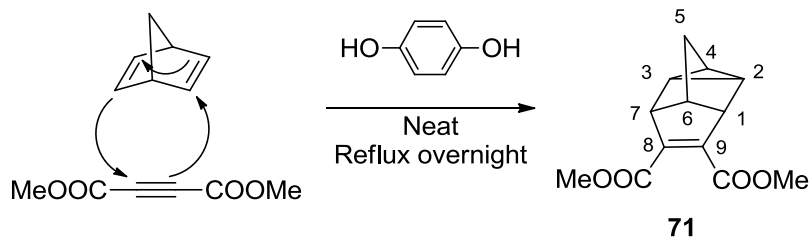
A solution of 2,5-norbornadiene (36.5 mL, 0.34 mol), MeOH (1 mL), dimethylacetylene dicarboxylate (13.0 mL, 0.11 mol) and hydroquinone (175 mg, 0.002 mol) was heated to reflux overnight. The light yellow solution was concentrated under reduced pressure and the residue was purified by a silica gel column chromatography. The product **71** was obtained in the fractions eluted with (Hex:EtOAc, 9:1) as an orange oil (20.25 g, 82%). The spectroscopical and analytical data were in accord with the ones described in the literature.[106]

(1R, 2R, 3S, 7S)-Tetracyclo[4.3.0.0²,⁴.0³,⁷]non-8-ene-8,9-dicarboxylic acid, 72.[106]
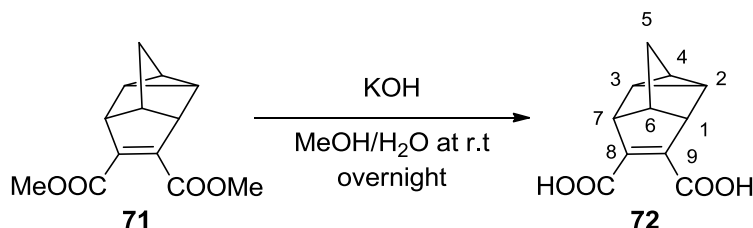
A solution of potassium hydroxide (58.45 g, 90.8 mol) in water (160 mL) was added to a solution of **71** (20.25 g, 86.4 mol) in MeOH (425 mL). The solution was left stirring at room temperature overnight. The MeOH was removed under reduced pressure and the remaining solution was acidified with HCl 5N (160 mL) until no more precipitate was formed. The suspension was extracted with EtOAc (3 x 500 mL) and the combined organic phases were dried over Na₂SO₄, filtered and concentrated under reduced pressure to yield **72** as a light brown solid (15.33 g, 86%). The spectroscopical and analytical data were in accord with the ones described in the literature.[106]

(1R, 2R, 3S, 7S, 8R, 9S)-Tetracyclo[4.3.0.0²,⁴.0³,⁷]nonane-8endo,9endo-dicarboxylic acid, 76.[152]
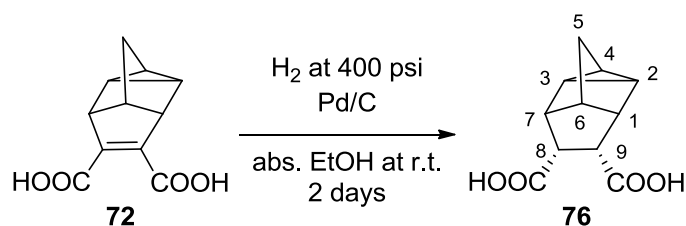
A solution of **72** (2.00 g, 9.70 mmol) and palladium on activated charcoal (800 mg, 5% in Pd) in absolute EtOH (100 mL) was set in a reactor with hydrogen at 400 psi for 2 days. The black suspension was filtered and the clear solution concentrated under reduced pressure to yield **76** as a white solid (1.79 g, 90%). An analytical sample was obtain by crystallization from acetonitrile. The spectroscopical and analytical data were in accord with the ones described in the literature.[152]

(2R, 3S, 7R, 8S, 9S, 10R)-5-Azapentacyclo[6.4.0.0²,¹⁰.0³,⁷.0⁹,¹¹]dodecane-4,6-dione, 77.
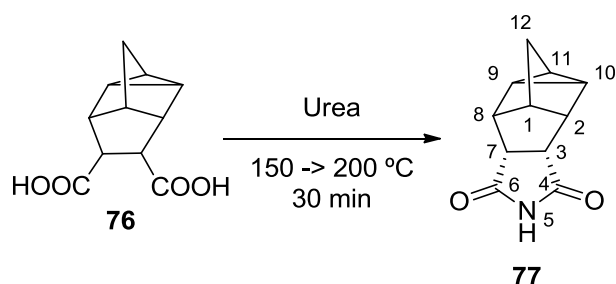
A mixture of **76** (1.03 g, 4.95 mmol) and urea 99.5% (1.49 g, 24.7 mmol) was heated to 150°C until the urea melted. Then the temperature was raised to 220°C for 30 min. The brown paste was redissolved in water (50 mL) and DCM (50 mL). The first organic phase was separated and the aqueous phase was extracted with DCM (5 x 50 mL). The combined organic phases were dried over Na₂SO₄, filtered and concentrated under reduced pressure to yield **77** as a yellow solid (737 mg, 79%).

---

[152] Russell, G. A.; Holland, G. W.; Chang, K.-Y.; Keske, R. G.; Mattox, J.; Chung, C. S. C.; Stanley, K.; Schmitt, K.; Blankespoor, R.; Kosugi, Y. *J. Am. Chem. Soc.* **1974**, 96, *23*, 7237.

Analytic and spectroscopic data of **77**:

Melting point 211-212 °C

IR (KBr) ν 3446, 3185, 3064, 2953, 2931, 2864, 2737, 1750, 1705, 1384, 1354, 1327, 1312, 1289, 1261, 1223, 1178, 1121, 1072, 1001, 993, 936, 797, 749, 706, 650, 632, 604, 538 cm^{-1}.

^{1}H NMR (400 MHz, CDCl$_3$) δ 1.08 [dd, J = 4.8 Hz, J' = 0.8 Hz, 2 H, 9(10)-H], 1.26 (t, J = 4.8 Hz, 1 H, 11-H), 1.59 (t, J = 1.2 Hz, 2 H, 12-H$_2$), 2.11 (broad s, 1 H, 1-H), 2.45 [broad s, 2 H, 2(8)-H], 3.24 [dd, J = 3.2 Hz, J' = 2.0 Hz, 2 H, 3(7)-H], 8.40 (broad s, 1 H, NH).

^{13}C NMR (100.6 MHz, CDCl$_3$) δ 11.2 [CH, C9(10)], 12.8 (CH, C11), 31.2 (CH$_2$, C12), 44.2 [CH, C3(7)], 45.6 (CH, C1), 48.8 [CH, C2(8)], 179.1 [C=O, C4(6)].

MS (GC), m/e (%); main ions: 189 (M^{+}, 67), 118 (92), 117 [(M-C$_2$H$_2$NO$_2$$^{+}$), 100], 115 (23), 92 (11), 91 (28), 65 (9), 58 (9).

Accurate mass:

Calculated for [C$_{11}$H$_{11}$NO$_2$+H]$^+$:   190.0863

Found: 190.0867

(2R, 3S, 7R, 8S, 9S, 10R)-5-Azapentacyclo[6.4.0.0^{2,10}.0^{3,7}.0^{9,11}]dodecane hydrochloride, 78·HCl.

To a solution of **77** (627 mg, 3.31 mmol) in dry toluene (22 mL) was added dropwise Red-Al 65% in toluene (5.05 mL, 16.57 mmol). The mixture was heated to reflux for 2 days. The black solution was quenched with KOH 30% aq. (10 mL) and the organic phase was separated. The aqueous layer was extracted with DCM (3 x 20 mL) and the combined organic phases were dried over Na$_2$SO$_4$, filtered and concentrated under reduced pressure. The yellow oil was redissolved in EtOAc and HCl/Et$_2$O 1.2N was added until no more precipitate was formed. It was filtered under vacuo and **78·HCl** was obtained as a light brown solid (305 mg, 47%).

Analytic and spectroscopic data of **78·HCl**:

Melting point: 208-209 °C

IR (KBr) ν 3435, 3209, 3081, 3046, 2983, 2899, 2954, 2938, 2870, 2752, 2725, 2620, 2559, 2443, 1569, 1467, 1457, 1399, 1344, 1305, 1274, 1256, 1231, 1146, 1062, 1000, 987, 945, 890, 875, 830, 817, 770, 695, 654 cm^{-1}.

^{1}H NMR (400 MHz, CD$_3$OD) δ 1.16 [d, J = 5.2 Hz, 2 H, 9(10)-H], 1.31 (t, J = 5.2 Hz, 1 H, 11-H), 1.56 (t, J = 1.2 Hz, 2 H, 12-H$_2$), 2.11 (m, 1 H, 1-H), 2.13 [m, 2 H, 2(8)-H], 3.00 [dd, J = 7.2 Hz, J' = 3.2 Hz, 2 H, 3(7)-H], 3.24 [m, 2 H, 4(6)-H$_a$], 3.42 [dd, J = 12 Hz, J' = 3.2 Hz, 2 H, 4(6)-H$_b$].

^{13}C NMR (100.6 MHz, CD$_3$OD) δ 11.4 [CH, C9(10)], 15.2 (CH, C11), 31.4 (CH$_2$, C12), 45.2 [CH, C3(7)], 46.9 (CH, C1), 47.3 [CH, C2(8)], 49.0 [CH$_2$, C4(6)].

MS (DI), m/e (%); main ions: 162 (10), 161 (M$^{·+}$, 84), 160 (56), 132 (14), 131 (12), 129 (12), 120 (20), 118 (21), 117 (47), 116 (13), 115 (30), 107 (18), 106 (17), 95 (28), 94 (50), 93 (15), 58 (91), 83 (14), 82 (28), 81 (35), 80 (90), 79 (16), 78 (27), 78 (26), 69 (11), 68 (100), 67 (25), 65 (18), 56 (12), 51 (11).

Elemental analysis:

| Calculated for C$_{11}$H$_{15}$N·HCl: | | C 66.83% | H 8.16% |
| N 7.08% | Cl 17.93% | | |

| Calculated for C$_{11}$H$_{15}$N·HCl·0.3H$_2$O·0.15HCl | | C 63.34% | H 8.09% |
| N 6.72% | Cl 19.55% | | |

| Found: | | C 63.30% | H 8.04% |
| N 6.71% | Cl 19.78% | | |

(2R, 3S, 7R, 8S, 9S, 10R)-5-Amidino-5-azapentacyclo[6.4.0.0²,¹⁰.0³,⁷.0⁹,¹¹]dodecane hydrochloride, 79·HCl.

A mixture of **78·HCl** (305 mg, 1.54 mmol), 1-*H*-pyrazole-1-carboxamidine monohydrochloride (271 mg, 1.85 mmol) and triethylamine (0.4 mL, 2.78 mmol) was dissolved in acetonitrile (12 mL). The yellow suspension was heated to mild reflux for 6 hours and was left at 4 °C overnight. The precipitate was separated and **79·HCl** was obtained as a light orange solid (258 mg, 70%). An analytical sample was obtained by crystallization from isopropanol.

Analytic and spectroscopic data of **79·HCl**:

Melting point: 153-154 °C

IR (KBr) ν 3567, 3482, 3344, 3304, 3190, 3138, 3066, 2995, 2958, 2945, 2881, 2861, 2677, 1627, 1508, 1467, 1458, 1367, 1342, 1304, 1284, 1249, 1225, 1189, 1160, 1073, 1036, 957, 937, 832, 802, 787, 775, 644, 582 cm⁻¹.

¹H NMR (400 MHz, CD₃OD) δ 1.00 [dd, J = 5.2, J' = 0.8 Hz, 2 H, 9(10)-H], 1.20 (t, J = 5.2 Hz, 1 H, 11-H), 1.55 (t, J = 1.2 Hz, 2 H, 12-H₂), 2.02 (broad s, 1 H, 1-H), 2.13 [broad s, 2 H, 2(8)-H], 2.97 [m, 2 H, 3(7)-H], 3.39 [m, 2 H, 4(6)-H$_a$], 3.65 [dd, J = 10.8 Hz, J' = 1.2 Hz, 2 H, 4(6)-H$_b$].

¹³C NMR (100.6 MHz, CD₃OD) δ 10.7 [CH, C9(10)], 13.9 (CH, C11), 31.5 (CH₂, C12), 44.8 [CH, C3(7)], 45.9 (CH, C1), 48.5 [CH, C2(8)], 50.1 [CH₂, C4(6)], 155.7 [C=NH]

MS (DI), m/e (%); main ions: 204 (15), 203 (M·⁺, 100), 202 (13), 160 (49), 137 (13), 131 (10), 129 (28), 128 (14), 124 (19), 117 (25), 116 (12), 115 (26), 111 (39), 110 (97), 95 (11), 94 (21), 93 (12), 91 (49), 85 (51), 82 (17), 80 (24), 79 (14), 78 (15), 77 (23), 72 (20), 68 (68), 67 (14), 65 (16).

Elemental analysis:

Calculated for $C_{12}H_{17}N_3 \cdot HCl$: C 60.12% H 7.57%
  N 17.53% Cl 14.79%

Calculated for $C_{12}H_{17}N_3 \cdot HCl \cdot 0.75H_2O \cdot 0.05HCl$ C 56.50% H 7.73%
  N 16.47% Cl 14.59%

Found: C 56.55% H 7.59%
  N 16.62% Cl 14.49%

2. **4-Azapentacyclo[5.3.2.0^{2,6}.0^{8,10}]dodecane and related compounds**

(1R, 2R, 6S, 7S, 8S, 10R)-4-Azapentacyclo[5.3.2.0²,⁶.0⁸,¹⁰]dodec-11-ene-3,5-dione, 80.[113]

To a solution of 1,3,5-cycloheptatriene (9.21 g, 100 mmol) in xylene (150 mL) was added maleimide (9.71 g, 100 mmol) and the mixture was refluxed for 3 hours. On cooling to 4-5 ºC a solid was separated, which was filtered and washed with xylene and hexane to give imide **80** (14.2 g, 76% yield).

Spectroscopic data of **80**:

¹H NMR (400 MHz, CDCl$_3$) δ 0.23 (complex signal, 2 H, 9-H$_2$), 1.06 [m, 2 H, 8(10)-H], 3.00 [m, 2 H, 2(6)-H], 3.37 [m, 2 H, 1(7)-H], 5.79 [m, 2 H, 11(12)-H].

¹³C NMR (100.6 MHz, CDCl$_3$) δ 4.8 (CH$_2$, C9), 9.7 [CH, C8(10)], 33.3 [CH, C1(7)], 46.6 [CH, C2(6)], 127.7 [CH, C11(12)], 178.8 [C=O, C3(5)].

(1R, 2R, 6S, 7S, 8S, 10R)-4-Azapentacyclo[5.3.2.0^{2,6}.0^{8,10}]dodec-11-ene hydrochloride, 81·HCl.

A solution of imide **80** (8.00 g, 42.3 mmol) in dry and degassed toluene (280 mL) was cooled down to 5° C with an ice bath. Sodium bis(2-methoxyethoxy) aluminium hydride (64.5 mL, 65% solution in toluene, 211.4 mmol) was added dropwise and the resulting solution was heated to reflux and stirred for 2 days. The solution was allowed to cool down to room temperature and 30% aqueous KOH (300 mL) was added dropwise. The organic phase was separated and the aqueous layer was extracted with dichloromethane (3 x 250 mL). The combined organic extracts were dried over Na_2SO_4, filtered and concentrated under vacuo to give a red oil. This oil was dissolved in EtOAc and treated with an excess of a 1.2 N ethereal solution of HCl and was allow to stand at 0 °C for 24 hours. The suspension was filtered to get **81·HCl** as a white solid (6.54 g, 79%). An analytical sample of **81·HCl** was obtained by crystallization from MeOH/Et$_2$O.

Analytic and spectroscopic data of **81·HCl**:

Melting point: 197-198 °C

IR (KBr) ν 3430, 2932, 2894, 2765, 2519, 2640, 1569, 1466, 1450, 1422, 1395, 1383, 1355, 1301, 1281, 1245, 1170, 1132, 1068, 1026, 1016, 936, 902, 841, 824, 758, 731, 649, 591, 580 cm^{-1}

^{1}H NMR (400 MHz, CD$_3$OD) δ 0.23 (complex signal, 2 H, 9-H$_2$), 1.05 [m, 2 H, 8(10)-H], 2.75 [m, 2 H, 2(6)-H], 2.82 [dm, J = 12.0 Hz, 2 H, 3(5)-H$_a$], 2.95 [m, 2 H, 1(7)-H], 3.38 [dd, J = 12.0 Hz, 2 H, 3(5)-H$_b$], 5.91 [m, 2 H, 11(12)-H].

^{13}C NMR (100.6 MHz, CD$_3$OD) δ 5.5 (CH$_2$, C9), 11.1 [CH, C8(10)], 35.5 [CH, C1(7)], 44.8 [CH, C2(6)], 50.4 [CH$_2$, C3(5)], 130.7 [CH, C11(12)].

MS (DI), m/e (%); main ions: 161 (M$^{·+}$, 5), 94 (14), 93 (16), 92 (19), 91 (47), 81 (12), 80 (20), 68 (100), 67 (35).

Elemental analysis:

Calculated for $C_{11}H_{15}N \cdot HCl$ C 66.83%   H 8.16%   N 7.08%
     Cl 17.93%

Found: C 66.55%   H 8.13%   N 7.00%
     Cl 17.81%

(1R, 2R, 6S, 7S, 8S, 10R)-4-Amidino-4-azapentacyclo[5.3.2.0^{2,6}.0^{8,10}]dodec-11-ene hydrochloride, 82·HCl.

A solution of **81·HCl** (1.15 g, 5.83 mmol) in water (30 mL) was basified to pH = 14 with a 10 N aqueous solution of NaOH. It was then extracted with EtOAc (3 x 50mL) and the joined organic phases were dried over Na_2SO_4, filtered and concentrated under vacuo (yellow oil, 900 mg, 5.55 mmol, 95% yield). To a suspension of this oil in acetonitrile (35 mL), 1*H*-pyrazole-1-carboxamidine monohydrochloride (1.08 g, 7.40 mmol) was added. The suspension was heated to reflux for 6 hours. The yellow precipitate was filtered to give **82·HCl** as yellow crystals (1.13 g, 85%). An analytical sample was obtained by crystallization from MeOH/Et$_2$O.

Analytic and spectroscopic data of **82·HCl**:

Melting Point: 248−249 °C (dec.)

IR (KBr) ν 3468, 3410, 3327, 3135, 3047, 3025, 2997, 2948, 2880, 2414, 1669, 1620, 1527, 1470, 1434, 1374, 1363, 1281, 1169, 1085, 1045, 1015, 973, 854, 819, 766, 710, 645 cm^{-1}

^{1}H NMR (400 MHz, CD$_3$OD) δ 0.15-0.23 (complex signal, 2 H, 9-H$_2$), 1.02 [m, 2 H, 8(10)-H], 2.81 [m, 2 H, 2(6)-H], 2.92 [broad s, 2 H, 1(7)-H], 3.12 [dd, J = 10.8 Hz, J' = 3.4 Hz, 2 H, 3(5)-H$_a$], 3.52 [m, 2 H, 3(5)-H$_b$], 5.85 [m, 2 H, 11(12)-H].

^{13}C NMR (100.6 MHz, CD$_3$OD) δ 4.7 (CH$_2$, C9), 10.7 [CH, C8(10)], 37.0 [CH, C1(7)], 45.1 [CH, C2(6)], 52.4 [CH$_2$, C3(5)], 130.1 [CH, C11(12)], 155.5 (C, CNH).

MS (DI), m/e (%); main ions: 203 (M$^{.+}$, 15), 126 (13), 125 (32), 124 (28), 115 (15), 114 (16), 113 (50), 112 (78), 111 (55), 110 (14), 92 (25), 91 (70), 77 (14), 69 (43), 68 (100), 67 (18), 65 (13).

Elemental analysis:

Calculated for C$_{12}$H$_{17}$N$_3$·HCl	C 60.12%	H 7.57%
N 17.53% Cl 14.79%		
Calculated for C$_{12}$H$_{17}$N$_3$·HCl·0.25 H$_2$O:	C 59.01%	H 7.53%
N 17.20% Cl 14.51%		
Found:	C 59.03%	H 7.62%
N 17.45% Cl 14.57%		

(1R, 2R, 6S, 7S, 8S, 10R)-4-Amidino-4-azapentacyclo[5.3.2.0^{2,6}.0^{8,10}]dodecane hydrochloride, 83·HCl.

To a solution of **82·HCl** (377 mg, 1.57 mmol) in absolute EtOH (35 mL), Pd on activated charcoal (78 mg, ca. 10% Pd) was added and the resulting suspension was hydrogenated at room temperature and at 150 psi of H$_2$ overnight. The black suspension was filtered to furnish **83·HCl** as an off-white powder (290 mg, 77%). An analytical sample was obtained by crystallization from MeOH/Et$_2$O.

Analytic and spectroscopic data of **83·HCl**:

Melting Point 208−209 ºC

IR (KBr) ν 3311, 3124, 3007, 2993, 2949, 2924, 2907, 1653, 1602, 1529, 1484, 1465, 1378, 1352, 1337, 1299, 1283, 1208, 1185, 1171, 1136, 1071, 1024, 936, 805, 642, 539, 487 cm^{-1}

^{1}H NMR (400 MHz, CD$_3$OD) δ 0.51 [dt, J = 6.2 Hz, J' = 7.8 Hz, 1 H, 9-H$_a$], 0.87 [dt, J = 6.2 Hz, J' = 3.6 Hz, 1 H, 9-H$_b$], 1.02 [m, 2 H, 8(10)-H], 1.18 [broad d, J = 10.0 Hz, 2 H, 11(12)-H$_a$], 1.29 [broad d, J = 10.0 Hz, 2 H, 11(12)-H$_b$], 1.92 [broad s, 2 H, 1(7)-H], 2.70 [m, 2 H, 2(6)-H], 3.48 [m, 2 H, 3(5)-H$_a$], 3.54 [dt, J = 11.2 Hz, J' = 2.0 Hz, 2 H, 3(5)-H$_b$].

^{13}C NMR (100.6 MHz, CD$_3$OD) δ 5.4 (CH$_2$, C9), 15.8 [CH, C8(10)], 18.4 [CH$_2$, C11(12)], 30.4 [CH, C1(7)], 40.9 [CH, C2(6)], 51.0 [CH$_2$, C3(5)], 156.1 (C, $\underline{C}$NH).

MS (DI), m/e (%); main ions: 205 (M$^{·+}$, 46), 204 (29), 138 (11), 112 (100), 111 (36), 110 (30), 91 (19), 79 (17), 72 (17), 68 (42).

Elemental analysis:

Calculated for C$_{12}$H$_{19}$N$_3$·HCl	C 59.62%	H 8.34%
N 17.38% Cl 14.66%		
Calculated for C$_{12}$H$_{19}$N$_3$·HCl·0.33 H$_2$O:	C 58.17%	H 8.41%
N 16.96% Cl 14.31%		
Found:	C 58.17%	H 8.23%
N 17.09% Cl 14.58%		

(1R, 2R, 6S, 7S, 8S, 10R)-4-Azapentacyclo[5.3.2.0²,⁶.0⁸,¹⁰]dodecane hydrochloride, 84·HCl.

To a solution of **81·HCl** (200 mg, 1.00 mmol) in absolute EtOH (35 mL), Pd on activated charcoal (5%, 40 mg) was added. The black suspension was set in a hydrogenator at 150 psi of H_2 and was stirred at room temperature overnight. The black suspension was filtered and **84·HCl** was recovered as an off-white solid (190 mg, 95%). An analytical sample was obtained by crystallization from 2-propanol.

Analytic and spectroscopic data of **84·HCl**:

Melting point 227-228 °C

IR (KBr) ν 3421, 3073, 2935, 2755, 2646, 2585, 2460, 2363, 1590, 1447, 1423, 1347, 1100, 1058, 1028, 999, 902, 881, 812, 798, 752, 723, 662, 526 cm⁻¹

¹H NMR (400 MHz, CD$_3$OD) δ 0.59 (dt, J = 6.0 Hz, J' = 7.6 Hz, 1 H, 9-H$_a$), 0.97 (dt, J = 6.0 Hz, J' = 3.6 Hz, 1 H, 9-H$_b$), 1.04 [m, 2 H, 8(10)-H], 1.25 [broad d, J = 8.8 Hz, 2 H, 11(12)-H$_a$], 1.42 [broad d, J = 8.8 Hz, 2 H, 11(12)-H$_b$], 1.96 [broad s, 2 H, 1(7)-H], 2.68 [m, 2 H, 2(6)-H], 3.16 [dd, J = 12.0 Hz, J' = 6.8 Hz, 2 H, 3(5)-H$_a$], 3.42 [dd, J = 12.0 Hz, J' = 8.6 Hz, 2 H, 3(5)-H$_b$].

¹³C NMR (100.6 MHz, CD$_3$OD) δ 6.9 [CH$_2$, C9], 16.7 [CH, C8(10)], 17.9 [CH$_2$, C11(12)], 28.1 [CH, C1(7)], 41.2 [CH, C2(6)], 48.6 [CH$_2$, C3(5)].

MS (DI), m/e (%); main ions: 163 (M⁺, 35), 162 (15), 134 (73), 105 (12), 94 (14), 93 (13), 92 (12), 91 (35), 80 (20), 79 (30), 77 (25), 70 (100), 68 (62), 67 (21).

Elemental analysis:

Calculated for C₁₁H₁₇N·HCl	C 66.15%	H 9.08%	N 7.01%
Cl 17.75%			
Calculated for C₁₁H₁₇N·HCl·0.33 H₂O:	C 64.24%	H 9.14%	N 6.81%
Cl 17.24%			
Found:	C 64.43%	H 8.96%	N 6.94%
Cl 17.55%			

(1R, 2R, 6S, 7S, 8S, 10R)-4-[(*tert*-Butoxycarbonyl)-4-piperidinyl]-4-azatetracyclo[5.3.2.0²,⁶.0⁸·¹⁰]dodec-11-ene, 85.

A solution of **81·HCl** (1.15 g, 5.83 mmol) in water (30 mL) was basified to pH = 14 with a 10 N aqueous solution of NaOH. It was then extracted with EtOAc (3 x 50mL) and the joined organic phases were dried over Na_2SO_4, filtered and concentrated under vacuo (yellow oil, 945 mg, 5.83 mmol, quantitative yield). The yellow oil was dissolved in MeOH (20 mL) in a round bottom flask fitted with a $CaCl_2$ tube then sodium cyanoborohydride (1.06 g, 16.91 mmol), 1-Boc-4-piperidone (1.39 g, 7.00 mmol) and glacial acetic acid (0.67 mL) were added to the solution. It was stirred at room temperature for 8 hours, then more sodium cyanoborohydride (1.06 g, 16.91 mmol) and more 1-Boc-4-piperidone (1.39 g, 7.00 mmol) were added. The yellow solution was stirred at room temperature overnight. It was concentrated under vacuo and the yellow oil was redissolved in water (50 mL) and extracted with EtOAc (3 x 50 mL). The organic phase was dried over Na_2SO_4, filtered and concentrated under vacuo (clear sticky solid, 3.90 g). The clear solid was columnated through silica gel and **85** was obtained in the EtOAc fractions as an off-white solid (1.52 g, 75%). An analytical sample was obtained by crystallization from MeOH/Et₂O.

Analytic and spectroscopic data of **85**:

Melting point 176-177 °C

IR (KBr): 3004, 2980, 2683, 2612, 2330, 2203, 2163, 1684, 1455, 1420, 1364, 1264, 1170, 1150, 1113, 1068, 1047, 1016, 974, 944, 866, 841, 814, 768, 733 cm⁻¹.

^{1}H NMR (500 MHz, CDCl$_3$) δ 0.21 (m, 1 H, 9-H$_b$), 0.27 (td, J = 7.5 Hz, J' = 5.5 Hz, 1 H, 9-H$_a$), 1.01 [m, 2 H, 8(10)-H],], 1.44 [s, 9 H, *tert*-butyl], 1.65 [qd, J = 12.5 Hz, J' = 2.5 Hz, piperidine-C3'(5')-H$_{ax}$], 1.94 [m, 2 H, piperidine-C3'(5')-H$_{eq}$], 2.39 [broad s, 2 H, 3(5)-H$_a$], 2.68 [broad s, 2 H, piperidine-C2'(6')-H$_{ax}$], 2.81 [m, 2 H, 2(6)-H], 2.93 [broad s, 3 H, 1(4',7)-piperidine-C4], 3.60 [broad s, 2 H, 3(5)-H$_b$], 4.21 [broad s, 2 H, piperidine-C2'(6')-H$_{eq}$], 5.86 [m, 2 H, 11(12)-H].

^{13}C NMR (100.6 MHz, CDCl$_3$) δ 5.59 (CH$_2$, C9), 10.1 [CH, C8(10)], 28.1 [CH$_2$, C3'(5')-piperidine], 28.5 [CH$_3$, CH$_3$-*tert*-butyl], 33.5 [CH, C1(7)], 41.9 [CH$_2$, C2'(6')-piperidine], 42.2 [CH, C2(6)], 54.8 [CH$_2$, C3(5)], 62.4 (CH, C4'-piperidine), 80.6 (C, C-*tert*-butyl), 129.6 [HC=CH, C11(12)], 154.2 (C=O).

MS (DI), m/e (%); main ions: 344 (M^{+}, 26), 287 [(M-C$_4$H$_9$)$^+$, 34], 243 [(M-COOC$_4$H$_9$)$^+$, 12), 195 (C$_5$H$_9$O$_2$$^{·+}$, 100), 188 (14), 151 (15), 94 (19), 57(27)

Accurate mass:

Calculated for [C$_{21}$H$_{32}$N$_2$O$_2$+H]$^+$:   345.2537

Found: 345.2533

(1R, 2R, 6S, 7S, 8S, 10R)-4-(4-Piperidinyl)-4-azatetracyclo[5.3.2.0^{2,6}.0^{8,10}]dodec-11-ene dihydrochloride, 86·2HCl.
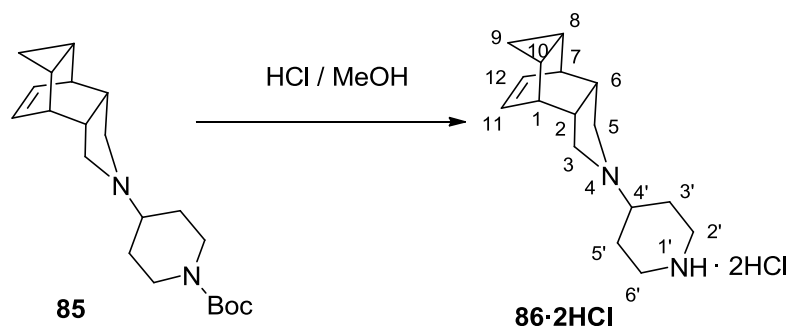
To a solution of **85** (760 mg, 2.20 mmol) in methanol (25 mL), a 0.8 N HCl solution in methanol (30 mL) was added. The resulting clear solution was heated to reflux and stirred for 30 min. It was then allowed to cool down to room temperature and was concentrated under vacuo to give a white solid, that was crystallized from MeOH/Et$_2$O to give **86·2HCl** as a white solid (700 mg, quantitative).

Analytic and spectroscopic data of **86·2HCl**:

Melting point >250 ºC (dec.)

IR (KBr) ν 3479, 3405, 2945, 2804, 2733, 2642, 2585, 2496, 2363, 1630, 1458, 1437, 1239, 1157, 1044, 974, 842, 766, 727, 679, 583 cm^{-1}

^{1}H NMR (400 MHz, CD$_3$OD) δ 0.28 (m, 2 H, 9-H$_2$), 1.04 [m, 2 H, 8(10)-H$_2$], 2.00 [dm, J = 13.6 Hz, 2 H, piperidine-C3'(5')-H$_{ax}$], 2.35 [d, J = 13.6 Hz, 2 H, piperidine-C3'(5')-H$_{eq}$], 2.59 [broad s, 2 H, 3(5)-H$_a$], 2.76 [broad s, 2 H, 2(6)-H], 2.96 [broad s, 2 H, 1(7)-H], 3.07 [td, J = 13.2 Hz, J' = 2.8 Hz, 2 H, piperidine-C2'(6')-H$_{ax}$], 3.40 (tt, J = 13.0 Hz, J' = 4.0 Hz, 1 H, piperidine-C4-H), 3.54 [dm, J = 13.2 Hz, 2 H, piperidine-C2'(6')-H$_{eq}$], 3.78 [broad s, 2 H, 3(5)-H$_b$], 5.90 [m, 2 H, 11(12)-H].

^{13}C NMR (100.6 MHz, CD$_3$OD) δ 5.8 (CH$_2$, C9), 10.9 [CH, C8(10)], 26.7 [CH$_2$, C3'(5')-piperidine], 34.4 [CH, C1(7)], 43.5 [CH$_2$, C2'(6')-piperidine], 43.8 [CH, C2(6)], 56.6 [CH$_2$, C3(5)], 60.1 (CH, C4'-piperidine), 130.5 [CH, C11(12)].

MS (DI), m/e (%); main ions: 244 (M$^{·+}$, 23), 200 (14), 189 (27), 188 (25), 164 (18), 163 (57), 162 (33), 160 (14), 152 (100), 151 (43), 120 (12), 108 (43), 107 (26), 97 (35), 96 (15), 95 (15), 94 (50), 91 (35), 86 (15), 85 (58), 84 (50), 83 (41), 82 (20), 69 (27), 68 (44), 58 (16), 57 (28), 55 (26).

Elemental analysis:

Calculated for C$_{16}$H$_{24}$N$_2$·2HCl	C 60.27%	H 8.26%
N 8.83% Cl 22.35%		
Calculated for C$_{16}$H$_{24}$N$_2$·2.15HCl·H$_2$O:	C 56.59%	H 8.33%
N 8.22% Cl 22.37%		
Found:	C 56.39%	H 8.33%
N 8.42% Cl 22.37%		

(1R, 2R, 6S, 7S, 8S, 10R)-4-(4-Piperidinyl)-4-azatetracyclo[5.3.2.0²,⁶.0⁸,¹⁰]dodecane dihydrochloride, 87·2HCl.
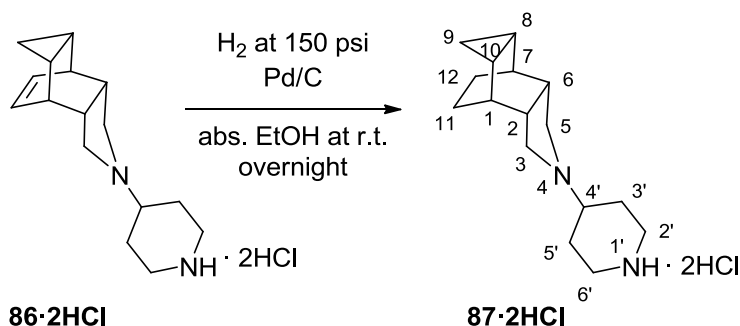
To a solution of **86·2HCl** (200 mg, 0.63 mmol) in absolute EtOH (35 mL), Pd on activated charcoal (40 mg, ca. 10% Pd) was added and the resulting suspension was hydrogenated at room temperature and at 150 psi of H_2 overnight. The black suspension was filtered and **87·2HCl** was recovered as a white solid (170 mg, 85%). An analytical sample was obtained by crystallization from MeOH.

Melting point >300 ºC (dec.)

IR (KBr) ν 3422, 2929, 2889, 2840, 2779, 2726, 2646, 2608, 2495, 2453, 2419, 2371, 1609, 1473, 1399, 1364, 1288, 1098, 1078, 879, 841, 800, 610, 510 cm⁻¹

¹H NMR (400 MHz, CD₃OD) δ 0.59 (td, J = 7.6 Hz, J' = 6 Hz, 1 H, 9-H_a), 1.00 (m, 1 H, 9-H_b), 1.04 [m, 2 H, 8(10)-H], 1.26 [broad d, J = 8.8 Hz, 2 H, 11(12)-H_a], 1.55 [broad d, J = 8.8 Hz, 2 H, 11(12)-H_b], 1.98 [s, 2 H, 1(7)-H], 2.07 [m, 2 H, piperidine-3'(5')-H_{ax}], 2.45 [d, J = 13.2 Hz, 2 H, piperidine-3'(5')-H_{eq}], 2.69 [broad s, 2 H, 2(6)-H], 3.07 [broad s, 2 H, 3(5)-H_a], 3.12 [td, J = 13.2 Hz, J' = 2.8 Hz, 2 H, piperidine-2'(6')-H_{ax}], 3.58 [d, J = 13.2 Hz, 2 H, piperidine-2'(6')-H_{eq}], 3.63 (m, 1 H, piperidine-4'-H), 3.78 [broad s, 2 H, 3(5)-H_b]

¹³C NMR (100.6 MHz, CD₃OD) δ 7.0 (CH₂, C9), 16.7 [CH, C8(10)], 17.7 [CH₂, C11(12)], 26.9 [CH₂, C2'(6')-piperidine], 27.0 [CH, C1(7)], 40.4 [CH, C2(6)], 43.6 [CH₂, C3'(5')-piperidine], 54.5 [CH₂, C3(5)], 60.2 (CH, C4'-piperidine).

MS (DI), m/e (%); main ions: 205 (47), 204 (28), 112 (100), 111 (36), 110 (30), 91 (19), 79 (16), 72 (17), 68 (41).

Elemental analysis:

Calculated for $C_{16}H_{26}N_2 \cdot 2HCl$ C 60.18%   H 8.84%
     N 8.77%   Cl 22.21%

Calculated for $C_{16}H_{26}N_2 \cdot 2HCl \cdot 0.5\ H_2O$:   C 58.53%   H 8.90%
     N 8.53%   Cl 21.60%

Found: C 58.57%   H 8.67%
     N 8.48%   Cl 21.53%

3. **14-Azaheptacyclo[8.6.1.0²,⁵.0³,¹¹0⁴,⁹.0⁶,¹⁷.0¹²,¹⁶]heptadecane and related compounds**

(1R, 2R, 6S, 7S, 8S, 11R)-4-Azatetracyclo[5.4.2.0²,⁶.0⁸,¹¹]tridec-9,12-diene-3,5-dione, 93.[119]
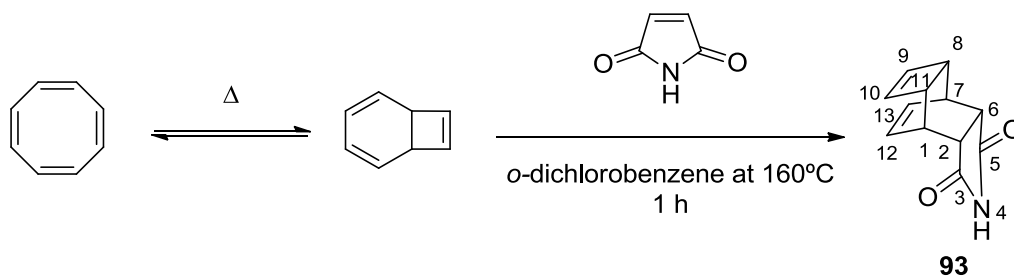
In a 3-necked roundbottom flask, maleimide (4.66 g, 48.0 mmol) was dissolved in *ortho*-dichlorobenzene (53 mL). To the white suspension was added dropwise cyclooctatetraene (5.00 g, 48.0 mmol) dissolved in *ortho*-dichlorobenzene (7 mL). The yellow suspension was heated to 160 °C for 1 hour. The yellow solution was allowed to cool down to room temperature, the precipitate was filtered under vacuo and washed with hexane. **93** was obtained as a light yellow solid (7.57 g, 78%). Its spectroscopic and analytical data were in accord with the ones described in the literature.[119]

(1R, 2S, 3R, 4R, 7S, 8S, 9R, 10S, 11S, 15R)-4,5,6,7-Tetrachloro-18,18-dimethoxy-13-azahexacyclo[8.5.2.1⁴,⁷.0²,⁹.0³,⁸.0¹¹,¹⁵]octadeca-5,16-diene-12,14-dione, 97.
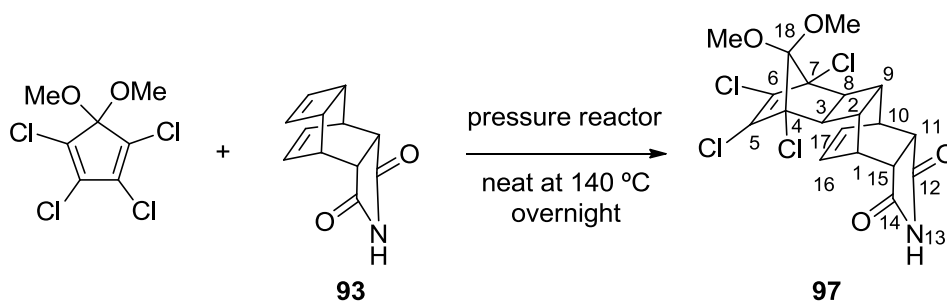
A mixture of **93** (4.00 g, 19.9 mmol) and 5,5-dimethoxy-1,2,3,4-tetrachlorocyclopentadiene (11.30 mL, 64.4 mmol) were mixed in a pressure reactor and heated to 140 °C overnight. The brownish paste was concentrated under vacuo and the crude was purified by silica column chromatography. The EtOAc fractions consisted of **97** as a light yellow solid (8.23 g, 89%).

Analytic and spectroscopic data of **97**:

Melting point > 300 °C

181

IR (KBr) ν 3366, 3048, 2987, 2948, 1761, 1717, 1451, 1338, 1296, 1231, 1176, 1119, 1031, 981, 938, 830, 794, 777, 750, 702, 661, 631, 611 cm^{-1}.

^{1}H NMR (400 MHz, CDCl$_3$) δ: 2.11 [m, 2 H, 2(9)-H], 2.54 [m, 2H, 3(8)-H], 2.74 [t, J = 1.2 Hz, 2 H, 11(15)-H], 3.26 [m, 2 H, 1(10)-H], 3.49 [s, 3H, -OC$\underline{H}_3$], 3.51 [s, 3H, -OC$\underline{H}_3$], 6.43 [dd, J = 4.4 Hz, J' = 3.2 Hz, 2 H, 16(17)-H], 7.95 (broad s, 1 H, NH).

^{13}C NMR (100.6 MHz, CDCl$_3$) δ: 34.8 [CH, C1(10)], 38.1 [CH, C2(9)], 43.7 [CH, C11(15)], 50.4 [CH, C3(8)], 51.8 [CH$_3$, -OC$\underline{H}_3$], 52.3 [CH$_3$, -OC$\underline{H}_3$], 76.7 [C, C4(7)], 128.8 (C, C18), 130.7 [C, C5(6)], 133.1 [CH, C16(17)], 177.7 [C=O, C12(14)].

MS (GC), rt = 31.1 min, m/e (%); main ions: 430 [(M-Cl)$^+$, 100], 295 (12), 281 (25), 255 (94), 207 (80), 179 (15), 112 (25), 103 (18), 78 (95), 59 (66).

Accurate mass:

Calculated for [C$_{19}$H$_{17}$Cl$_4$NO$_4$+H]$^+$: 463.9984

Found: 463.9978

(1R, 2S, 3R, 4S, 7S, 8S, 9R, 10S, 11S)-13-Azahexacyclo[8.5.2.1^{4,7}.0^{2,9}.0^{3,8}.0^{11,15}]octadeca-5,16-diene-12,14,18-trione, 99.
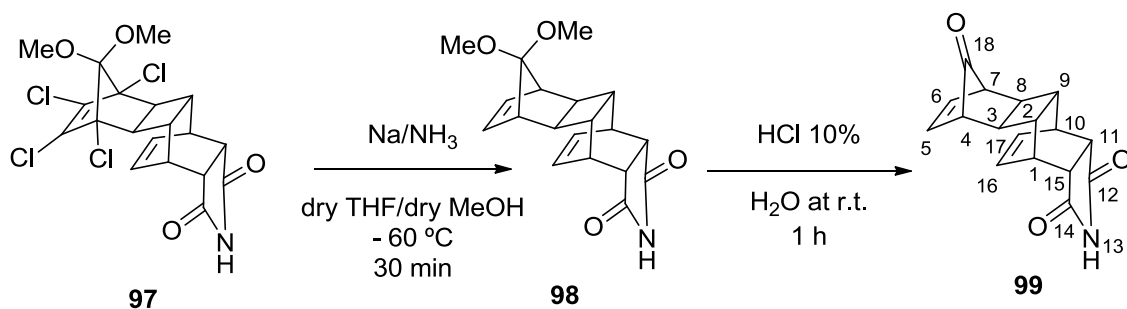
A solution of **97** (9.00 g, 19.3 mmol) in dry THF (60 mL) and dry MeOH (9 mL) was carefully added to freshly distilled ammonia (500 mL aprox.) at - 60 °C. Sodium (5.6 g, 24.2 mmol) was carefully added in small portions over 15 min. The dark blue solution was stirred for another 15 min and it was quenched with NH$_4$Cl. The white suspension was allowed to warm up to room temperature and was stirred overnight. The white precipitate was acidified with HCl aq. 10% (200 mL) and was left stirring for 1 hour. The white solution was extracted with DCM (3 x 150 mL), the organic phase was dried over Na$_2$SO$_4$, filtered and concentrated under vacuo. The white solid obtained was purified by silica gel column chromatography. In the (DCM 99.2: MeOH) fractions, **99** was obtained as a white solid (2.24 g, 41%).

Analytic and spectroscopic data of **99**:

Melting point 202-203 °C

IR (KBr) v 3263, 3083, 3040, 2997, 2939, 1795, 1780, 1695, 1363, 1297, 1226, 1193, 1104, 1067, 999, 941, 888, 879, 717, 686 cm^{-1}.

^{1}H NMR (400 MHz, CDCl$_3$) δ: 1.85 [m, 2 H, 2(9)-H], 2.33 [td, J = 3.2 Hz, J' = 2 Hz, 2 H, 3(8)-H], 2.64 [t, J = 1.6 Hz, 2 H, 11(15)-H], 2.99 [quint, J = 2.8 Hz, 2 H, 4(7)-H], 3.21 [m, 2 H, 1(10)-H], 6.46 [dd, J = 4.8 Hz, J' = 3.2 Hz, 2 H, 16(17)-H], 6.80 [t, J = 2 Hz, 5(6)-H], 8.03 (broad s, 1 H, NH).

^{13}C NMR (100.6 MHz, CDCl$_3$) δ: 35.2 [CH, C1(10)], 37.5 [CH, C3(8)], 41.7 [CH, C2(9)], 43.9 [CH, C11(15)], 50.1 [CH, C4(7)], 133.8 [CH, C16(17)], 134.0 [CH, C5(6)], 178.2 [C=O, C12(14)], 200.0 (C=O, C18).

MS (GC), rt = 24.5 min, m/e (%); main ions: 253 [(M-CO)$^{·+}$, 53], 187 (14), 175 (29), 165 (15), 155 (28), 128 (15), 116 (23), 104 (35), 91 (30), 78 (100).

Accurate mass:

Calculated for [C$_{17}$H$_{15}$NO$_3$+H]$^+$:   282.1125

Found: 282.1118

(1R, 2R, 3S, 4S, 5R, 6S, 9R, 10S, 11S, 12S, 16R, 17R)-14-Azaheptacyclo[8.6.1.0^{2,5}.0^{3,11}0^{4,9}.0^{6,17}.0^{12,16}]heptadec-7-ene-13,15-dione, 101.
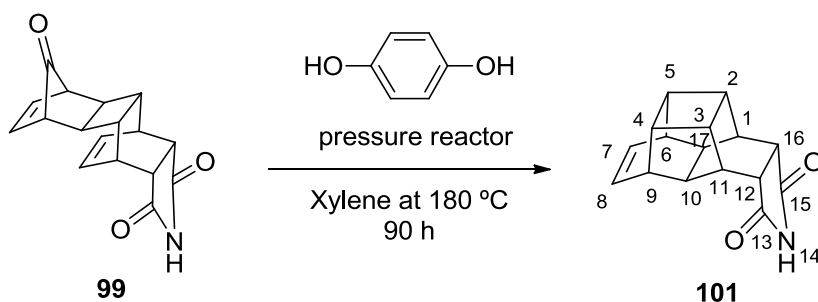
A mixture of **99** (500 mg, 1.98 mmol) and hydroquinone (33 mg, 0.29 mmol) in a pressure reactor was dissolved in xylene (50 mL). The white suspension was heated to 180 °C for 90 hours. The yellowish suspension was allowed to cool down to room temperature and was concentrated under vacuo. The solid obtained was purified through silica gel by column chromatography and **101** was collected in the (DCM 99.2: MeOH) fractions as a white solid (438 mg, 44%) that was used in the next step without further purification.

Analytic and spectroscopic data of **101**:

Melting point 299-300 °C

IR (KBr) ν 3230, 3073, 1975, 1945, 2903, 2735, 1773, 1698, 1359, 1342, 1290, 1229, 1175, 1149, 1064, 1019, 938, 798, 741, 706, 686, 630 cm⁻¹.

¹H NMR (400 MHz, CDCl₃) δ 1.76 (m, 2 H), 2.16 (m, 2 H), 2.33 (m, 2 H), 2.55 (m, 2 H), 2.68 (m, 2 H), 2.81 (m, 2 H), 6.22 [dd, J = 4.8 Hz, J' = 3.2 Hz, 2H, 7(8)-H], 8.0 (broad s, 1 H, NH).

¹³C NMR (100.6 MHz, CDCl₃) δ: 34.3 (CH), 37.1 (CH), 37.6 (CH), 39.4 (CH), 39.5 (CH), 39.8 (CH), 130.6 [CH, C7(8)], 180.2 [C, C13(15)].

MS (GC), rt = 24.6 min, m/e (%); main ions: 253 (M·⁺, 47), 187 (13), 182 (12), 181 (12), 175 (26), 165 (14), 155 (26), 128 (15), 116 (22), 104 (34), 91 (27), 78 (100).

(1R, 2R, 3S, 4S, 5R, 6S, 9R, 10S, 11S, 12S, 16R, 17R)-14-Azaheptacyclo[8.6.1.0²,⁵.0³,¹¹0⁴,⁹.0⁶,¹⁷.0¹²,¹⁶]heptadec-7-ene, hydrochloride, 102·HCl.
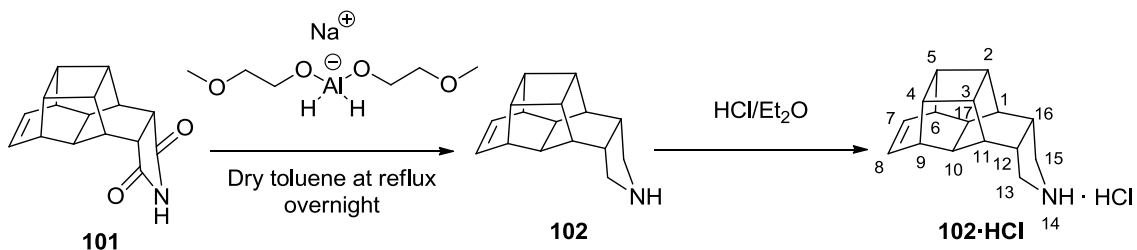
To a solution of **101** (427 mg, 1.69 mmol) in dry and degassed toluene (16 mL) was added dropwise Red-Al® 65% in toluene (2.60 mL, 8.43 mmol). The solution was stirred at 107 °C overnight. The solution was then allowed to cool down to room temperature and it was quenched with an aqueous 30% solution of KOH (15 mL) added dropwise. The organic phase was separated and the aqueous phase was extracted with DCM (3 x 35 mL). All the organic phases were put together, dried over Na₂SO₄, filtered and concentrated under vacuo to give an orange oil (421 mg). The oil was dissolved in EtOAc and HCl/Et₂O 0.66N was added until no more precipitate was formed. The suspension was filtered under vacuo and **102·HCl** was obtained as an off-white solid (325 mg, 74%). An analytical sample was obtained by crystallization from MeOH/Et₂O.

Analytic and spectroscopic data of **102·HCl**:

Melting point 282-283 ºC (dec.)

IR (KBr) ν 3041, 2918, 2902, 2726, 2602, 2484, 2376, 1594, 1395, 1373, 1347, 1300, 1255, 910, 828, 809, 685 cm^{-1}.

^{1}H NMR (400 MHz, CD$_3$OD) δ 1.79 [broad s, 2 H, 1(11)-H], 1.87 [m, 2 H, 10(17)-H], 2.30 [m, 2 H, 4(5)-H], 2.44 [m, 2 H, 12(16)-H], 2.54 [m, 2 H, 6(9)-H], 2.63 [m, 2 H, 2(3)-H], 3.12 [m, 2 H, 13(15)-H$_a$], 3.56 [m, 2 H, 13(15)-H$_b$], 6.27 [dd, J = 4.6 Hz, J' = 3.0 Hz, 2H, 7(8)-H].

^{13}C NMR (100.6 MHz, CD$_3$OD) δ: 34.7 [CH, C12(16)], 36.7 [CH, C1(11)], 37.3 [CH, C10(17)], 39.4 [CH, C2(3)], 40.8 [CH, C4(5)], 41.2 [CH, C6(9)], 51.4 [CH$_2$, C13(15)], 131.9 [CH, C7(8)].

MS (DI), m/e (%); main ions: 225 (M$^{·+}$, 100), 165 (9), 128 (9), 115 (16), 91 (18), 80 (22), 78 (14), 68 (49).

Elemental analysis:

Calculated for C$_{16}$H$_{19}$N·HCl:	C 73.41%	H 7.70%	N 5.35%
Cl 13.54%			
Calculated for C$_{16}$H$_{19}$N·HCl·0.25 H$_2$O:	C 72.16%	H 7.76%	N 5.26%
Cl 13.31%			
Found:	C 72.16%	H 7.74%	N 5.07%
Cl 13.25%			

(1R, 2R, 3S, 4S, 5R, 6S, 9R, 10S, 11S, 12S, 16R, 17R)-14-Azaheptacyclo[8.6.1.0^{2,5}.0^{3,11}0^{4,9}.0^{6,17}.0^{12,16}]heptadecane, hydrochloride, 103·HCl.
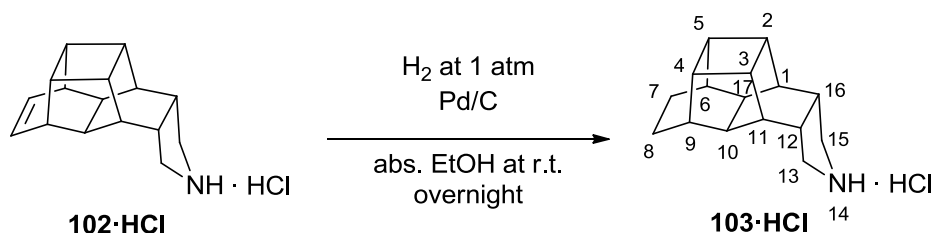
In an roundbottom flask, **102·HCl** (111 mg, 0.42 mmol) was dissolved in absolute EtOH (15 mL) and palladium on activated charcoal (235 mg, 5% in Pd) was added. The flask was fitted with a balloon filled with H_2 at atmospheric pressure and the black suspension was stirred at room temperature overnight. It was then filtered and the clear solution was concentrated under vacuo to yield **103·HCl** as a white solid (89 mg mg, 79%). An analytical sample was obtained by crystallization from MeOH/Et$_2$O.

Analytic and spectroscopic data of **103·HCl**:

Melting point 292-293 °C (dec.)

IR (KBr) ν 2958, 2930, 2897, 2853, 2748, 2599, 2462, 1588, 1452, 1419, 1350, 1312, 1290, 1262, 1049, 1025, 902, 825, 660 cm^{-1}.

^{1}H NMR (400 MHz, CD$_3$OD) δ: 1.43 [m, 2 H, 6(9)-H], 1.55 [m, 2 H, 7(8)-H$_a$], 1.63 [broad s, 2 H, 1(11)-H], 1.81 [m, 2 H, 7(8)-H$_b$], 2.23 [m, 2 H, 10(17)-H], 2.44 [m, 2 H, 12(16)-H], 2.57-2.65 [complex signal, 4 H, 2(3)-H and 4(5)-H], 3.19 [m, 2 H, 13(15)-H$_a$], 3.57 [m, 2 H, 13(15)-H$_b$].

^{13}C NMR (100.6 MHz, CD$_3$OD) δ: 19.9 [CH$_2$, C7(8)], 34.7 [CH, C12(16)], 35.6 [CH, C6(9)], 36.8 [CH, C10(17)], 38.0 [CH, C1(11)], 39.9 [CH, C2(3)]*, 41.2 [CH, C4(5)]*, 51.6 [CH$_2$, C13(15)].

MS (GC), m/e (%); main ions: 227 (M^{+}, 100), 155 (5), 141 (6), 128 (8), 117 (10), 105 (5), 91 (19), 79 (11), 68 (10).

Elemental analysis:

Calculated for C$_{16}$H$_{21}$N·HCl:	C 72.85%	H 8.41%	N 5.31%
Cl 13.44%			
Calculated for C$_{16}$H$_{21}$N·HCl·0.25H$_2$O:	C 71.62%	H 8.45%	N 5.22%
Cl 13.21%			
Found:	C 71.89%	H 8.49%	N 5.00%
Cl 13.35%			

(1R, 2R, 3S, 4S, 5R, 6S, 9R, 10S, 11S, 12S, 16R, 17R)-14-Amidino-14-azaheptacyclo[8.6.1.0²,⁵.0³,¹¹0⁴,⁹.0⁶,¹⁷.0¹²,¹⁶]heptadec-7-ene, hydrochloride, 104·HCl.
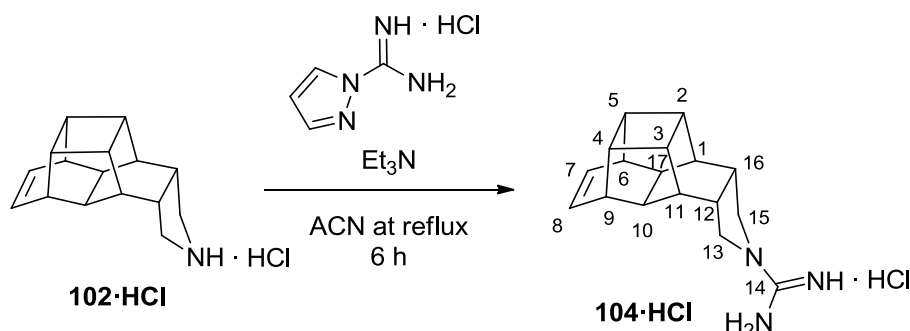
A solution of **102·HCl** (85 mg, 0.32 mmol) in water (10 mL) was basified to pH = 14 with a 10 N aqueous solution of NaOH. It was then extracted with EtOAc (3 x 15mL) and the joined organic phases were dried over Na_2SO_4, filtered and concentrated under vacuo (yellow oil, 70 mg, 0.31 mmol, 96% yield). To a suspension of this oil in acetonitrile (3 mL), 1*H*-pyrazole-1-carboxamidine monohydrochloride (55 mg, 0.37 mmol) was added. The suspension was heated to reflux for 6 hours and was left at 4 °C overnight. The yellow precipitate was filtered to give **104·HCl** as an off-white solid (29 mg, 31%).

Analytic and spectroscopic data of **104·HCl**:

Melting point 224-225 °C (dec.)

IR (KBr) ν 3309, 3125, 2940, 1635, 1627, 1375, 1351, 1295, 1255, 1182, 1147, 1118, 1073, 828, 805, 690 cm⁻¹.

¹H NMR (400 MHz, CD₃OD) δ 1.72 [complex signal, 4 H, 10(17)-H and 1(11)-H], 2.28 [m, 2 H, 4(5)-H], 2.47-2.55 [complex signal, 4 H, 6(9)-H and 12(16)-H], 2.61 [m, 2 H, 2(3)-H], 3.55-3.62 [complex signal, 4 H, 13(15)-H₂], 6.25 [dd, *J* = 4.8 Hz, *J'* = 2.8 Hz, 2 H, 7(8)-H].

¹³C NMR (100.6 MHz, CD₃OD) δ 33.5 [CH, C12(16)], 36.4 [CH, C1(11)], 37.2 [CH, C2(3)], 37.9 [CH, C10(17)], 39.8 [CH, C4(5)], 40.0 [CH, C6(9)], 52.0 [CH₂, C13(15)], 130.5 [CH, C7(8)], 154.6 (C=NH).

MS (DI), m/e (%); main ions: 267 (M·⁺, 100), 266 (99), 225 (17), 224 (43), 165 (9), 117 (10), 115 (16), 91 (17), 85 (63), 78 (15), 68 (32).

Accurate mass:

Calculated for $[C_{17}H_{22}N_3+H]^+$:   268.1808

Found: 268.1811

(1R, 2R, 3S, 4S, 5R, 6S, 9R, 10S, 11S, 12S, 16R, 17R)-14-Amidino-14-azaheptacyclo[8.6.1.0^{2,5}.0^{3,11}0^{4,9}.0^{6,17}.0^{12,16}]heptadecane, hydrochloride, 105·HCl.
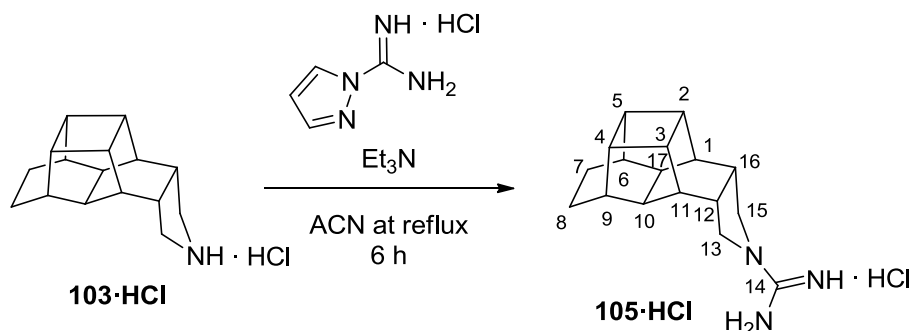
A solution of **103·HCl** (82 mg, 0.31 mmol) in water (10 mL) was basified to pH = 14 with a 10 N aqueous solution of NaOH. It was then extracted with EtOAc (3 x 15mL) and the joined organic phases were dried over Na_2SO_4, filtered and concentrated under vacuo (yellow oil, 67 mg, 0.29 mmol, 92% yield). To a suspension of this oil in acetonitrile (3 mL), 1*H*-pyrazole-1-carboxamidine monohydrochloride (52 mg, 0.29 mmol) was added. The suspension was heated to reflux for 6 hours and was left at 4 °C overnight. The yellow precipitate was filtered to give **105·HCl** as an off-white solid (38 mg, 42%).

Analytic and spectroscopic data of **105·HCl**:

Melting point >300 °C

IR (KBr) ν 3300, 3176, 3118, 2945, 2900, 2856, 1628, 1458, 1298, 1258, 1098, 830, 729 cm^{-1}.

^{1}H NMR (400 MHz, CD$_3$OD) δ 1.39 [m, 2H, 6(9)-H], 1.55 [m, 4 H, 7(8)-H$_a$ and 1(11)-H], 1.78 [m, 2 H, 7(8)-H$_b$], 2.10 [broad s, 2 H, 10(17)-H], 2.52 [m, 2 H, 12(16)-H], 2.60 [m, 4 H, 2(3)-H and 4(5)-H], 3.57-3.67 [complex signal, 4 H, 13(15)-H$_2$].

^{13}C NMR (100.6 MHz, CD$_3$OD) δ 19.9 [CH$_2$, C7(8)], 35.0 [CH, C12(16)], 35.8 [CH, C6(9)], 37.4 [CH, C10(17)], 40.4 [CH, C2(3)]*, 40.5 [CH, C1(11)]*, 40.7 [CH, C4(5)]*, 53.6 [CH$_2$, C13(15)], 156.1 (C=NH).

MS (DI), m/e (%); main ions: 269 (M$^{·+}$, 83), 226 (57), 141 (6), 129 (8), 117 (10), 91 (18), 85 (C$_3$H$_7$N$_3$$^{·+}$, 100), 79 (11), 68 (11).

Accurate mass:

Calculated for [C$_{17}$H$_{24}$N$_3$+H]$^+$:   270.1965

Found: 273.1963

4. **7,8-Diethyl-3-azatetracyclo[5.2.1.1^{5,8}.0^{1,5}]undecane, 12-azapentacyclo[6.5.1.1^{3,10}.0^{1,10}.0^{3,8}]pentadecane and related compounds**

Cis-1,5-diethylbicyclo[3.3.0]octane-3,7-dione, 108.[127b]

To a solution of sodium bicarbonate (28 g) in water (1800 mL) was added dimethyl 1,3-acetonedicarboxylate (348.3 g, 2.0 mol) and 3,4-hexanedione (114.3 g, 1.0 mol). The mixture was stirred at room temperature for 24 hours. The off-white precipitate was filtered under vacuo, washed with water and dried under vacuo obtaining the tetraester **106** (492.2 g) that was used in the next step without further purification.

A mixture of HCl aq. 10% (150 mL), glacial AcOH (450 mL) and tetraester **106** (26.76 g, 6.28 mmol) was heated under reflux for 7 hours. The resulting solution was allowed to cool down overnight and was then poured into a beaker containing dichloromethane (2 L). The mixture was neutralized with an aqueous saturated solution of $NaHCO_3$ (9 L) while stirring mechanically. The organic phase was separated, concentrated to a lesser volume, dried over Na_2SO_4, filtered and concentrated under vacuo to give the known[127b] diketone **108** (9.59 g, 42% yield over 2 steps).

Analytic and spectroscopic data of **108**:

Melting point 79-80 ºC

IR (KBr) ν 2968, 2944, 2884, 2865, 2746, 1734, 1460, 1460, 1402, 1333, 1301, 1247, 1228, 1191, 1156, 1082, 1060, 1040, 1019, 1000, 980, 965, 822, 792, 768, 636, 611 cm⁻¹.

¹H NMR (400 MHz, $CDCl_3$) δ 0.92 [t, *J* = 7.2 Hz, 6 H, C1(5)-CH₂C$\underline{H}$₃], 1.55 [q, *J* = 7.2 Hz, 4 H, C1(5)-C$\underline{H}$₂CH₃], 2.27 [d, *J* = 19.6 Hz, 4 H, 2(4,6,8)-H$_{endo}$], 2.43 [d, *J* = 19.6 Hz, 4 H, 2(4,6,8)-H$_{exo}$].

¹³C NMR (100.6 MHz, $CDCl_3$) δ 10.0 [CH₃, C1(5)-CH₂$\underline{C}$H₃], 26.8 [CH₂, C1(5)-$\underline{C}$H₂CH₃], 48.3 [CH₂, C2(4,6,8)], 50.1 [C, C1(5)], 216.7 [C=O, C3(7)].

MS (DI), m/e (%); main ions: 194 (M·⁺, 27), 109 (11), 97 (44), 69 (100).

Cis-1,5-diethylbicyclo[3.3.0]octane-3,7-dione bishydrazone, 110.

To a solution of diketone **108** (15.0 g, 77.2 mmol) in absolute EtOH (225 mL) was added triethylamine (173 mL, 1.25 mmol) and hydrazine monohydrate (39.9 mL, 0.82 mmol). The mixture was heated to reflux for 3 hours. The dark yellow solution obtained was allowed to cool down to room temperature, it was then concentrated to a third of its volume and it was left at 4 °C overnight. The white precipitate was filtered, washed with cold 96% ethanol and dried under vacuum to give **110** (*anti* isomer) as white needles (14.95 g, 87%).

Analytic and spectroscopic data of **110**:

Melting point 139-140 °C

IR (KBr) ν 3390, 3372, 3193, 2962, 2939, 2876, 2827, 1636, 1459, 1423, 1338, 1291, 1223, 1056, 826, 791, 675, 591, 513 cm^{-1}.

^{1}H NMR (400 MHz, CDCl$_3$) δ 0.90 [t, J = 7.4 Hz, 6 H, C1(5)-CH$_2$C$\underline{H}_3$], 1.38 [q, J = 7.4 Hz, 4 H, C1(5)-C$\underline{H}_2$CH$_3$], 2.11 [dd, J = 18.0 Hz, J' = 0.8 Hz, 2H, 4(8)-H$_{endo}$], 2.23 [dd, J = 18.0 Hz, J' = 1.6 Hz, 2 H, 4(8)-H$_{exo}$], 2.37 [dd, J = 17.0 Hz, J' = 0.8 Hz, 2 H, 2(6)-H$_{endo}$] , 2.46 [dd, J = 17.0 Hz, J' = 1.6 Hz, 2 H, 2(6)-H$_{exo}$], 4.84 (s, 4 H, 2 NH$_2$).

^{13}C NMR (100.6 MHz, CDCl$_3$) δ 9.8 [CH$_3$, C1(5)-CH$_2$$\underline{C}H_3$], 26.0 [CH$_2$, C1(5)-$\underline{C}H_2CH_3$], 35.2 [CH$_2$, C4(8)], 42.2 [CH$_2$, C2(6)], 52.4 [C, C1(5)], 157.7 [C=N, C3(7)].
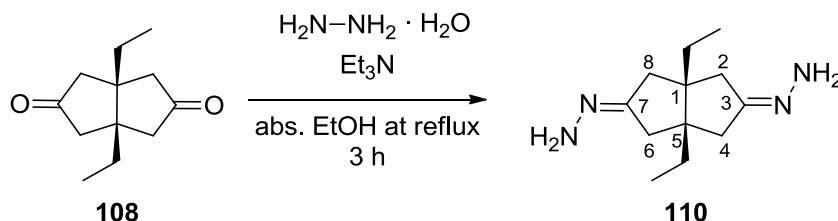
MS (DI), m/e (%); main ions: 222 (M$^{\cdot+}$, 11), 206 (100), 193 (27), 152 (19), 151 (29), 150 (13), 149 (12), 91 (14).

Elemental analysis:

Calculated for C$_{12}$H$_{14}$N$_4$:	C 64.83%	H 9.97%	N 25.20%
Found:	C 64.78%	H 10.09%	N 25.11%

Mixture of *cis*-1,5-diethyl-3,7-diiodobicyclo[3.3.0]octa-2,7-diene and *cis*-1,5-diethyl-3,7-diiodobicyclo[3.3.0]octa-2,6-diene (*syn*- and *anti*-112).
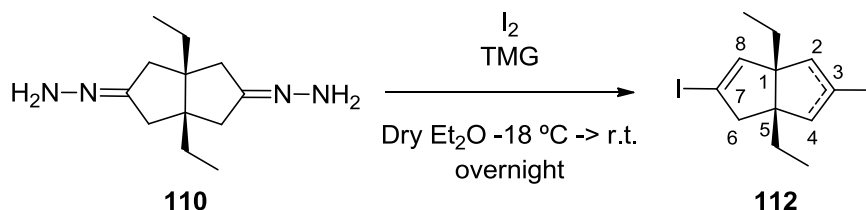
To a stirred suspension of bis-hydrazone **110** (1.0 g, 4.5 mmol) in dry diethyl ether (72 mL) under an argon atmosphere, tetramethylguanidine (8.5 ml, 67.5 mmol) was added. The mixture was cooled to −18 °C and solid iodine (6.88 g, 27.1 mmol) was added in small portions during 1 hour. When the addition was over, the mixture was allowed to warm to room temperature and stirring was continued for 15 hours. The organic layer was washed with $Na_2S_2O_3$ (10% aqueous solution, 5 × 30 ml) and brine (2 × 30 ml). The organic layer was dried (Na_2SO_4), filtered and concentrated under reduced pressure to give an orange solid that was purified by column chromatography (silica gel, *n*-hexane) to give a mixture of *syn*- and *anti*-**112** (876 mg, 47% yield). From some selected fractions, pure *syn*-**112** was obtained and was fully characterized.

Analytic and spectroscopic data of *syn*-**112**:

Melting point 63-64 °C (*n*-hexane)

IR (KBr) ν 3446, 2960, 2926, 2874, 1601, 1457, 1430, 1377, 1281, 1148, 1097, 1034, 1015, 964, 893, 853, 805, 790, 745 cm⁻¹.

¹H NMR (400 MHz, CDCl₃) δ 0.90 [t, *J* = 7.2 Hz, 3 H, C1-CH₂CH₃]*, 0.91 [t, *J* = 7.6 Hz, 3 H, C5-CH₂CH₃]*, 1.42 [q, *J* = 7.2 Hz, 2 H, C1-CH₂CH₃]*, 1.43 [q, *J* = 7.2 Hz, 2 H, C5-CH₂CH₃]*, 2.50 [dd, *J* = 16.4 Hz, *J'* = 2 Hz, 2 H, 4(6)-H$_{endo}$], 2.62 [dd, *J* = 16.4 Hz, *J'* = 2 Hz, 2 H, 4(6)-H$_{exo}$], 6.01 [t, *J* = 2 Hz, 2 H, 2(8)-H].

¹³C NMR (100.6 MHz, CDCl₃) δ 9.5 [CH₃, C1-CH₂CH₃]*, 9.9 [CH₃, C5-CH₂CH₃]*, 25.7 [CH₂, C1-CH₂CH₃]*, 26.0 [CH₂, C5-CH₂CH₃]*, 54.8 [CH₂, C4(6)], 58.0 (C, C5), 70.8 (C, C1), 92.5 [C-I, C3(7)], 142.4 [CH, C2(8)].

MS (GC), m/e (%); main ions (*syn* and *anti*): rt (19.5 min): 414 (M·⁺, 15), 287 [(M-I⁺), 56], 160 [(M-2I)·⁺, 100], 145 [(C₁₁H₁₃)⁺, 31], 131 [(C₁₀H₁₁)⁺, 48], 115 (20), 91 [(C₇H₇)⁺, 21]; rt (19.6 min): 414 (M·⁺, 15), 385 [(M-C₂H₅)⁺, 100], 258 [(M-2C₂H₅)·⁺, 10], 131 [(C₁₀H₁₁)⁺, 22], 115 (11), 91 [(C₇H₇)⁺, 21].

Elemental analysis:

Calculated for $C_{12}H_{16}I_2$:	C 34.81%	H 3.89%	I 61.30%
Calculated for $C_{12}H_{16}I_2 \cdot 0.13$ Hexane:	C 36.11%	H 4.23%	I 59.67%
Found:	C 36.16%	H 4.23%	I 59.67%

Mixture of dimethyl 1,5-diethyl-*cis*-bicyclo[3.3.0]octa-2,7-diene-3,7-dicarboxylate and dimethyl 1,5-diethyl-*cis*-bicyclo[3.3.0]octa-2,6-diene-3,7-dicarboxylate (*syn*- and *anti*-114).
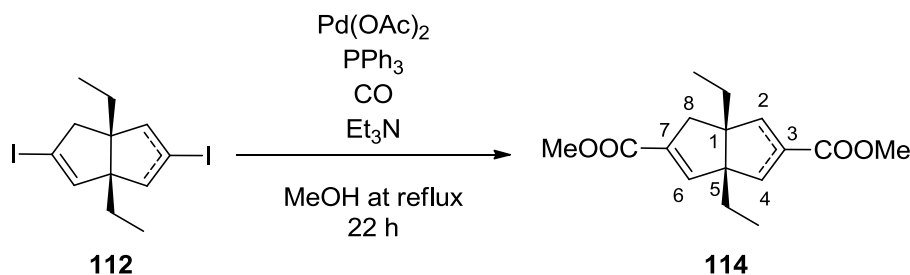
A mixture of **112** (5.65 g, 13.65 mmol), triphenylphosphine (706 mg, 2.69 mmol), Pd(OAc)$_2$ (316 mg, 1.41 mmol), methanol (175 mL) and triethylamine (11.4 mL, 82.2 mmol) was purged with CO for 10 min and stirred and heated under reflux for 22 h under CO (about 1 atm). The black suspension was allowed to cool to room temperature and was evaporated in vacuo to dryness. The residue was taken in dichloromethane (200 mL) and filtered. The orange filtrate was washed with HCl (10% aqueous solution, 3 × 200 mL), NaHCO$_3$ (saturated aqueous solution, 3 × 200 mL) and brine (200 mL). The organic layer was dried (anhydrous Na$_2$SO$_4$), filtered and concentrated in vacuo to dryness to give a mixture of *syn*- and *anti*-**114** as a brown oil. Column chromatography (silica gel, hexanes to ethyl acetate / hexanes mixture 2/8) gave a mixture of *syn*- and *anti*-**114** (in the approx. ratio of 1:1, ^{1}H NMR or GC/MS) as a yellowish oil (2.36 g, 62% yield).

Analytic and spectroscopic data of *syn*- and *anti*-**114**:

IR (ATR) ν 2964, 2851, 1713, 1634, 1460, 1435, 1381, 1352, 1317, 1239, 1217, 1190, 1159, 1128, 1076, 961, 908, 892, 855, 797, 773, 749, 738, 687, 554 cm^{-1}.

^{1}H NMR (400 MHz, CDCl$_3$) δ *syn*-**114** 0.93 (t, J = 7.4 Hz, 3 H, C1-CH$_2$C$\underline{H}_3$), 0.97 (t, J = 7.4 Hz, 3 H, C5-CH$_2$C$\underline{H}_3$), 1.36-1.64 (complex signal, 4 H, C1-C$\underline{H}_2$CH$_3$ and C5-C$\underline{H}_2$CH$_3$), 2.45 [dd, J = 16.4 Hz, J' = 1.8 Hz, 2 H, 4(6)-H$_a$], 2.58 [dd, J = 16.4 Hz, J' = 1.8 Hz, 2 H, 4(6)-H$_b$], 3.70 [s, 6 H, C3(7)-CO$_2$C$\underline{H}_3$], 6.59 [t, J = 1.8 Hz, 2 H, 2(8)-H]; *anti*-**114** 0.93 [t, J = 7.4 Hz, 6 H, C1(5)-CH$_2$C$\underline{H}_3$], 1.36-1.64 [complex signal, 4 H, C1(5)-C$\underline{H}_2$CH$_3$], 2.49 [dd, J = 16.4 Hz, J' = 2.8 Hz, 2 H, 4(8)-H$_a$], 2.68 [broad d, J = 17.2 Hz, 2 H, 4(8)-H$_b$], 3.71 [s, 6 H, C3(7)-CO$_2$C$\underline{H}_3$], 6.60 [d, J = 1.6 Hz, 2 H, 2(6)-H].

^{13}C NMR (100.6 MHz, CDCl$_3$) δ *syn*-**114** 9.4 (CH$_3$, C1-CH$_2\underline{C}$H$_3$)*, 9.8 (CH$_3$, C5-CH$_2\underline{C}$H$_3$)*, 25.5 (CH$_2$, C1-$\underline{C}$H$_2$CH$_3$)*, 26.3 (CH$_2$, C5-$\underline{C}$H$_2$CH$_3$)*, 42.5 [CH$_2$, C4(6)], 51.5 (CH$_3$, 2 CO$_2\underline{C}$H$_3$), 55.6 (C, C5), 68.4 (C, C1), 134.9 [C, C3(7)], 150.3 [CH, C2(6)], 165.6 (C, $\underline{C}$O$_2$CH$_3$); *anti*-**114** 9.9 [CH$_3$, C1(5)-CH$_2\underline{C}$H$_3$], 27.6 [CH$_2$, C1(5)-$\underline{C}$H$_2$CH$_3$-*anti*], 40.7 [CH$_2$, C4(8)], 51.4 (CH$_3$, 2 CO$_2\underline{C}$H$_3$), 61.2 [C, C1(5)], 132.9 [C, C3(7)], 144.0 [CH, C2(8)], 165.6 (C, $\underline{C}$O$_2$CH$_3$).

MS (GC), m/e (%); main ions (*syn* and *anti*): rt (19.9 min): 278 (M$^{·+}$, 23), 249 [(M-C$_2$H$_5$)$^+$, 14], 247 (49), 246 [(M-CH$_3$OH)$^{·+}$, 100], 219 (27), 218 [(M-HCO$_2$CH$_3$)$^{·+}$, 92], 217 (57), 203 (18), 193 [(C$_{12}$H$_{17}$O)$^+$, 91], 189 [(M-C$_2$H$_5$-HCO$_2$CH$_3$)$^+$, 69], 187 (29), 186 (16), 161 (37), 159 [(C$_{12}$H$_{16}$)$^{·+}$, 87], 157 (25), 145 (20), 133 (20), 131 (32), 130 (22), 129 [(C$_{10}$H$_{10}$), 57], 128 (27), 117 (22), 115 (38), 105 (26), 93 (22), 91 [(C$_7$H$_7$)$^+$, 37], 77 (18); rt (20.0 min): 278 (M$^{·+}$, 12), 249 [(M-C$_2$H$_5$)$^+$, 26], 247 (20), 219 (46), 218 [(M-HCO$_2$CH$_3$)$^{·+}$, 100], 217 (27), 189 [(M-C$_2$H$_5$-HCO$_2$CH$_3$)$^+$, 31], 159 [(C$_{12}$H$_{16}$)$^{·+}$, 49], 129 [(C$_{10}$H$_{10}$)$^{·+}$, 28], 115 (16), 91 [(C$_7$H$_7$)$^+$, 15].

Accurate mass:

Calculated for [C$_{16}$H$_{22}$O$_4$+H]$^+$: 279.1591

Found: 279.1593

Mixture of *endo,endo-*, *endo,exo-* and *exo,exo-* dimethyl 1,5-diethyl-*cis*-bicyclo[3.3.0]octane-3,7-dicarboxylate, 116
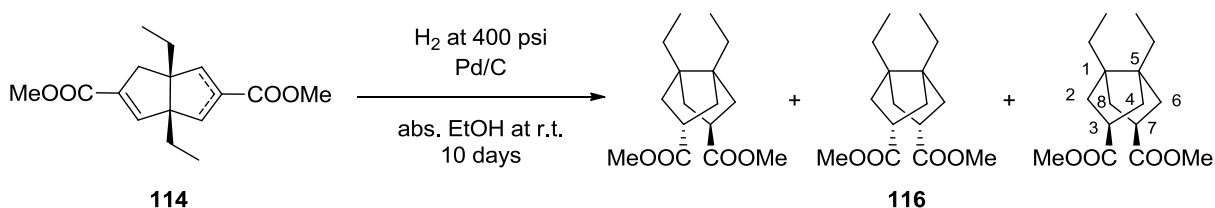
A mixture of **114** (4.45 g, 16.0 mmol) was dissolved in absolute ethanol (120 mL), Pd on charcoal (1.34 g, 54% water content, ca. 5% Pd, equivalent to 31 mg of Pd) was added and the resulting mixture was hydrogenated at 400 psi at room temperature for 7 days. The suspension was filtered, and the solvent was evaporated in vacuo to give a mixture of *endo,endo-*, *endo,exo-* and *exo,exo-* stereoisomers of **116** (3.47 g, 77% yield) as an oil.

Analytic and spectroscopic data of **116**:

IR (ATR) ν 2959, 2878, 1730, 1458, 1434, 1364, 1265, 1192, 1171, 1042, 1027, 930, 830, 761, 668 cm^{-1}.

^{1}H NMR (500 MHz, CDCl$_3$) δ *endo,endo-***116** 0.87 [t, J = 7.5 Hz, 3 H, C1(5)-CH$_2$C<u>H</u>$_3$], 1.24 [q, J = 7.5 Hz, 4 H, C1(5)-C<u>H</u>$_2$CH$_3$], 1.89 [dd, J = 13.5 Hz, J' = 10.0 Hz, 4 H, 2(4,6,8)-H$_a$], 1.98 [dd, J = 13.5 Hz, J' = 8.5 Hz, 4 H, 2(4,6,8)-H$_b$], 2.88 [m, 2 H, 3(7)-H], 3.67 [s, 6 H, 3(7)-CO$_2$C<u>H</u>$_3$]; *endo,exo-***116** and *exo,exo-***116** 0.88 [t, J = 7.5 Hz, 3 H, C1(5)-CH$_2$C<u>H</u>$_3$], 0.89 [t, J = 7.5 Hz, 3 H, C1(5)-CH$_2$C<u>H</u>$_3$], 1.26-1.39 (complex signal, C1(5)-C<u>H</u>$_2$CH$_3$], 1.54 (d, J = 12.5 Hz), 1.59 (d, J = 11.0 Hz), 1.75 (t, J = 12.5 Hz), 1.88 (m) and 2.03 (dd, J = 14.5 Hz, J' = 7.0 Hz) (CH$_2$), 2.59 (tt, 1 H, J = 14.0 Hz, J' = 9.0 Hz), 2.75 (tt, 1 H, J = 14.5 Hz, J' = 9.0 Hz) and 2.87 (m) (CH), 3.66 (s, 6 H, OC<u>H</u>$_3$), 3.67 (s, 6 H, OC<u>H</u>$_3$).

^{13}C NMR (125.7 MHz, CDCl$_3$) δ *endo,endo-***21c** 9.9 [CH$_3$, C1(5)-CH$_2$<u>C</u>H$_3$], 25.8 [CH$_2$, C1(5)-<u>C</u>H$_2$CH$_3$-*anti*], 38.2 [CH$_2$, C2(4,6,8)], 51.7 (CH$_3$, 2 CO$_2$<u>C</u>H$_3$), 57.3 [C, C1(5)], 177.2 (C, <u>C</u>O$_2$CH$_3$); *endo,exo-***21c** and *exo,exo-***21c** 10.0 (CH$_3$), 10.2 (CH$_3$), 28.0 (CH$_2$), 30.9 (CH$_2$), 40.2 (CH), 40.5 (CH$_2$), 41.5 (CH), 41.9 (CH$_2$), 42.7 (CH), 43.1 (CH$_2$), 51.60 (CH$_3$), 51.62 (CH$_3$), 55.2 (C), 55.3 (C), 176.1 (C), 176.2 (C), 176.5 (C).

MS (GC), m/e (%); main ions (only two peaks were observed): rt (19.6 min): 282 (M$^{\cdot+}$, 2), 251 (37), 250 [(M-CH$_3$OH)$^{\cdot+}$, 100], 222 (36), 221 (22), 218 [(M-2CH$_3$OH)$^{\cdot+}$, 61], 193 (55), 191 (41), 190 (98), 183 (27), 163 (43), 162 (34), 161 (42), 142 (18), 136 (17), 135 (38), 134 (16), 133 [(C$_{10}$H$_{14}$)$^{\cdot+}$, 78], 122 (21), 121(39), 110 (18), 107 [(C$_8$H$_{10}$)$^{\cdot+}$, 53], 105 (30), 93 (39), 91 (33), 79 (34), 77 (18), 59 (18), 55 (24); rt (19.7 min): 282 (M$^{\cdot+}$, 2), 251 (28), 250 [(M-CH$_3$OH)$^{\cdot+}$, 73], 222 (48), 221 (38), 218 [(M-2CH$_3$OH)$^{\cdot+}$, 56], 193 (47), 191 (31), 190 (28), 181 (16), 163 (66), 162 (26), 161 (47), 158 (98), 149 (21), 142 (32), 136 (24), 135 (38), 133 [(C$_{10}$H$_{14}$)$^{\cdot+}$, 100], 126 (21), 124 (29), 123 (31), 121 (60), 110 (20), 107 [(C$_8$H$_{10}$)$^{\cdot+}$, 90], 105 (43), 95 (27), 93 (64), 91 (52), 81 (35), 79 (59), 77 (32), 67 (27), 59 (34), 55 (44).

Accurate mass:

Calculated for [C$_{16}$H$_{26}$O$_4$+H]$^+$: 283.1904

Found: 283.1897

Dimethyl 3,7-diethyltricyclo[3.3.0.0^{3,7}]octane-1,5-dicarboxylate, 118.
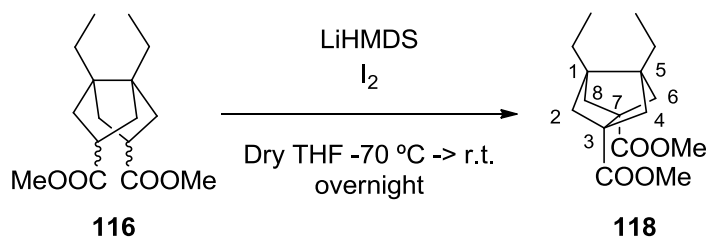
A solution of LiHMDS was prepared by reacting a solution of HMDS (3.56 mL, 17.0 mmol) in anhydrous THF (14 mL) with *n*-butyllithium (8.0 mL, 2.0 M in hexanes, 16.0 mmol) at -68°C under argon for 1 h. Then, a solution of a stereoisomeric mixture of diesters **116** (2.0 g, 7.08 mmol) in anhydrous THF (14 mL) was added dropwise keeping the temperature at -68°C. Stirring was continued for 1 h at this temperature and then a solution of iodine (1.80 g, 7.08 mmol) in anhydrous THF (32 mL) was added dropwise. The mixture was maintained 1 h at -68°C and then allowed to warm to room temperature over 15 h. The mixture was acidified with HCl (10% aqueous solution) until pH 2 (10 mL) and the THF was removed *in vacuo*. The remaining aqueous phase was extracted with diethyl ether (4 × 50 mL) and the combined organic extracts were washed with $Na_2S_2O_3$ (10% aqueous solution, 3 × 100 mL) and brine (2 × 100 mL), dried (Na_2SO_4), filtered and evaporated to dryness under reduced pressure to furnish a dark red oil. Column chromatography of this residue (silica gel, hexanes / ethyl acetate, 9 / 1) gave diester **118** (930 mg, 47% yield) as an orange oil.

Analytic and spectroscopic data of **118**:

IR (ATR) ν 2962, 2891, 1732, 1479, 1459, 1435, 1378, 1325, 1301, 1285, 1219, 1192, 1155, 1132, 1081, 1063, 1042, 1002, 942, 915, 775, 763, 730, 647 cm^{-1}.

^{1}H NMR (400 MHz, CDCl$_3$) δ 0.90 [t, *J* = 7.4 Hz, 6 H, C3(7)-CH$_2$C$\underline{H}_3$], 1.57 [d, *J* = 7.0 Hz, 4 H, 2(4,6,8)-H$_a$], 1.59 [q, *J* = 7.4 H, 4 H, C3(7)-C$\underline{H}_2$CH$_3$], 2.01 [d, *J* = 7.0 Hz, 4 H, 2(4,6,8)-H$_b$], 3.67 [s, 6 H, CO$_2$C$\underline{H}_3$].

^{13}C NMR (100.6 MHz, CDCl$_3$) δ 10.0 [CH$_3$, C3(7)-CH$_2$$\underline{C}H_3$], 22.7 [CH$_2$, C3(7)-$\underline{C}H_2CH_3$], 51.6 (CH$_3$, 2 CO$_2$$\underline{C}H_3$), 52.9 [CH$_2$, C2(4,6,8)], 53.0 [C, C3(7)], 57.3 [C, C1(5)], 173.6 (C, $\underline{C}$O$_2$CH$_3$).

MS (GC), m/e (%); main ions: 280 (M$^{.+}$, 1), 249 (41), 248 (25), 220 (100), 191 (67), 189 (28), 181 (72), 180 (25), 179 (44), 161 (87), 160 (27), 149 (88), 133 (20), 131 (37), 121 (60), 119 (30), 105 (38), 93 (31), 91 (49), 77 (21).

Accurate mass:

Calculated for $[C_{16}H_{24}O_4+H]^+$:   281.1753

Found: 281.1750

3,7-Diethyltricyclo[3.3.0.0^{3,7}]octane-1,5-dicarboxylic acid, 120.
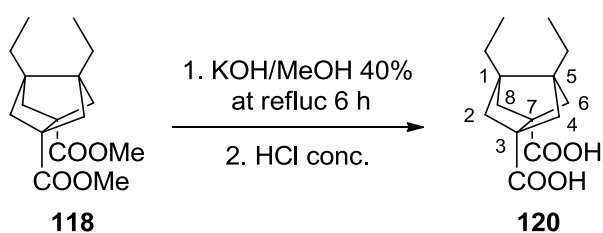
A mixture of **118** (2.32 g, 8.28 mmol) and a solution of KOH (40%) in MeOH (24 mL) was heated under reflux for 3 h. Water (24 mL) was added and heating under reflux was continued for 6 h more. The solution was made acidic with conc. aqueous HCl (25 mL) and concentrated in vacuo. The dark solid was extracted with boiling diethyl ether (6 × 50 mL). The combined organic extracts were dried (Na$_2$SO$_4$), filtered and evaporated to dryness under reduced pressure to furnish **120** (1.32 g, 63% yield) as a pale yellow solid.

Analytic and spectroscopic data of **120**:

Melting point 205-206 ºC

IR (KBr) ν 2971, 2930, 2705, 2604, 1702, 1420, 1312, 1235, 1151, 1091, 938, 729 cm^{-1}.

^{1}H NMR (400 MHz, CDCl$_3$) δ 0.91 [t, J = 7.2 Hz, 6 H, C3(7)-CH$_2$CH$_3$], 1.56-1.64 [complex signal, 8 H, C3(7)-CH$_2$CH$_3$ and 2(4,6,8)-H$_a$], 2.03 [d, J = 7.6 Hz, 4 H, 2(4,6,8)-H$_b$], 10.65 (broad s, 2 H, CO$_2$H).

^{13}C NMR (100.6 MHz, CDCl$_3$) δ 10.0 [CH$_3$, C3(7)-CH$_2$CH$_3$], 22.7 [CH$_2$, C3(7)-CH$_2$CH$_3$], 52.7 [CH$_2$, C2(4,6,8)], 53.3 [C, C3(7)], 57.9 [C, C1(5)], 180.1 [C=O, C9(11)].

MS (DI), m/e (%); main ions: 234 [(M-H$_2$O)$^{\cdot+}$, 5], 206 [(M-HCO$_2$H)$^{\cdot+}$, 55], 177 (67), 167 (100), 166 (37), 165 (31), 163 (33), 162 (47), 149 (63), 137 (18), 133 (28), 131 (23), 121 (54), 119 (23), 107 (21), 105 (40), 93 (46), 91 (60), 79 (34), 77 (38), 69 (19), 57 (29).

Accurate mass:

Calculated for [C$_{14}$H$_{20}$O$_4$+H]$^+$:　　　　253.1434

Found:　　　　253.1428

7,8-Diethyl-3-azatetracyclo[5.2.1.1^{5,8}.0^{1,5}]undeca-2,4-dione, 122.
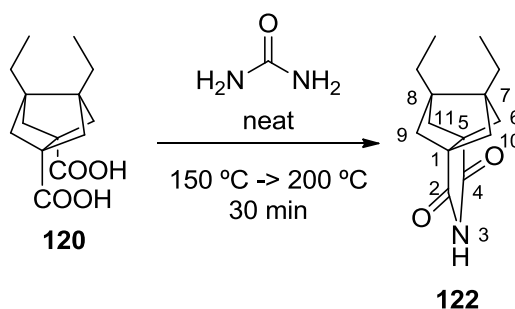
A mixture of diacid **120** (1.12 g, 4.44 mmol) and urea (1.33 g, 95% purity, 22.2 mmol) was heated slowly to 135 ºC. When the mixture melted it was heated to 180 ºC for 30 min and cooled. Water (100 mL) was added and the suspension was extracted with CH$_2$Cl$_2$ (6 × 100 mL). The combined organic extracts were dried with anhydrous Na$_2$SO$_4$, filtered and concentrated in vacuo to dryness to give imide **122** as a white solid (0.91 g, 87% yield). An analytical sample of **122** was obtained by crystallization from CH$_2$Cl$_2$ / n-pentane.

Analytic and spectroscopic data of **122**:

Melting point 209-210 ºC

IR (KBr) ν 3404, 3198, 3072, 2962, 1761, 1707, 1464, 1353, 1210, 1143, 1061, 830, 725, 618, 506 cm^{-1}.

^{1}H NMR (400 MHz, CDCl$_3$) δ 0.92 [t, J = 7.6 Hz, 6 H, C7(8)-CH$_2$CH$_3$], 1.63 [q, J = 7.6 Hz, 4 H, C7(8)-CH$_2$CH$_3$], 1.80 [broad d, J = 7.2 Hz, 4 H, 6(9,10,11)-H$_a$], 1.96 [broad d, J = 7.2 Hz, 4 H, 6(9,10,11)-H$_b$], 8.13 (broad s, 1H, NH).

^{13}C NMR (100.6 MHz, CDCl$_3$) δ 10.0 [CH$_3$, C7(8)-CH$_2$CH$_3$], 22.8 [CH$_2$, C7(8)-CH$_2$CH$_3$], 52.1 [CH$_2$, C6(9,10,11)], 56.6 [C, C7(8)], 57.2 [C, C1(5)], 177.7 (C, CO).

MS (GC), m/e (%); main ions: 233 (M$^+$, 34), 163 (16), 162 (96), 148 (100), 147 (20), 133 (80), 106 (18), 105 (35), 91 (40), 77 (16).

Accurate mass:

Calculated for [C$_{14}$H$_{19}$NO$_2$+H]$^+$:   234.1489

Found: 234.1499

7,8-Diethyl-3-azatetracyclo[5.2.1.1^{5,8}.0^{1,5}]undecane (2R,3R)-tartrate, [124·(2R,3R)-tartrate].

122   **124**   **124·tartrate**
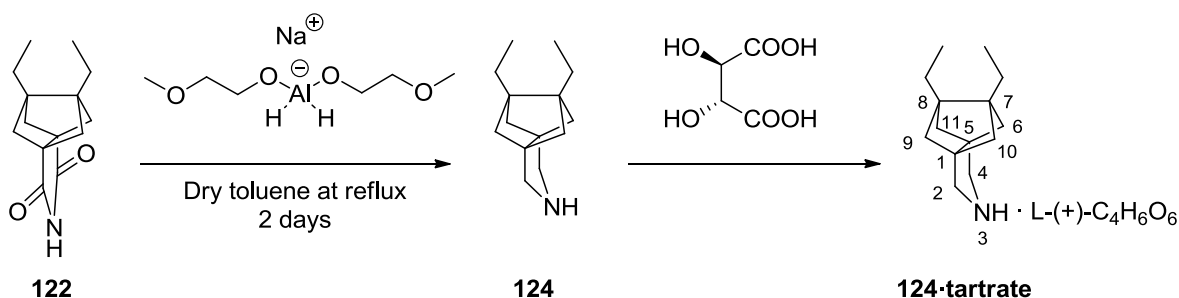
To a stirred solution of imide **122** (907 mg, 3.89 mmol) in anhydrous toluene (32 mL) at 0 °C, sodium bis-(2-methoxyethoxy)aluminium hydride (5.95 mL, 65% solution in toluene, 5.95 mmol) was added dropwise. When the addition was finished, the solution was heated under reflux for 72 h. The mixture was cooled to 0 °C (ice-water bath), treated with 30% aq solution of KOH until basic pH and stirred at room temperature for 1 h. The organic layer was separated and the aqueous one was extracted with CH$_2$Cl$_2$ (3 × 30 mL). The combined organic layers were dried with anhydrous Na$_2$SO$_4$, filtered and evaporated in vacuo to give amine **124** as an orange oil (326 mg). The amine was dissolved in methanol (5 mL) and treated with (2R,3R)-tartaric acid (170 mg, 1.13 mmol) dissolved in the minimum amount of methanol. The mixture was concentrated in vacuo to yield **124** as its (2R,3R)-tartrate as a yellow solid (459 mg, 33% yield). An analytical sample of **124·(2R,3R)-tartrate** was obtained by crystallization from MeOH/Et$_2$O.

Analytic and spectroscopic data of **124·(2R,3R)-tartrate**:

Melting point 165-166 °C

IR (KBr) ν 3422, 3321, 2958, 2882, 1718, 1585, 1455, 1407, 1303, 1263, 1210, 1130, 1068, 899, 834, 784, 680, 618 cm⁻¹.

^{1}H NMR (400 MHz, CD$_3$OD) δ 0.93 [t, J = 7.6 Hz, 6 H, C7(8)-CH$_2$C$\underline{H}$$_3$], 1.53 [broad d, J = 7.2 Hz, 4 H, 6(9,10,11)-H$_a$], 1.61 [q, J = 7.6 Hz, 4 H, C7(8)-C$\underline{H}$$_2CH_3$], 1.76 [broad d, J = 7.2 Hz, 4 H, 6(9,10,11)-H$_b$], 3.27 [s, 4 H, 2(4)-H2], 4.39 [s, 2 H, C$\underline{H}$(OH)-CO$_2$H].

^{13}C NMR (100.6 MHz, CD$_3$OD) δ 10.5 [CH$_3$, C7(8)-CH$_2$$\underline{C}H_3$], 24.2 [CH$_2$, C7(8)-$\underline{C}H_2CH_3$], 47.6 [CH$_2$, C2(4)], 53.3 [CH$_2$, C6(9,10,11)], 57.9 [C, C1(5)]*, 58.0 [C, C7(8)]*, 74.4 [CH, $\underline{C}$H(OH)], 177.6 (C, CO$_2$H).

MS (GC), m/e (%); main ions: 205 [(C$_{14}$H$_{23}$N)$^{·+}$, 7], 190 (11), 176 (16), 163 (21), 162 (100), 161 (14), 147 (27), 136 (20), 133 (21), 120 (15), 119 (21), 107 (15), 105 (23), 91 (37).

Elemental analysis:

Calculated for C$_{18}$H$_{29}$NO$_6$:	C 60.83%	H 8.22%	N 3.94%
Calculated for C$_{18}$H$_{29}$NO$_6$·0.25H$_2$O	C 60.06%	H 8.26%	N 3.89%
Found:	C 60.06%	H 8.51%	N 4.06%

3-Amidino-7,8-diethyl-3-azatetracyclo[5.2.1.1^{5,8}.0^{1,5}]undecane hydrochloride, 126·HCl.

124   **126·HCl**
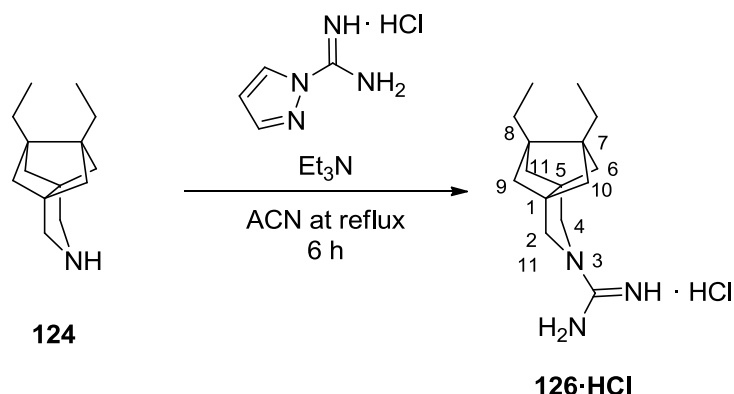
A solution of **124·tartrate** (459 mg, 1.29 mmol) in aqueous 5N KOH (15 mL) was extracted with EtOAc (3 x 20 mL). The organic phase was dried over Na$_2$SO$_4$, filtered and concentrated under vacuo to yield **124** (264 mg, 1.29 mmol) as a yellow waxy solid. A solution of **124** (264 mg, 1.29 mmol), Et$_3$N (0.30 mL, 2.06 mmol) and 1*H*-pyrazole-1-carboxamidine hydrochloride (226 mg, 1.54 mmol) in acetonitrile (10 mL) was heated at 70 °C for 6 h. Then, the suspension was allowed to stand overnight in the freezer (4 °C) and the solid was separated by filtration in vacuo and washed with diethyl ether to give guanidine **126·HCl** as a yellow solid (242 mg, 76% yield). An analytical sample was obtained by crystallization from *t*-butanol.

Analytic and spectroscopic data of **126·HCl**:

Melting point 231-232 °C (dec.)

IR (KBr) ν 3291, 3220, 3173, 3102, 2957, 2877, 2364, 2337, 1603, 1556, 1455, 1369, 1290, 1112, 1077, 946, 899, 677 cm^{-1}.

^{1}H NMR (400 MHz, CD$_3$OD) δ 0.93 [t, *J* = 7.6 Hz, 6 H, C7(8)-CH$_2$CH$_3$], 1.58 [broad d, *J* = 6.6 Hz, 4 H, 6(9,10,11)-H$_a$], 1.61 [q, *J* = 7.6 Hz, 4 H, C7(8)-CH$_2$CH$_3$], 1.72 [broad d, *J* = 6.6 Hz, 4 H, 6(9,10,11)-H$_b$], 3.51 [s, 4 H, 2(4)-H].

^{13}C NMR (100.6 MHz, CD$_3$OD) δ 10.5 [CH$_3$, C7(8)-CH$_2$CH$_3$], 24.2 [CH$_2$, C7(8)-CH$_2$CH$_3$], 49.8 [CH$_2$, C2(4)], 54.6 [CH$_2$, C6(9,10,11)], 57.5 [C, C1(5)]*, 57.9 [C, C7(8)]*, 156.7(C, C=NH).

MS (DI), m/e (%); main ions: 247 (M$^{.+}$, 34), 246 (26), 232 (100), 192 (33), 178 (33), 177 (20), 162 (18), 159 (14), 119 (28), 112 (24), 105 (20), 91 (35), 79 (15), 72 (68).

Elemental analysis:

| Calculated for $C_{15}H_{26}ClN_3$: | C 63.47% | H 9.23% | N 14.80% |
| | Cl 12.49% | | |

| Calculated for $C_{15}H_{26}ClN_3 \cdot 0.3H_2O$ | C 62.29% | H 9.27% | N 14.53% |
| | Cl 12.26% | | |

| Found: | C 61.90% | H 9.16% | N 14.93% |
| | Cl 12.31% | | |

Tricyclo[4.3.3.0^{1,6}]dodecane-8,11-dione, 109.[127a]
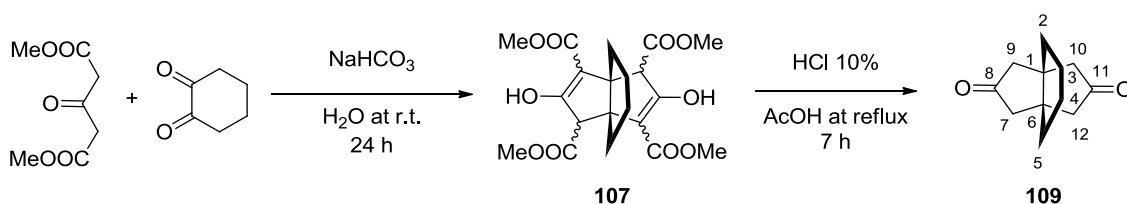
To a solution of sodium bicarbonate (11.2 g) in water (800 mL) was added dimethyl 1,3-acetonedicarboxylate (140.0 g, 0.8 mol) and 1,2-cyclohexanedione (44.8 g, 0.4 mol). The mixture was stirred at room temperature for 2 weeks. The yellow precipitate was filtered under vacuo, washed with water and dried under vacuo obtaining the tetraester **107** (128.9 g) that was used in the next step without further purification.

A mixture of HCl aq. 5N (110 mL) and tetraester **107** (4.49 g, 16.5 mmol) was heated under reflux for 15 hours. The resulting brown solution was allowed to cool down overnight and was neutralized with aqueous 5N NaOH (85 mL) and an aqueous saturated solution of NaHCO$_3$ (20 mL). The solution was extracted with dichloromethane (4 x 100 mL) and the organic phase was dried over Na$_2$SO$_4$, filtered and concentrated under vacuo to give the known[127a] diketone **109** (1.21 g, 38% yield over 2 steps).

Analytic and spectroscopic data of **109**:

Melting point 200-201 °C

IR (KBr) ν 3449, 2925, 2865, 1732, 1453, 1427, 1403, 1354, 1292, 1273, 1260, 1223, 1207, 1177, 1156, 1076, 1041, 1023, 959, 926, 891, 844, 816, 772, 687, 646, 537 cm^{-1}.

^{1}H NMR (400 MHz, CDCl$_3$) δ 1.54 [br s, 8 H, 2(3,4,5)-H2], 2.25 [d, J = 19.6 Hz, 4 H, 7(9,10,12)-H$_{endo}$], 2.43 [d, J = 19.6 Hz, 4 H, 7(9,10,12)-H$_{exo}$].

^{13}C NMR (100.6 MHz, CDCl$_3$) δ 21.1 [CH$_2$, C3(4)], 216.9 [C=O, C8(11)], 31.6 [CH$_2$, C2(5)], 44.7 [C, C1(6)], 49.0 [CH$_2$, C7(9,10,12)].

MS (DI), m/e (%); main ions: 192 (M$^{.+}$, 100), 150 (29), 136 (18), 122 (14), 108 (46), 94 (37), 80 (37).

Tricyclo[4.3.3.0^{1,6}]dodecane-8,11-dione bishydrazone, 111.
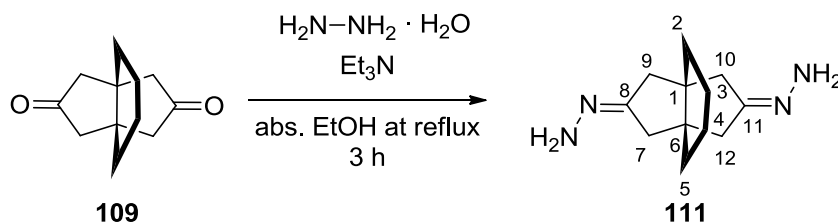
To a solution of diketone **109** (37.3 g, 0.19 mol) in absolute EtOH (525 mL) was added triethylamine (431 mL, 3.11 mmol) and hydrazine monohydrate (97.4 mL, 2.02 mmol). The mixture was heated to reflux for 3 hours. The dark yellow solution obtained was allowed to cool down to room temperature, it was then concentrated to a third of its volume and it was left at 4 °C overnight. The orange precipitate was filtered, washed with cold 96% ethanol and dried under vacuum to give **111** as an orange sticky solid (42.5 g, 99%). An analytical sample (*syn*-isomer) was obtained by crystallized from chloroform

Analytic and spectroscopic data of *syn*-**111**:

Melting point 142-143 °C

IR (KBr) ν 3353, 3195, 2921, 2862, 2841, 1654, 1444, 1420, 1339, 1267, 1225, 1079, 872, 862, 813, 687, 507 cm^{-1}.

^{1}H NMR (400 MHz, CDCl$_3$) δ 1.45 [broad s, 8 H, 3(4)-H$_2$ and 2(5)-H$_2$], 2.15 [dd, J = 18.0 Hz, J' = 1.6 Hz, 2 H, 9(10)-H$_a$], 2.32 [dd, J = 17.0 Hz, J' = 1.6 Hz, 2 H, 7(12)-H$_b$], 2.34 [dd, J = 18.0 Hz, J' = 1.8 Hz, 2 H, 9(10)-H$_b$], 2.47 [broad d, J = 17.2 Hz, 2 H, 7(12)-H$_a$], 4.85 (broad s, 4 H, NH$_2$).

^{13}C NMR (100.6 MHz, CDCl$_3$) δ 21.3 (CH$_2$, C3)*, 21.6 (CH$_2$, C4)*, 30.4 (CH$_2$, C2)*, 32.1 (CH$_2$, C5)*, 37.5 [broad CH$_2$, C9(10)], 42.5 [broad CH$_2$, C7(12)], 46.4 (C, C1)*, 47.6 (C, C5)*, 157.5 [C=N, C3(7)].

MS (DI), m/e (%); main ions: 220 (M$^{·+}$, 19), 204 (100), 191 (18), 188 (25), 150 (39), 149 (39), 148 (23), 105 (16), 91 (30), 79 (17).

Accurate mass:

Calculated for [C$_{12}$H$_{20}$N$_4$+H]$^+$:   221.1761

Found: 221.1756

Mixture of 8,11-diiodotricyclo[4.3.3.0^{1,6}]dodeca-7,11-diene and 8,11-diiodotricyclo[4.3.3.0^{1,6}]dodeca-7,10-diene (*syn-* and *anti-*113).
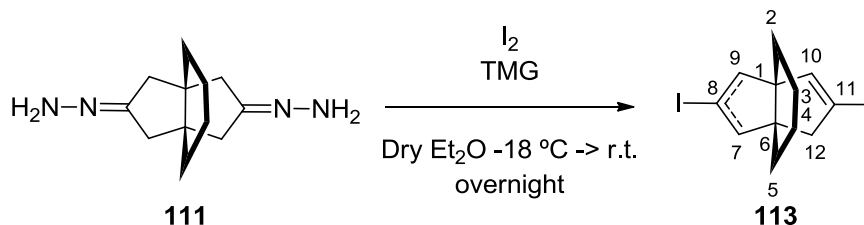
To a stirred suspension of bis-hydrazone **111** (1.0 g, 4.54 mmol) in dry diethyl ether (50 mL) under an argon atmosphere, tetramethylguanidine (8.6 ml, 68.1 mmol) was added. The mixture was cooled to −18 ºC and solid iodine (9.22 g, 36.3 mmol) was added in small portions during 1 hour. When the addition was over, the mixture was allowed to warm to room temperature and stirring was continued for 15 hours. The organic layer was washed with Na$_2$S$_2$O$_3$ (10% aqueous solution, 5 × 50 ml) and brine (2 × 50 ml). The organic layer was dried (Na$_2$SO$_4$), filtered and concentrated under reduced pressure to give a pink solid that was purified by column chromatography (silica gel, *n*-hexane) to give a mixture of *syn-* and *anti-***113** (1.07 g, 57% yield). An analytical sample was obtained by crystallization with *n*-pentane.

Analytic and spectroscopic data of *syn*-**113**:

Melting point 91-92 °C

IR (KBr) ν 3404, 3042, 2916, 2843, 1599, 1436, 1270, 1210, 1097, 1074, 989, 856, 790, 739, 594 cm^{-1}.

^{1}H NMR (400 MHz, CDCl$_3$) δ *anti*-**113** 1.25-1.72 [complex signal, 8 H, 2(5)-H$_2$ and 3(4)-H$_2$], 2.51 [dd, J = 16.4 Hz, J' = 1.6 Hz, 2 H, 9(12)-H$_a$], 2.62 [dd, J = 16.4 Hz, J' = 2.4 Hz, 2 H, 9(12)-H$_b$], 5.85 [m, 2 H, 7(10)-H]; δ *syn*-**113** 1.25-1.55 [complex signal, 8 H, 2(5)-H$_2$ and 3(4)-H$_2$], 2.54 [m, 4 H, 9(10)-H$_2$], 5.88 [t, J = 2.0 Hz, 2 H, 7(12)-H].

^{13}C NMR (100.6 MHz, CDCl$_3$) δ *anti*-**113** 19.0 [CH$_2$, C3(4)], 31.0 [CH$_2$, C2(5)], 52.6 [CH$_2$, C9(12)], 59.0 [C, C1(6)], 91.1 [C, C8(11)], 148.5 [CH, C7(10)]; δ *syn*-**113** 19.7 (CH$_2$, C3)*, 20.8 (CH$_2$, C4)*, 31.4 (CH$_2$, C2)*, 31.8 (CH$_2$, C5)*, 53.2 (C, C1), 55.9 [CH$_2$, C9(10)], 65.9 (C, C6), 92.6 [C, C8(11)], 143.9 [CH, C7(12)].

MS (GC), m/e (%); main ions (*syn* and *anti*): rt (20.2 min): 412 (M$^{\cdot+}$, 26), 285 [(M-I)$^+$, 40], 158 [(M-2I)$^{\cdot+}$, 100], 157 (51), 143 (24), 130 (34), 129 (48), 128 (28), 117 (27), 116 (22), 115 (49), 102 (23), 91 (40); rt (20.3 min): 412 (M$^{\cdot+}$, 13), 285 [(M-I)$^+$, 84], 158 [(M-2I)$^{\cdot+}$, 100], 143 (17), 130 (26), 129 (35), 128 (23), 117 (18), 115 (34), 102 (11), 91 (23).

Elemental analysis:

Calculated for C$_{12}$H$_{14}$I$_2$:   C 34.98%   H 3.42%   I 61.60%

Found: C 34.87%   H 3.34%   I 61.49%

Mixture of dimethyl tricyclo[4.3.3.0^{1,6}]dodeca-7,11-diene-8,11-dicarboxylate and dimethyl tricyclo[4.3.3.0^{1,6}]dodeca-7,10-diene-8,11-dicarboxylate (*syn-* and *anti*-115).
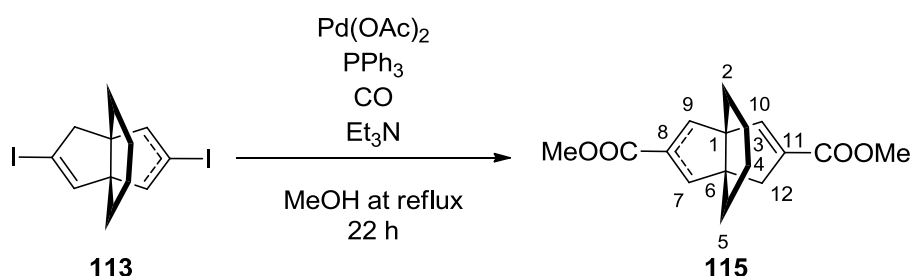
A mixture of **113** (5.70 g, 13.7 mmol), triphenylphosphine (719 mg, 7.74 mmol), Pd(OAc)$_2$ (308 mg, 1.37 mmol), methanol (180 mL) and triethylamine (11.4 mL, 82.2 mmol) was purged with CO for 10 min and stirred and heated under reflux for 22 h under CO (about 1 atm). The black suspension was allowed to cool to room temperature and was evaporated in vacuo to dryness. The residue was taken in dichloromethane (200 mL) and filtered. The orange filtrate was washed with HCl (10% aqueous solution, 3 × 200 mL), NaHCO$_3$ (saturated aqueous solution, 3 × 200 mL) and brine (200 mL). The organic layer was dried (anhydrous Na$_2$SO$_4$), filtered and concentrated in vacuo to dryness to give a mixture of *syn-* and *anti*-**115** as a black oil. Column chromatography (silica gel, hexanes to ethyl acetate / hexanes mixture 2/8) gave a mixture of *syn-* and *anti*-**115** (in the approx. ratio of 1:1, ^{1}H NMR or GC/MS) as a white solid (2.43 g, 64% yield).

Analytic and spectroscopic data of *syn-* and *anti*-**115**:

Melting point 71-72 °C (hexane).

IR (KBr) ν 3026, 3001, 2954, 2921, 2899, 2853, 1713, 1627, 1609, 1437, 1352, 1282, 1264, 1244, 1224, 1206, 1194, 1106, 1084, 979, 950, 898, 777, 749, 602, 552 cm^{-1}.

^{1}H NMR (400 MHz, CDCl$_3$) δ *anti*-**115** 1.20-1.83 [complex signal, 8 H, 2(5)-H$_2$ and 3(4)-H$_2$], 2.58 [dd, J = 16.2 Hz, J' = 1.6 Hz, 2 H, 9(12)-H$_a$], 2.65 [dd, J = 16.4 Hz, J' = 2.8 Hz, 2 H, 9(12)-H$_b$], 3.70 (s, 6 H, CO$_2$C$\underline{H}_3$), 6.47 [m, 2 H, 7(10)-H]; δ *syn*-**115** 1.25-1.60 [complex signal, 8 H, 2(5)-H$_2$ and 3(4)-H$_2$], 2.50 [m, 4 H, 9(10)-H$_2$], 3.71 (s, 6 H, CO$_2$C$\underline{H}_3$), 6.47 [m, 2 H, 7(12)-H].

^{13}C NMR (100.6 MHz, CDCl$_3$) δ *anti*-**115** 19.7 [CH$_2$, C3(4)], 31.4 [CH$_2$, C2(5)], 43.6 [CH$_2$, C9(12)], 51.5 (CH$_3$, CO$_2$C̲H$_3$), 56.0 [C, C1(6)], 135.2 [C, C8(11)], 151.9 [CH, C7(10)], 165.9 (C, C̲O$_2$CH$_3$); δ *syn*-**115** 20.5 (CH$_2$, C3)*, 21.0 (CH$_2$, C4)*, 31.6 (CH$_2$, C2)*, 32.3 (CH$_2$, C5)*, 39.6 [CH$_2$, C9(10)], 50.7 (C, C1), 51.5 (CH$_3$, CO$_2$C̲H$_3$), 63.2 (C, C6), 132.2 [C, C8(11)], 145.5 [CH, C7(12)], 166.0 (C, C̲O$_2$CH$_3$).

MS (GC), m/e (%); main ions: 276 (M$^{\cdot+}$, 40), 244 (100), 217 (48), 216 (42), 185 (34), 184 (18), 157 (47), 131 (16), 129 (29), 128 (17), 117 (21), 115 (28), 91 (21).

Accurate mass:

Calculated for [C$_{16}$H$_{20}$O$_4$+H]$^+$: 277.1434

Found: 277.1435

Mixture of *endo,endo*- and *endo,exo*- dimethyl tricyclo[4.3.3.0^{1,6}]dodecane-8,11-dicarboxylate, 117.
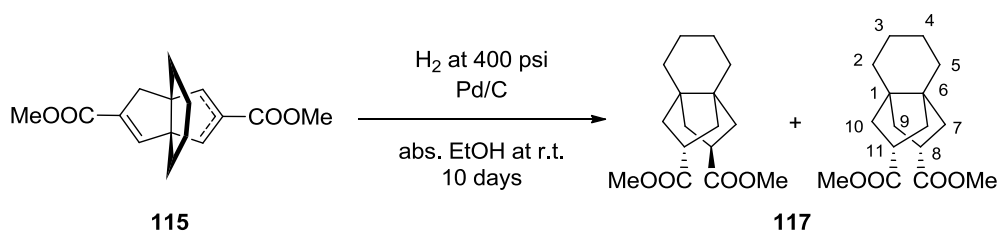
A mixture of **115** (5.43 g, 19.7 mmol) was dissolved in absolute ethanol (120 mL), Pd on charcoal (1.09 g, 54% water content, ca. 5% Pd, equivalent to 25.1 mg of Pd) was added and the resulting mixture was hydrogenated at 400 psi at room temperature for 14 days. The suspension was filtered, and the solvent was evaporated in vacuo to give a mixture of *endo,endo*- and *endo,exo*-stereoisomers of **117** (4.06 g, 74% yield) as a yellow oil.

Analytic and spectroscopic data of **117**:

IR (ATR) ν 2924, 2861. 1730, 1700, 1460, 1434, 1364, 1308, 1278, 1192, 1167, 1121, 1020, 930, 890, 830, 761, 722 cm^{-1}.

^{1}H NMR (400 MHz, CDCl$_3$) δ 1.20-1.52 [complex signal, 8 H, 2(5)-H$_2$ and 3(4)-H$_2$], 1.87-2.02 [complex signal, 8 H, 7(9,10,12)-H$_2$], 2.93-3.11 [complex signal, 2 H, 8(11)-H], 3.67 (s, 6 H, CO$_2$CH̲$_3$).

^{13}C NMR (100.6 MHz, CDCl$_3$) δ *endo,exo*-**117** 20.8 [CH$_2$, C3(4)], 31.1 [CH$_2$, C2(5)], 39.6 (CH) and 40.9 (CH) (C8 and C11), 40.1 (CH$_2$) and 41.1 (CH$_2$) [C7(9) and C10(12)], 51.69 [C, C1(6)], 51.8 (CH$_3$, CO$_2$<u>C</u>H$_3$), 177.3 (C, <u>C</u>O$_2$CH$_3$); δ *endo,endo*-**117** 21.6 [CH$_2$, C3(4)], 32.3 [CH$_2$, C2(5)], 40.1 [CH, C8(11)], 40.7 [CH$_2$, C7(9,10,12)], 50.7 (C, C1), 51.6 [C, C1(6)], 51.72 (CH$_3$, CO$_2$<u>C</u>H$_3$), 177.3 (C, <u>C</u>O$_2$CH$_3$).

MS (GC), m/e (%); main ions: 280 (M$^{\cdot+}$, 2), 248 [(M-CH$_3$OH)$^{\cdot+}$, 100], 220 [(M-HCO$_2$H)$^{\cdot+}$, 82], 216 (59), 189 (36), 188 (58), 179 (52), 161 (83), 158 (30), 147 (25), 134 (55), 121 (59), 119 (87), 105 (37), 93 (52), 91 (76), 79 (45), 77 (25).

Accurate mass:

Calculated for [C$_{16}$H$_{24}$O$_4$+H]$^+$:   281.1747

Found: 281.1747

Dimethyl tetracyclo[6.2.1.1^{3,10}.0^{3,8}]dodecane-1,10-dicarboxylate, 119
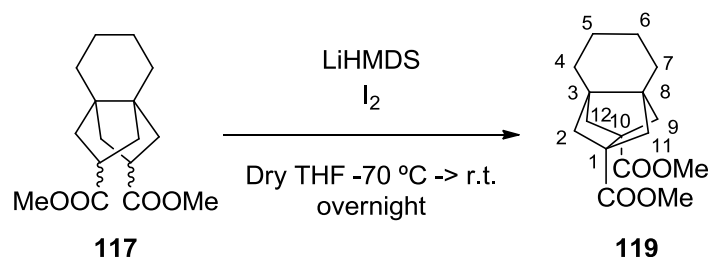
A solution of LiHMDS was prepared by reacting a solution of HMDS (2.50 mL, 11.73 mmol) in anhydrous THF (10 mL) with *n*-butyllithium (5.0 mL, 2.0 M in hexanes, 10.0 mmol) at -68°C under argon for 1 h. Then, a solution of a stereoisomeric mixture of diesters **117** (1.37 g, 4.89 mmol) in anhydrous THF (10 mL) was added dropwise keeping the temperature at -68°C. Stirring was continued for 1 h at this temperature and then a solution of iodine (1.24 g, 4.89 mmol) in anhydrous THF (22 mL) was added dropwise. The mixture was maintained 1 h at -68°C and then allowed to warm to room temperature over 15 h. The mixture was acidified with HCl (10% aqueous solution) until pH 2 (10 mL) and the THF was removed *in vacuo*. The remaining aqueous phase was extracted with diethyl ether (4 × 50 mL) and the combined organic extracts were washed with Na$_2$S$_2$O$_3$ (10% aqueous solution, 3 × 100 mL) and brine (2 × 100 mL), dried (Na$_2$SO$_4$), filtered and evaporated to dryness under reduced pressure to furnish a dark red oil. Column chromatography of this residue (silica gel, hexanes to hexanes / ethyl acetate, 87 / 13) gave diester **119** (771 mg, 57% yield) as a yellow solid.

Analytic and spectroscopic data of **119**:

Melting point 72-73 °C (hexanes).

IR (ATR) ν 3432, 2937, 2856, 1734, 1455, 1436, 1301, 1198, 1176, 1115, 1080, 1031, 930, 799, 758, 566 cm^{-1}.

^{1}H NMR (400 MHz, CDCl$_3$) δ 1.57 [m, 4 H, 5(6)-H$_2$], 1.65 [m, 4 H, 4(7)-H$_2$], 1.77 [d, J = 7.2 H, 4 H, 2(9,11,12)-H$_a$], 1.87 [d, J = 7.2 Hz, 4 H, 2(9,11,12)-H$_b$], 3.66 [s, 6 H, CO$_2$C$\underline{H}_3$].

^{13}C NMR (100.6 MHz, CDCl$_3$) δ 18.8 [CH$_2$, C5(6)], 25.4 [CH$_2$, C4(7)], 48.0 [C, C3(8)], 51.6 (CH$_3$, 2 CO$_2\underline{C}$H$_3$), 53.9 [CH$_2$, C2(9,11,12)], 57.5 [C, C1(10)], 173.5 (C, $\underline{C}$O$_2$CH$_3$).

MS (DI), m/e (%); main ions: 279 [(M+H)$^+$, 13], 247 (32), 246 (51), 237 (31), 219 (25), 205 (17), 203 (19), 196 (13), 188 (18), 179 (53), 177 (30), 164 (55), 159 (37), 147 (63), 133 (16), 131 (25), 119 (100), 117 (29), 115 (19), 105 (25), 91 (64), 79 (21), 77 (21).

Accurate mass:

Calculated for [C$_{16}$H$_{22}$O$_4$+H]$^+$:   279.1591

Found: 279.1588

Tetracyclo[6.2.1.1^{3,10}.0^{3,8}]dodecane-1,10-dicarboxylic acid, 121.
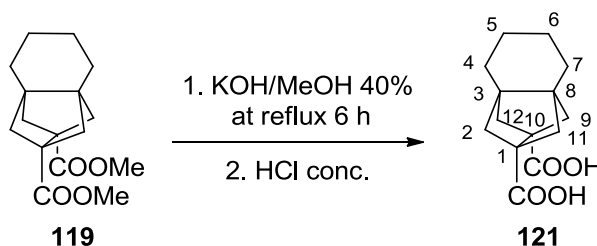
A mixture of **119** (722 mg, 2.59 mmol) and a solution of KOH (40%) in MeOH (7 mL) was heated under reflux for 3 h. Water (7 mL) was added and heating under reflux was continued for 6 h more. The solution was made acidic with conc. aqueous HCl (10 mL) and concentrated in vacuo. The dark solid was extracted with boiling diethyl ether (6 × 40 mL). The combined organic extracts were dried (Na$_2$SO$_4$), filtered and evaporated to dryness under reduced pressure to furnish **121** (520 mg, 80% yield) as a pale yellow solid.

Analytic and spectroscopic data of **121**:

Melting point 239-240 °C

IR (ATR) ν 2931, 2859, 2693, 2592, 1696, 1418, 1299, 1236, 1201, 1083, 1038, 885, 714, 600 cm^{-1}.

^{1}H NMR (400 MHz, CDCl$_3$) δ 1.58 [m, 4 H, 5(6)-H$_2$], 1.66 [m, 4 H, 4(7)-H$_2$], 1.81 [d, J = 7.4 H, 4 H, 2(9,11,12)-H$_a$], 1.91 [d, J = 7.4 Hz, 4 H, 2(9,11,12)-H$_b$], 9.88 [very broad s, 2 H, CO$_2$H̲].

^{13}C NMR (100.6 MHz, CDCl$_3$) δ 18.8 [CH$_2$, C5(6)], 25.3 [CH$_2$, C4(7)], 48.3 [C, C3(8)], 53.7 [CH$_2$, C2(9,11,12)], 58.0 [C, C1(10)], 179.9 (C, C̲O$_2$CH$_3$).

MS (GC), m/e (%); main ions: 250 (M$^{·+}$, 3), 232 [(M-H$_2$O)$^{·+}$, 48], 204 (37), 165 (78), 164 (28), 160 (30), 159 (36), 150 (67), 147 (53), 146 (26), 145 (26), 131 (44), 119 (89), 117 (53), 115 (28), 105 (30), 93 (17), 92 (20), 91 (100), 79 (33), 77 (40), 65 (20).

Accurate mass:

Calculated for [C$_{14}$H$_{18}$O$_4$-H]$^-$:   249.1132

Found: 249.1135

12-Azapentacyclo[6.5.1.1^{3,10}.0^{1,10}.0^{3,8}]pentadecane-11,13-dione, 123.
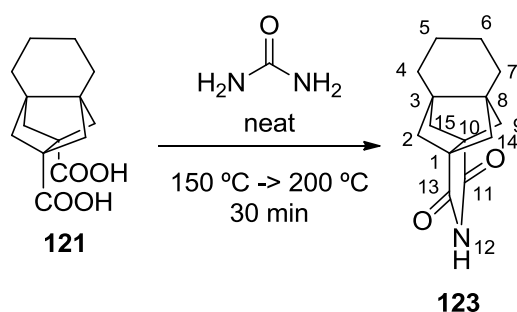
A mixture of diacid **121** (520 mg, 2.10 mmol) and urea (624 mg, 95% purity, 10.4 mmol) was heated slowly to 135 °C. When the mixture melted it was heated to 180 °C for 30 min and cooled. Water (50 mL) was added and the suspension was extracted with CH$_2$Cl$_2$ (6×50 mL). The combined organic extracts were dried with anhydrous Na$_2$SO$_4$, filtered and concentrated in vacuo to dryness to give imide **123** as a white solid (400 g, 83% yield). An analytical sample of **123** was obtained by crystallization from CH$_2$Cl$_2$ / n-pentane.

Analytic and spectroscopic data of **123**:

Melting point 202-203 °C

IR (ATR) ν 3404, 3189, 3079, 2934, 1758, 1706, 1473, 1396, 1354, 1213, 1140, 1061, 840, 733, 618 cm^{-1}.

^{1}H NMR (400 MHz, CDCl$_3$) δ 1.58 [m, 4 H, 5(6)-H$_2$], 1.70 [m, 4 H, 4(7)-H$_2$], 1.83 [d, J = 7.2 H, 4 H, 2(9,14,15)-H$_a$], 1.99 [d, J = 7.2 Hz, 4 H, 2(9,14,15)-H$_b$], 8.09 [broad s, 1 H, N$\underline{H}$].

^{13}C NMR (100.6 MHz, CDCl$_3$) δ 18.7 [CH$_2$, C5(6)], 25.5 [CH$_2$, C4(7)], 52.2 [C, C3(8)], 53.0 [CH$_2$, C2(9,14,15)], 56.9 [C, C1(10)], 177.5 [C, C11(13)].

MS (GC), m/e (%); main ions: 231 (M$^{.+}$, 27), 160 (23), 146 (100), 145 (49), 131 (15), 118 (21), 117 (35), 91 (31).

Accurate mass:

Calculated for [C$_{14}$H$_{17}$NO$_2$+NH$_4$]$^+$:   249.1598

Found: 249.1607

12-Azapentacyclo[6.5.1.1³,¹⁰.0¹,¹⁰.0³,⁸]pentadecane (2R,3R)-tartrate, [125·(2R,3R)-tartrate].
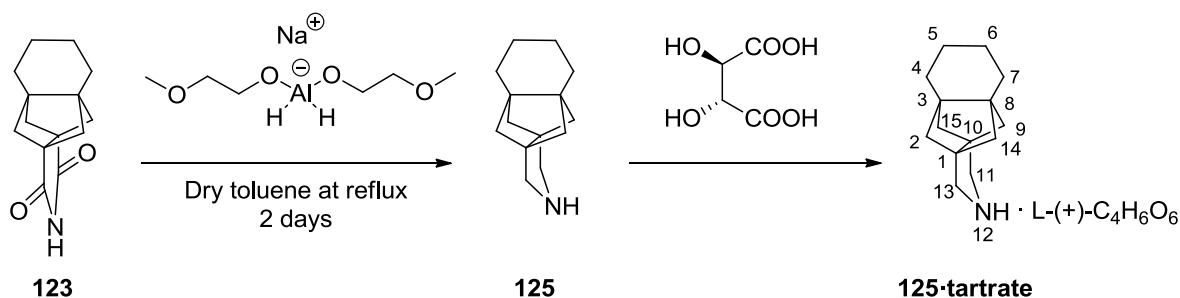
To a stirred solution of imide **123** (378 mg, 1.51 mmol) in anhydrous toluene (14 mL) at 0 °C, sodium bis-(2-methoxyethoxy)aluminium hydride (2.30 mL, 65% solution in toluene, 7.55 mmol) was added dropwise. When the addition was finished, the solution was heated under reflux for 72 h. The mixture was cooled to 0 °C (ice-water bath), treated with 30% aq solution of KOH until basic pH and stirred at room temperature for 1 h. The organic layer was separated and the aqueous one was extracted with CH_2Cl_2 (3×30 mL). The combined organic layers were dried with anhydrous Na_2SO_4, filtered and evaporated in vacuo to give amine **125** as an orange oil (386 mg). The amine was dissolved in methanol (5 mL) and treated with (2R,3R)-tartaric acid (140 mg, 0.93 mmol) dissolved in the minimum amount of methanol. The mixture was concentrated in vacuo to yield **125** as its (2R,3R)-tartrate as a pale yellow solid (442 mg, 83% yield). An analytical sample of **125·(2R,3R)-tartrate** was obtained by crystallization from dichloromethane/methanol.

Analytic and spectroscopic data of **125·(2R,3R)-tartrate**:

Melting point 124-125 °C

IR (ATR) ν 3377, 2931, 2542, 2360, 1715, 1585, 1475, 1450, 1351, 1296, 1118, 1069, 983, 897, 834, 690 cm⁻¹.

^1H NMR (400 MHz, CD_3OD) δ 1.57-1.72 [complex signal, 12 H, 5(6)-H_2, 4(7)-H_2 and 2(9,14,15)-H_a], 1.75 [broad d, J = 6.8 Hz, 4 H, 2(9,14,15)-H_b], 3.27 [s, 4 H, 11(13)-H_2], 4.36 [s, 2 H, C$\underline{H}$(OH)-CO_2H]

^{13}C NMR (100.6 MHz, CD_3OD) δ 20.0 [CH_2, C5(6)], 26.8 [CH_2, C4(7)], 47.3 [CH_2, C11(13)], 52.9 [C, C3(8)], 54.3 [CH_2, C2(9,14,15)], 58.2 [C, C1(10)], 74.7 (CH, $\underline{C}H(OH)$], 178.2 (C, CO_2H).

MS (DI), m/e (%); main ions: 203 [$(C_{14}H_{21}N)^{+}$, 62], 202 (43), 188 (100), 175 (21), 160 (39), 148 (77), 146 (28), 134 (95), 133 (43), 132 (34), 131 (33), 121 (79), 120 (36), 119 (26), 118 (23), 117 (40), 106 (24), 105 (29), 94 (19), 93 (19), 92 (20), 91 (79), 82 (26), 80 (29), 79 (29), 77 (30), 70 (29).

Accurate mass:

Calculated for $[C_{14}H_{21}N+H]^{+}$:	204.1747
Found:	204.1748

Elemental analysis:

Calculated for $C_{18}H_{27}NO_6$:	C 61.17%	H 7.70%	N 3.96%
Calculated for $C_{18}H_{27}NO_6 \cdot 1MeOH$	C 59.20%	H 8.11%	N 3.63%
Found:	C 59.41%	H 8.08%	N 3.47%

12-Amidino-12-azapentacyclo[6.5.1.1^{3,10}.0^{1,10}.0^{3,8}]pentadecane hydrochloride, 127·HCl.

125   **127·HCl**
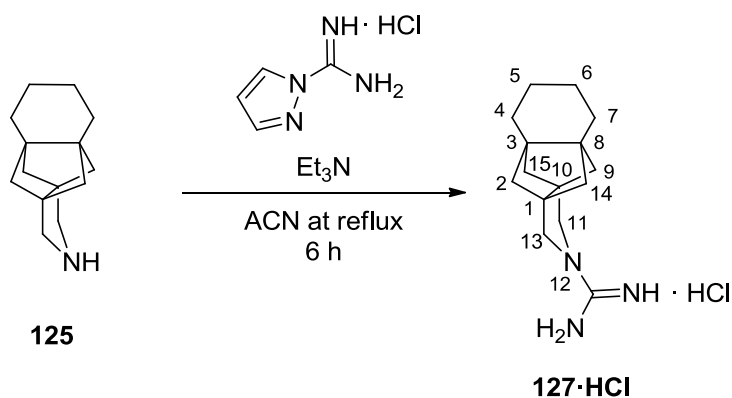
A solution of **125·tartrate** (481 mg, 1.22 mmol) in aqueous 5N KOH (15 mL) was extracted with EtOAc (3 x 20 mL). The organic phase was dried over Na_2SO_4, filtered and concentrated under vacuo to yield **125** as an orange waxy solid (249 mg, 1.22 mmol). A suspension of **125** (249 mg, 1.22 mmol), Et$_3$N (0.14 mL, 0.98 mmol) and 1*H*-pyrazole-1-carboxamidine hydrochloride (215 mg, 1.47 mmol) in acetonitrile (9.5 mL) was heated at 70 °C for 6 h. Then, the suspension was allowed to stand overnight in the freezer (4 °C) and the solid was separated by filtration in vacuo and washed with diethyl ether to give guanidine **127·HCl** as a yellow solid (215 mg, 63% yield). An analytical sample was obtained by crystallization from *t*-butanol.

Analytic and spectroscopic data of **127·HCl**:

Melting point 254-255 °C (dec.)

IR (ATR) ν 3303, 3178, 2926, 2871, 2371, 1647, 1616, 1464, 1361, 1293, 1127, 1035, 958, 929, 775, 701, 609, 559 cm^{-1}.

^{1}H NMR (400 MHz, CD$_3$OD) δ 1.55-1.65 [complex signal, 8 H, 5(6)-H$_2$ and 2(9,14,15)-H$_a$], 1.69 [m, 4 H, 4(7)-H$_2$], 1.80 [broad d, J = 6.8 Hz, 4 H, 2(9,14,15)-H$_b$], 3.50 [s, 4 H, 11(13)-H$_2$].

^{13}C NMR (100.6 MHz, CD$_3$OD) δ 20.0 [CH$_2$, C5(6)], 26.8 [CH$_2$, C4(7)], 49.4 [CH$_2$, C11(13)], 52.8 [C, C3(8)], 55.6 [CH$_2$, C2(9,14,15)], 57.8 [CH$_2$, C1(10)], 156.7 (C, CN).

MS (GC), m/e (%); main ions: 245 [(C$_{15}$H$_{23}$N$_3$)$^{·+}$, 91], 230 (39), 217 (72), 190 (100), 171 (21), 162 (58), 148 (38), 143 (23), 131 (31), 129 (25), 120 (30), 117 (27), 112 (56), 111 (27), 105 (27), 91 (69), 79 (29), 77 (32), 72 (39), 60 (30).

Elemental analysis:

Calculated for C$_{15}$H$_{24}$ClN$_3$:	C 63.93%	H 8.58%	N 14.91%
Calculated for C$_{15}$H$_{24}$ClN$_3$·0.25H$_2$O	C 62.92%	H 8.62%	N 14.68%
Found:	C 63.04%	H 8.55%	N 14.49%

5. **7,8,9,10-Tetramethyl-3-azapentacyclo[7.2.1.1^{5,8}.0^{1,5}.0^{7,10}]tridecane and related compounds**

3,4,8,9-Tetramethyl-12-oxatricyclo[4.4.3.0^{1,6}]trideca-3,8-diene-11,13-dione, 130.[138]

130
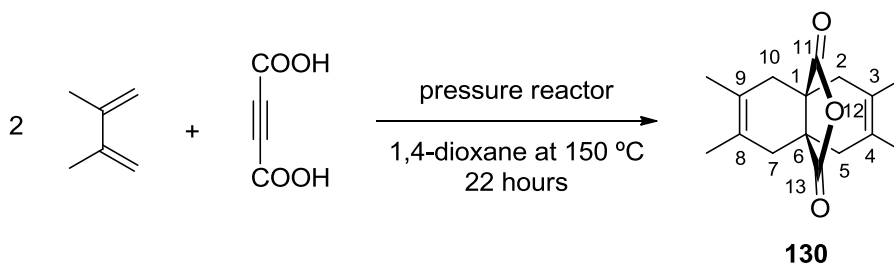
A suspension of acetylene dicarboxylic acid (1.00 g, 8.77 mmol) and 2,3-dimethyl-1,3-butadiene (5.00 mL, 43.8 mmol) in 1,4-dioxane (2 mL) was heated in a pressure reactor to 150 °C for 22 hours. The yellow solution was allowed to cool down and was concentrated under vacuo to yield a light yellow solid (2.78 g). The solid was cristallized from CH_2Cl_2/pentane to give the known [138] anhydride **130** as a light yellow solid (1.95 g, 86%).

Analytical and spectroscopic data of **130**:

Melting point: 152-153 °C

IR (KBr) ν 2992, 2912, 2860, 1845, 1826, 1766, 1435, 1382, 1351, 1313, 1283, 1217, 1165, 960, 760, 657, 616, 567 cm^{-1}.

^{1}H NMR (400 MHz, CDCl$_3$) δ: 1.66 [d, J = 1.2 Hz, 12 H, 3(4,8,9)-C$\underline{H}_3$], 2.16 [broad d, J = 14.8 Hz, 4 H, 2(5,7,10)-H$_a$], 2.43 [d, J = 14.8 Hz, 4 H, 2(5,7,10)-H$_b$].

^{13}C NMR (100.6 MHz, CDCl$_3$) δ: 18.9 [CH$_3$, C3(4,8,9)-$\underline{C}$H$_3$], 38.6 [CH$_2$, C2(5,7,10], 53.0 [C, C1(6)], 127.6 [C, C3(4,8,9)], 177.4 [C, C11(12)].

MS (GC), m/e (%); main ions: 260 (M$^{\cdot+}$, 35), 232 (26), 187 [(C$_{14}$H$_{19}^+$, 100)], 173 (64), 171 (23), 163 (30), 159 (15), 146 (15), 145 (46), 143 (16), 142 (13), 141 (20), 133 (14), 132 (29), 131 (33), 129 (18), 128 (22), 119 (55), 115 (22), 106 (16), 105 (25), 91 (45), 82 (69), 77 (30), 67 (38).

3,4,8,9-tetramethylbicyclo[4.4.0]deca-3,8-diene-1,6-dicarboxylic acid, 131.
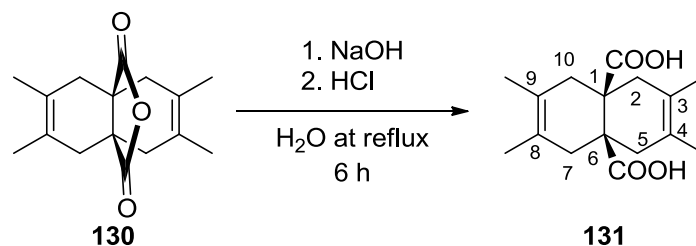
A mixture of the anhydride **130** (500 mg, 1.92 mmol) in an aqueous solution of 5 N NaOH (5 mL) was heated to reflux for 6 hours. The orange suspension was allowed to cool down to room temperature and it was then filtered under vacuo, the residue was recovered as an off white solid that was redissolved in water, acidified with conc. HCl and filtered under vacuo to yield **131** as a white solid (57 mg). A second fraction of **131** was obtained as follows. The aqueous filtrate was washed with Et_2O (4 x 15 mL) and the aqueous phase was acidified again with conc. HCl. The suspension was filtered under vacuo, the residue was recovered as a very pale brown solid (284 mg). Both solids obtained were put together to give a total amount of 341 mg (64% yield) of **131**.

Analytical and spectroscopic data of **131**:

Melting point: 223-224 ºC

IR (KBr) ν 2915, 2865, 2680, 2364, 1697, 1454, 1438, 1400, 1372, 1325, 1291, 1219, 1139, 1116, 1024, 929, 882, 837, 779, 725, 694, 585 cm^{-1}.

^{1}H NMR (400 MHz, CD_3OD) δ: 1.59 [s, 12 H, 3(4,8,9)-C$\underline{H}_3$], 2.11 [d, J = 16.8 Hz, 4 H, 2(5,7,10)-H$_a$], 2.52 [d, J = 16.8 Hz, 4 H, 2(5,7,10)-H$_b$].

^{13}C NMR (100.6 MHz, CD_3OD) δ: 18.7 [CH$_3$, C3(4,8,9)-$\underline{C}$H$_3$], 41.1 [CH$_2$, C2(5,7,10], 46.3 [C, C1(6)], 123.6 [C, C3(4,8,9)], 179.6 (C=O).

MS (GC), m/e (%); main ions: 260 [(M-H_2O)$^{·+}$, 50), 232 (32), 187 ($C_{14}H_{19}^+$, 100), 174 (11), 173 (56), 171 (28), 163 (22), 159 (14), 146 (14), 145 (40), 143 (14), 142 (15), 141 (16), 131 (25), 129 (18), 119 (51), 115 (19), 105 (19), 91 (38), 82 (46), 77 (24), 67 (20).

3,4,8,9-Tetramethyl-12-azatricyclo[4.4.3.0^{1,6}]deca-3,8-diene-11,13-dione, 132.
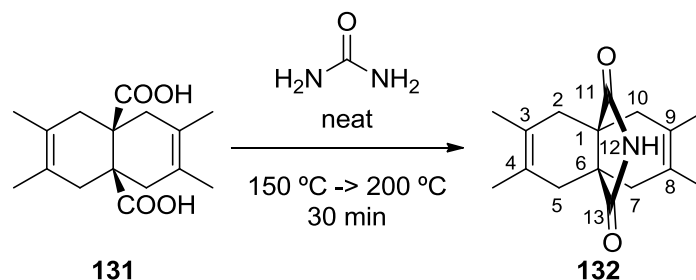
A mixture of diacid **131** (200 mg, 0.72 mmol) and urea (216 mg, 3.59 mmol) was heated slowly to 135 °C. When the mixture melted it was heated to 180 °C for 30 min and cooled. Water (5 mL) was added and the suspension was extracted with CH_2Cl_2 (6 × 4 mL). The combined organic extracts were washed with brine (1 × 5 mL), dried with Na_2SO_4, filtered and concentrated in vacuo to dryness to give imide **132** as a white solid (193 mg, 75% yield). An analytical sample of **132** was obtained by crystallization from CH_2Cl_2/pentane.

Analytical and spectroscopic data of **132**:

Melting point: 197-198 °C

IR (ATR) ν 3202, 3072, 2983, 2928, 2859, 1775, 1706, 1659, 1439, 1364, 1322, 1186, 1106, 982, 829, 739, 677 cm^{-1}.

^1H NMR (400 MHz, $CDCl_3$) δ: 1.63 [d, J = 1.2 Hz, 12 H, 3(4,8,9)-CH_3], 2.07 [d, J = 14.2 Hz, 4 H, 2(5,7,10)-H_a], 2.35 [d, J = 14.2 Hz, 4 H, 2(5,7,10)-H_b], 8.23 (broad s, 1H, NH).

^{13}C NMR (100.6 MHz, $CDCl_3$) δ: 19.1 [CH_3, C3(4,8,9)-CH_3], 38.7 [CH_2, C2(5,7,10)], 52.9 [C, C1(6)], 127.4 [C, C3(4,8,9)], 182.8 [C, C11(13)].

MS (GC), m/e (%); main ions: 259 (M^{·+}, 49), 188 (24), 177 (25), 173 (15), 162 [($C_{12}H_{18}^{·+}$, 100)], 144 (13), 133 (16), 132 (10), 119 (18), 91 (13).

Accurate mass:

Calculated for $[C_{16}H_{21}NO_2+H]^+$:   260.1645

Found: 260.1649

7,8,9,10-Tetramethyl-3-azapentacyclo[7.2.1.1^{5,8}.0^{1,5}.0^{7,10}]tridecane-2,4-dione, 133.
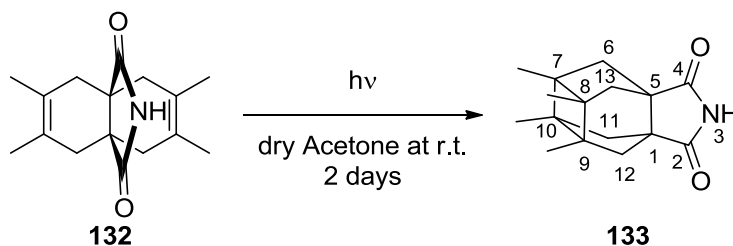
A solution of **132** (630 mg, 2.43 mmol) in dry and degassed acetone (70 mL) placed in a quartz reactor was irradiated with a 125 W Hg lamp for 2 days under Ar atmosphere. The dark yellow solution was concentrated under vacuo to give a yellow paste (1.08 g). The paste was purified by column chromatography (silica gel, hexane/EtOAc mixtures). With hexane/EtOAc (85/15) was recovered starting material (190 mg), while with hexane/EtOAc (80/20) imide **133** was obtained (160 mg, 36% b.r.s.m.) as a white solid.

Analytical and spectroscopic data of **133**:

Melting point: 272-273 °C

IR (ATR) ν 3167, 3054, 2953, 2919, 2868, 1770, 1704, 1452, 1374, 1345, 1312, 1268, 1173, 1154, 1108, 1052, 1018, 842, 739, 628 cm^{-1}.

^{1}H NMR (400 MHz, CDCl$_3$) δ: 1.01 [s, 12 H, 7(8,9,10)-C$\underline{\text{H}}_3$], 1.32 [d, J = 11.4 Hz, 4 H, 6(11,12,13)-H$_a$], 1.83 [d, J = 11.4 Hz, 4 H, 6(11,12,13)-H$_b$], 8.58 (broad s, 1H, NH).

^{13}C NMR (100.6 MHz, CDCl$_3$) δ: 15.2 [CH$_3$, C7(8,9,10)-$\underline{\text{C}}$H$_3$], 40.5 [CH$_2$, C6(11,12,13)], 46.1 [C, C7(8,9,10)], 50.6 [C, C1(5)], 180.9 [C, C2(4)].

MS (GC), m/e (%); main ions: 259 (M$^{·+}$, 74), 188 [(C$_{14}$H$_{20}$)$^{·+}$, 39], 177 (36), 173 (17), 162 [(C$_{12}$H$_{18}$)$^{·+}$, 100], 145 (13), 133 (14), 119 (17), 91 (17).

Accurate mass:

Calculated for [C$_{16}$H$_{21}$NO$_2$+H]$^+$:   260.1645

Found: 260.1643

7,8,9,10-Tetramethyl-3-azapentacyclo[7.2.1.1^{5,8}.0^{1,5}.0^{7,10}]tridecane hydrochloride, 134·HCl.
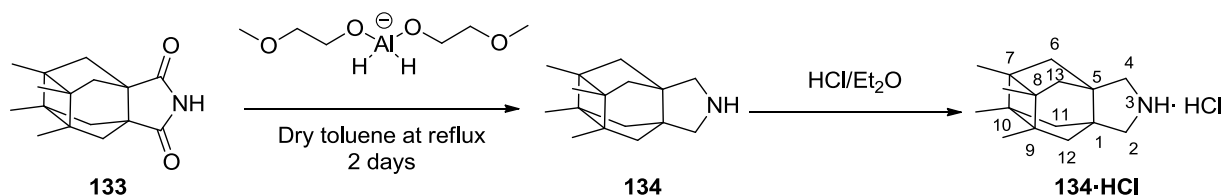
To a stirred solution of imide **133** (210 mg, 0.81 mmol) in anhydrous toluene (7 mL) at 0 °C, sodium bis-(2-methoxyethoxy)aluminium hydride (1.2 mL, 70% solution in toluene, 4.05 mmol) was added dropwise. When the addition was finished, the solution was heated under reflux for 72 h. The mixture was cooled to 0 °C (ice-water bath), treated with 30% aq solution of KOH until basic pH and stirred at room temperature for 1 h. The organic layer was separated and the aqueous one was extracted with CH_2Cl_2 (3 × 10 mL). The combined organic layers were dried with anhydrous Na_2SO_4, filtered and evaporated in vacuo to give amine **134** as an orange oil (232 mg). The oil was taken in ethyl acetate and HCl/Et_2O was added until no more precipitate was formed. The suspension was filtered under vacuo and **134·HCl** was recovered as an off-white solid (154 mg, 71%). An analytical sample of this product was obtained by cristallization from CH_2Cl_2/*n*-pentane.

Analytical and spectroscopic data of **134·HCl**:

Melting point: >300 °C (dec.)

IR (ATR) ν 2918, 2907, 2869, 2824, 2734, 2696, 2675, 2559, 2533, 2471, 1612, 1594, 1454, 1435, 1364, 1314, 1282, 1240, 1201, 1159, 1134, 1124, 1090, 1037, 1002, 979, 916 cm^{-1}.

^{1}H NMR (400 MHz, CD_3OD) δ: 0.95 [d, J = 11.0 Hz, 4 H, 6(11,12,13)-H$_a$], 1.00 [s, 12 H, C7(8,9,10)-CH3], 1.84 [d, J = 11.0 Hz, 4 H, 6(11,12,13)-H$_b$], 3.35 [s, 4 H, 2(4)-H$_2$].

^{13}C NMR (100.6 MHz, CD_3OD) δ: 15.7 [CH$_3$, C7(8,9,10)-$\underline{C}$H3], 42.7 [CH$_2$, C6(11,12,13)], 46.7 [C, C7(8,9,10)], 48.8 [C1(5)], 52.7 [CH$_2$, C2(4)].

MS (DI), m/e (%); main ions: 231 (M$^{·+}$, 100), 230 (58), 216 (25), 201 (14), 188 (36), 187 (31), 186 (60), 185 (19), 173 (20), 172 (17), 171 (65), 160 (14), 159 (23), 157 (16), 149 (26), 148 (94), 146 (47), 145 (34), 134 (20), 132 (23), 119 (40), 105 (21), 93 (17), 91 (36), 79 (18), 77 (21).

Elemental analysis:

Calculated for $C_{16}H_{25}N \cdot HCl$:	C 71.75%	H 9.78%	N 5.23%
Calculated for $C_{16}H_{25}N \cdot HCl \cdot 0.6H_2O$	C 68.70%	H 9.84%	N 5.01%
Found:	C 68.98%	H 9.70%	N 4.79%

3-Amidino-7,8,9,10-tetramethyl-3-azapentacyclo[7.2.1.1^{5,8}.0^{1,5}.0^{7,10}]tridecane hydrochloride, 135·HCl.
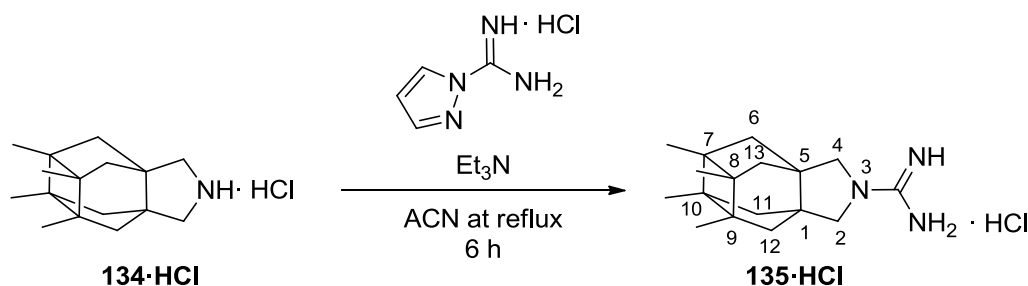
A suspension of **134** (187 mg, 0.70 mmol), Et$_3$N (0.15 mL, 1.05 mmol) and 1*H*-pyrazole-1-carboxamidine hydrochloride (123 mg, 0.84 mmol) in acetonitrile (7.5 mL) was heated at 70 °C for 6 h. Then, the suspension was allowed to stand overnight in the freezer (4 °C) and the solid was separated by filtration in vacuo and washed with diethyl ether to give guanidine **135·HCl** as a white solid (142 mg, 66% yield). An analytical sample of this product was obtained by crystallization from *t*-butanol.

Analytical and spectroscopic data of **135·HCl**:

Melting point: >300 °C (dec.)

IR (ATR) ν 3178, 2854, 2914, 2868, 1771, 1704, 1697, 1651, 1555, 1455, 1374, 1347, 1312, 1269, 1173, 1154, 1052, 842, 739, 628 cm^{-1}.

^{1}H NMR (400 MHz, CD$_3$OD) δ: 0.95 [d, J = 11.0 Hz, 4 H, 6(11,12,13)-H$_a$], 1.00 [s, 12 H, C7(8,9,10)-CH$_3$], 1.87 [d, J = 11.0 Hz, 4 H, 6(11,12,13)-H^b], 3.59 [s, 4 H, 2(4)-H$_2$].

^{13}C NMR (100.6 MHz, CD$_3$OD) δ: 15.8 [CH$_3$, C7(8,9,10)-$\underline{C}$H$_3$], 43.9 [CH$_2$, C6(11,12,13)], 46.6 [C, C7(8,9,10)], 49.5 [C1(5)], 54.6 [CH$_2$, C2(4)], 156.6 (C=NH).

MS (DI), m/e (%); main ions: 273 (M$^{\cdot+}$, 85), 272 (18), 192 (25), 191 (100), 190 (76), 176 (15), 171 (65), 148 (15), 132 (12), 119 (11), 105 (10), 91 (17), 72 (26).

Elemental analysis:

Calculated for C$_{17}$H$_{27}$N$_3$·HCl:	C 65.89%	H 9.11%	N 13.56%
Cl 11.44%			
Calculated for C$_{17}$H$_{27}$N$_3$·1.1HCl·0.6H$_2$O	C 62.75%	H 9.11%	N 12.91%
Cl 11.98%			
Found:	C 62.47%	H 8.84%	N 13.06%
Cl 11.72%			

6. **3,4,8,9-tetramethyltetracyclo[4.4.0.0^{3,9}.0^{4,8}]dec-1(6)-ene and related compounds**

3,4,8,9-Tetramethyl-3-oxapentacyclo[7.2.1.1^{5,8}.0^{1,5}.0^{7,10}]tridecane-2,4-dione, 144.[138]
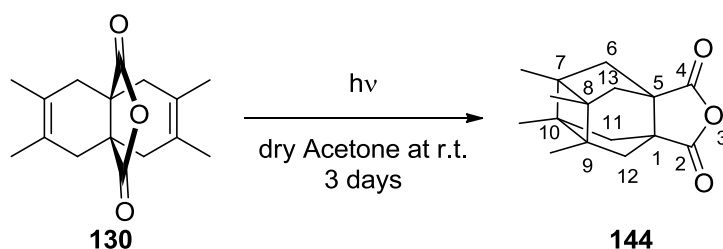
A solution of **130** (881 mg, 3.38 mmol) in dry and degassed acetone (100 mL) in a quartz reactor under argon atmosphere, was irradiated with a 125 W Hg lamp for 3 days. The dark yellow solution was concentrated under vacuo to give a yellow paste. The paste was purified by silica gel column chromatography. The starting material was recovered in the early (hexane/ethyl acetate, 95:5) fractions (314 mg) and the known [138] anhydride **144** was obtained as a white solid in the late (hexane/ethyl acetate, 95:5) fractions (171 mg, 30% b.r.s.m.).

Analytical and spectroscopic data of **144**:

Melting point: 189-190 °C.

IR (KBr) ν 2959, 2927, 2865, 1851, 1791, 1783, 1457, 1385, 1372, 1307, 1283, 1256, 1226, 1210, 1160, 1138, 1013, 995, 917, 759, 739, 619 cm^{-1}.

^{1}H NMR (400 MHz, CDCl$_3$) δ: 1.03 [s, 12 H, 7(8,9,10)-C$\underline{H}_3$], 1.37 [d, J = 11.2 Hz, 4 H, 6(11,12,13)-H$_a$], 1.96 [d, J = 11.6 Hz, 4 H, 6(11,12,13)-H$_b$].

^{13}C NMR (100.6 MHz, CDCl$_3$) δ: 15.1 [CH$_3$, C7(8,9,10)-$\underline{C}$H$_3$], 40.8 [CH$_2$, C6(11,12,13)], 45.9 [C, C7(8,9,10)], 49.5 [C, C1(5)], 174.9 [C, C2(4)].

MS (GC), m/e (%); main ions: 260 (M$^{·+}$, 4), 232 (47), 187 (100), 173 (78), 163 (21), 159 (16), 145 (39), 131 (29), 119 (44), 105 (22), 91 (47), 82 (46), 77 (40), 67 (22), 53 (12).

Elemental analysis:

Calculated for C$_{16}$H$_{20}$O$_3$: C 73.82% H 7.74%

Found: C 73.67% H 7.93%

3,4,8,9-Tetramethyltetracyclo[4.4.0.0^{3,9}.0^{4,8}]decane-1,6-dicarboxylic acid, 145.
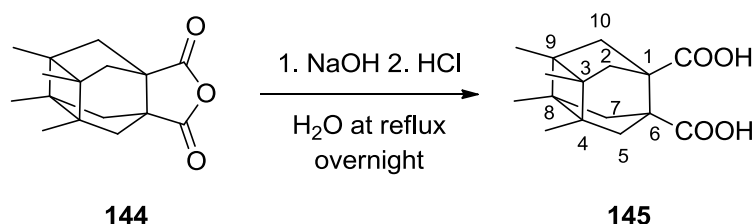
A solution of anhydride **144** (4.17 g, 16.0 mmol) in methanol (50 mL) and 10 N NaOH (200 mL) was heated to reflux for 18 h. The suspension was allowed to cool down to room temperature, the methanol was removed by distillation and the solid was filtered. The solid was partitioned between 5 N HCl (200 mL) and ethyl acetate (200 mL). The two layers were separated and the aqueous one was extracted with ethyl acetate (200 mL). The combined organic extracts were dried over anhydrous Na$_2$SO$_4$, filtered and concentrated under reduced pressure to give **145** (3.66 g, 82% yield) as a white solid.

Analytical and spectroscopic data of **145**:

Melting point: 209-210 °C.

IR (KBr) ν 3000-2400 (2953, 2921, 2867, 2673, 2570), 1717, 1429, 1299, 1218, 1176, 1116, 1061, 1030, 1013, 877, 771, 720 cm^{-1}.

^{1}H NMR (400 MHz, DMSO-d$_6$) δ: 0.92 (s, 12 H, 3(4,8,9)-CH$_3$], 0.98 [d, J = 11.6 Hz, 4 H, 2(5,7,10)-H$_a$], 1.97 [d, J = 11.6 Hz, 4 H, 2(5,7,10)-H$_b$].

^{13}C NMR (100.6 MHz, CD$_3$OD) δ: 15.7 [CH$_3$, 3(4,8,9)-$\underline{C}$H$_3$], 43.5 [CH$_2$, C2(5,7,10)], 46.4 [C, C3(4,8,9)], 53.7 [C, C1(6)], 179.1 (C, CO$_2$H).

MS (GC), m/e (%); main ions: 260 [(M-H$_2$O)$^{·+}$, 5], 232 (51), 187 (100), 173 (73), 163 (19), 159 (15), 145 (34), 131 (23), 119 (37), 105 (17), 91 (36), 82 (37), 77 (31), 67 (17).

Accurate mass:

Calculated for [C$_{16}$H$_{21}$O$_4$-H]$^{-}$:   277.1445

Found: 277.1448

1,6-Diiodo-3,4,8,9-tetramethyltetracyclo[4.4.0.0³,⁹.0⁴,⁸]decane, 146.
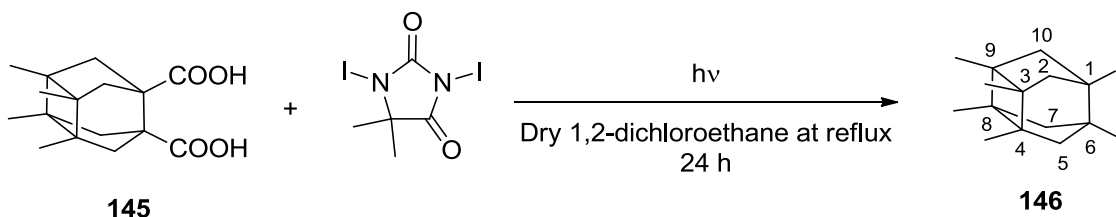
To a solution of diacid **145** (2.50 g, 9.0 mmol) in 1,2-dichloroethane (60 mL) was added 1,3-diiodo-5,5-dimethylhydantoin (8.53, 22.5 mmol). The resulting orange solution was irradiated (2 x 60 W tungsten bulb) at reflux for 24 h. The suspension was cooled to room temperature and filtered. The solid was washed with dichloromethane (2 x 25 mL). The combined filtrate and washings were washed with 10% aqueous solution of $Na_2S_2O_3$ (3 x 100 mL). The organic layer was washed with 2 N NaOH (1 x 100 mL), dried over Na_2SO_4, filtered and concentrated under vacuum to obtain 2.94 g of a mixture of starting **146** and some anhydride **144**. Purification by column chromatography (silica gel, *n*-hexane) gave **146** as a colourless solid (2.03 g, 51% yield).

Analytical and spectroscopic data of **146**:

Melting point: 234-235 °C.

IR (KBr) ν 2923, 2859, 1717, 1448, 1384, 1369, 1298, 1270, 1208, 1187, 1102, 935, 820, 790, 708, 654 cm⁻¹.

¹H NMR (400 MHz, CDCl₃) δ: 0.92 (s, 12 H, 3(4,8,9)-CH₃], 1.62 [d, *J* = 12.0 Hz, 4 H, 2(5,7,10)-Hₐ], 2.69 [d, *J* = 12.0 Hz, 4 H, 2(5,7,10)-Hᵦ].

¹³C NMR (100.6 MHz, CDCl₃) δ: 14.3 [CH₃, C3(4,8,9)-CH₃], 47.0 [C, C3(4,8,9)], 48.7 [C, C1(6)], 53.7 [CH₂, C2(5,7,10)].

MS (GC), m/e (%); main ions: 442 (M⁺, 2), 315 (46), 187 (100), 173 (46), 159 (13), 145 (34), 131 (16), 119 (23), 105 (11), 91 (20), 77 (12).

Elemental analysis:

Calculated for $C_{14}H_{20}I_2$:	C 38.03%	H 4.56%
Calculated for $C_{14}H_{20}I_2 \cdot 0.1$ Hexane:	C 38.91%	H 4.79%
Found:	C 38.94%	H 4.49%

12,13,14,17-Tetramethyl-2,9-diphenyl-19-oxaheptacyclo[10.3.2.1²,⁹.1¹⁰,¹³.0¹,¹⁰.0³,⁸.0¹⁴,¹⁷]nonadeca-3,5,7-triene, 147.
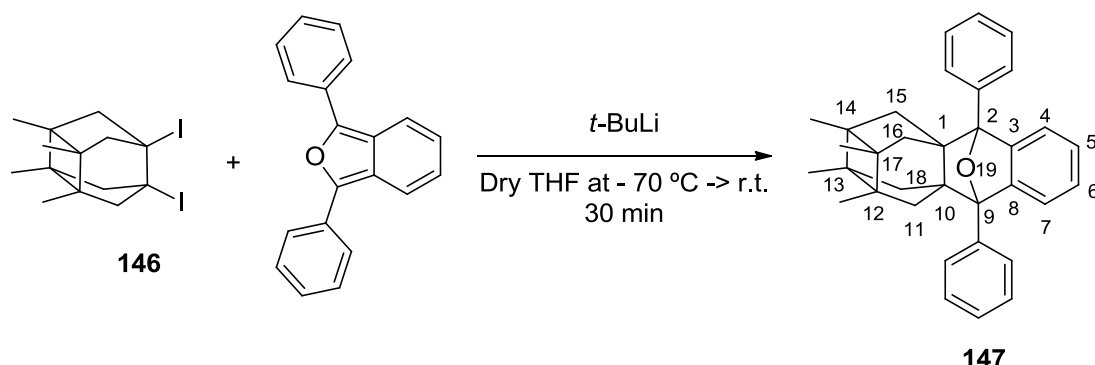
To a cold (-67°C) solution of **146** (252 mg, 0.6 mmol) and 1,3-diphenylisobenzofuran (186 mg, 0.68 mmol) in anhydrous THF (10 mL) a solution of *t*-butyllithium (1.6 M in pentane, 0.61 mL, 0.97 mmol) was slowly added under stirring. The reaction mixture was kept at this temperature for 30 min and then it was allowed to warm to room temperature. Methanol (5 mL) and water (10 mL) were added dropwise and the mixture was extracted with diethyl ether (3 x 50 mL). The combined organic extracts were dried over Na_2SO_4, filtered and concentrated in vacuo to dryness to give a yellow oil. Purification by column chromatography (ethyl acetate/*n*-hexane mixtures) gave **147** (96 mg, 37% yield) as a pale yellow solid.

Analytical and spectroscopic data of **147**:

Melting point: 182-183 °C.

IR (KBr) ν 3061, 3024, 2943, 2913, 2860, 1597, 1457, 1446, 1370, 1342, 1302, 1272, 1217, 1178, 1155, 1119, 1021, 1001, 975, 936, 839, 745, 712, 698, 674 cm⁻¹.

¹H NMR (500 MHz, CDCl₃) δ: 0.42 [d, *J* = 11.5 Hz, 2 H, 11(16)-H$_a$], 0.80 (s, 6 H) and 0.85 (s, 6 H) [C12(17)-C$\underline{H}_3$ and C13(14)-C$\underline{H}_3$], 0.94 [dd, *J* = 11.0 Hz, *J'* = 2.5 Hz, 2 H, 15(18)-H$_b$], 1.06 [d, *J* = 11.0 Hz, 2 H, 15(18)-H$_a$], 1.51 [dd, *J* = 11.5 Hz, *J'* = 2.5 Hz, 2 H, 11(16)-H$_b$], 7.15 [m, 2 H, 5(6)-H], 7.32 [m, 2 H, 4(7)-H], 7.37 (tt, 2 H, *J* = 7.5 Hz, *J'* = 1.5 Hz, Ar-H$_{para}$), 7.49 (broad t, *J* = 7.5 Hz, 4 H, Ar-H$_{meta}$), 7.78 (d, *J* = 8.0 Hz, *J'* = 1.5 Hz, 4 H, Ar-H$_{ortho}$).

¹³C NMR (125.7 MHz, CDCl₃) δ: 15.6 (CH₃) and 15.8 (CH₃) [C12(17)-CH₃ and C13(14)-CH₃], 39.2 [CH₂, C11(16)], 41.0 [CH₂, C15(18)], 44.6 [C, C12(17)], 45.4 [C, C13(14)], 55.3 [C, C1(10)], 88.8 [C, C2(9)], 119.6 [CH, C4(7)], 125.0 (CH, C$_{ortho}$-C₆H₅), 126.1 [CH, C5(6)], 127.0 (CH, C$_{para}$-C₆H₅), 128.2 (CH, C$_{meta}$-C₆H₅), 138.3 (C, C$_{ipso}$-C₆H₅), 146.7 [C, C3(8)].

MS (GC), m/e (%); main ions: 458 ($M^{\cdot+}$, 1), 353 (36), 270 (100), 241 (13), 193 (5), 165 (8), 105 (5), 77 (4).

Accurate mass:

Calculated for $[C_{34}H_{34}O+H]^+$: 459.2682

Found: 459.2680

Elemental analysis:

Calculated for $C_{34}H_{34}O$: C 89.04%   H 7.47%

Calculated for $C_{34}H_{34}O \cdot 0.05\ CH_2Cl_2$: C 88.35%   H 7.43%

Found: C 88.10%   H 7.63%

3,4,8,9-Tetramethyltetracyclo[4.4.0.0^{3,9}.0^{4,8}]decane, 148,

3,3',4,4',8,8',9,9'-octamethyl-bis[tetracyclo[4.4.0.0^{3,9}.0^{4,8}]dec-1-yl], 149,

4,5,6,7,12,13,16,17-octamethylnonacyclo[8.4.4.1^{2,5}.1^{6,9}.0^{1,10}.0^{2,9}.0^{4,7}.0^{12,17}.0^{13,16}]eicosane, 143.
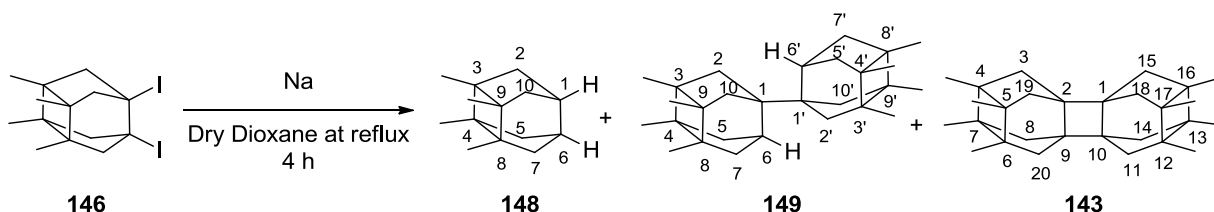
Finely cut sodium (0.49 g, 21.5 mmol) was added to boiling anhydrous 1,4-dioxane (25 mL) and the mixture was heated with stirring under an argon atmosphere until the metal melted. Then, solid **140** (0.95 g, 2.15 mmol) was added and the mixture was heated under reflux for 4 h. The reaction mixture was allowed to cool to room temperature and filtered through Celite®. The solid residue was washed with diethyl ether and *n*-pentane and the combined filtrate and washings were concentrated under reduced pressure to give a white solid residue (151 mg, aprox. 35% yield). GC/MS spectrometry showed the presence of three main components with the following retention times, *m/z* of the molecular ions and relative areas (12.3 min, 190, 20.8%; 24.2 min, 376, 11.5%; 25.1 min, 378, 45.6%). By sublimation (100°C/1 atm), pure tetracycle **142** was obtained (19 mg, 5% yield).

Analytical and spectroscopic data of **148**:

Melting point: 189-190 °C.

IR (KBr) ν 3447, 2946, 2864, 1458, 1381, 1369, 1323, 1116, 1096, 1028, 927 cm⁻¹.

¹H NMR (400 MHz, CDCl$_3$) δ: 0.56 [d, *J* = 11.0 Hz, 4 H, 2(5,7,10)-H$_a$], 0.93 (s, 12 H, 3(4,8,9)-CH$_3$], 1.70 [d, *J* = 11.0 Hz, 4 H, 2(5,7,10)-H$_b$], 2.24 [s, 2 H, 1(6)-H].

¹³C NMR (100.6 MHz, CDCl$_3$) δ: 15.8 [CH$_3$, C3(4,8,9)-$\underline{C}$H$_3$], 32.9 [CH, C1(6)], 38.1 [CH$_2$, C2(5,7,10)], 45.3 [C, C3(4,8,9)].

MS (GC), m/e (%); main ions: 190 (M·⁺, 43), 120 (100), 119 (30), 108 (31), 107 (34), 105 (51), 95 (16), 93 (39), 91 (34), 77 (19).

The solid remaining after concentration of the mother liquors was washed with dichloromethane to give pure dihydrodimer **149** (37 mg, 9% yield).

Analytical and spectroscopic data of **149**:

Melting point: 199-200 °C.

IR (KBr) ν 2943, 2861, 1457, 1381, 1371, 1324, 1258, 1224, 1095, 1061, 1033, 799 cm^{-1}.

^{1}H NMR (400 MHz, CDCl$_3$) δ: 0.62 [d, J = 11.6 Hz, 4 H, 2(2',10,10')-H$_a$], 0.69 [dd, J = 11.2 Hz, J' = 2.8 Hz, 4 H, 5(5',7,7')-H$_a$], 0.91 (s, 12 H) and 0.93 (s, 12 H) [3(3',9,9')-CH$_3$, and 4(4',8,8')-CH$_3$], 1.62 [d, J = 11.2 Hz, 4 H, 2(2',10,10')-H$_b$], 1.71 [dd, J = 11.2 Hz, J' = 1.4 Hz, 4 H, 5(5',7,7')-H$_b$], 2.31 [m, 2 H, 6(6´)-H].

^{13}C NMR (100.6 MHz, CDCl$_3$) δ: 15.8 (CH$_3$), 16.1 (CH$_3$), 36.9 [CH, C6(6´)], 39.2 [CH$_2$, C2(2',10,10')], 39.4 [CH$_2$, C5(5',7,7')], 44.8 (C), and 45.3 (C) [C3(3',9,9') and C4(4',8,8')], 47.5 [C, C1(1')].

MS (GC), m/e (%); main ions: 378 (M$^{.+}$, 21), 296 (49), 214 (18), 189 (65), 188 (68), 187 (20), 173 (33), 133 (21), 120 (25), 119 (100), 107 (50), 105 (29), 95 (54), 93 (16), 91 (34), 80 (19), 67 (20).

Elemental analysis:

Calculated for C$_{28}$H$_{42}$:	C 88.82%	H 11.18%
Calculated for C$_{28}$H$_{42}$·0.1CH$_2$Cl$_2$:	C 87.18%	H 10.99%
Found:	C 87.43%	H 11.11%

By recrystallization of the remaining mixture from *n*-pentane, pure dimer **143** (36 mg, 9% yield) was isolated by filtration.

Analytical and spectroscopic data of **143**:

Melting point: >300 °C.

IR (KBr) ν 2945, 2860, 1699, 1445, 1382, 1297, 1215, 1115 cm^{-1}.

^{1}H NMR (400 MHz, CDCl$_3$) δ: 0.64 [d, J = 13.5 Hz, 8 H, 3(8,11,14,15,18,19,20)-H$_a$], 0.91 (s, 24 H, 4(5,6,7,12,13,16,17)-CH$_3$], 1.97 [d, J = 13.5 Hz, 8 H, 3(8,11,14,15,18,19,20)-H$_b$].

^{13}C NMR (100.6 MHz, CDCl$_3$) δ: 15.8 [CH$_3$, C4(5,6,7,12,13,16,17)-$\underline{C}$H$_3$], 38.9 [CH$_2$, C3(8,11,14,15,18,19,20)], 45.3 [C, C4(5,6,7,12,13,16,17)], 47.0 [C, C1(2,9,10)].

MS (GC), m/e (%); main ions: 376 (M^{+}, 12), 190 (24), 189 (17), 188 (69), 187 (100), 186 (55), 185 (15), 173 (71), 171 (34), 145 (21), 131 (16), 119 (42), 105 (17), 91 (19), 79 (15).

Elemental analysis:

Calculated for $C_{28}H_{40}$:   C 89.29%   H 10.71%

Found: C 89.07%   H 10.71%

REFERENCES

1. Rossman, J. S.; Lamb, R. A. *Virology* **2011**, *411*, 229.

2. Molinari, N.-A. M.; Ortega-Sanchez, I. R.; Messonnier, M. L.; Thompson, W. W.; Wortley, P. M.; Weintraub, E.; Bridges, C. B. *Vaccine* **2007**, *25*, 5086.

3. a) De Clercq, E. *Nat. Rev. Drug Discov.* **2006**, *5*, 1015. b) Beigel, J.; Bray, M. *Antiviral Res.* **2008**, *78*, 91. c) Krug, R. M.; Aramini, J. M. *Trends Pharmacol. Sci.* **2009**, *30*, 269. d) Das, K.; Aramini, J. M.; Ma, L.-C.; Krug, R. M.; Arnold, E. *Nat. Struct. Mol. Biol.* **2010**, *17*, 530. e) Du, J.; Cross, T. A.; Zhou, H.-X. *Drug Discov. Today* **2012**, *17*, 1111. f) Das, K. *J. Med. Chem.* **2012**, *55*, 6263. g) Lee, S. M.-Y.; Yen, H.-L. *Antiviral Res.* **2012**, *96*, 391. h) Vanderlinden, E.; Naesens, L. *Med. Res. Rev.* **2014**, *34*, 301.

4. a) Camps, P.; Pérez, F.; Vázquez, S.; Font-Bardia, M.; Solans, X. *Angew. Chem. Int. Ed. Engl.* **1995**, *34*, 912. b) Camps, P.; Estiarte, M. A.; Vázquez, S.; Pérez, F. *Synth. Commun.* **1995**, *25*, 1287. c) Camps, P.; Luque, F. J.; Orozco, M.; Pérez, F.; Vázquez, S. *Tetrahedron Lett.* **1996**, *37*, 8605. d) Camps, P.; Pérez, F.; Vázquez, S. *Tetrahedron* **1997**, *53*, 9727. e) Lange, H.; Schäfer, W.; Gleiter, R.; Camps, P.; Vázquez, S. *J. Org. Chem.* **1998**, *63*, 3478. f) Camps, P.; Fernández, J. A.; Vázquez, S.; Font-Bardia, M.; Solans, X. *Angew. Chem. Int. Ed. Engl.* **2003**, *42*, 4049. g) Vázquez, S.; Camps, P. *Tetrahedron* **2005**, *61*, 5147. h) Camps, P.; Muñoz, M. R.; Vázquez, S. *Tetrahedron* **2006**, *62*, 7645. i) Duque, M. D.; Camps, P.; Profire, L.; Montaner, S.; Vázquez, S.; Sureda, F. X.; Mallol, J.; López-Querol, M.; Naesens, L.; De Clercq, E.; Prathalingam, S. R.; Kelly, J. M. *Bioorg. Med. Chem.* **2009**, *17*, 3198. j) Duque, M. D.; Camps, P.; Torres, E.; Valverde, E.; Sureda, F. X.; López-Querol, M.; Camins, A.; Prathalingam, S. R.; Kelly, J. M.; Vázquez, S. *Bioorg. Med. Chem.* **2010**, *18*, 46.

5. a) Brankston, G.; Gitterman, L.; Hirji, Z.; Lemieux, C.; Gardam, M. *Lancet Infect. Dis.* **2007**, *7*, 257. b) Weber, T. P.; Stilianakis, N. I. *J. Infect.* **2008**, *57*, 361.

6. Lowen, A. C.; Mubareka, S.; Steel, J.; Palese, P. *PLoS Pathog.* **2007**, *3*, 1470.

7. CDC. Flu symptoms & severity http://www.cdc.gov/flu/about/disease/symptoms.htm (accessed Feb 25, 2014).

8. NIH. Antigenic drift http://www.niaid.nih.gov/topics/flu/research/basic/pages/antigenicdriftillustration.aspx (accessed Feb 25, 2014).

9. NIH. Antigenic shift http://www.niaid.nih.gov/topics/flu/research/basic/pages/antigenicshiftillustration.aspx (accessed Feb 25, 2014).

10. a) Rello, J.; Rodríguez, A.; Ibañez, P.; Socias, L.; Cebrian, J.; Marques, A.; Guerrero, J.; Ruiz-Santana, S.; Marquez, E.; Del Nogal-Saez, F.; Alvarez-Lerma, F.; Martínez, S.; Ferrer, M.; Avellanas, M.; Granada, R.; Maraví-Poma, E.; Albert, P.; Sierra, R.; Vidaur, L.; Ortiz, P.; Prieto del Portillo, I.; Galván, B.; León-Gil, C. *Crit. Care* **2009**, *13*, R148. b) Perez-Padilla, R.; de la Rosa-Zamboni, D.; Ponce de Leon, S.; Hernandez, M.; Quiñones-Falconi, F.; Bautista, E.; Ramirez-Venegas, A.; Rojas-Serrano, J.; Ormsby, C. E.; Corrales, A.; Higuera, A.; Mondragon, E.; Cordova-Villalobos, J. A. *N. Engl. J. Med.* **2009**, *361*, 680.

11. Bouvier, N. M.; Palese, P. *Vaccine* **2008**, *26*, D49.

12. a) Reid, A. H.; Taubenberger, J. K.; Fanning, T. G. *Microbes Infect.* **2001**, *3*, 81. b) Taubenberger, J. K.; Morens, D. M. *Emerg. Infect. Dis.* **2006**, *12*, 15. c) Oxford, J. S.; Lambkin, R.; Elliot, A.; Daniels, R.; Sefton, A.; Gill, D. *Vaccine* **2006**, *24*, 6742. d) Kilbourne, E. D. *Emerg. Infect. Dis.* **2006**, *12*, 9.

13. Jones, J. C.; Baranovich, T.; Marathe, B. M.; Danner, A. F.; Seiler, J. P.; Franks, J.; Govorkova, E. A.; Krauss, S.; Webster, R. G. *J. Virol.* **2014**, *88*, 1175.

14. a) Rajagopal, S.; Treanor, J. *Semin. Respir. Crit. Care Med.* **2007**, *28*, 159. b) Taubenberger, J. K.; Kash, J. C. *Cell Host Microbe* **2010**, *7*, 440.

15. a) Cox, N. J.; Fukuda, K. *Infect. Dis. Clin. North Am.* **1998**, *12*, 27. b) Neumann, G.; Noda, T.; Kawaoka, Y. *Nature* **2009**, *459*, 931.

16. Nicoll, A. A new decade, a new seasonal influenza: the Council of the European Union Recommendation on seasonal influenza vaccination http://www.eurosurveillance.org/ViewArticle.aspx?ArticleId=19458 (accessed Feb 28, 2014).

17. CDC. First Human Avian Influenza A (H5N1) Virus Infection Reported in Americas http://www.cdc.gov/flu/news/first-human-h5n1-americas.htm (accessed Feb 28, 2014).

18. Abdel-Ghafar, A.; Chotpitayasunondh, T.; Zhancheng, G.; Hayden, F.; Hien, N.; de Jong, M.; Naghdaliyev, A.; Peiris, J.; Shindo, N.; Soeroso, S.; Uyeki, T. *N Engl J Med* **2008**, *358*, 261.

19. WHO. Influenza at the human-animal interface. June 2014 http://www.who.int/influenza/human_animal_interface/Influenza_Summary_IRA_HA _interface_27June14.pdf?ua=1 (accessed Oct. 07th, 2014).

20. a) Cohen, J.; Enserink, M. *Science* **2009**, *324*, 1496. b) Michaelis, M.; Doerr, H. W.; Cinatl, J. *Med. Microbiol. Immunol.* **2009**, *198*, 175. c) Dawood, F. S.; Iuliano, A. D.; Reed, C.; Meltzer, M. I.; Shay, D. K.; Cheng, P.-Y.; Bandaranayake, D.; Breiman, R. F.; Brooks, W. A.; Buchy, P.; Feikin, D. R.; Fowler, K. B.; Gordon, A.; Hien, N. T.; Horby, P.; Huang, Q. S.; Katz, M. A.; Krishnan, A.; Lal, R.; Montgomery, J. M.; Mølbak, K.; Pebody, R.; Presanis, A. M.; Razuri, H.; Steens, A.; Tinoco, Y. O.; Wallinga, J.; Yu, H.; Vong, S.; Bresee, J.; Widdowson, M.-A. *Lancet Infect. Dis.* **2012**, *12*, 687.

21. WHO. Human infections with avian influenza A (H7N9) virus http://www.who.int/influenza/human_animal_interface/influenza_h7n9/riskassessme nt_h7n9_27june14.pdf?ua=1 (accessed Oct. 7th, 2014).

22. a) Lamb, R. A. *Am. J. Respir. Crit. Care Med.* **2013**, *188*, 1. b) Horby, P. *Nature* **2013**, *496*, 399.

23. WHO. *Bull. World Health Organ.* **1980**, *58*, 585.

24. Krystal, M.; Fitch, W. M.; Palese, P. *Virology* **1988**, *163*, 112.

25. Cheung, T. K. W.; Poon, L. L. M. *Ann. N. Y. Acad. Sci.* **2007**, *1102*, 1.

26. Kaiser, J. *Science* **2006**, *312*, 380.

27. Varghese, J. N.; Colman, P. M. *J. Mol. Biol.* **1991**, *221*, 473.

28. Air, G. M. *Influ. Other Respir. Viruses* **2012**, *6*, 245.

29. Sharma, M.; Yi, M.; Dong, H.; Qin, H.; Peterson, E.; Busath, D. D.; Zhou, H.-X.; Cross, T. A. *Science* **2010**, *330*, 509. (PDB: 2LOJ)

30. Pinto, L. H.; Holsinger, L. J.; Lamb, R. A. *Cell* **1992**, *69*, 517.

31. Goh, G. K.-M.; Dunker, A. K.; Uversky, V. N. *Virol. J.* **2008**, *5*, 126.

32. Boivin, S.; Cusack, S.; Ruigrok, R. W. H.; Hart, D. J. *J. Biol. Chem.* **2010**, *285*, 28411.

33. Chen, W.; Calvo, P. A.; Malide, D.; Gibbs, J.; Schubert, U.; Bacik, I.; Basta, S.; O'Neill, R.; Schickli, J.; Palese, P.; Henklein, P.; Bennink, J. R.; Yewdell, J. W. *Nat. Med.* **2001**, *7*, 1306.

34. Bornholdt, Z. A.; Prasad, B. V. V. *Nature* **2008**, *456*, 985.

35. Akarsu, H.; Burmeister, W. P.; Petosa, C.; Petit, I.; Müller, C. W.; Ruigrok, R. W. H.; Baudin, F. *EMBO J.* **2003**, *22*, 4646.

36. O'Neill, R. E.; Talon, J.; Palese, P. *EMBO J.* **1998**, *17*, 288.

37. Paterson, D.; Fodor, E. *PLoS Pathog.* **2012**, *8*, e1003019.

38. WHO. Recommended composition of influenza virus vaccines for use in the 2014-2015 northern hemisphere influenza season: http://www.who.int/influenza/vaccines/virus/recommendations/2014_15_north/en/ (accessed Apr 15, 2014).

39. de Vries, E.; Tscherne, D. M.; Wienholts, M. J.; Cobos-Jiménez, V.; Scholte, F.; García-Sastre, A.; Rottier, P. J. M.; de Haan, C. a M. *PLoS Pathog.* **2011**, *7*, e1001329.

40. Torres, E.; Duque, M. D.; Vanderlinden, E.; Ma, C.; Pinto, L. H.; Camps, P.; Froeyen, M.; Vázquez, S.; Naesens, L. *Antiviral Res.* **2013**, *99*, 281.

41. Basu, A.; Antanasijevic, A.; Wang, M.; Li, B.; Mills, D. M.; Ames, J. A.; Nash, P. J.; Williams, J. D.; Peet, N. P.; Moir, D. T.; Prichard, M. N.; Keith, K. A.; Barnard, D. L.; Caffrey, M.; Rong, L.; Bowlin, T. L. *J. Virol.* **2014**, *88*, 1447.

42. a) Oxford, J.S.; Galbraith, A. *Pharmacol. Ther.* **1980**, *11*, 181. b) Belshe, R. B.; Burk, B.; Newman, F.; Cerruti, R. L.; Sim, I. S.; *J. Infect. Dis.* **1989**, *159*, 430

43. WHO. Guidelines on the use of vaccines and antivirals during influenza pandemics. http://whqlibdoc.who.int/hq/2004/WHO_CDS_CSR_RMD_2004.8_eng.pdf?ua=1 (accessed on 15th October 2014).

44. a) Hubsher, G.; Haider, M.; Okun, M. S. *Neurology* **2012**, *78*, 1096. b) WHO. Laboratory methodologies for testing the antiviral susceptibility of influenza viruses: M2 ion channel inhibitor. http://www.who.int/influenza/gisrs_laboratory/antiviral_susceptibility/m2inhibitor/en/ (accessed on 15th October 2014).

45. York, A.; Fodor, E. *RNA Biol.* **2013**, *10*, 1274.

46. a) Pleschka, S.; Wolff, T.; Ehrhardt, C.; Hobom, G.; Planz, O.; Rapp, U. R.; Ludwig, S. *Nat. Cell Biol.* **2001**, *3*, 301. b) Watanabe, K.; Takizawa, N.; Katoh, M.; Hoshida, K.; Kobayashi, N.; Nagata, K. *Virus Res.* **2001**, *77*, 31. c) Chen, J.; Huang, S.; Chen, Z. *J. Gen. Virol.* **2010**, *91*, 2474.

47. Kash, J. C.; Goodman, A. G.; Korth, M. J.; Katze, M. G. *Virus Res.* **2006**, *119*, 111.

48. Takeuchi, K.; Lamb, R. A. *J. Virol.* **1994**, *68*, 911.

49. Schmidt, N. W.; Mishra, A.; Wang, J.; DeGrado, W. F.; Wong, G. C. L. *J. Am. Chem. Soc.* **2013**, *135*, 13710.

50. von Itzstein, M. *Nat. Rev. Drug Discov.* **2007**, *6*, 967.

51. a) Nguyen, J. T.; Smee, D. F.; Barnard, D. L.; Julander, J. G.; Gross, M.; de Jong, M. D.; Went, G. T. *PLoS One* **2012**, *7*, e31006. b) Seo, S.; Englund, J. A.; Nguyen, J. T.; Pukrittayakamee, S.; Lindegardh, N.; Tarning, J.; Tambyah, P. A.; Renaud, C.; Went, G. T.; de Jong, M. D.; Boeckh, M. J. *Antivir. Ther.* **2013**, *18*, 377.

52. a) Wang, J.; Kim, S.; Kovacs, F.; Cross, T. A. *Protein Sci.* **2001**, *10*, 2241. b) Hong, M.; DeGrado, W. F. *Protein Sci.* **2012**, *21*, 1620.

53. Wang, J.; Qiu, J. X.; Soto, C.; DeGrado, W. F. *Curr. Opin. Struct. Biol.* **2011**, *21*, 68.

54. Miao, Y.; Qin, H.; Fu, R.; Sharma, M.; Can, T. V; Hung, I.; Luca, S.; Gor'kov, P. L.; Brey, W. W.; Cross, T. A. *Angew. Chem. Int. Ed. Engl.* **2012**, *51*, 8383.

55. Okada, A.; Miura, T.; Takeuchi, H. *Biochemistry* **2001**, *40*, 6053.

56. Stouffer, A. L.; Acharya, R.; Salom, D.; Levine, A. S.; Di Costanzo, L.; Soto, C. S.; Tereshko, V.; Nanda, V.; Stayrook, S.; DeGrado, W. F. *Nature* **2008**, *451*, 596.

57. Schnell, J. R.; Chou, J. J. *Nature* **2008**, *451*, 591.

58. Williams, J. K.; Zhang, Y.; Schmidt-Rohr, K.; Hong, M. *Biophys. J.* **2013**, *104*, 1698.

59. a) Hu, J.; Fu, R.; Nishimura, K.; Zhang, L.; Zhou, H.-X.; Busath, D. D.; Vijayvergiya, V.; Cross, T. A. *Proc. Natl. Acad. Sci. U. S. A.* **2006**, *103*, 6865. b) Phongphanphanee, S.; Rungrotmongkol, T.; Yoshida, N.; Hannongbua, S.; Hirata, F. *J. Am. Chem. Soc.* **2010**, *132*, 9782.

60. Hu, F.; Schmidt-Rohr, K.; Hong, M. *J. Am. Chem. Soc.* **2012**, *134*, 3703.

61. Bankura, A.; Klein, M. L.; Carnevale, V. *Chem. Phys.* **2013**, *422*, 156.

62. Acharya, R.; Carnevale, V.; Fiorin, G.; Levine, B. G.; Polishchuk, A. L.; Balannik, V.; Samish, I.; Lamb, R. A.; Pinto, L. H.; DeGrado, W. F.; Klein, M. L. *Proc. Natl. Acad. Sci. U. S. A.* **2010**, *107*, 15075.

63. Carnevale, V.; Fiorin, G.; Levine, B. G.; DeGrado, W. F.; Klein, M. L. *J. Phys. Chem. C* **2010**, *114*, 20856.

64. Pinto, L. H.; Lamb, R. A. *J. Biol. Chem.* **2006**, *281*, 8997.

65. Hu, F.; Luo, W.; Hong, M. *Science* **2010**, *330*, 505.

66. Leiding, T.; Wang, J.; Martinsson, J.; DeGrado, W. F.; Arsköld, S. P. *Proc. Natl. Acad. Sci. U. S. A.* **2010**, *107*, 15409.

67. Ma, C.; Fiorin, G.; Carnevale, V.; Wang, J.; Lamb, R. A; Klein, M. L.; Wu, Y.; Pinto, L. H.; DeGrado, W. F. *Structure* **2013**, *21*, 2033.

68. Hay, A. J.; Wolstenholme, A. J.; Shekel, J. J.; Smith, M. H. *EMBO J.* **1985**, *4*, 3021.

69. Pielak, R. M.; Schnell, J. R.; Chou, J. J. *Proc. Natl. Acad. Sci. U. S. A.* **2009**, *106*, 7379.

70. Rosenberg, M. R.; Casarotto, M. G. *Proc. Natl. Acad. Sci. U. S. A.* **2010**, *107*, 13866.

71. a) Ohigashi, Y.; Ma, C.; Jing, X.; Balannik, V.; Pinto, L. H.; Lamb, R. A. *Proc. Natl. Acad. Sci. U. S. A.* **2009**, *106*, 18775. b) Pielak, R. M.; Oxenoid, K.; Chou, J. J. *Structure* **2011**, *19*, 1655.

72. a) Cady, S. D.; Schmidt-Rohr, K.; Wang, J.; Soto, C. S.; Degrado, W. F.; Hong, M. *Nature* **2010**, *463*, 689. b) Cady, S. D.; Wang, J.; Wu, Y.; DeGrado, W. F.; Hong, M. *J. Am. Chem. Soc.* **2011**, *133*, 4274.

73. Andreas, L. B.; Barnes, A. B.; Corzilius, B.; Chou, J. J.; Miller, E. A.; Caporini, M.; Rosay, M.; Griffin, R. G. *Biochemistry* **2013**, *52*, 2774.

74. Gu, R.-X.; Liu, L. A.; Wei, D.-Q.; Du, J.-G.; Liu, L.; Liu, H. *J. Am. Chem. Soc.* **2011**, *133*, 10817.

75. Khurana, E.; Devane, R. H.; Dal Peraro, M.; Klein, M. L. *Biochim. Biophys. Acta* **2011**, *1808*, 530.

76. Ghosh, A.; Wang, J.; Moroz, Y. S.; Korendovych, I. V; Zanni, M.; DeGrado, W. F.; Gai, F.; Hochstrasser, R. M. *J. Chem. Phys.* **2014**, *140*, 235105.

77. Gu, R.-X.; Liu, L. A.; Wang, Y.-H.; Xu, Q.; Wei, D.-Q. *J. Phys. Chem. B* **2013**, *117*, 6042.

78. Ouyang, B.; Chou, J. J. *Biochim. Biophys. Acta* **2014**, *1838*, 1058.

79. Balannik, V.; Carnevale, V.; Fiorin, G.; Levine, B. G.; Lamb, R. A.; Klein, M. L.; Degrado, W. F.; Pinto, L. H. *Biochemistry* **2010**, *49*, 696.

80. Suzuki, H.; Saito, R.; Masuda, H.; Oshitani, H.; Sato, M.; Sato, I. *J. Infect. Chemother.* **2003**, *9*, 195.

81. Wang, J.; Ma, C.; Fiorin, G.; Carnevale, V.; Wang, T.; Hu, F.; Lamb, R. A.; Pinto, L. H.; Hong, M.; Klein, M. L.; DeGrado, W. F. *J. Am. Chem. Soc.* **2011**, *133*, 12834.

82. a) Pielak, R. M.; Chou, J. J. *Biochem. Biophys. Res. Commun.* **2010**, *401*, 58. b) Gu, R.-X.; Liu, L. A.; Wei, D.-Q. *Trends Pharmacol. Sci.* **2013**, *34*, 571.

83. Furuse, Y.; Suzuki, A.; Oshitani, H. *Antimicrob. Agents Chemother.* **2009**, *53*, 4457.

84. Grambas, S.; Bennett, M. S.; Hay, A. J. *Virology* **1992**, *191*, 541.

85. a) Dong, H.; Yi, M.; Cross, T. A.; Zhou, H. *Chem. Sci.* **2013**, *4*, 2776. b) Wei, C.; Pohorille, A. *Biophys. J.* **2013**, *105*, 2036. c) Alhadeff, R.; Assa, D.; Astrahan, P.; Krugliak, M.; Arkin, I. T. *Biochim. Biophys. Acta* **2014**, *1838*, 1068.

86. Jackson, G. G.; Muldoon, R. L.; Akers, L. W. *Antimicrob. Agents Chemother.* **1963**, *161*, 703.

87. Davies, W. L.; Grunert, R. R.; Haff, R. F.; McGahen, J. W.; Neumayer, E. M.; Paulshock, M.; Watts, J. C.; Wood, T. R.; Hermann, E. C.; Hoffmann, C. E. *Science* **1964**, *144*, 862.

88. Tsunoda, A.; Maassab, H. F.; Cochran, K. W.; Eveland, W. C. *Antimicrob. Agents Chemother.* **1965**, *5*, 553.

89. Duque, M. D.; Torres, E.; Valverde, E.; Barniol, M.; Guardiola, S.; Rey, M.; Vázquez, S. In *Recent Advances in Pharmaceutical Science*; 2011; Vol. I pp. 1655–1663.

90. Wang, J.; Ma, C.; Balannik, V.; Pinto, L. H.; Lamb, R. A.; Degrado, W. F. *ACS Med. Chem. Lett.* **2011**, *2*, 307.

91. a) Fytas, G.; Stamatiou, G.; Foscolos, G. B.; Kolocouris, A.; Kolocouris, N.; Witvrouw, M.; Pannecouque, C.; De Clercq, E. *Bioorg. Med. Chem.* **1997**, 7, 1887. b) Stamatiou, G.; Foscolos, G. B., Fytas, G., Kolocouris, A.; Kolocouris, N.; Pannecouque, C.; Witvrouw, M.; Padalko, E.; Neyts, J.; De Clercq, E. *Bioorg. Med. Chem.* **2003**, 11, 5485. c) Zoidis, G.; Fytas, C.; Papanastasiou, I.; Foscolos, G. B.; Fytas, G.; Padalko, E.; De Clercq, E.; Naesens, L.; Neyts, J.; Kolocouris, N. *Bioorg. Med. Chem.* **2006**, *14*, 3341. d) Tataridis, D.; Fytas, G.; Kolocouris, A.; Fytas, C.; Kolocouris, N.; Foscolos, G. B.; Padalko, E., Neyts, J.; De Clercq, E. *Bioorg. Med. Chem.* **2007**, 17, 692.

92. Zhang, W.; Xu, J.; Liu, F.; Li, C.; Jie, Y.; Chen, S.; Li, Z.; Liu, J.; Chen, L.; Zhou, G. *Chinese J. Chem.* **2010**, *28*, 1417.

93. a) Kolocouris, A.; Tataridis, D.; Fytas, G.; Mavromoustakos, T.; Foscolos, G. B.; Kolocouris, N.; De Clercq, E. *Bioorg. Med. Chem. Lett.* **1999**, *9*, 3465. b) Stamatiou, G.; Kolocouris, A.; Kolocouris, N.; Fytas, G.; Foscolos, G. B.; Neyts, J.; De Clercq, E. *Bioorg. Med. Chem. Lett.* **2001**, *11*, 2137. c) Setaki, D.; Tataridis, D.; Stamatiou, G.; Kolocouris, A.; Foscolos, G. B.; Fytas, G.; Kolocouris, N.; Padalko, E.; Neyts, J.; De Clercq, E. *Bioorg. Chem.* **2006**, *34*, 248.

94. a) Beare, A. S.; Hall, T. S.; Tyrrell, D. A. J. *Lancet* **1972**, *299*, 1039. b) Mathur, A.; Beare, A. S.; Reed, S. E. *Antimicrob. Agents Chemother.* **1973**, *4*, 421. c) Togo, Y. *Antimicrob. Agents Chemother.* **1973**, *4*, 641.

95. a) Kolocouris, N.; Foscolos, G. B.; Kolocouris, A.; Marakos, P.; Pouli, N.; Fytas, G.; Ikeda, S.; De Clercq, E. *J. Med. Chem.* **1994**, *37*, 2896. b) Gkeka, P.; Eleftheratos, S.; Kolocouris, A.; Cournia, Z. *J. Chem. Theory Comput.* **2013**, *9*, 1272.

96. a) Zoidis, G.; Tsotinis, A.; Kolocouris, N.; Kelly, J. M.; Prathalingam, S. R.; Naesens, L.; De Clercq, E. *Org. Biomol. Chem.* **2008**, *6*, 3177. b) Zoidis, G.; Kolocouris, N.; Naesens, L.; De Clercq, E. *Bioorg. Med. Chem.* **2009**, *17*, 1534.

97. a) Wang, J.; Wu, Y.; Ma, C.; Fiorin, G.; Wang, J.; Pinto, L. H.; Lamb, R. A.; Klein, M. L.; Degrado, W. F. *Proc. Natl. Acad. Sci. U. S. A.* **2013**, *110*, 1315. b) Wang, J.; Ma, C.; Wang, J.; Jo, H.; Canturk, B.; Fiorin, G.; Pinto, L. H.; Lamb, R. A.; Klein, M. L.; DeGrado, W. F. *J. Med. Chem.* **2013**, *56*, 2804. c) Williams, J. K.; Tietze, D.; Wang, J.; Wu, Y.; DeGrado, W. F.; Hong, M. *J. Am. Chem. Soc.* **2013**, *135*, 9885.

98. Kurtz, S.; Luo, G.; Hahnenberger, K. M.; Brooks, C.; Gecha, O.; Ingalls, K.; Numata, K.; Krystal, M. *Antimicrob. Agents Chemother.* **1995**, *39*, 2204.

99. a) Wang, J.; Cady, S. D.; Balannik, V.; Pinto, L. H.; DeGrado, W. F.; Hong, M. *J. Am. Chem. Soc.* **2009**, *131*, 8066. b) Balannik, V.; Wang, J.; Ohigashi, Y.; Jing, X.; Magavern, E.; Lamb, R. A.; DeGrado, W. F.; Pinto, L. H. *Biochemistry* **2009**, *48*, 11872.

100. Wang, J.; Ma, C.; Wu, Y.; Lamb, R. A.; Pinto, L. H.; DeGrado, W. F. *J. Am. Chem. Soc.* **2011**, *133*, 13844.

101. Zhao, X.; Li, C.; Zeng, S.; Hu, W. *Eur. J. Med. Chem.* **2011**, *46*, 52.

102. Torres, E., Synthesis of polycyclic compounds with antiviral activity. Ph.D. Thesis, University of Barcelona, Barcelona, Spain, 2013.

103. Duque, M. D.; Ma, C.; Torres, E.; Wang, J.; Naesens, L.; Juárez-Jiménez, J.; Camps, P.; Luque, F. J.; DeGrado, W. F.; Lamb, R. A.; Pinto, L. H.; Vázquez, S. *J. Med. Chem.* **2011**, *54*, 2646.

104. Rey-Carrizo, M.; Torres, E.; Ma, C.; Barniol-Xicota, M.; Wang, J.; Wu, Y.; Naesens, L.; DeGrado, W. F.; Lamb, R. A.; Pinto, L. H.; Vázquez, S. *J. Med. Chem.* **2013**, *56*, 9265.

105. Camps, P.; Duque, M. D.; Vázquez, S.; Naesens, L.; De Clercq, E.; Sureda, F. X.; López-Querol, M.; Camins, A.; Pallàs, M.; Prathalingam, S. R.; Kelly, J. M.; Romero, V.; Ivorra, D.; Cortés, D. *Bioorg. Med. Chem.* **2008**, *16*, 9925.

106. Forman, M. A.; Moran, C.; Herres, J. P.; Stairs, J.; Chopko, E.; Pozzessere, A.; Kerrigan, M.; Kelly, C.; Lowchyj, L.; Salandria, K.; Gallo, A.; Loutzenhiser, E. *J. Org. Chem.* **2007**, *72*, 2996.

107. a) Wynne, A. M. *J. Chem. Educ.* **1987**, *64*, 180. b) Schaber, P. M.; Colson, J.; Higgins, S.; Thielen, D.; Anspach, B.; Brauer, J. *Thermochim. Acta* **2004**, *424*, 131. c) Bernhard, A. M.; Peitz, D.; Elsener, M.; Wokaun, A.; Kröcher, O. *Appl. Catal. B Environ.* **2012**, *115-116*, 129.

108. Kalo, J.; Ginsburg, D.; Vogel, E. *Tetrahedron* **1977**, *33*, 1177.

109. Bernatowicz, M. S.; Wu, Y.; Matsueda, G. R. *J. Org. Chem.* **1992**, *57*, 2497.

110. Bingcai, G.; Chen, X.; Zhang, H. In *Ion channels. Methods in Molecular Biology*; 2nd Ed. Gamper, N., Ed.; Springer: New York, 2013; pp. 79–89.

111. Shimbo, K.; Brassard, D. L.; Lamb, R. A.; Pinto, L. H. *Biophys. J.* **1996**, *70*, 1335.

112. Riss, T. L.; Moravec, R. A.; Niles, A. L.; Benink, H. A.; Worzella, T. J.; Minor, L. In *Assay Guidance Manual*; Sittampalam, G. S., Ed.; Eli Lilly & Company and the National Center for Advancing Translational Sciences, 2013.

113. Abou-Gharbia, M.; Patel, U. R.; Webb, M. B.; Moyer, J. A.; Andree, T. H.; Muth, E. A. *J. Med. Chem.* **1988**, *31*, 1382.

114. McNamara, O. A.; Maguire, A. R. *Tetrahedron* **2011**, *67*, 9.

115. Martin, J. G.; Hill, R. K. *Chem. Rev.* **1961**, *61*, 537.

116. a) Borch, R. F.; Bernstein, M. D.; Durst, H. D. *J. Am. Chem. Soc.* **1971**, *93*, 2897. b) Lane, C. F. *Synthesis* **1975**, 135.

117. Kolocouris, A.; Tzitzoglaki, C.; Johnson, F. B.; Zell, R.; Wright, A. K.; Cross, T. A.; Tietjen, I.; Fedida, D.; Busath, D. D. *J. Med. Chem.* **2014**, *57*, 4629.

118. Meneghesso, S.; Vanderlinden, E.; Stevaert, A.; McGuigan, C.; Balzarini, J.; Naesens, L. *Antiviral Res.* **2012**, *94*, 35.

119. Arya, V. P.; Shenoy, S. J. *Indian J. Chem., Sect. B.* **1976**, *14*, 780.

120. a) Drake, L. R.; Stowe, S. C.; Partansky, A. M. *J. Am. Chem. Soc.* **1946**, *68*, 2521. b) Woodward, R. B.; Hoffmann, R. *Angew. Chem. Int. Ed. Engl.* **1969**, *8*, 781.

121. Magnusson, G. *J. Org. Chem.* **1985**, *50*, 1998.

122. Srikrishna, A. *Synth. Commun.* **1990**, *20*, 279.

123. Dye, J. L. *Science* **2003**, *301*, 607.

124. Smith, M. B.; March, J. *March's Advanced Organic Chemistry*, 6th ed.; Wiley: New Jersey, 2007.

125. Ayats, C.; Camps, P.; Duque, M. D.; Font-Bardia, M.; Muñoz, M. R.; Solans, X.; Vázquez, S. *J. Org. Chem.* **2003**, *68*, 8715.

126. a) Weiss, U.; Edwards, J. M. *Tetrahedron Lett.* **1968**, *47*, 4885. b) Yang, S.; Cook, J. M. *J. Org. Chem.* **1976**, *41*, 1903. c) Bertz, S. H.; Cook, J. M.; Gawish, A.; Weiss, U. *Org. Synth.* **1986**, *64*, 27.

127. a) Weber, R. W.; Cook, J. M. *Can. J. Chem.* **1978**, *56*, 189. b) Makhseed, S.; McKeown, N. B. *Chem. Commun.* **1999**, 255.

128. a) Barton, D. H. R.; Bashiardes, G.; Fourrey, J.-L. *Tetrahedron Lett.* **1983**, *24*, 1605. b) Barton, D. H. R.; Bashiardes, G.; Fourrey, J. *Tetrahedron* **1988**, *44*, 147. c) Barton, D. H. R.; Chen, M.; Jászberényi, J. C.; Taylor, D. K.; Hartz, R. A.; Smith, A. B. *Org. Synth.* **1997**, *74*, 101.

129. a) Schoenberg, A.; Bartoletti, I.; Heck, R. F. *J. Org. Chem.* **1974**, *39*, 3318. b) Barnard, C. F. J. *Organometallics* **2008**, *27*, 5402.

130. Ivanoff, D.; Spassoff, A.; *Bull. Soc. Chim. Fr.* **1935**, *2*, 76-78.

131. Rathke, M. W.; Lindert, A. *J. Am. Chem. Soc.* **1971**, *93*, 4605.

132. Ito, Y.; Konoike, T.; Saegusa, T. *J. Am. Chem. Soc.* **1975**, *97*, 2912.

133. Frazier, R. H.; Harlow, R. L. *J. Org. Chem.* **1980**, *45*, 5408.

134. Kise, N.; Tokioka, K.; Aoyama, Y.; Matsumura, Y. *J. Org. Chem.* **1995**, *60*, 1100.

135. a) Baran, P. S.; DeMartino, M. P. *Angew. Chem. Int. Ed. Engl.* **2006**, *45*, 7083. b) DeMartino, M. P.; Chen, K.; Baran, P. S. *J. Am. Chem. Soc.* **2008**, *130*, 11546.

136. Renaud, P.; Fox, M. A. *J. Org. Chem.* **1988**, *53*, 3745.

137. Ma, C.; Polishchuk, A. L.; Ohigashi, Y.; Stouffer, A. L.; Schön, A.; Magavern, E.; Jing, X.; Lear, J. D.; Freire, E.; Lamb, R. A.; DeGrado, W. F.; Pinto, L. H. *Proc. Natl. Acad. Sci. U. S. A.* **2009**, *106*, 12283.

138. a) Avila, W. B.; Silva, R. A. *J. Chem. Soc. D Chem. Commun.* **1970**, 94. b) Ashkenazi, P.; Ginsburg, D. *Tetrahedron* **1979**, *35*, 1317.

139. a) Tada, M.; Kokubo, T.; Sato, T. *Tetrahedron* **1972**, *28*, 2121. b) Kosugi, H.; Sekiguchi, S.; Ryu-ichi, S.; Uda, H. *Bull. Chem. Soc. Jpn.* **1976**, *49*, 520. c) Loufty, R. O.; De Mayo, P. *Can. J. Chem.* **1972**, *50*, 3465.

140. a) Theophanous, F. A.; Tasiopoulos, A. J.; Nicolaides, A.; Zhou, X.; Johnson, W. T. G.; Borden, W. T. *Org. Lett.* **2006**, *8*, 3001. b) Camps, P.; Colet, G.; Delgado, S.; Muñoz, M. R.; Pericàs, M. A.; Solà, L.; Vázquez, S. *Tetrahedron* **2007**, *63*, 4669. c) Pillekamp, M.; Alachraf, W.; Oppel, I. M.; Dyker, G. *J. Org. Chem.* **2009**, *74*, 8355. d) Gavrish, S. P. *J. Comput. Chem.* **2012**, *33*, 2173. e) Ioannou, S.; Krassos, H.; Nicolaides, A. V. *Tetrahedron* **2013**, *69*, 8064.

141. Vázquez, S.; Camps, P. *Tetrahedron* **2005**, *61*, 5147.

142. Vazquez, S. *J. Chem. Soc. Perkin Trans. 2* **2002**, 2100.

143. Volland, W. V; Davidson, E. R.; Borden, W. T. *J. Am. Chem. Soc.* **1979**, *101*, 533.

144. Daday, C.; Smart, S.; Booth, G. H.; Alavi, A.; Filippi, C. *J. Chem. Theory Comput.* **2012**, *8*, 4441.

145. a) Biethan, U.; Gizycki, U. V.; Musso, H. *Tetrahedron Lett.* **1965**, *6*, 1477. b) Musso, H.; Biethan, U. *Chem. Ber.* **1967**, *100*, 119. c) Musso, H.; Klusacek, H. *Chem. Ber.* **1970**, *103*, 3076. d) Ahlquist, B.; Almenningen, A.; Benterud, B.; Traetteberg, M.; Bakken, P.;

Lüttke, W. *Chem. Ber.* **1992**, *125*, 1217. e) Cupas, C. A.; Hodakowski, L. *J. Am. Chem. Soc.* **1974**, *96*, 4668. f) Hamon, D. P. G.; Taylor, G. F. *Tetrahedron Lett.* **1974**, *15*, 155 g) Hamon, D. P. G.; Taylor, G. F. *Aust. J. Chem.* **1976**, *29*, 1721.

146. a) Balasubramanian, M. *Chem. Rev.* **1962**, *62*, 591. b) Sauers, R. R. *J. Chem. Educ.* **2000**, *77*, 332. c) Kakhiani, K.; Lourderaj, U.; Hu, W.; Birney, D.; Hase, W. L. *J. Phys. Chem. A* **2009**, *113*, 4570.

147. During the writing of this thesis, M. Barniol repeated this reaction with a 400 W mercury lamp and irradiating during 5 days, she obtained **138** in 70% yield.

148. Kulbitski, K.; Nisnevich, G.; Gandelman, M. *Adv. Synth. Catal.* **2011**, *353*, 1438.

149. Mo, Y. *Org. Lett.* **2006**, *8*, 535.

150. Alden, R. A.; Kraut, J.; Traylor, T. G. *J. Am. Chem. Soc.* **1968**, *90*, 74.

151. Camps, P.; Colet, G.; Delgado, S.; Muñoz, M. R.; Pericàs, M. A.; Solà, L.; Vázquez, S. *Tetrahedron* **2007**, *63*, 4669.

152. Russell, G. A.; Holland, G. W.; Chang, K.-Y.; Keske, R. G.; Mattox, J.; Chung, C. S. C.; Stanley, K.; Schmitt, K.; Blankespoor, R.; Kosugi, Y. *J. Am. Chem. Soc.* **1974**, 96, *23*, 7237.